PALEOPRODUCTIVITY AND OXYGEN MINIMUM CONDITIONS ON THE PERU MARGIN DURING THE QUATERNARY: MICROPALEONTOLOGIC AND GEOCHEMICAL ANALYSIS OF MODERN AND ANCIENT SEDIMENTS

A THESIS SUBMITTED TO THE GRADUATE DIVISION OF THE UNIVERSITY OF HAWAI'I IN PARTIAL FULFILLMENT OF THE REQUIREMENTS FOR THE DEGREE OF

MASTER OF SCIENCE

IN

GEOLOGY AND GEOPHYSICS

DECEMBER 1994

BY

Richard Knight

Thesis Committee:

Craig R. Glenn, Chairperson
Johanna Resig
Brian Popp

We certify that we have read this thesis and that, in our opinion, it is satisfactory in scope and quality as a thesis for the degree of Master of Science in Geology and Geophysics.

Craig R. Glenn

Chairperson

Abstract

Analysis of modern and ancient sediment from the Peru margin indicates that surface productivity on the margin has been persistently high during the Quaternary with relatively higher rates of production during interglacial stages. The oxygen minimum zone has continually intersected the sediment water interface on the Peru margin at depths of approximately 200 to 600m and, in general, has moved in relation to sea level change (i.e., moving landward during times of rising sea level).

Sediment ages are determined through oxygen isotope stratigraphy and organic carbon weight percent. The organic carbon content of modern sediment from the Peru margin is principally controlled by surface primary productivity and is the main proxy used to interpret productivity in ancient sediments from ODP Leg 112 drilling cores. Benthic foraminifera populations from modern sediments reveal four principle assemblages that distinguish four environments: middle shelf, low oxygen; midshelf/upper slope, oxygen minimum; lower slope, dysaerobic; and deep, relatively well oxygenated . The presence of these assemblages in ODP core sediments reveal the environments of deposition.

Table of Contents

List of Tables

List of Figures

Chapter 1

Introduction and Study Area Description

Purpose of This Research

Marine phosphorites have been located and described along many of the world's continental margins often in areas with strong coastal upwelling and high biological productivity. Along the Peru shelf and upper slope extensive modern phosphorite deposits have been identified. The modern phosphorites which occur on the continental shelf of Peru may be analogous to some large phosphate deposits on land. Studying these presently forming phosphorites on the Peru margin offers a unique opportunity to evaluate the processes responsible for their formation; these processes may lend insight into the formation of ancient phosphorite deposits.

The research presented in this thesis is part of a larger project aimed at investigating environmental factors controlling the formation of phosphorite on the Peru margin. Among the factors that may affect the formation of phosphorite are sea level change, position and intensity of the oxygen minimum zone, paleoproductivity, bottom current activity, sedimentation rates, and sediment reworking. My research analyzes modern and ancient sediments from this region. The scope of this research is restricted mainly to the analysis of oxygen minimum conditions and productivity on the Peru Margin during the Quaternary. In later research, these results may aid in assessing the influence of such factors on the formation of phosphorite on the Peru shelf. I do not consider phosphogenesis in this thesis.

Recently, two cruises have collected sediment samples from the Peru coast. In 1986, The Ocean Drilling Program (ODP) Leg 112 retrieved sections of marine sediment from six sites drilled on the Peru shelf; they include Sites 679, 680, 681, 684, 686, 687 (Fig. 1.1). The sites were chosen to allow tracking of seaward-landward and latitudinal shifts

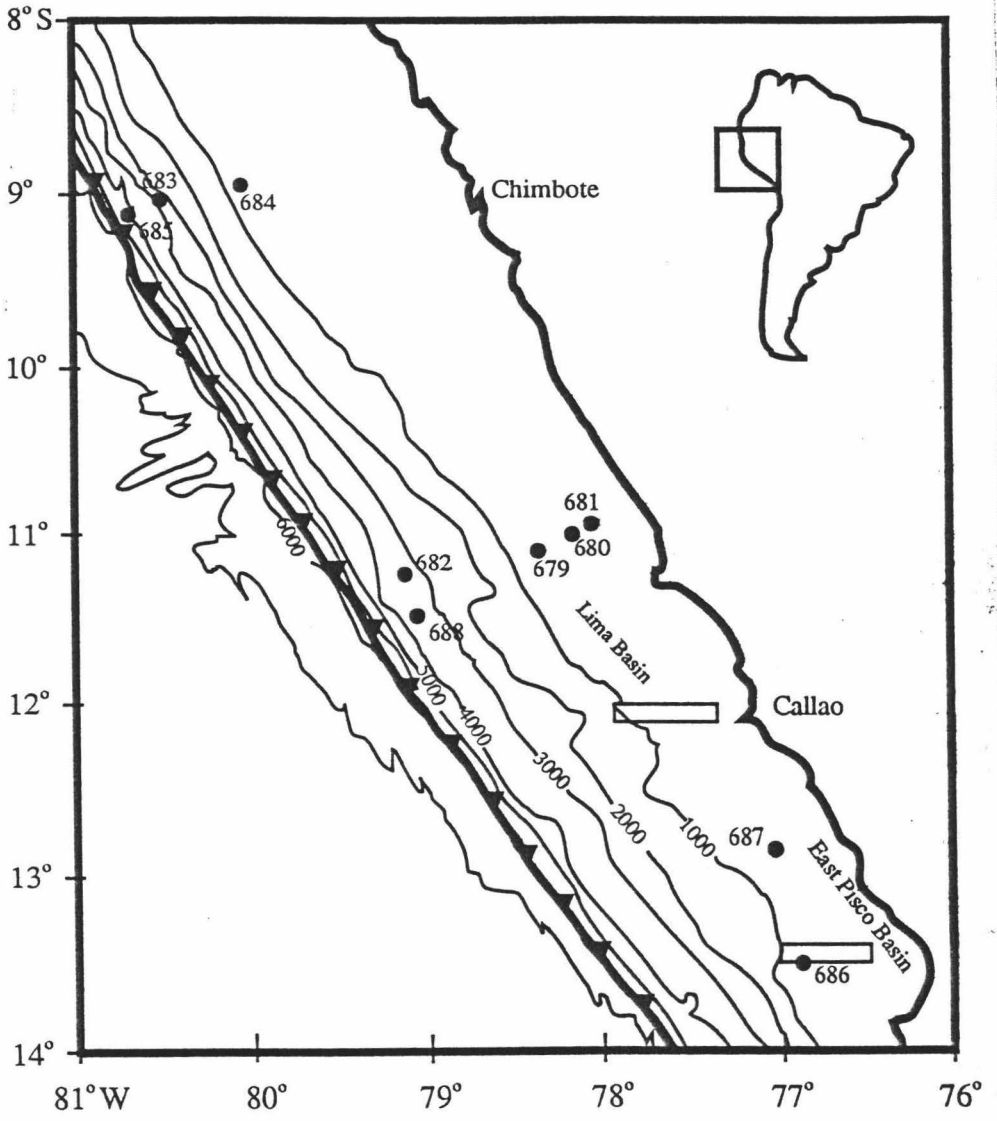

Figure 1.1. Location of ODP Leg 112 coring sites. Rectangular boxes are transect areas during the R/V Seward Johnson cruise. Submersible operations were conducted within the boxes centered at 12°S and 13.5°S ; modified after von Huene et al. (1988).

in the upwelling centers. In 1992, the R/V Seward Johnson cruise collected a large suite of surface sediments from gravity cores and submersible operations (see Fig. 1.1).

This thesis is divided into two major parts: analysis of the modern surface sediments, and analysis of the ODP core sediments. The surface sediments are analyzed with respect to organic-carbon content, the $\delta^{13}C$ of benthic foraminifera, bottom water dissolved oxygen, sea floor sediment facies, benthic foraminiferal assemblages, surface primary productivity, and sedimentology. Based on these analyses, conclusions are drawn about the modern surface samples and they are used to interpret the results of the analysis of the ancient sediments of the ODP cores. The ODP core sediments are analyzed with respect to benthic foraminiferal populations, $\delta^{18}O$ and $\delta^{13}C$ of benthic and planktonic foraminifera, organic-carbon and inorganic-carbon content, sulfur content, and sedimentology and these data are interpreted to determine changes in the bottom water oxygen level, sea level change, changes in productivity, and isotope stages.

My research improves the understanding of Quaternary paleoceanography of the Peru Margin through advances in age assignments to core sediment, and interpretation of geochemical content and micropaleontologic assemblages in its sediments. This research is a high resolution study of the upper 18 m of core sediment. The fine sampling interval of the ODP cores will distinguish higher frequency patterns in environmental indicators that were not observable in studies of samples taken at longer intervals (e.g., Resig 1990, Oberhänsli et al. 1990).

Previous Research

Several studies relative to this research have analyzed the sediment from the Peru Margin with respect to its paleoceanography (e.g., Oberhänsli et al., 1990; Schrader et al., 1990; Schrader et al. 1991; Wefer et al., 1990). These and other studies have attempted to determine changes in intensity and position of upwelling in the region through the analy-

sis of diatom and benthic foraminiferal assemblages, organic and inorganic carbon content, percentage of fish debris, sediment size fractions, etc.

Variations in paleoproductivity has been studied through analysis of organic-carbon content (Müller and Suess, 1979; Müller et al., 1983; and in Suess and Thiede, 1983; Sarnthein et al., 1988; articles in Berger et al., 1989), $\delta^{13}C$ of benthic foraminifera, diatom assemblages (e.g., Schrader, 1992), benthic foraminiferal assemblages (Oberhänsli et al., 1990), and Uk_{37} (Farrington et al., 1989). Heinze & Wefer (1992) studied the benthic foraminifera in Hole 680B and they concluded that the relative percentages of key foraminifer species (*Nonoinella auris, Bolivina costata,* and *Bolivina humilis*) indicated changes in upwelling. They found that upwelling was enhanced during interglacial periods, that is, $\delta^{18}O$-stages 1, 3, 5, 7, 9, and 11. Schrader and Sorknes (1990a) investigated the composition of the diatom flora in Holes 681A and 686A. Their results allowed them to identify variations in the upwelling intensity off Peru over the last 400,000 years. They assinged ages by transferring Wefer et al.'s (1990) oxygen isotope stages from Hole 680B to Holes 681A, and 686A through a correlation of the diatom flora in all three holes. Time intervals with increased upwelling were found in sections of $\delta^{18}O$-stages 3, 5, 7, and 8, while the upwelling intensity was reduced in $\delta^{18}O$-stages 2, 6, and 10 (Schrader & Sorknes, 1990a). These results largely correspond to the upwelling history interpreted from the distribution pattern of benthic foraminifera in Hole 680B by Heinze and Wefer (1992). In a more recent paper, Schrader & Sorknes (1990b) revised the stratigraphy and concluded from marine diatom assemblages that paleoproductivity is not in phase with the general glacial-interglacial cycles and that the largest swings in the magnitude of paleoproductivity seem to occur across oxygen isotope stage boundaries.

Benthic foraminiferal assemblages are good indicators of environmental conditions such as oxygen content, and depth. Benthic foraminiferal species have been studied and

documented along the Peru margin and they have been classified into various assemblages that relate to depth, oxygen content, and current activity (e.g., Ingle et al., 1980; Resig, 1981,1990). Resig (1990) defined several different assemblages that indicate minimum oxygen environments, environments of increased current activity, and shallow shelf environments. Heinze & Wefer (1992) also identified benthic foraminifer species that indicate relatively high velocities of the Peruvian Undercurrent, upwelling activity and well oxygenated bottom waters (0.5->6 ml/l O_2).

Assigning ages to sediments from the Peru margin has proven difficult. The most promising method of assigning ages is through oxygen isotope stratigraphy of foraminifera. Unfortunately, in these cores, benthic and planktonic foraminifera are not present in many intervals, making it difficult or impossible to generate a useful oxygen isotope curve. Hole 680B did, however, contain enough benthic foraminifera for analysis and Wefer et al. (1990) assigned glacial stages to this hole. In Hole 680B, they noticed that low $\delta^{18}O$ oxygen isotope values corresponded to high organic-carbon weight percentages. Using this correlation, they proposed that the organic-carbon weight percent curve may be used as a proxy for the $\delta^{18}O$ curve and they assigned glacial stages to Hole 686B in this way. Other age assignments for these ODP core sediments have been attempted by correlating diatom marker horizons and sedimentary features that are believed to be contemporaneous (Schrader, 1992a). Other methods have placed ages on various sections of sediment in the cores: Matuyama/Bruhnes magnetic reversal boundary, nannofossils, etc (Suess, von Huene et al., 1988).

The oxygen minimum zone that occurs on the Peru margin is due to the oxidation of organic matter in the water column, and to a deficient oxygen supply at the ocean floor. The organic-carbon contents of the marine sediments deposited in anoxic environments are usually very high (1% to 20%), and researchers have suggested that the dissolved oxygen content of the bottom water influences the degree of organic carbon preservation.

The relation between anoxic bottom waters and preserved organic matter is not clear. At present, evidence suggests that there is not a direct relation between oxygen levels and microbial organic carbon degradation. Bacterial degradation rates have been shown to be nearly equal in anoxic and oxic environments (Lee, 1992; Foree and McCarty, 1970; Orr and Gaines, 1974). Studying the Guaymas Basin in the Gulf of California, Calvert et al. (1992) found that both the concentration and the nature of the organic matter in the sediments of this highly productive marginal marine basin are not related to the concentration of dissolved oxygen in the bottom waters. However, oxygen levels may restrict burrowing metazoa. These metazoa may increase organic matter decomposition through active consumption and bioirrigation which increases the residence time of the organic matter in the oxygenated zone where it may be decomposed more efficiently. Therefore, low oxygen levels may effect organic carbon preservation by restricting the activity of burrowing metazoa and thus increasing the rate of preservation of organic matter (Demaison and Moore, 1980).

Oceanographic and geologic setting.

The sediments analyzed in this research were recovered from the outer shelf-upper slope area of the Peru Margin. Stratigraphically, this area is complicated. Previous facies distribution analyses show many erosional unconformities, alternating laminated and bioturbated muds and reworked and winnowed phosphorite sand and silt layers (DeVries and Percy, 1982; Reimers and Seuss, 1983; Molina-Cruz, 1984) (Fig. 1.2). The cause of the unconformities and winnowed layers is thought to be scouring by poleward flowing currents that are influenced by the rise and fall of sea level (Reimers and Seuss, 1983).

The surface and subsurface circulation off the Peruvian coast is similar to the model of Csandy (1990) and was described by Smith et al. (1971). High primary productivity is maintained through the upwelling process where intermediate water is brought to the

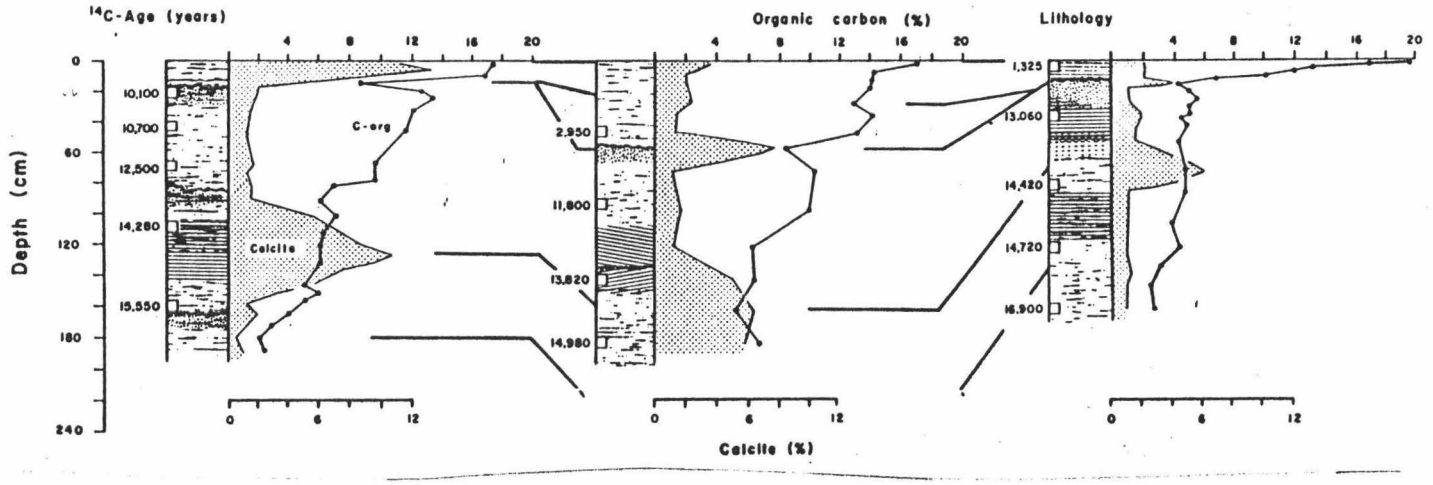

Figure 1.2. Stratigraphic sections from 15 cm-diameter cores. Represents sedimentation NW-SE along approximately 300 km of the present day depositional axis of the upper slope mud lens facies and illustrates erosional unconformities (Reimers and Suess, 1983).

surface by Eckman transport dynamics caused by the southeast trade winds. These intermediate waters are cold and nutrient rich and are supplied by the Poleward Undercurrent(Smith et al., 1971; Barber and Smith, 1981); high nutrient content in the surface waters gives rise to high primary production (Zuta and Guillén, 1970; Blasco, 1971; DeMendiola, 1981). Marine planktonic diatoms are the main part of the biomass (DeMendiola, 1981).

The upwelling process is periodically interrupted by El Niño events which represent an ENSO anomaly (El Niño Southern Oscillation). During El Niño events, primary surface productivity is reduced, however, the physical oceanographic process of upwelling does not need to be reduced. The reduction in productivity may be a result of upwelling a source of water intruding from the north that is warmer and poorer in nutrients compared with normal conditions (Philander 1983; Canby 1984).

Two prominent structural ridges, subparallel to onshore Andean trends, control the distribution of the offshore Cenozoic sedimentary basins. The Coastal Cordillera, which surfaces north of lat. 6°S and south of lat. 14°S, can be traced onto the offshore as an Outer Shelf High; it evidently has a core of Precambrian and Paleozoic metasediments and crystalline rocks. A series of shelf basins is situated between the outer-shelf high and the Andean Cordillera (Fig. 1.3). From north to south, these are the, Salaverry, and East Pisco Basins. A second set of upper-slope basins flanks the outer-shelf high to the southwest, limited seaward by an upper-slope ridge of deformed sediment. From north to south, these are the Trujillo, Lima, and West Pisco Basins.

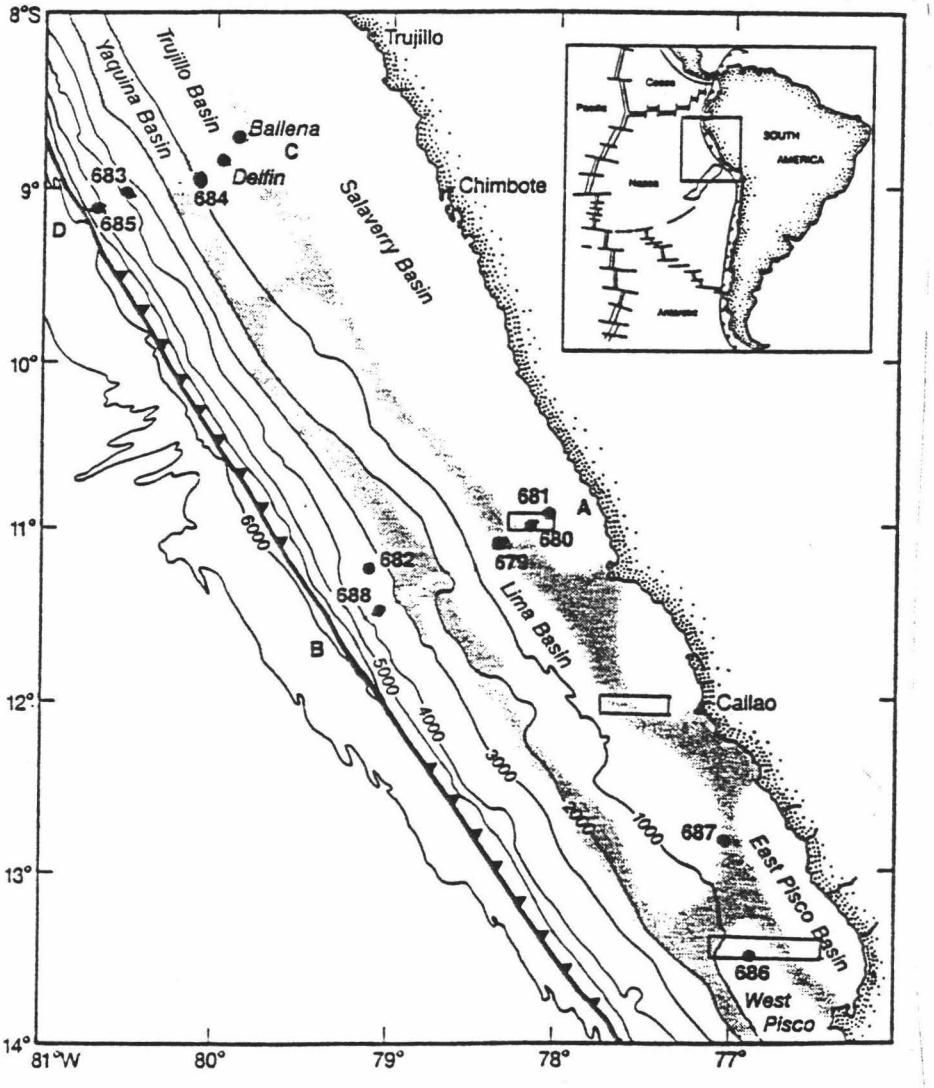

Figure 1.3. ODP Leg 112 drilling sites and R/V Seward Johnson transects (rectangles) shown with respect to depositional basins on the Peru/Chile Margin; modified from Thornburg and Kulm (1981).

Chapter 2
Material, Methods and Calculations

Sample Acquisition

The sediment samples used for this research were obtained from drilling cores taken during ODP Leg 112 in 1986 and from box cores and gravity cores retrieved during the R/V Seward Johnson cruise in September and October 1992. ODP holes sampled include those from Sites 679B, 680A, 681A, 686A, and 687A. Two 20 cm^3 plugs were taken at approximately 25 cm intervals throughout the top 15-17 meters of these ODP sites. The plugs are approximately 2.5 cm wide and the samples were taken perpendicular to the axis of the cores with the midpoint being the reported depth of each sample. 50 surface sediment samples were taken from the tops of Seward Johnson box and gravity cores and from Johnson Sealink submersible operations. The uppermost layer of sediment (< 1 cm) from these cores was removed for analysis.

Micropaleontology Analysis

Foraminiferal Census Counts

The 20 cm^3 samples were dried at 45° C for 24 hours and weighed. The dried sediment was soaked in water before sieving. No chemicals were used to disaggregate the sediments. All samples were wet-sieved on a screen with 62 μm openings and then dried again. The dried sand fraction was divided by an OTTO-style microsplitter until roughly 200 to 500 benthic specimens remained. Different benthic foraminifer species were identified and counted and their percentage frequencies were recorded.

Taxonomy

Taxonomy follows the generic classification adopted by Loeblich and Tappan (1987). Illustrations of foraminiferal species analyzed in this study can be found in Resig (1981, 1990).

Oxygen and carbon stable isotope analysis

Foraminifer Selection

Sieved and dried sediments were picked for benthic and planktonic foraminifera for light stable isotope analyses. The benthic foraminifer *Bolivina humilis* thrives in the Peru Margin's oxygen minimum zone and was a logical choice for analysis. Only easily identifiable specimens showing no trace of foreign particles were used for isotope analysis. The average number of individual tests per isotope analysis was 20. The averaga dimension of benthic foraminifers selected for analysis was approximately 0.5 mm.

CO_2 Gas Liberation

A glass vial containing the foraminifer tests is placed in the deep well of a reaction tube (Fig. 2.1 shows a schematic diagram of the apparatus use for CO_2 gas liberation and collection). Approximately 1 ml of 100% phosphoric acid is injected into the side finger of the reaction tube. The reaction tube is placed on a vacuum line and evacuated to approximately 0.4 mbar. Dissolved air is removed from the phosphoric acid with the aid of a hot air blower. The evacuation takes approximately one hour. The evacuated reaction tube with its sample is then sealed and removed from the vacuum line and placed in a water bath at 50 °C for approximately one hour. When the phosphoric acid and the foraminifer tests have reached 50 °C the reaction tube is tilted and the phosphoric acid is allowed to enter the deep finger and dissolve the foraminifer tests. The reaction is allowed to proceed in the water bath for approximately one hour. Samples during this research typically generated 2 to 6 μMol of CO_2 gas.

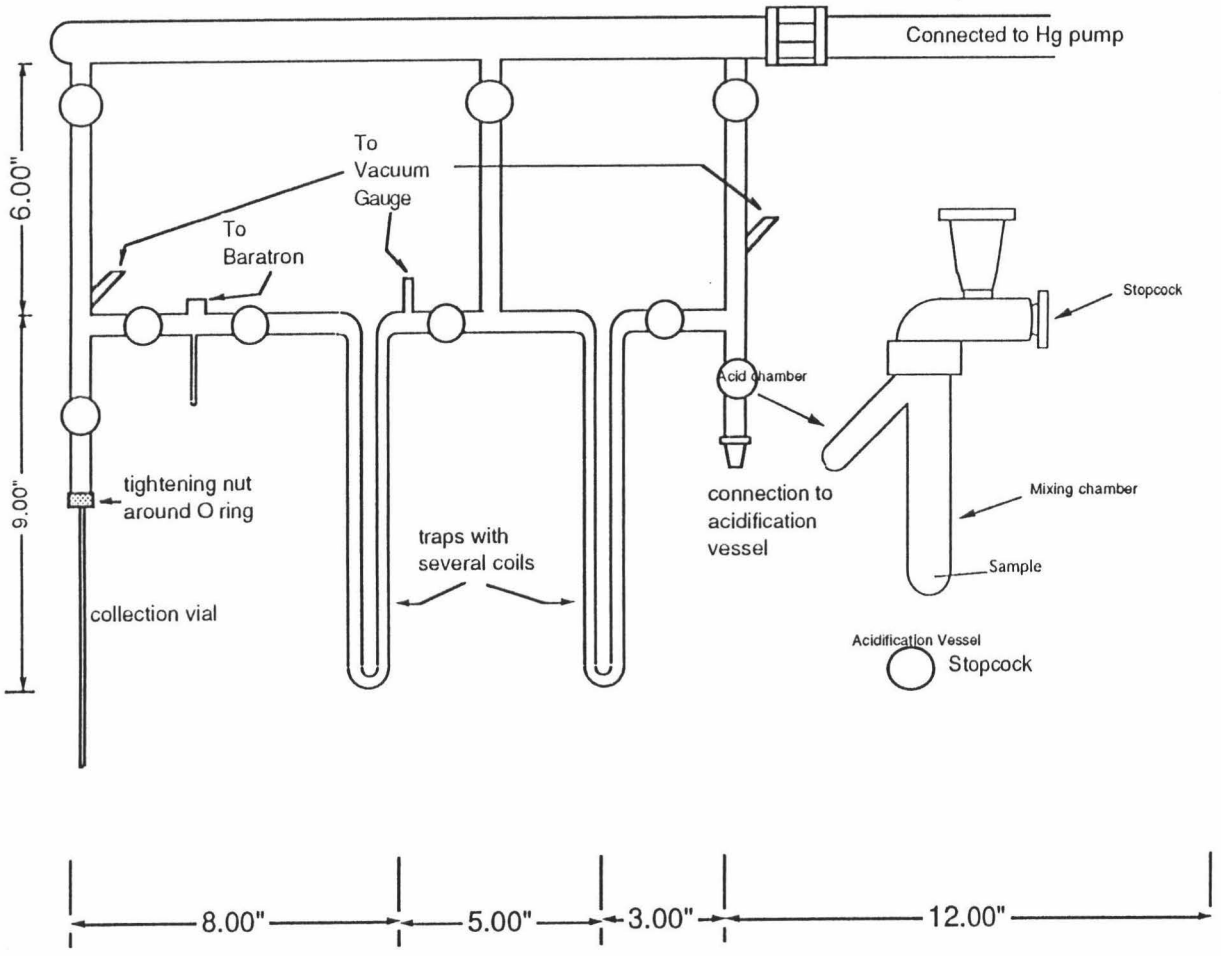

Figure 2.1. Schematic diagram of apparatus used to extract CO_2 gas from foraminifer samples.

CO_2 Gas Extraction

The reaction tube with the evolved CO_2 gas is placed on an extraction line (Fig. 2-1). The extraction line is evacuated. An H_2O trap is created by immersing a glass tube coil in a pentane slurry. The pentane slurry consists of a mixture of pentane and liquid nitrogen. It maintains a temperature above the boiling point of CO_2 and below the freezing point of water thus allowing CO_2 to pass while freezing any water in the sample gas. A path to the H_2O trap is isolated on the extraction line and the sample gas is allowed to enter. A path is then opened to a CO_2 trap. The CO_2 trap is achieved by immersing a glass tube coil in liquid nitrogen. The CO_2 in the sample gas is allowed to condense. The extraction line is then opened to the vacuum pump. This will remove any nonvolatile gases in the sample. The condensed sample in the CO_2 trap is isolated with a small finger reservoir beneath a Baratron meter. The sample is transferred to the collection finger by immersing the finger in liquid nitrogen and slowly heating the glass coil which traps the CO_2. The condensed sample is isolated beneath the Baratron meter and the CO_2 is allowed to sublime. The Baratron registers a pressure which can be used to calculate the size of the gas sample in micro moles. A path from the small collection finger is opened to a six millimeter collection tube. The gas is condensed in the six millimeter collection tube by immersing the tube in liquid nitrogen. The collection tube is sealed at the top by heating with a torch and removed.

Analysis of CO_2 Gas With the Mass Spectrometer

Carbon and oxygen isotope analyses were performed on a Finnegan 252 Mass Spectrometer. The mass spectrometer consists of three essential parts: a source of a positively charged mono-energetic beam of ions, a magnetic analyzer, and an ion collector. All three parts of the mass spectrometer are evacuated to pressures of the order of 10^{-6} to 10^{-9}

mm Hg. During analysis of a CO_2 gas sample, the sample gas is allowed to leak into the source through a small orifice while the system is being pumped. The molecules are then ionized by bombardment with electrons. The resulting positively charged ions are accelerated by a high voltage field and are collimated into a beam by means of suitably spaced slit plates. The ion beam enters a magnetic field generated by an electromagnet whose pole pieces are carefully shaped and positioned in such a way that the magnetic field lines are perpendicular to the direction of travel of the ions. The magnetic field deflects the ions into circular paths whose radii are proportional to the masses of the isotopes, that is, the heavier ions are deflected less than the lighter ones. The pole pieces of the magnet are shaped so that the ion beams converge as they leave the magnetic fields. The separated ion beams continue through the analyzer tube to the collector, where an image of the source slit is formed by the ion optic effect to the magnetic field.

The ion collector consists of a metallic cup positioned behind a slit plate. The accelerating voltage in the source and the magnetic field are adjusted in such a way that one of the resolved ion beams is focused through the collector slit and enters the detector cup while the other ion beams collide with the grounded slit plate, or metallic walls of the flight tube, and are neutralized. The beam that enters the collector cup is neutralized by the electrons that flow from ground to the collector through a resistor. The voltage difference generated across the terminals of this resistor is amplified and measured with a voltmeter. A mass analysis of several isotopes is obtained by varying either the magnetic field or the acceleration voltage in such a way that the separated ion beams are focused into the collector in succession. The resulting signal forms the mass spectrum of the element (Faure, 1986).

The reproducibility of the carbon and oxygen isotope analyses of foraminifers was determined by analyzing different samples of foraminifers picked from the same sediment. When two foraminifer samples were analyzed from a sediment the reproducibility

is reported as the absolute difference between the two values. When three foraminifer samples were analyzed from a sediment the reproducibility is reported as the standard deviation of the values about the mean value.

Total Carbon and Inorganic Carbon Analysis

Total carbon and inorganic carbon content of sediment samples were determined through coulometric titration of evolved carbon dioxide gas as described below.

Coulometer -Principles of Operation

The coulometer cell is filled with a partially aqueous proprietary solution containing monoethanolamine and a calorimetric indicator. A platinum cathode and a silver anode are positioned in the cell and the assembly is positioned between a light source and a photodetector in the coulometer.

When a gas stream passes through the solution, CO_2 is quantitatively absorbed, reacting with monoethanolamine to form a titratable acid (hydroxyethylcarbamic acid). This acid causes the color indicator to fade. Photodetection monitors the change in the solution's color as percent transmittance (%T). As the %T increases, the titration current is automatically activated to stoichiometrically generate base at a rate proportional to %T. When the solution returns to its original color (original %T), the current stops. The titration current is continually measured and integrated to display milligrams of carbon (C) (Huffman, 1977).

Total Carbon

Dried sediments are ground to a fine powder. A sample of the powder is combusted in oxygen at 975 °C to convert organic and inorganic forms of carbon to CO_2. The sample combustion gases are swept through a barium/chromate scrubber to ensure com-

plete oxidation of carbon to CO_2. Non-carbon combustion products are removed from the gas stream by a series of chemical scrubbers. The CO_2 is then measured with the CO_2 Coulometer as described above.

Inorganic Carbon

A powdered sediment sample is placed in a test tube resting in a heating element. The sample is immersed in 5% perchloric acid. Any gas released is passed through a silver nitrate scrubber and the CO_2 is then measured with the CO_2 Coulometer as described above.

Total Sulfur Analysis

Sediments are ground to a fine powder. A sample of the powder is weighed in to a ceramic boat and covered with vanadium pentoxide (V_2O_5). The sample is introduced into a 1050 °C combustion furnace, and oxygen is introduced into a nitrogen carrier gas. the combustion products are passed over a combustion catalyst to ensure complete decomposition, and are also passed over copper to quantitatively convert all sulfur to SO_2. The SO_2 is swept into the coulometer cell, where it is quantitatively absorbed and coulometrically titrated.

The coulometer cell is filled with a solution which initially contains a slight excess of free iodine. When SO_2 enters the cell, iodine is consumed. The amperometric-sensing circuit detects the deficiency of iodine in the solution and caused iodine to be electrically generated at a rate proportional to the sensed deficiency. When all of the SO_2 has been titrated, the iodine is restored to its initial concentration. The total current used to generate the iodine is integrated by the coulometer and digitally displayed in milligrams of S.

Calculations

$\delta^{18}O$ and $\delta^{13}C$

Permil values are calculated using the formula

$$\delta = \frac{R_{sample} - R_{standard}}{R_{standard}} \times 1000$$

where R is the particular isotopic ratio (exp. $^{18}O/^{16}O$ for oxygen). All δ values are reported relative to PDB (Craig, 1957).

Mean

The mean (average) value of a series of data is calculated by the equation

$$\text{average} = \frac{\sum_{i=1}^{n} X_i}{n}$$

where X_i is the *i*th data point of data set, X, and n is the number of data points.

Median

The median is the value midway in the frequency distribution.

Standard Deviation

The standard deviation of a series of data is calculated by the equation

$$\text{standard deviation} = \sqrt{\frac{\sum_{i=1}^{n} X_i^2 - n\overline{X^2}}{n-1}}$$

where X_i is the *i*th data point of data set, X, and n is the number of data points.

Comparison of Averages

The average values of different data sets are compared using the Student t-test. The t score is determined using the following formula:

$$t = \frac{\overline{x_1} - \overline{x_2}}{\sqrt{\frac{(n_1 - 1)s_1^2 + (n_2 - 1)s_2^2}{n_1 + n_2 - 2}\left(\frac{1}{n_1} + \frac{1}{n_2}\right)}}$$

where x(bar) is the average value of a data set, n is the number of samples in a set, and s is the standard deviation of the data set.

A confidence level, α, is chosen. The degrees of freedom, ν, equals the sum of the samples in both sets minus 2. The values of t, α, and ν are compared to a t-statistics table (e.g., Table 2.11 in Davis, 1986).

R-mode Factor Analysis

R-mode analysis was applied to the surface sediment foraminifera population data. R-mode analysis is concerned with interrelations between variables, the variables here being the different foraminiferal species.

The foraminifera census data table matrix [X] with m variables (species) and n samples is converted to a square m × m covariance matrix

[R]=[X]'×[X]

Eigenvalues and eigenvectors are extracted from the matrix [R]. The eigenvectors are scaled by the square roots of their corresponding eigenvalues. The resulting vectors are factors with their individual elements being loadings which relate the factor to the individual variables. Multiplying the original data matrix by the scaled factor vectors produces R-mode scores which represent the influence of each factor on the individual samples (Davis, 1986).

Dry Bulk Density

To determine the dry bulk density, the sediment of a 20 cm^3 sample plug was dried and weighed. The weight was divided by the volume of the sediment. The original volume of the sediment was determined by measuring the length of sediment in the plug sample and multiplying the length by the area of the plug end.

Organic Carbon Flux

$$\text{Organic carbon accumulation} = \frac{[(Wt.\%C_{org})\rho S]}{100(C_{atomic\,wt.})}$$

where ρ = dry bulk density, S = bulk sedimentation rate. The units are Moles / Area / Time (mol cm^{-2} yr^{-1}) (Glenn and Arthur, 1984).

Porosity

The porosity equals the weight of water in a sample (determined by weighing the sediment before and after drying) divided by 1.027 (the approximate density of sea water) divided by the total volume of the sample.

Sand Fraction of Sediment

The sand fraction of a sediment sample is determined by dividing the bulk weight of the dried sediment sample into the dry weight of the sample after the sediment has been sieved through a 63 μm screen.

Chapter 3
Surface Sediment Analysis

Results

A total of 50 surface sediment samples collected during the R/V Seward Johnson cruisewere analyzed on the Peru/Chile Margin. No sediment from the top 1 cm of the ODP holes was available. Figures 3.1, and 3.2 show the collection site for each sample.

Various data of the present environmental conditions of the sediments were collected during the R/V Seward Johnson cruise. The data include dissolved oxygen levels, temperatures, salinities of overlying water bodies, water depths of sample sites, and strength of bottom water current velocities. These data for each sample location are summarized in Table 3.1.

Benthic Foraminifer Populations

The results of benthic foraminifer population counts of the surface sediments are summarized in Table 3.2. Assemblages in these sediments contain benthic foraminifer species typical in the region (Resig, 1981,1990). Dominant species include *Bolivina humilis, Pseudoparrella subperuviana, Bolivina plicata, Uvigerina* spp. and *Angulogerina carinata.* Population density is highly variable with ranges from less than 10 to more than 12,000 specimens per gram dry sediment.

Organic Carbon

Organic-carbon and carbonate total weight percentages are summarized in Table 3.3. Organic-carbon weight percentages are variable, but generally extremely high. Values range from less than 1% to more than 17%.

Reproduced organic-carbon analyses for sediments are summarized in Table 3.4. The

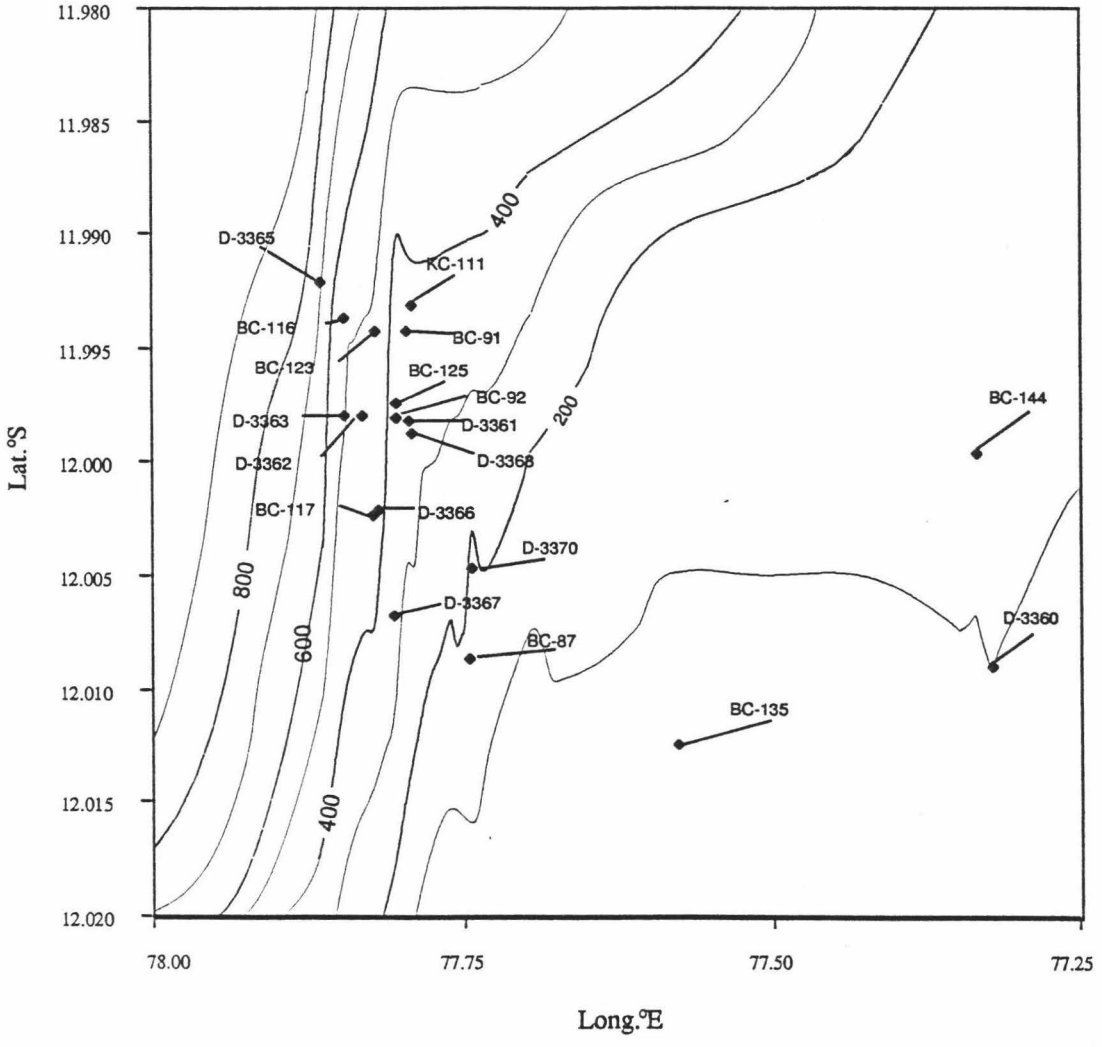

Figure 3.1. Location of surface sediment samples taken along the 12°S transect. Contours are sea floor bathymetry in meters.

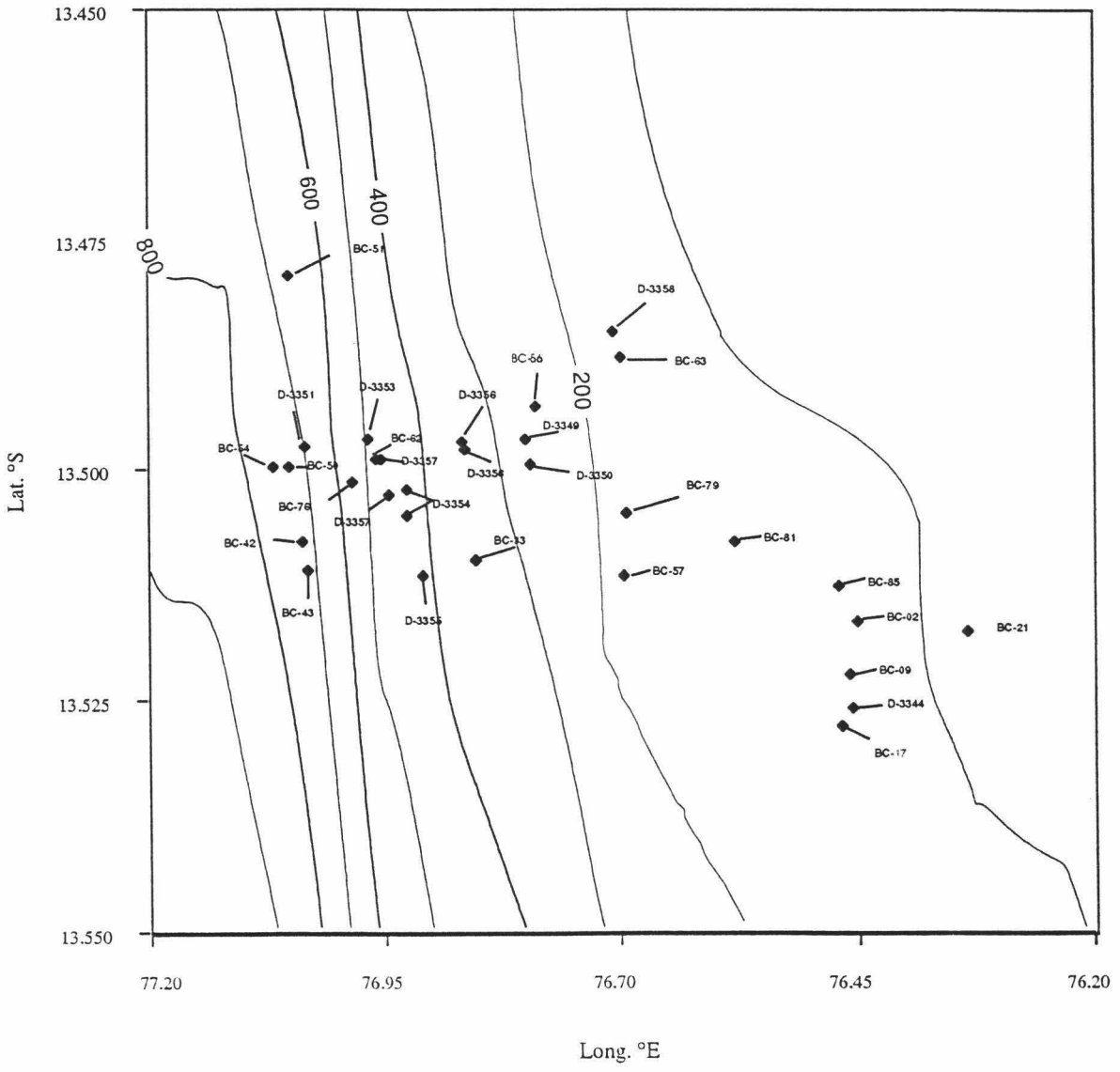

Figure 3.2. Location of surface sediment samples taken along the 13.5°S transect. Contours are sea floor bathymetry in meters.

maximum standard deviation was slightly over 1.00% while most of the standard deviations are well below 0.20%.

$\delta^{13}C$ Analysis

Carbon isotope analysis was concentrated on the species *Bolivina humilis*. This is the same species used to generate the carbon and oxygen isotope curves for Holes 679B and 680B (discussed in Chapter 4). In a number of samples, *B. humilis* was not available. When unavailable, *Bolivina plicata, Uvigerina peregrina* and *Uvigerina striata* were taken. Results of the carbon isotope analysis for the surface sediments are summarized in Table 3.5. Duplicate analyses were run on *B. humilis* specimens in two core samples. Two benthic foraminifer samples were analyzed from sediment sample D-3362 and three benthic foraminifer samples were analyzed from sediment sample BC-116 (Table 3.6). The $\delta^{13}C$ values for the two analyses from sediment sample D-3362 differed by 0.006 ‰. The $\delta^{13}C$ values for the three analyses from sediment sample BC-116 had a standard deviation of 0.075‰. This means that 64% of samples analyzed for $\delta^{13}C$ from this sediment should be within ± 0.075‰, 96% should be within ± 0.149‰, and 99% should be within ±0.224‰. A standard sample of NBS-19, analyzed with the foraminifer samples produced values within 0.009‰ of the expected $\delta^{13}C$ value and 0.043‰ of the expected $\delta^{18}O$ value.

Physical Properties

I determined porosity, dry bulk density, and the silt/sand fraction of the surface sediments. These data are summarized in Table 3.3.

Sedimentary Facies

Sedimentary facies are based on descriptions of box cores and on visual observations made during submersible operations during the R/V Seward Johnson cruise. At 12°S,

between 100 and 200 m depth, the sea-floor sediment is dominated by mud with blankets of *Thioploca* spp. bacterial mats. Below 200 m, the seafloor is almost entirely covered with gravely phosphorites, phosphorite hardgrounds or pelletal sands with the exception of a mud lens located at approximately 300 m (Fig. 3.3). At 13.5° S, muds dominate the outer shelf to a depth of approximately 150 m. Seaward of the mud facies, to a depth of 550m, the slope is dominated by phosphatic crusts, nodules and pavements. Another mud facies is located at 600-650m. Deeper, between 800 and 1100m the sea floor sediment is composed of coarse glauconitic sands (Fig 3.4) (Glenn et al., 1994).

Ages of Modern Sea-floor Phosphorite Samples

Absolute age data from phosphorite hardgrounds taken from the ocean floor during the R/V S. Johnson cruise have been provided by Dr. William Burnett at The Florida State University (Table 3.7). Absolute ages are determined through uranium-series dating (Burnett and Veeh, 1977).

Interpretations and Discussion

Organic Carbon Content—Controlling Factors

The amount of organic carbon preserved in sediments along the Peru coast is very high with average values from 3% to 7% and extreme values exceeding 15%. At present, a number of factors have been proposed that control burial and preservation: bulk sedimentation rate (Heath et al., 1977; Müller & Suess, 1979), water column oxygen (Demaison & Moore, 1980), water depth (Seuss 1980), benthic regeneration (Reimers & Suess, 1983b), and ecology (Walsh, 1981). Here, I examine the organic-carbon weight percentage of the surface sediments with respect to other data I have collected. I compare organic-carbon weight percentages to several factors: surface productivity, sea floor

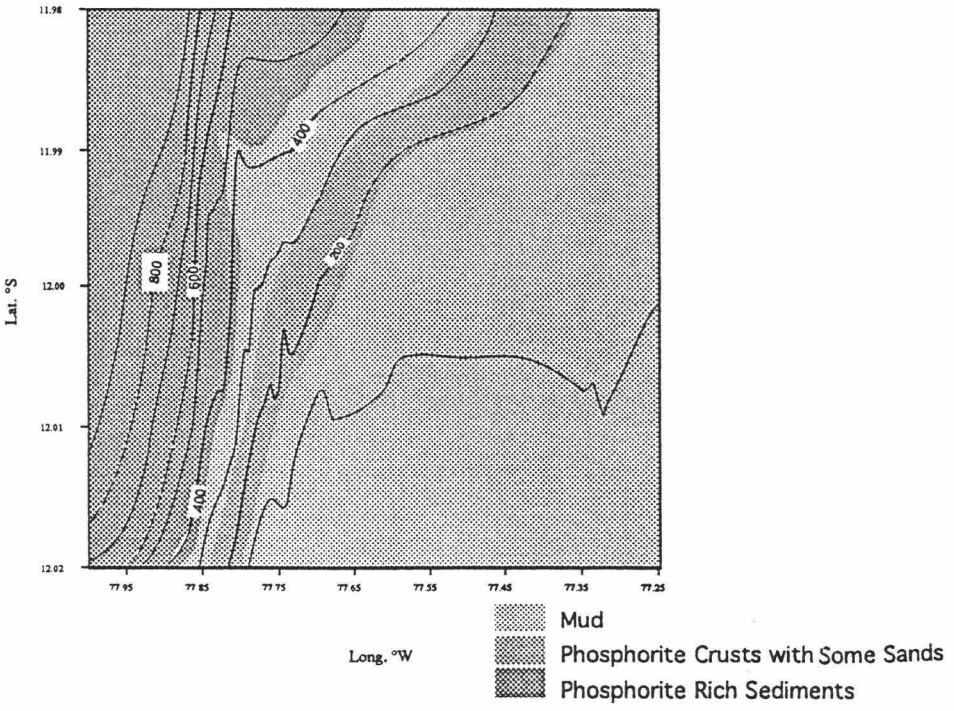

Figure 3.3. Distribution of sediment facies along 12°S transect.

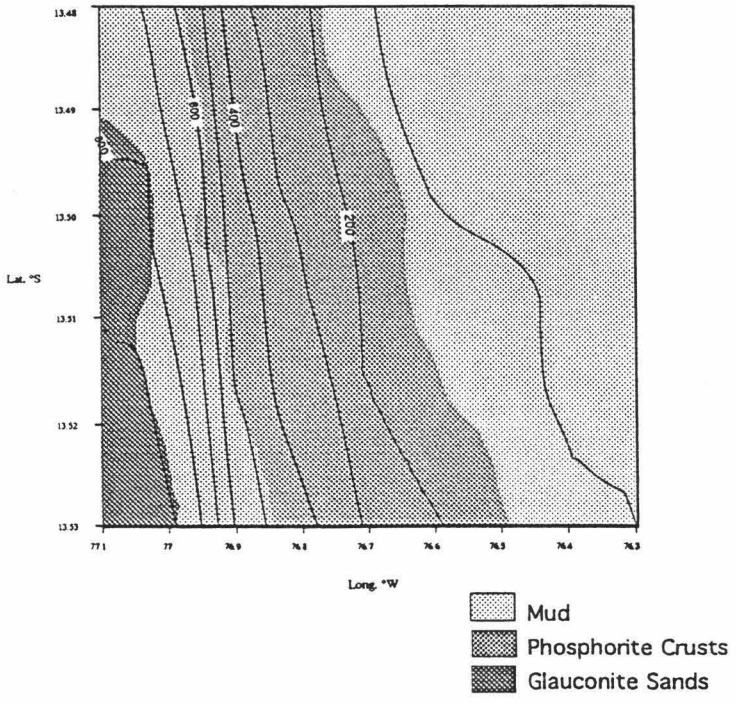

Figure 3.4. Distribution of sediment facies along 13.5°S transect.

sedimentary facies, dissolved oxygen content of bottom waters, porosity of the sediments, and bottom current velocity. The goal of the comparisons is to determine if the organic-carbon content in ancient sediments can reveal information about the state of these factors in the past.

Surface Productivity

Figure 3.5 shows the current zones of productivity on the Peru/Chile margin. The various productivity regions were determined by Zuta and Guillén (1970) and are based on 4,413 observations (2,823 corresponding to hydrographic stations) made during 41 cruises conducted from 1961 to 1968. Surface primary productivity measurements were made by determining the rate of fixation of radio carbon ^{14}C by phytoplankton following the method of Steeman Nielsem (1952). Samples were collected in van-Dorn bottles at depths corresponding to 100, 28, 10, and 2.8% of the intensity of surface light. ^{14}C was added to each sample and the sample was incubated at the same temperature as surface sea water and in natural sun light for approximately six hours. The average of the production values is used as the basis for defining the different regions. The location of the upwelling cells do persist from year to year. However, environmental changes in the area such as the nutrient content of the surface water, the amount of solar radiation, or the water temperature have a significant effect on primary production in the surface waters. These changes appear to be on a seasonal time scale with higher productivity occuring during the summer season and lower productivity occuring during the winter season. The averaging of the data collected during the eight years of study has likely greatly diminished any seasonal variation signals and possibly reflect well the time scale represented by the sediment samples used in this study. The contoured primary production values in Fig. 3.5 probably give a good indication of regions with significantly different surface productivities.

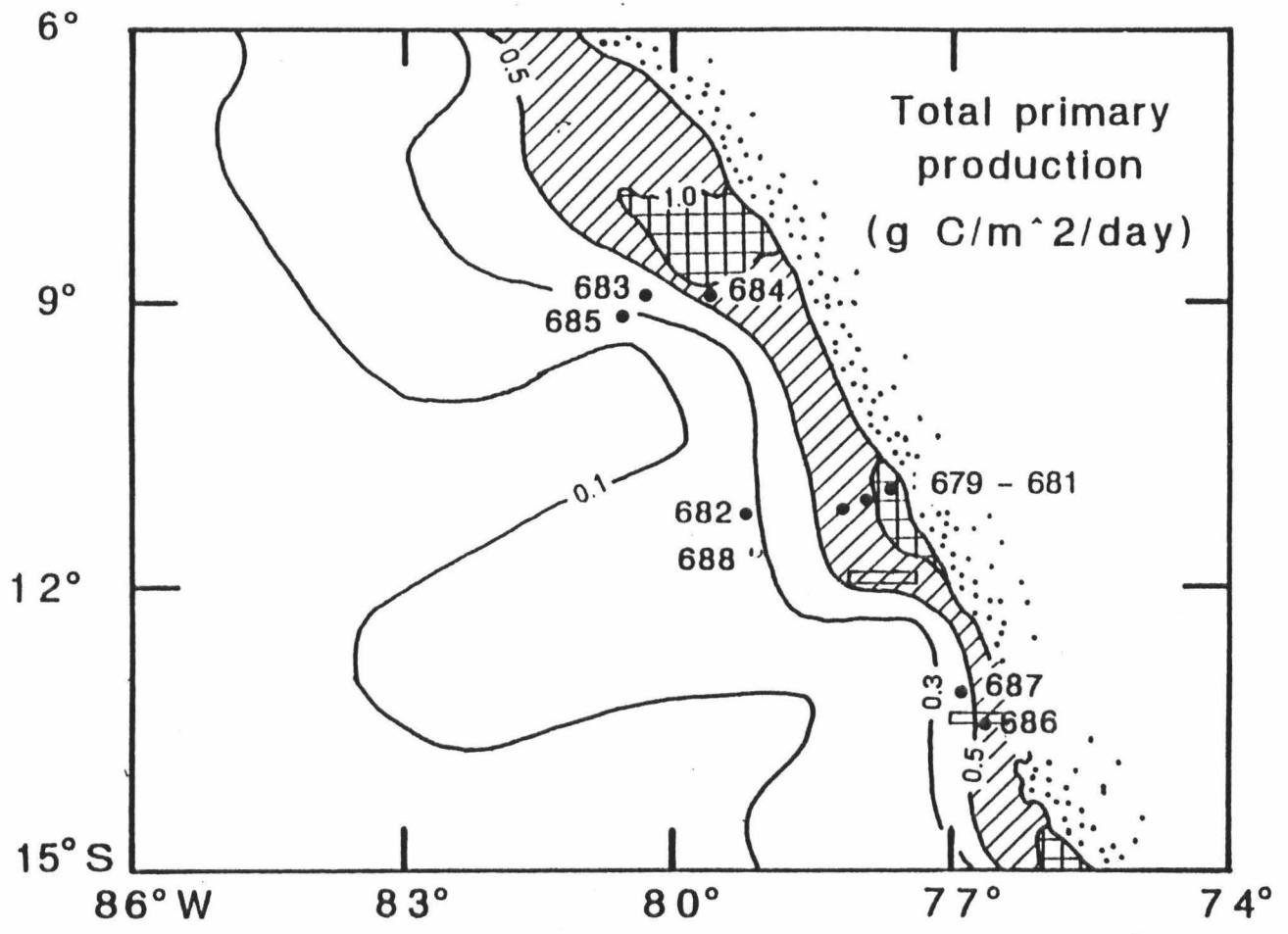

Figure 3.5. Distribution of ten-year average surface primary production along the Peru Margin (Zuta and Guillén, 1970); figure modified from Reimers and Suess (1983a).

The distribution of surface sediment samples and their organic-carbon contents are compared to the overlying surface water productivities (Figs. 3.6, and 3.7). Samples collected along the 12° S transect were beneath an area with total primary production in the range of 0.5 to 1.0 gC/m²/day with the western limit of the transect being very close to a lower productivity region of 0.3 to 0.5 g C/m²/day. Samples collected along the 13.5° S transect covered areas with a wider range of productivities; to the west of longitude 76.75° W productivity ranges from 0.3 to 0.5 g C/m²/day and to the east productivity ranges from 0.5 to 1.0 g C/m²/day. Organic-carbon contents are contoured in Figures 3.6, and 3.7. The highest organic carbon content values among the surface sediment samples do occur under the areas of highest production. Sediments under areas with total primary production of 0.3 to 0.5 g C/m²/day have an average organic-carbon content of 3.6% and a standard deviation of 2.1%. Under the higher production areas (0.5 to 1.0 g C/m²/day) the average organic-carbon content along 13.5° S is 7.8% and standard deviation 3.7%, and along 12° S the average is 6.7% and standard deviation is 5.4%. Along 12° S, the average is lower and the standard deviation is higher, probably, due to the proximity of a lower productivity region to the west; note the western end of the transect shows consistent low percentages of organic carbon. The pattern of organic-carbon contents is consistent with the patterns of surface productivity and indicates that the organic-carbon content of these sediments may be a semi-quantitative indicator of productivity.

Sedimentary Facies

The organic-carbon content of surface sediments is contoured and plotted in Figures 3.8, and 3.9 for 12° S and 13.5° S, respectiviely. At 12° S, the highest organic-carbon contents (<10%) are found at a depth of 300-400 m and correspond to a mud belt. Landward of this area, values remain relatively high (5-10%). Seaward of the mud belt, organic-carbon contents fall sharply (0-5%). The organic-carbon content of these sedi-

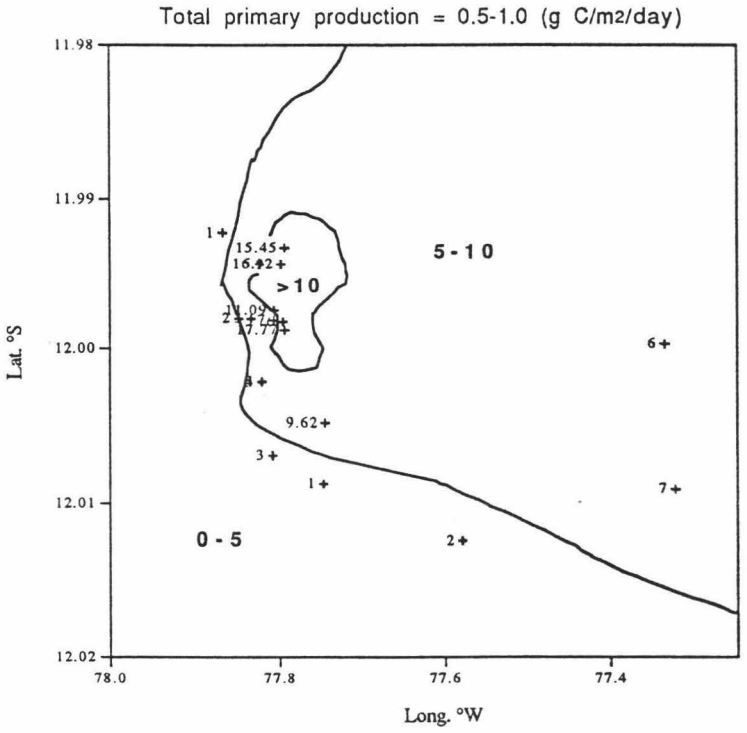

Figure 3.6. Contoured organic carbon weight percents of surface sediments along 12°S transect.

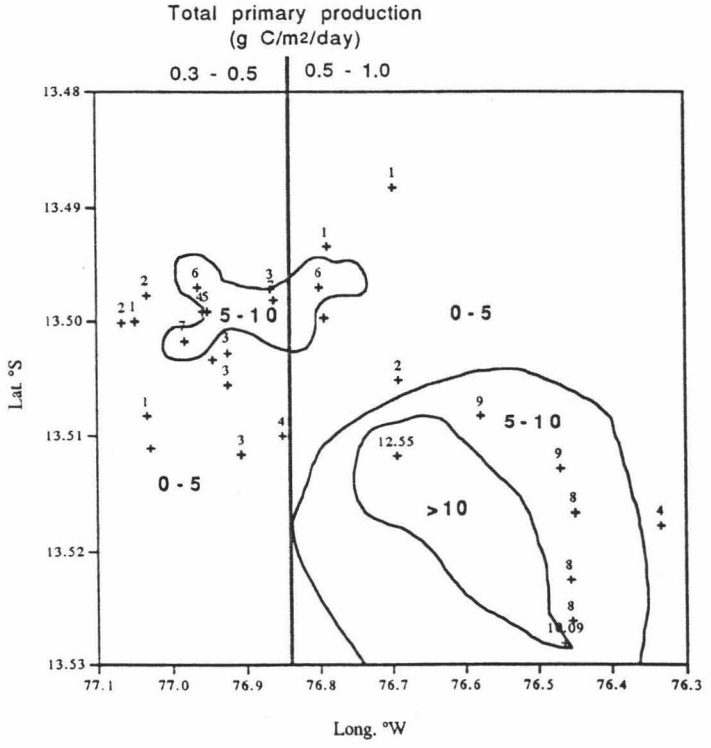

Figure 3.7. Contoured organic carbon weight percents of surface sediments along 13.5°S transect.

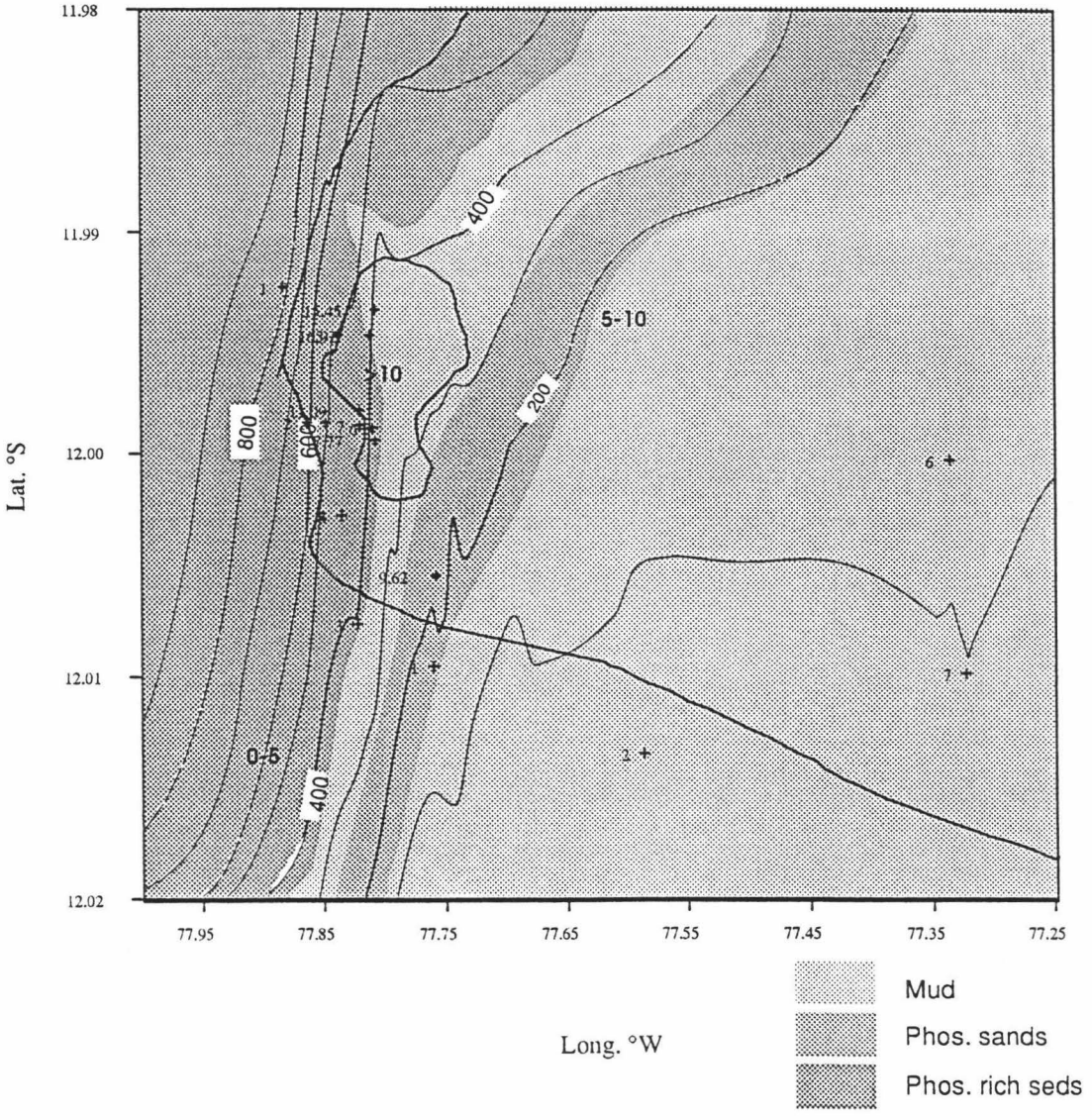

Figure 3.8. Contoured organic carbon weight percents plotted over sedimentary facies—12°S transect.

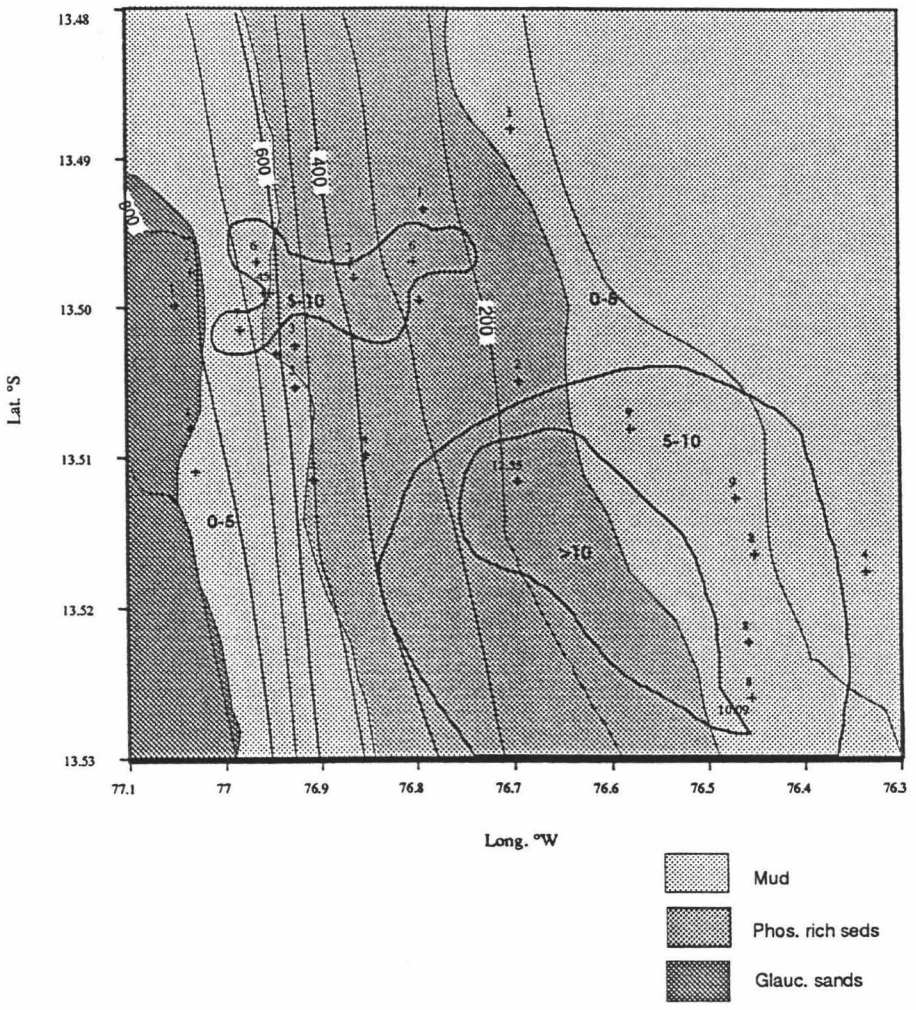

Figure 3.9. Contoured organic carbon weight percents plotted over sedimentary facies—13.5°S transect.

ments does seem to show a correlation with sediment type, although relatively low and high values are found in all sediments. At 13.5° S, in general, high organic-carbon contents (>5%) are found in both the mud facies and the phosphorite rich facies. The shallow mud facies does show relatively high values (8-10%) with two exceptions (1% and 4%). Glauconitic sands consistently contain very low organic-carbon contents (<3%).

My data reveal a rough relation between mud facies and relatively high organic-carbon content. Dilution may explain the pattern of organic-carbon content with the different sediment facies. Growth of phosphatic material will displace organic matter in the sediment. This displacement will tend to dilute the organic matter and reduce its percentage of the sediment regardless of any real organic-carbon flux changes.

Bottom-Water Dissolved Oxygen

Figures 3.10, and 3.11 shows the distribution of dissolved oxygen levels in bottom water along both the 12° S and 13.5° S transects. Figure 3.12 plots percent organic-carbon content of surface sediment samples versus dissolved-oxygen content of the overlying bottom water. In these sediments, samples with higher oxygen levels (> 10μMol) have consistently low organic carbon contents (<2.5%). While the organic-carbon content of sediments with low oxygen levels are highly variable (3% to 17%) they remain higher than the maximum value of sediments with oxygen levels above 10 μMol. These data indicate that oxygen levels and organic-carbon content are related but the relation is unclear. Much variability in sediments with low oxygen content indicate other controlling factors are involved.

The most direct explanation for the high organic carbon contents in low oxygen bottom waters is simply that a higher organic-carbon flux will consume more oxygen in the water column. Beyond this basic interaction, however, the relationship of dissolved

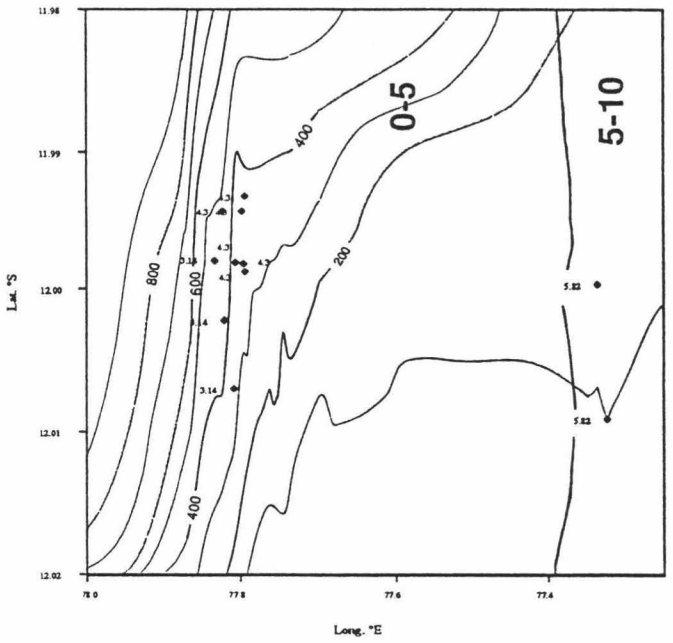

Figure 3.10. Contoured bottom water dissolved oxygen concentrations (µMol)—12°S.

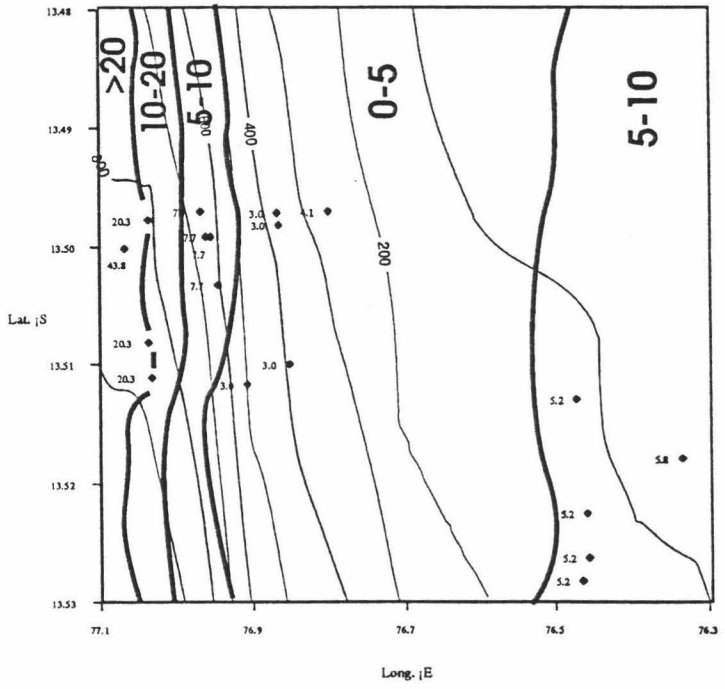

Figure 3.11. Contoured bottom water dissolved oxygen concentrations (µMol)—13.5°S.

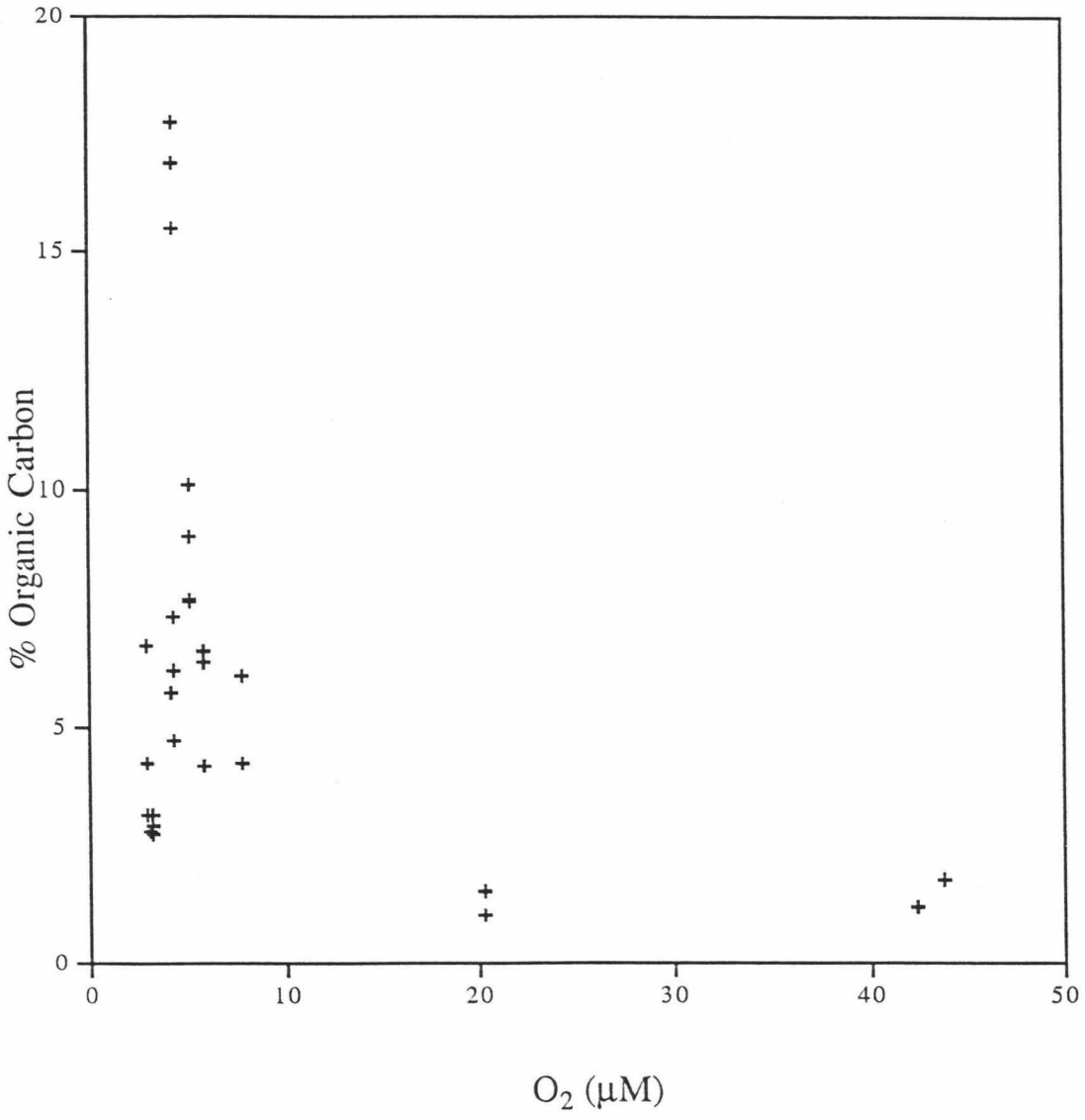

Figure 3.12. Organic carbon weight percent of surface sediments versus dissolved bottom water oxygen content (where available).

oxygen to organic-carbon preservation seems to be complicated or, perhaps, may not exist. As an example, Calvert et al. (1992) found no evidence for enhanced preservation of sedimentary organic matter in the oxygen minimum zone of the Gulf of California. With respect to how oxygen may control the preservation of organic carbon in sediment, consider that degradation of organic matter in seafloor sediments is influenced by bacterial and metazoan activity. With regard to bacterial degradation, research has shown that rates are nearly the same in oxic or anoxic environments (Lee, 1992). With regard to metazoans, the oxygen content of the bottom water does determine their activity, and decreased activity by metazoans will result in less organic matter degradation (Demaison et al., 1980). Researchers have noted that laminated muds reflect deposition beneath oxygen-poor waters that prevented colonization of the seafloor by a burrowing infauna. At the opposite extreme, burrowed, massive sediments indicate higher oxygen levels (Savdra and Bottjer, 1986). The modern sediments off Peru are dominantly unlaminated (Arthur et al., 1993). The restriction of burrowing infauna likely plays a role in organic-carbon preservation in sediments deposited in more anoxic environments.

The data in Figure 3.12 do have two gaps with respect to oxygen: between approximately 10-20μMol, and between 20-40μMol. Values predicted from the latter section very likely are similar to the values at 20μMol and 44μMol. Values in the former section, however, cannot be so easily predicted. I cannot tell where the organic-carbon contents reach a minimum. This leaves uncertainty about the oxygen levels for organic-carbon contents greater than 2.5-3.0%. I can tentatively conclude from these data that the dissolved oxygen content is related to the organic carbon content, and that sediments with organic-carbon contents greater than 2.5-3.0% were deposited in waters with less than 10μMol dissolved oxygen. But, the organic-carbon content of sediments from this upwelling region are only useful as a rough indicator of bottom-water oxygen levels.

Porosity

Percent organic carbon versus porosity is plotted in Figure 3.13. A rough trend is seen in the data. Increased porosity corresponds in a general way ($r^2 = 0.325$) to higher contents of organic-carbon. The relation is counterintuitive. Higher porosities should increase the mobility of carbon consuming organisms in sediment and more organic carbon should be degraded. The data reveal the opposite effect. An explanation for the opposite effect can be developed by noticing that the highest porosity values are found in very mud-rich sediments. Mud-rich sediments do have high porosities but they generally have very low permeabilities (Tucker, 1991). Although the sediments are very porous there may be relatively little communication possible between pore spaces. I speculate that this lack of communication may possibly impede the movement of organic carbon consuming organisms and, thus, retard organic carbon degradation.

Particle Size

A strong correlation has been observed between increasing particle surface area and increasing residual organic-carbon content from soil and sediment measurements (Mayer, 1994). This organic matter is hypothesized to reside in small cracks and crevasses on the surface of particles which are inaccessible to relatively large bacterial enzymes. The mud-sized particles (mainly clays) of the Peru Margin sediments will have a relatively very high surface area and adsorption of organic matter onto the sediment particle surfaces may explain the higher organic-carbon contents of these sediments.

Current Velocity

Under the influence of bottom currents, organic-carbon contents of sediments may be reduced due to resuspension that reintroduces fine particulate organic matter into the benthic boundary layer thereby increasing its residence time and the efficiency of benthic

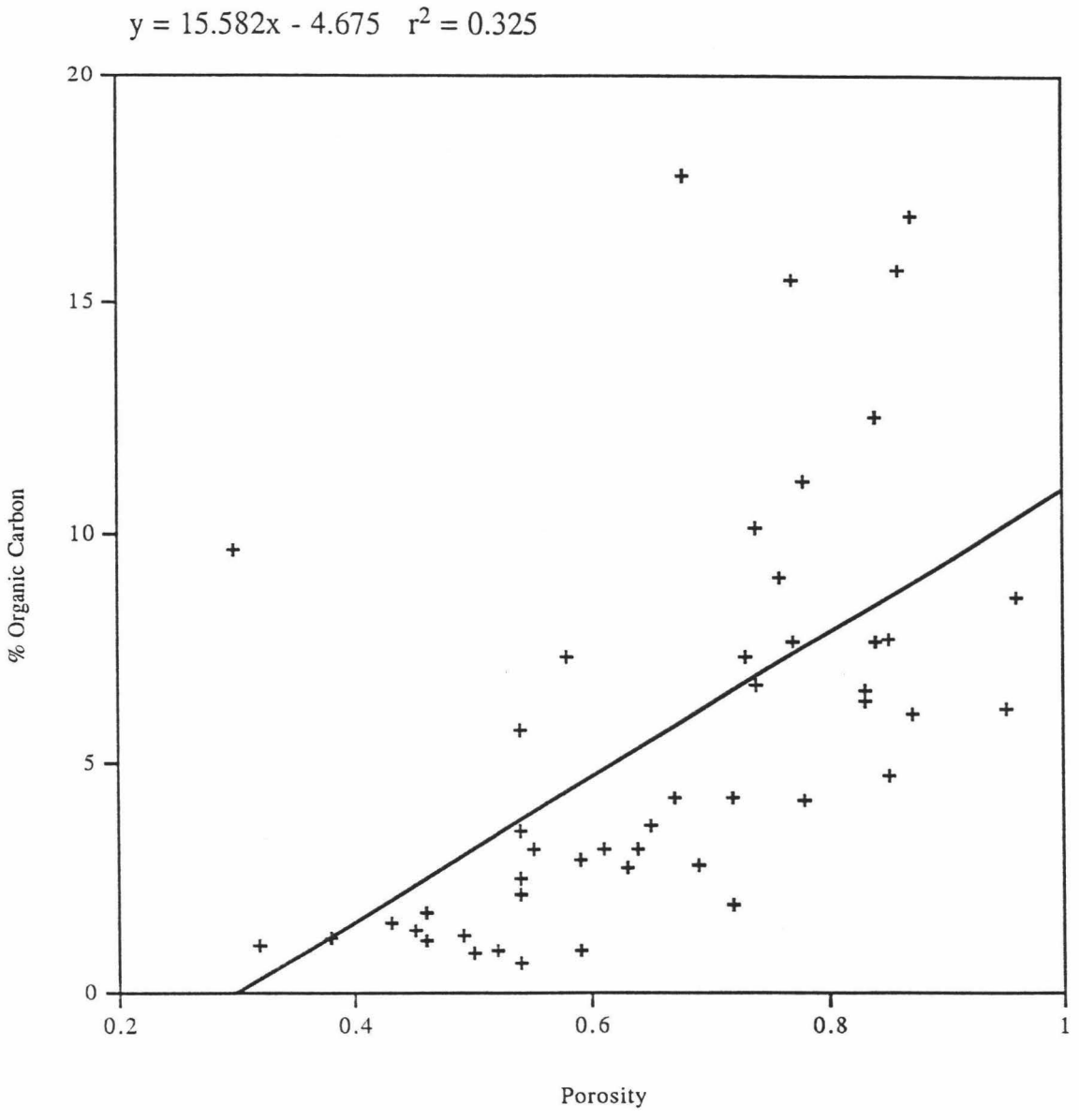

Figure 3.13. Organic carbon weight percent of surface sediments versus the porosity of the surface sediments. A linear regression through the points gives a correlation coefficient (r^2) of 0.325.

decomposition processes, or by causing material to be physically redistributed and winnowed (Reimers and Suess, 1983b). Bottom-water current velocities are plotted against organic-carbon percentages in Figure 3.14. The data reveal no strong correlation between current and organic-carbon content. Current vectors are plotted over a contoured map of organic-carbon distributions for 12° S and 13.5° S (Figs. 3.15, and 3.16). Again, the distributions do not indicate a relation between the strong bottom currents and areas of decreased organic-carbon content.

Light Stable Isotope Analysis of Benthic Foraminifera

Oxygen depletion in seawater is reflected by a proportional decrease in the $\delta^{13}C$ of dissolved inorganic carbon, the same carbon from which foraminifera manufacture their tests. Researchers have postulated that changes in the $\delta^{13}C$ composition of the tests of benthic foraminifer species may mirror the intensity of oxygen depletion (e.g., Vincent et al., 1981; Belanger et al., 1981). Therefore, changes in the $\delta^{13}C$ of benthic foraminifer tests may be a way to estimate the size and intensity of the oxygen minimum zone. Changes in the $\delta^{13}C$ of bottom seawater and seawater in sediment can also be the result of increased flux of marine organic material. Marine organic matter is isotopically light with respect to seawater. An increase in particulate organic-carbon (POC) flux will result in a higher percentage of organic carbon in the sediment and, thus, will decrease $\delta^{13}C$ values of the total dissolved carbon in the sediment and will increase the $\delta^{13}C$ gradient with depth in the sediment. If *B. humilis* precipitates its test in relation to the $\delta^{13}C$ gradient of CO_2 in sediment then a correlation should be present with respect to the sediment's organic-carbon content. Previous studies, however, have found evidence that both environmental (microhabitat) and vital effects determine the final $^{13}C/^{12}C$ ratio in foraminiferal tests (McCorkleet al., 1990). To date, no convincing evidence has been found that supports a correlation between the $\delta^{13}C$ of foraminifera tests and productivity or dis-

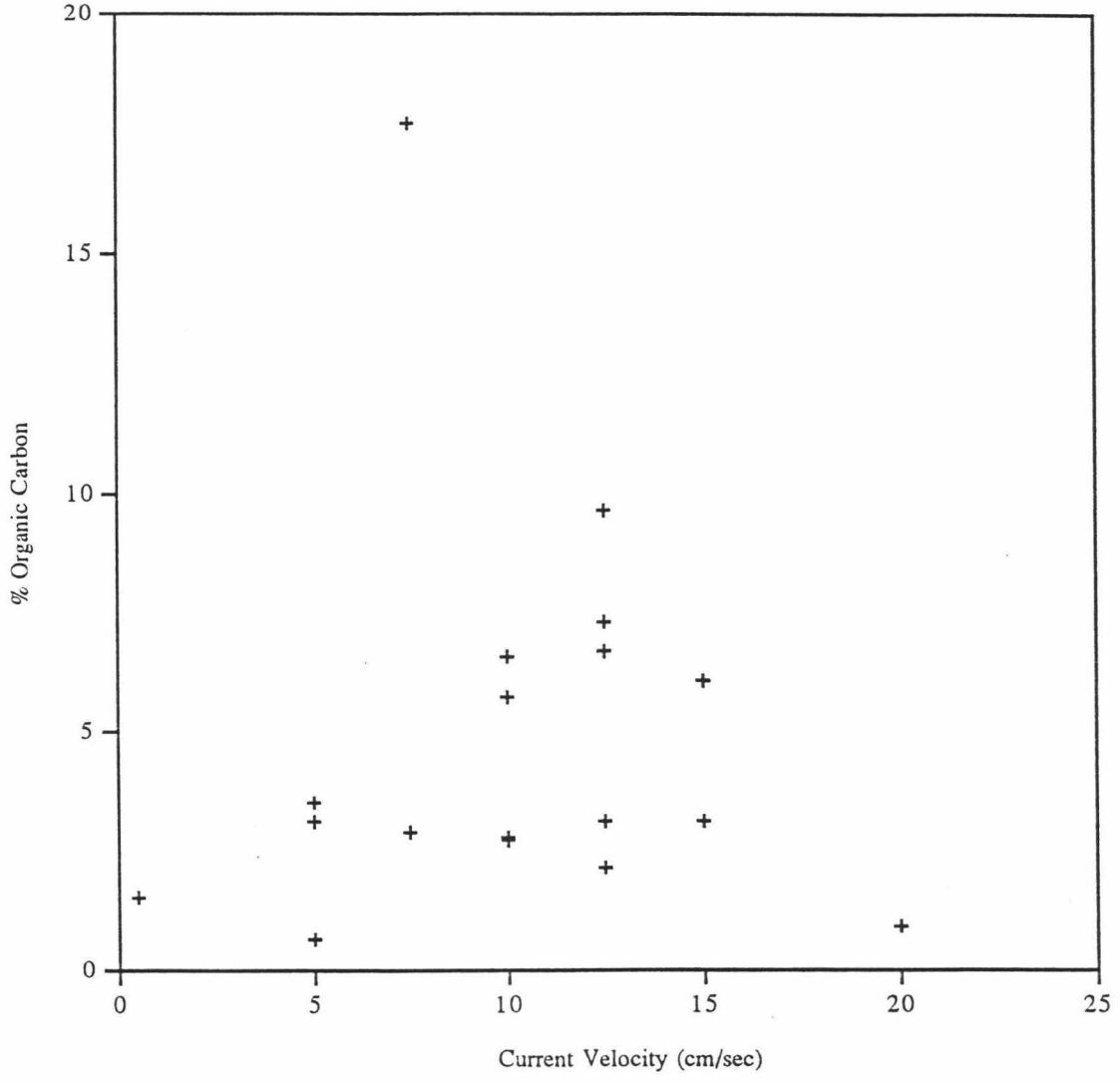

Figure 3.14. Organic carbon weight percent of surface sediments versus bottom water current velocity.

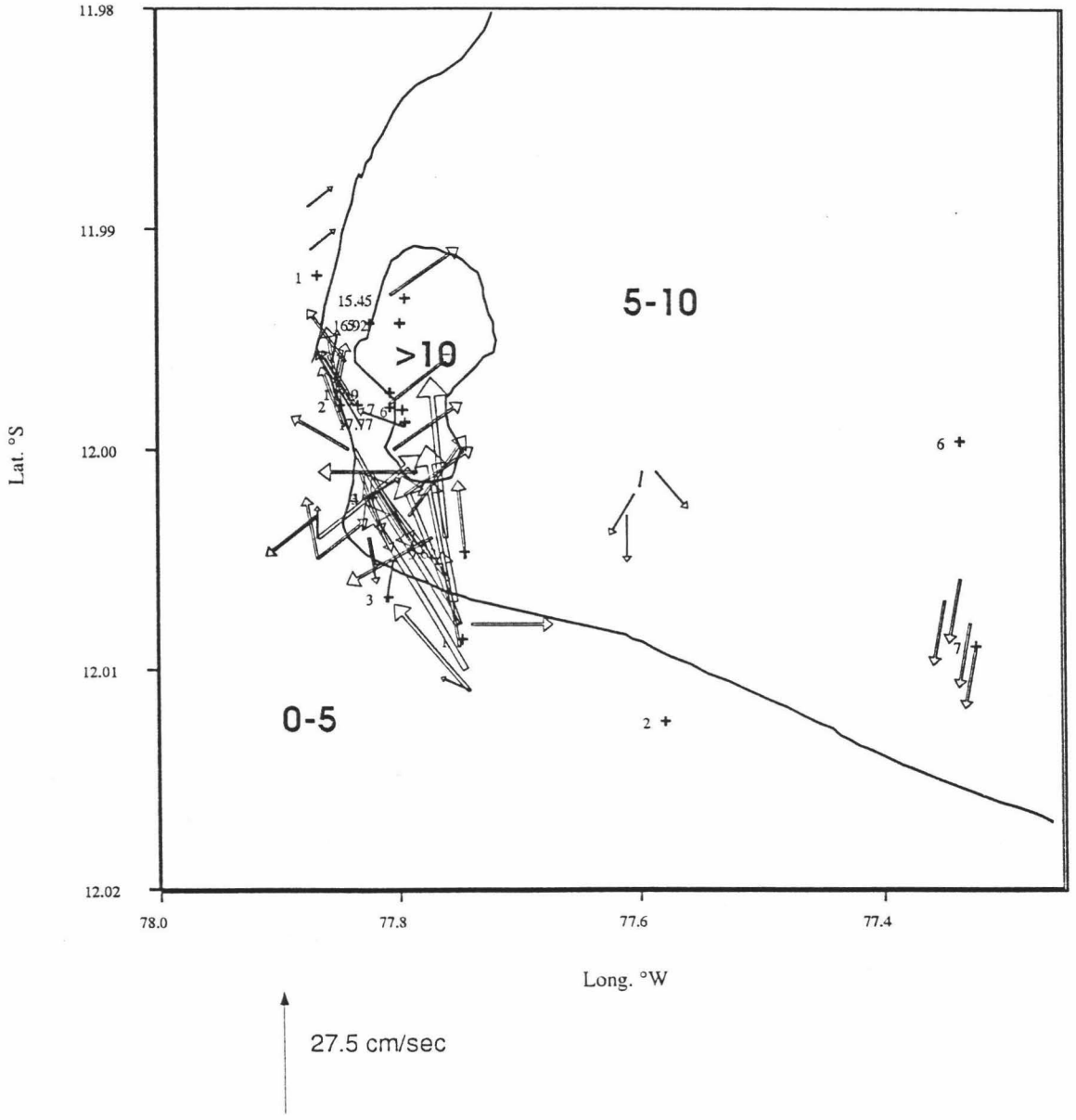

Figure 3.15. Contoured organic carbon weight percents with current velocity vectors—12°S.

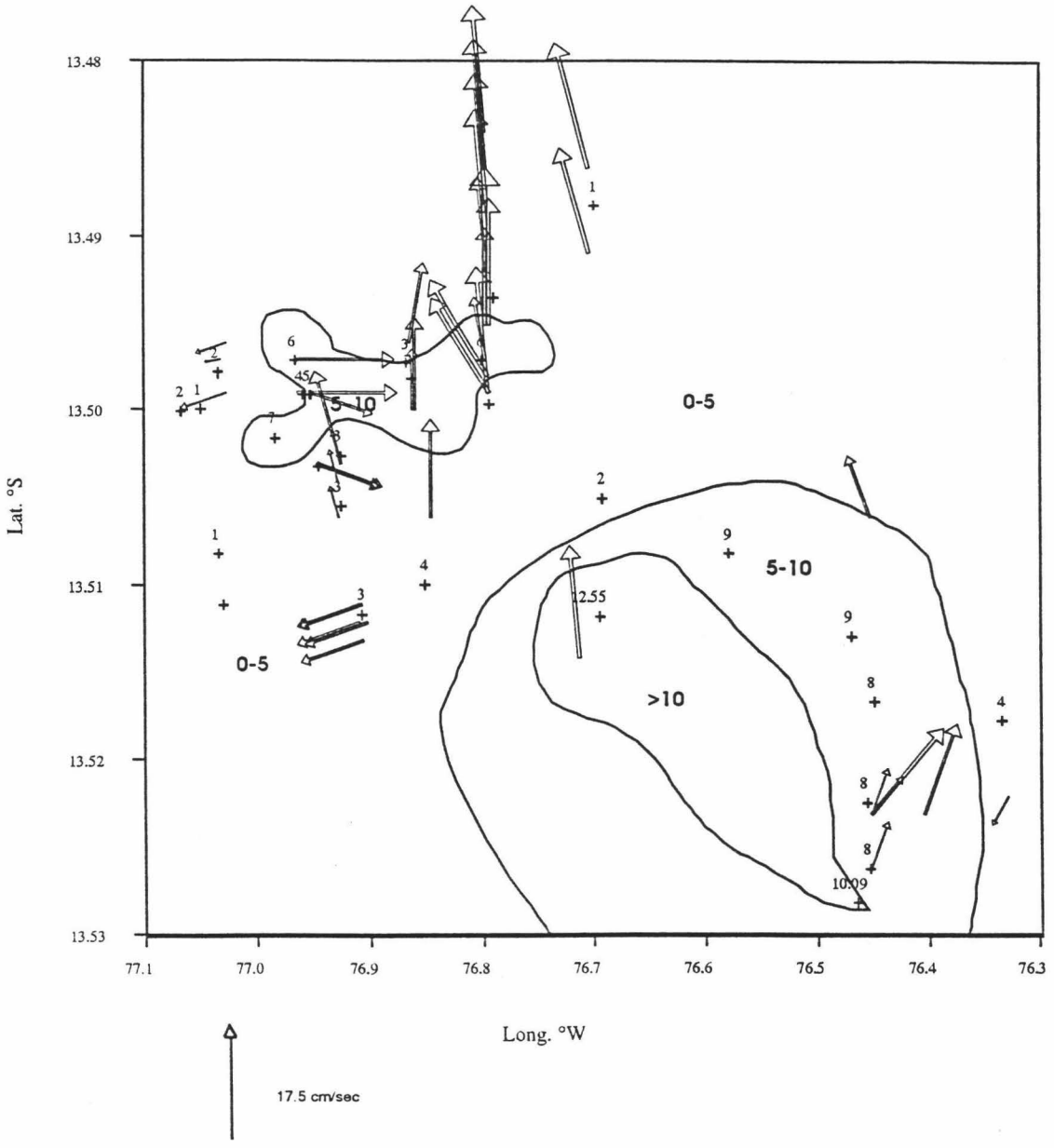

Figure 3.16. Contoured organic carbon weight percents with current velocity vectors—13.5°S.

solved oxygen (Schrader, 1992a; Wefer et al., 1983; Dunbar and Wefer, 1984; Grossman, 1984; Corliss, 1985; Zuhn et al., 1986). $\delta^{13}C$ and bottom-water oxygen levels are plotted in Figure 3.17. The pattern of the data is random. I can conclude from these data that no relation exists between $\delta^{13}C$ of the collected *B. humilis* and oxygen levels measured during the R/V Seward Johnson expedition.

A relatively high organic-carbon content in a sediment sample indicates that the sediment experienced a relatively high flux of particulate organic matter and was likely located beneath an area of relatively high surface productivity. As mentioned above, a higher flux of organic carbon should decrease the $\delta^{13}C$ values of dissolved HCO_3^- from which benthic foraminifera form their tests. I plot $\delta^{13}C$ vs. organic-carbon content in Figure 3.18. These data indicate no correlation. There are very significant variations of $\delta^{13}C$ over similar organic-carbon percents, e.g., at approximately 3% organic carbon the $\delta^{13}C$ values range from -0.5‰ to -3.3‰ vs. PDB. $\delta^{13}C$ values versus organic carbon are plotted for *B. plicata* and *Uvigerina* sp. in Figures 3.19, and 3.20. Again, no correlation is observed. I conclude that surface productivity, or at least organic-carbon content, does not strongly influence the $\delta^{13}C$ of benthic foraminifera.

Benthic Foraminiferal Assemblages

Factor Analysis

I performed an R-mode factor analysis on the percentage population counts of benthic foraminifera. The analysis revealed four principal factors. Together, the four factors account for 84% of the variance in the data set (Table 3.8). In the case of each factor, the species that represents the frequency distribution is designated nominal species for the associated assemblage. Together, the four factors explain nearly all the variance in the surface samples (Table 3.9). Characteristic information for individual factors is taken from samples with 50% or more of the variance explained by the factor.

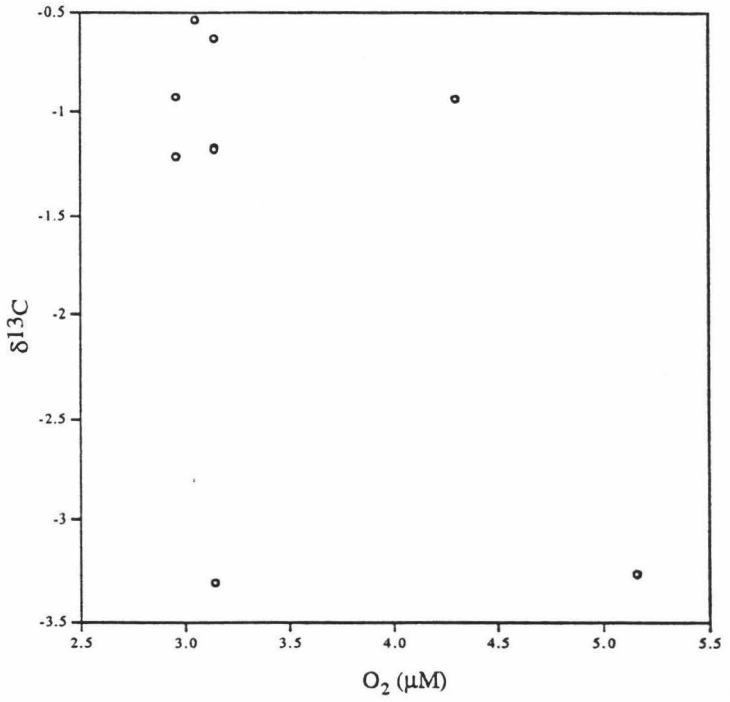

Figure 3.17. $\delta^{13}C$ of *B. humilis* from surface sediments versus dissolved oxygen content of overlying water collected in late October/early November, 1992.

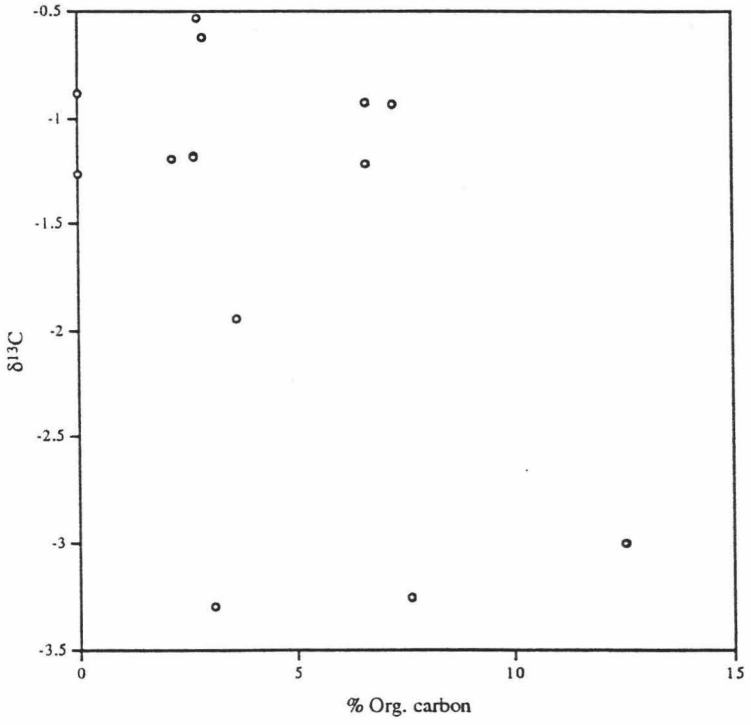

Figure 3.18. $\delta^{13}C$ of *B. humilis* from surface sediments versus organic carbon weight percent of the surface sediment collected in late October/early November, 1992.

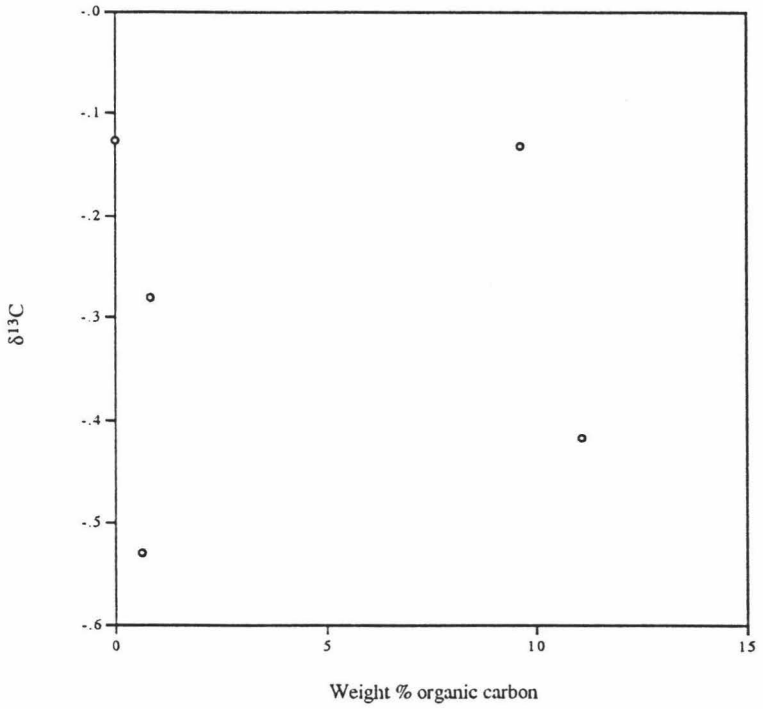

Figure 3.19. $\delta^{13}C$ of *B. plicata* from surface sediments versus organic carbon weight percent of the surface sediment.

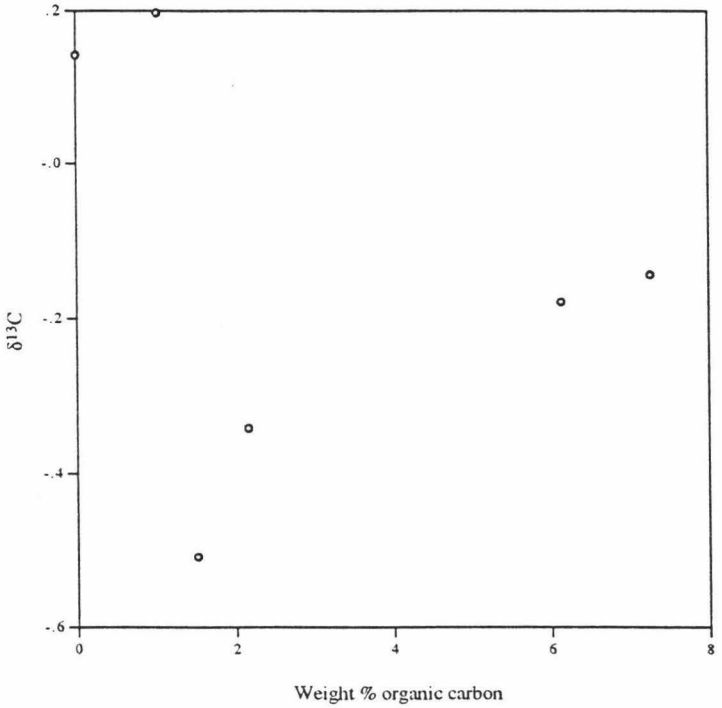

Figure 3.20 $\delta^{13}C$ of *Uvigerina* spp. from surface sediments versus organic carbon weight percent of the surface sediment.

Bolivina humilis assemblage (factor 1)

Depth range (m)= 172 to 595 ; Temp. (°C) = 5.6 to 12.8 (average = 10.11, median = 9.91) Salinity (‰) = 34.57 to 34.87 (average = 34.74, median = 34.72); O_2 (µMol) = 3.0 to 7.7 (average = 3.9, median = 3.1); Wt. % organic carbon = 0 to 17.8 (average = 5.0, median = 3.1). Key species: *Bolivina humilis*, % of population = 8 to 51 (average = 28, median = 30), f/g (foraminifers/gram dry sediment) = 2 to 2388 (average = 517, median = 61.9); *Bolivina plicata*, % of population = 5 to 65 (average = 29, median = 26), f/g = 4 to 1940 (average = 442.2, median = 67.9).

Remarks. 19 surface samples with foraminifera present were dominated at least 50% by this assemblage. This assemblage accounts for 33% of the variance in the entire data set. The assemblage represents a mid-shelf/upper-slope (172-595m), very low-oxygen environment (3.0-7.7µMol)with variable but, generally, very high organic-carbon contents (0-17%).

Bolivina costata assemblage (factor 2)

Depth range (m) = 73 to 309; Temp. (°C) = 11.8 to 13.7 (average = 13.0, median = 13.4); Salinity (‰) = 32.2 to 34.9 (average = 34.2, median = 34.9); O_2 (µMol) = 4.3 to 5.9 (average = 5.3, median = 5.5); Wt. % organic carbon = 4.1 to 7.6 (average = 6.1, median= 6.3). Key species: *Bolivina costata*, % of population = 65 to 100 (average = 88, median = 94), f/g = 2 to 376 (average = 65.4, median = 37.2).

Remarks. Only four surface samples were dominated by this assemblage. This assemblage accounts for 26% of the variance in the data set and represents a shelf to upper slope environment (73-309m) with high organic-carbon levels (4.1-7.6%). Oxygen concentrations are low, but the average dissolved oxygen level (5.3µMol) is slightly greater than the average dissolved oxygen level for the *B. humilis* assemblage (3.9µMol).

In previous work, it has been difficult to establish the depth range of *B. costata*. Low percentages (1 to 3 %) have been reported in slope samples, but this occurrence may be attributed to reworking of shallow sediment; samples have been recovered, however, from the eastern margin of the Nazca plate, where no shallow source of sediments is evident (Shepherd 1979; Resig, 1981). In this study, *B. costata* is a significant species only at shallow depths (<300m) but it does appear in low percentages down to about 500m depth (Fig. 3.21). This present study reconfirms a shallow shelf environment for this species as previously concluded (Resig 1981), but, due to the samples not being treated with protoplasmic stain, the depth range of the species cannot be more conclusively resolved.

Pseudoparella subperuviana assemblage (factor 3)

Depth range (m) = 546 to 800; Temp. (°C) = 5.6 to 10.5 (average = 8.1, median = 6.9); Salinity (‰) = 34.5 to 34.6; O_2 (µMol) = 7.7 to 20.3 (average = 11.92, median = 7.73); Wt. % organic carbon = 1.02 to 7.26 (average = 4.2%, median = 3.9%). Key Species: *Pseudoparella subperuviana*, % of population = 7 to 77 (average = 34, median = 30), f/g = 2.3 to 628.6 (average = 144.2, median = 60.4); *Uvigerina peregrina*, % of population = 0 to 55 (average = 25, median = 25), f/g = 0 to 108 (average = 41.4, median = 23.8); *Uvigerina striata*, % of population = 0 to 32 (average = 14, median = 9), f/g = 0 to 115 (average = 31.9, median = 14.3).

Remarks. Six surface sediment samples were dominated by this assemblage. This assemblage accounts for 15% of the variance in the data set and represents a deeper (545-800m), slightly more oxygenated (7.7-20.3µMol) environment with relatively low organic-carbon contents (1%-7.6%).

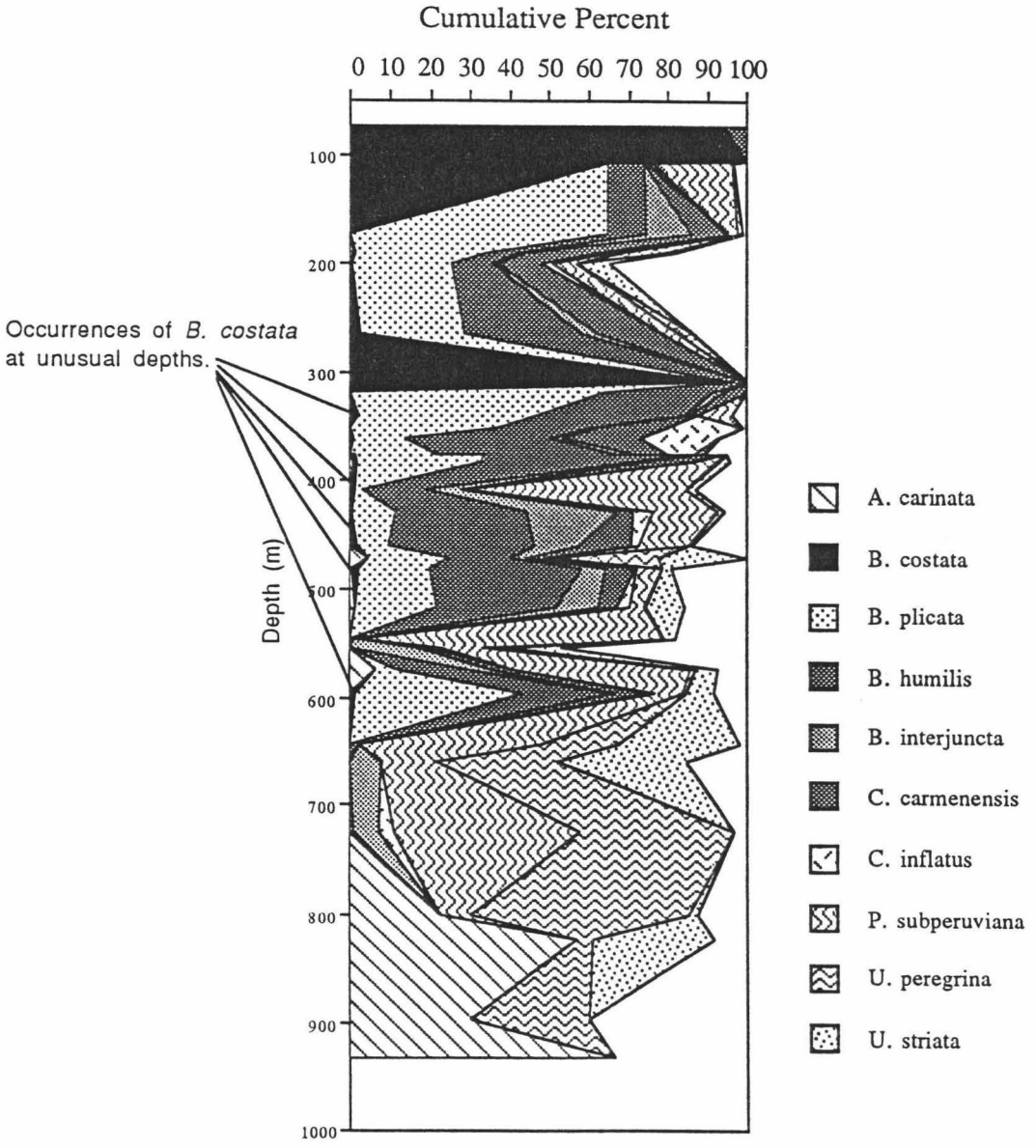

Figure 3.21. Percentage distribution of benthic foraminiferal assemblages with water depth.

Angulogerina carinata assemblage (factor 4)

Depth range (m) = 823 to 932; Temp. (°C) = 4.4 to 5.6 (average= 5.0, median= 5.0); Salinity = 34.5 to 34.5; O2 (μMol) = 20.3 to 42.4 (average= 31.3, median= 31.3); Wt. % organic carbon = 1.15% to 1.52% (average= 1.3%, median= 1.2%). Key Species: *Angulogerina carinata*, 30% to 67% of population (average= 51%, median= 57%), f/g - 1.7 to 7.5 (average= 4.0, median= 2.8); *Bolivina spissa*, 0% to 40% of population (average= 24%, median= 33%), f/g - 0 to 2.3 (average= 1.2, median= 1.4); *Uvigerina peregrina*, 0% to 30% of population (average= 11%, median= 4%), f/g - 0 to 1.7 (average= .76, median= .58).

Remarks. Only three surface samples were dominated by this assemblage. The lack of data makes the classification of this assemblage tenuous. The assemblage accounts for only 10% of the variance in the data set. It represents a deep (823-932m), cold water (4.4-5.6°C), relatively well-oxygenated (20.3-42.4μMol) environment with relatively very low organic-carbon content (1.15%-1.52%), and very sparse foraminiferal populations (<10 f/g).

Sample locations of benthic foraminifers are plotted on the substrate facies map for both 12°S and 13.5°S (Figures 3.22, and 3.23, respectively) and are contoured with respect to the dominant assemblage factor in each sample. Very few data are available for the assemblages of factors 2 and 3 at 12°S and the areas I have contoured for them are tenuous. The data distribution is better for 13.5°S and I can assign contoured regions with more confidence. The data form a clear pattern of distribution with each dominant factor occupying a separate region of the shelf or slope. This pattern indicates that benthic foraminiferal assemblages of ancient sediments will be useful in interpreting

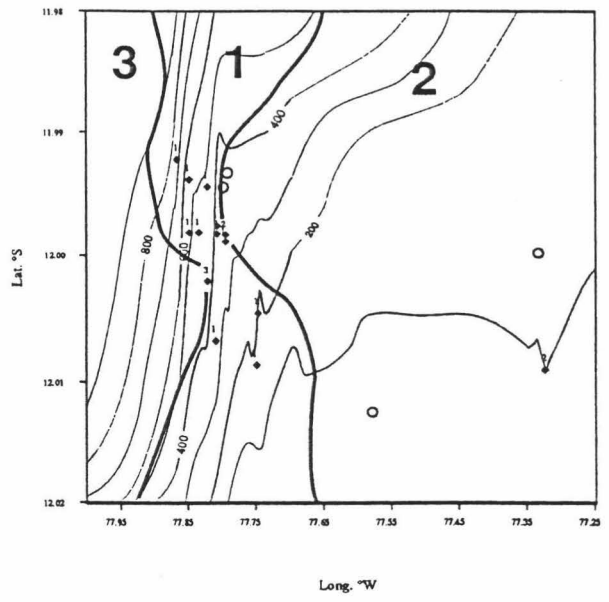

Figure 3.22. Locations of surface sediment samples collected along the 12°S transect contoured for the dominant foraminiferal assemblage. Open circles are sediment samples barren of benthic foraminifera.

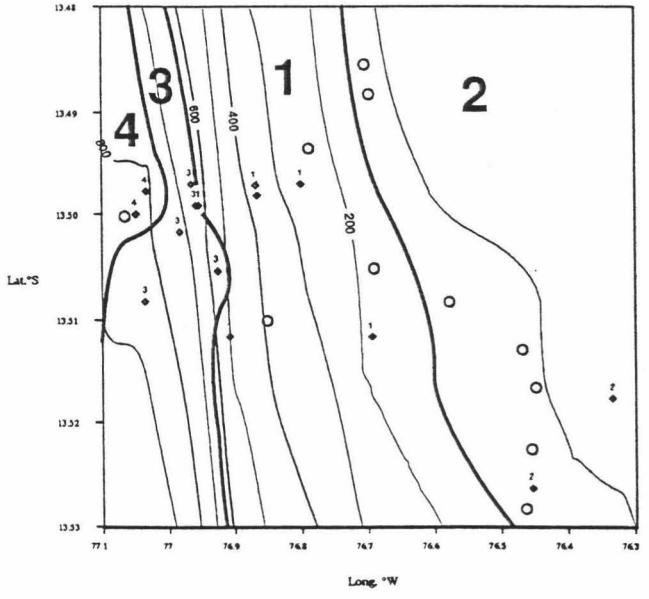

Figure 3.23. Locations of surface sediment samples collected along the 13.5°S transect contoured for the dominant foraminiferal assemblage. Open circles are sediment samples barren of benthic foraminifera.

depositional locations—at least with respect to depth compared to other samples. A cross-section view of the distribution of the four assemblages is illustrated in Figure 3.24.

Influence of Current on Benthic Foraminiferal Distribution

Resig (1990) distinguished assemblages from samples from ODP Leg 112 that seemed to represent a collection of robust species concentrated in foraminiferal sands through current action. This assemblage consisted of relatively large species and was found in what appears to be winnowed sediment. The most dominant species identified for this assemblage is *Angulogerina carinata* with other key species being *Bolivina plicata*, *Brizalina interjuncta*, *Cancris carmenensis*, *Cancris inflatus* and *Uvigerina* spp.

Bottom water current data was collected with several surface sediment samples during the R/V Seward Johnson cruise. As outlined below, analysis of these data is used to verify if any correlation does exist between current strength and foraminiferal assemblages.

Explanation of Current Data

Previous research has identified several current regimes along the Peru coast: the Peru Current — a northward-flowing surface current produced by prevailing south-east winds, the Poleward Undercurrent — a poleward undercurrent running counter to the Peru Current, and a northward flowing current of Antarctic Intermediate Water (AIW) (Wyrtki, 1967). The Peru Current is a surface current that extends to approximately 20 m depth (Brockman et al., 1980). The poleward undercurrent is observed below the Peru Current over the entire area between 6° and 17° S, Brockman et al. (1980) reported that current measurements indicate the poleward undercurrent is stronger and more persistent in the north, near 5°S, and is over the shelf with the current in contact with the sea floor; moving toward the south, the current strength decreases and moves out to the shelf/slope

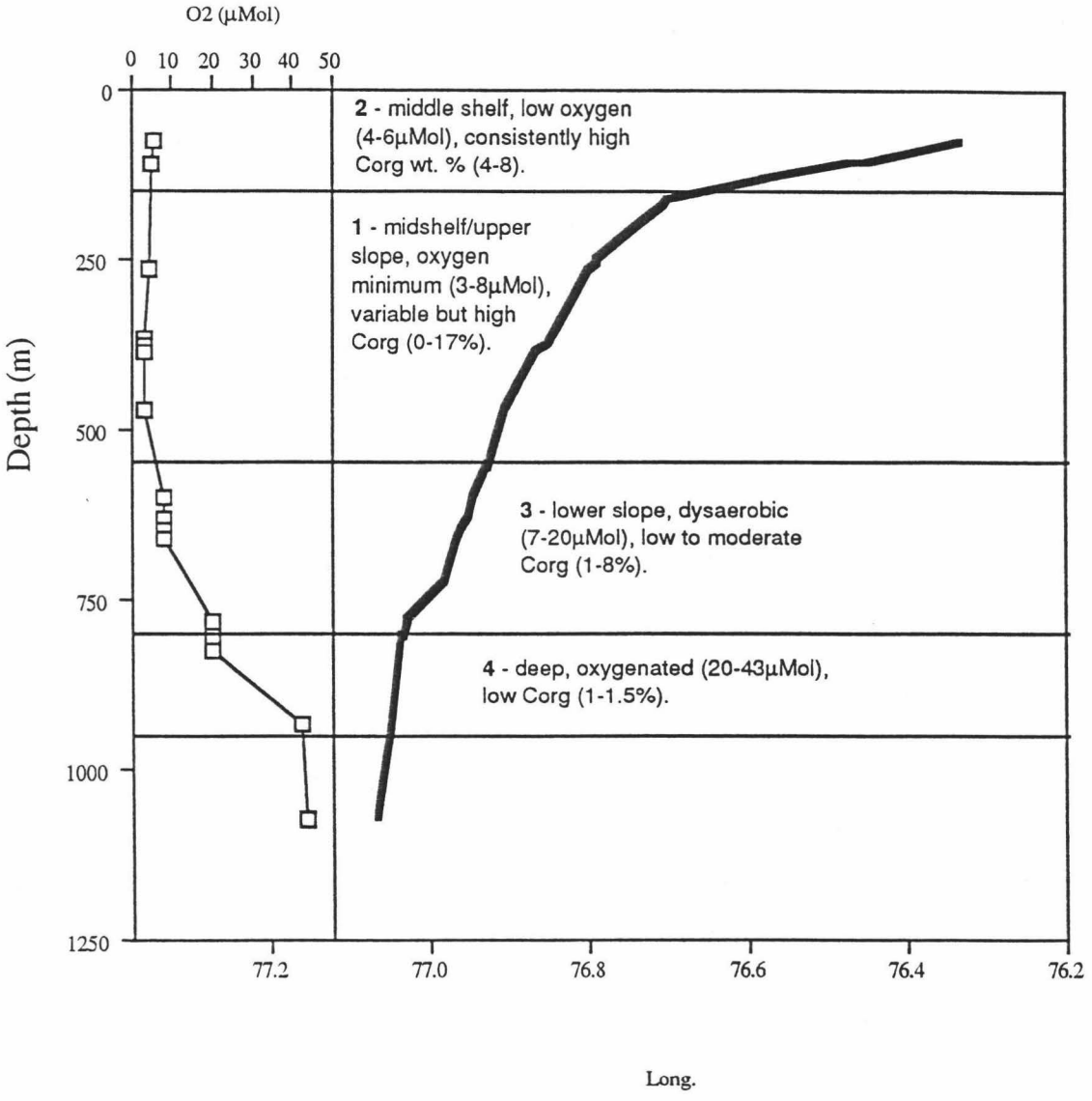

Figure 3.24. Cross sectional view of different areas dominated by the 4 major assemblages of benthic foraminifera on the Peru Margin and characteristic environmental conditions of each area.

break area and looses contact with the sea floor. They placed the flow core depth at approximately 90 m with mean current velocities of 6-16 cm/sec. In a more recent study, Huyer et al. (1990) found a well defined core of the Peru Undercurrent near 150m with a mean velocity of 10 cm/sec. The maximum geostrophic flow is just seaward of the shelf edge (at 10°S) between 150 and 200m depth with a velocity of 20 cm/sec. They found that the Peru Undercurrent extends from 50 to 350m depth. Huyer et al. (1990) also found that currents were very variable in both speed and direction at all frequencies. The AIW is found at depths of 500 to 900m and is northward flowing.

Current data were collected at 12°S and 13.5°S during submersible operations on the Peru coast during the R/V Seward Johnson cruise. The current measurements are illustrated in Figures 3.25 (12°S), and 3.26 (13.5°S). The bathymetry for the region is based on depth measurements taken during operations on the R/V Seward Johnson cruise. Contours were created by fitting a two-dimensional spline to the depth data.

At 12°S, in the region from 77.3° to 77.7° W, there was a predominantly southern trend to bottom water flow with current velocities approximately 10 cm/s. Depths of these data points are at approximately 100 and 150 m. The direction of flow and its shallow depths suggest that these currents are most likely associated with the Peru Undercurrent. Further to the west, in greater depths, the current activity becomes erratic. Current velocities range between 0 and 27.5 cm/s and directions are found northward, southward, and on- and off-shore. Despite the variability, a general pattern is observed. Flow, in the region west of 77.75° W, is generally equatorward with velocities reaching a maximum at the shallower depths and decreasing at greater depths. These northward-flowing currents may be associated with northward flowing AIW, but the depths of the current measurements with the highest velocity and the most persistent northward trend (see depth around 150 to 200m on Fig. 3.25) are much more shallow than the AIW (minimum depth ~500m). As described above, Huyer et al. (1990) found that flow in the

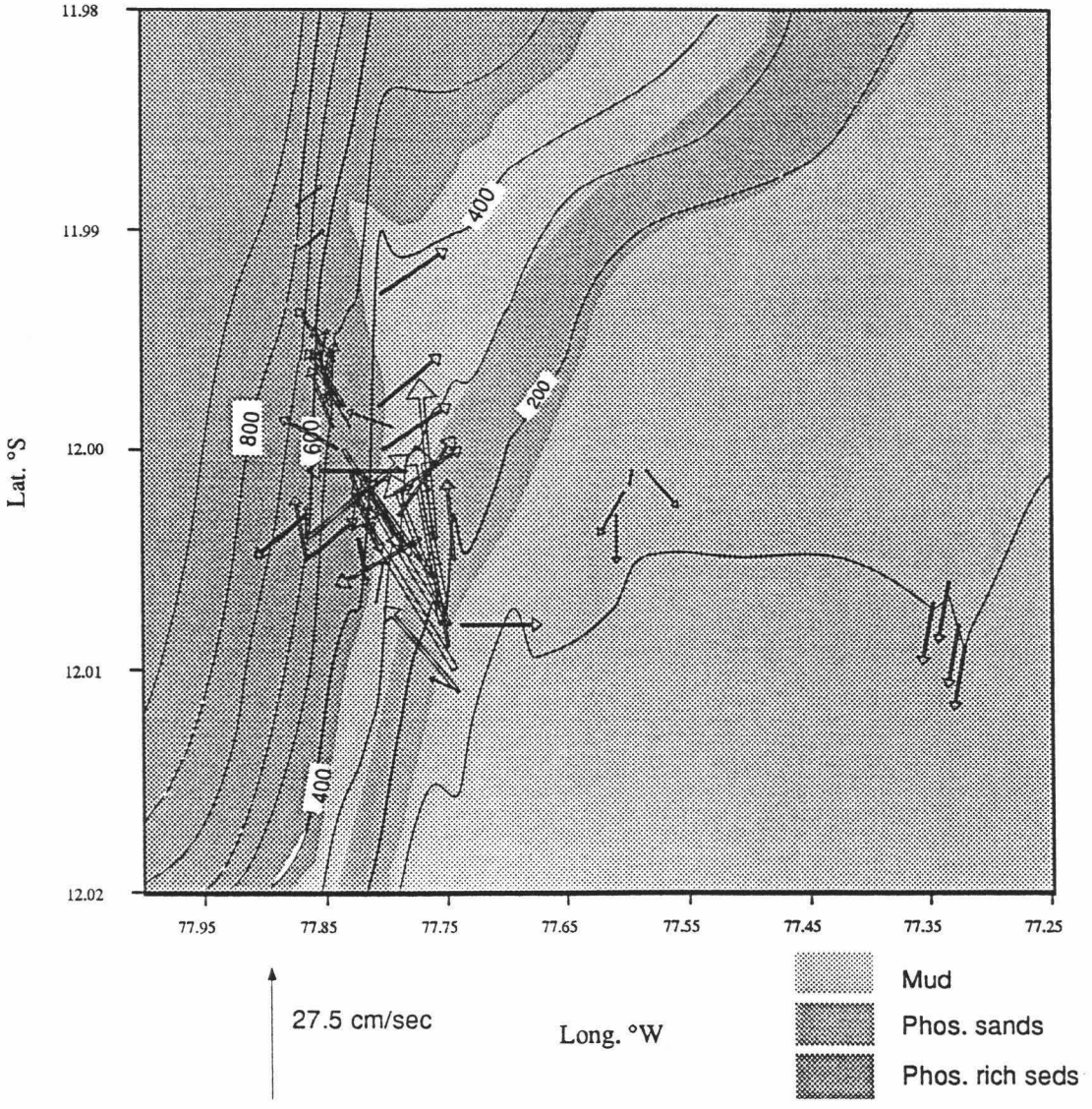

Figure 3.25. Velocity of bottom currents—12°S. Length of arrow is proportional to current velocity.

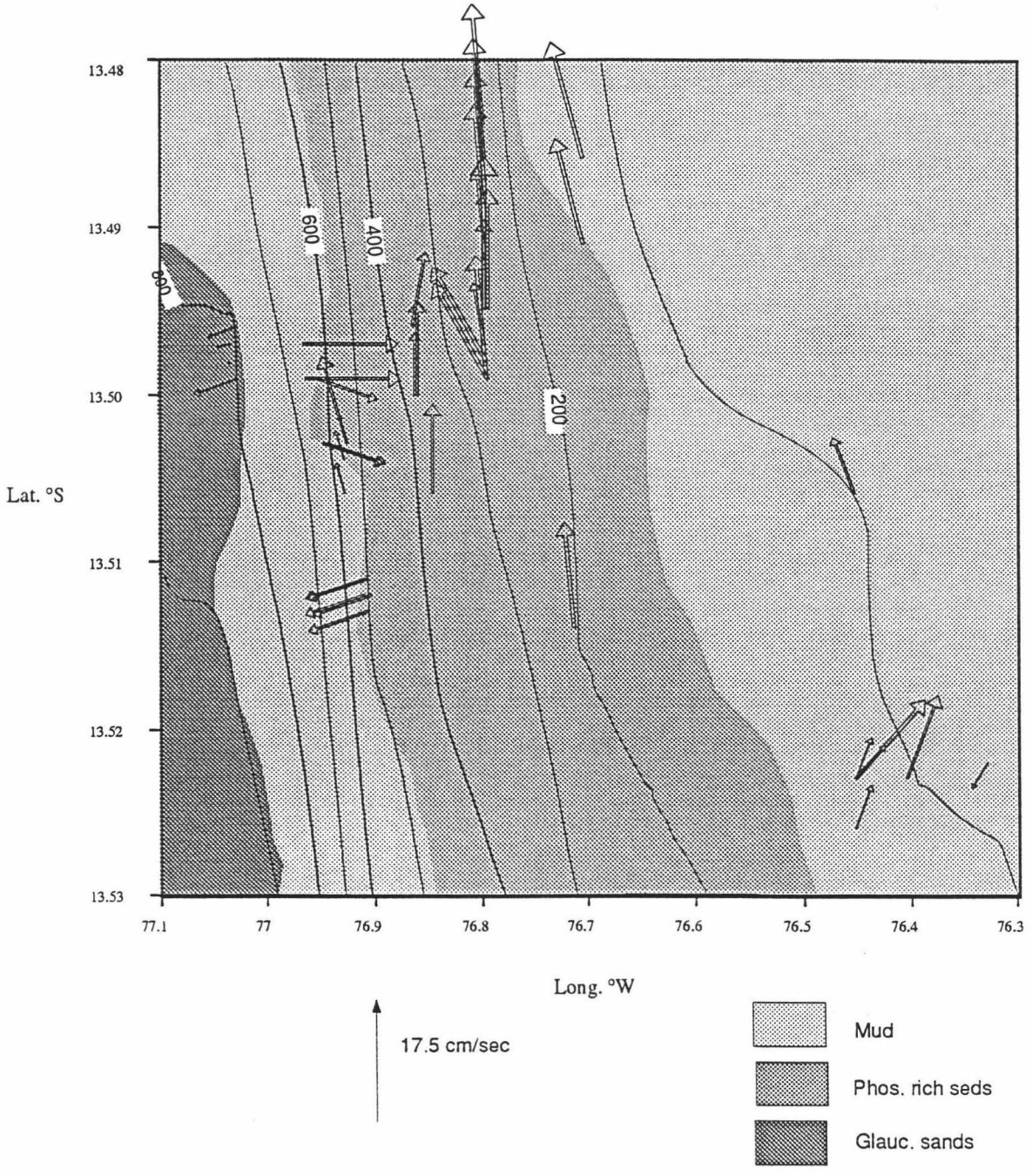

Figure 3.26. Velocity of bottom currents—13.5°S. Length of arrow is proportional to current velocity.

Peru Undercurrent is variable in direction and speed. Since the current measurements I present here were recorded only once at each location it is most likely that they are related to the Peru Undercurrent and that flow directions that deviate from a southerly trend are anomolies.

At 13.5° S, in the region east of 76.9° W and between 100 - 400m, the flow was consistently equatorward. Current velocity is generally lower near depths of 100 m (5-17 cm/s) and increases between 100-300 m (maximum = 25 cm/s). West of 76.9° W the current direction becomes variable with northward, on-shore and off-shore flows. Velocities are reduced slightly from the maximum region. None of the current data east of 76.9° W can be correlated well with the general poleward flow of the Peru Undercurrent, however, due to the depth of this region, the bottom water is most likely related to the Peru Undercurrent and are anomolous directions. These northward flowing currents are much too shallow to be associated with the northward-flowing AIW. At the reported depths of the AIW (~500-1000m) along the 13.5 °S transect, the current directions show no clear trend.

Correlation of Current Data with Foraminifer Distribution

Resig's (1990) 'current' species, *Angulogerina carinata*, *Bolivina plicata*, *Brizalina interjuncta*, *Cancris carmenensis*, *Cancris inflatus* and *Uvigerina* spp., are compared to the 1992 current activity; both the percentage (Fig. 3.27) and the number of foraminifers per gram dry sediment (Fig. 3.28) of foraminiferal populations are compared to current velocity.

Percentages

No strong increase in the percentage of population with increasing current velocity is observed for the species *A. carinata*, *B. interjuncta*, and *B. plicata*. (Fig. 3.27). *A.*

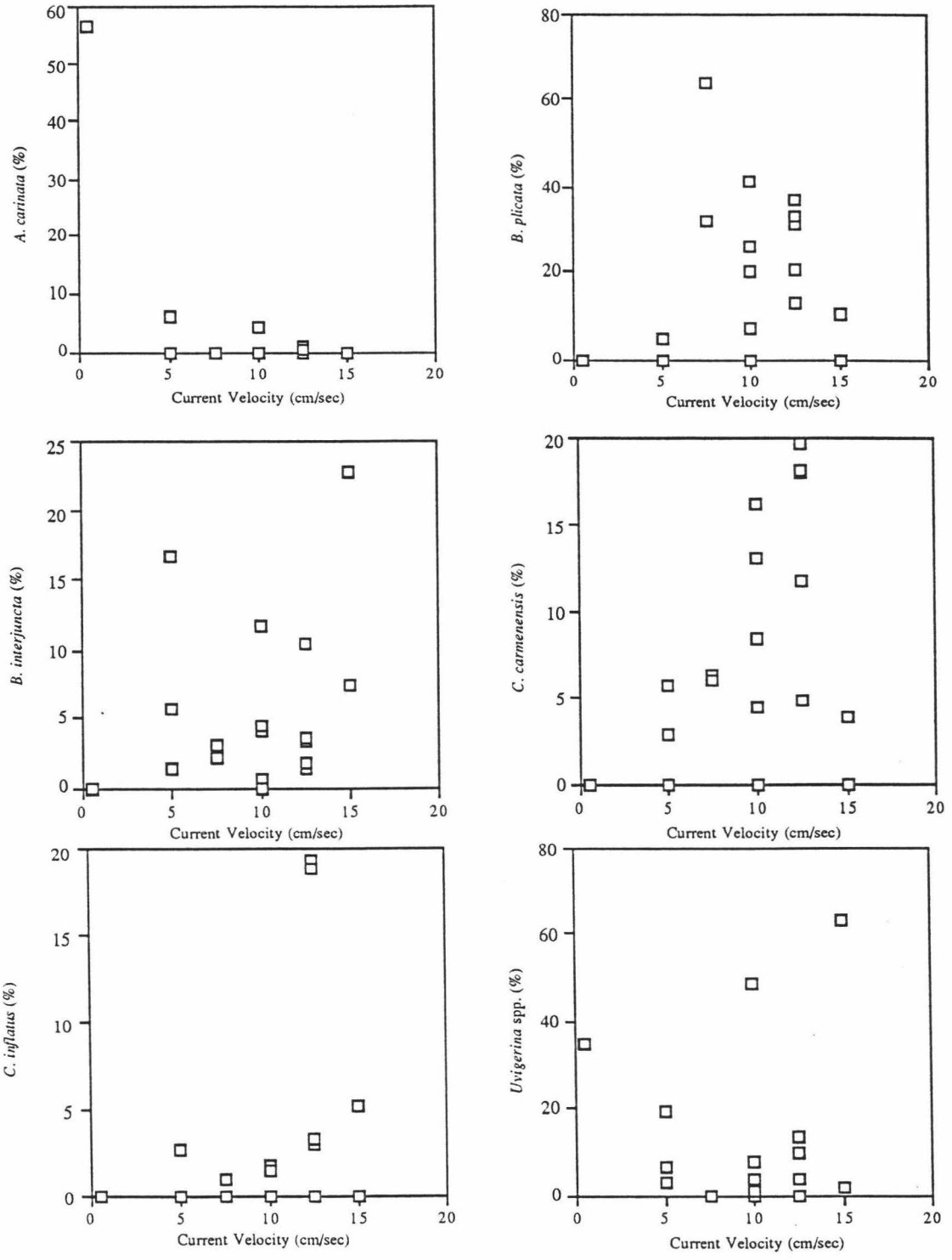

Figure 3.27. Percentage of various benthic foraminifer species per population versus bottom water current velocity.

carinata actually shows an inverse correlation to the 1992 current velocity. For the species *C. inflatus, C. carmenensis*, and *Uvigerina* spp., excluding samples in which no specimens were counted, there is a noticeable increase in the percentage of the population with increased current strength.

Current activity may have an effect on benthic foraminifer assemblages; it may tend to concentrate certain species and winnow others based on the shape or weight of a species. My results identify *C. inflatus, C, carmenesis*, and *Uvigerina* spp. as possible species that are concentrated by currents.

Foraminifers per gram dry sediment

The number of foraminifers per gram of some species in Resig's 'current' assemblage does show a significant increase with increased current velocity; these include *A. carinata, B. plicata, B. interjuncta*, and *Uvigerina* spp (Fig. 3.28). This trend is observed, however, in other species that were not considered by Resig to be species that are concentrated by currents. As examples, Figures 3.29, and 3.30 show the number of foraminifers per gram vs. current strength for *B. humilis* and *Buliminella subfusiformis*. Notice that the number of specimens per gram increases with current velocity. Current does seem to increase the number of foraminifers per gram but it does not seem to discriminate between species, concentrating all species more or less equally.

Barren Surface Sediment Samples

No benthic foraminifera were found in 16 of the 49 surface sediment samples analyzed for benthic foraminiferal assemblages. This is significant because vast barren intervals have been observed in the ODP cores from Leg 112 with no clear explanation for their absence. Aerobic dissolution of $CaCO_3$ by metabolic CO_2 is known to occur in these sediments and possibly plays a role in preservation (Wefer et al., 1983; Seuss et al.,

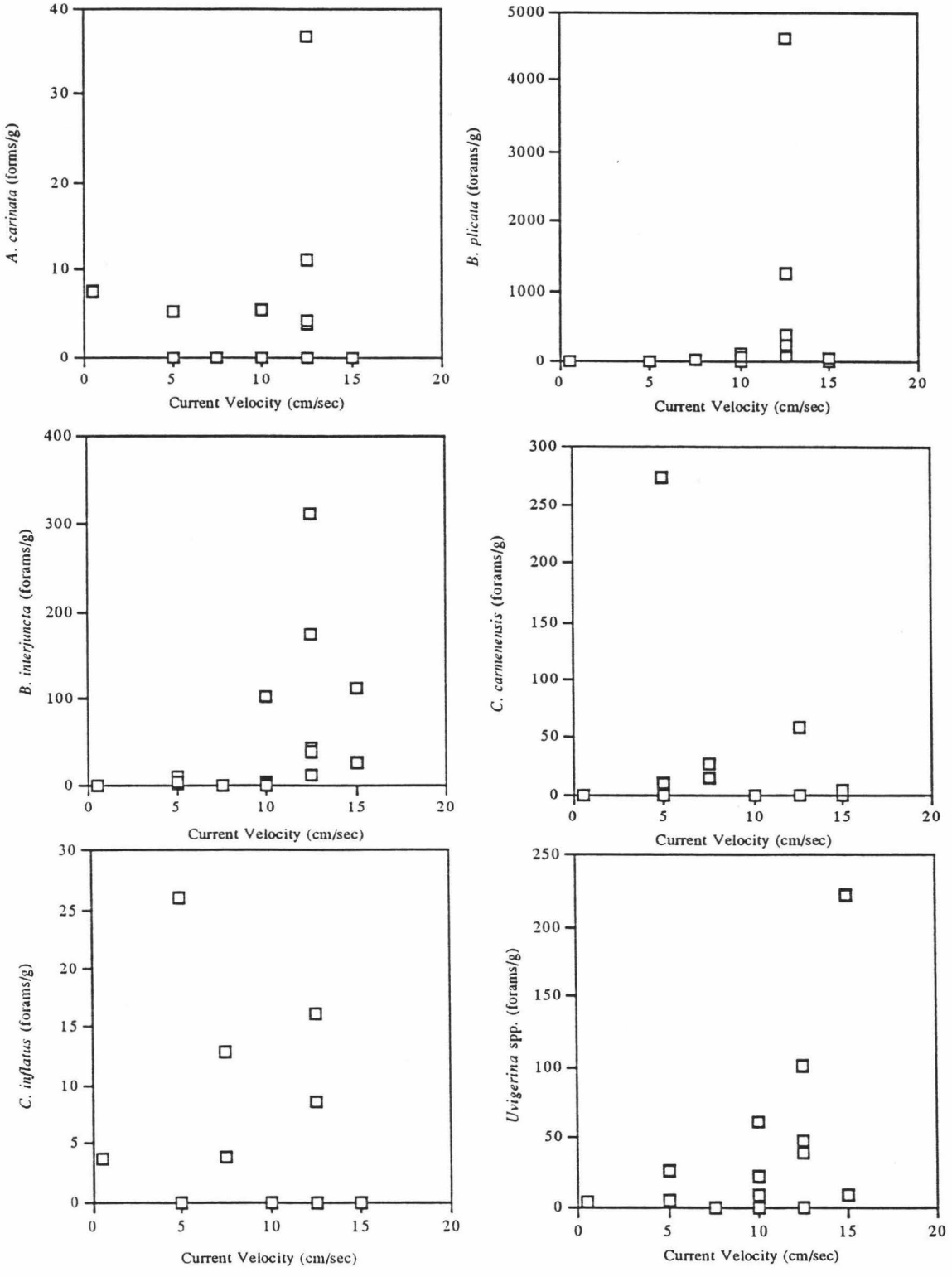

Figure 3.28. Concentration of various benthic foraminifer species versus bottom water current velocity.

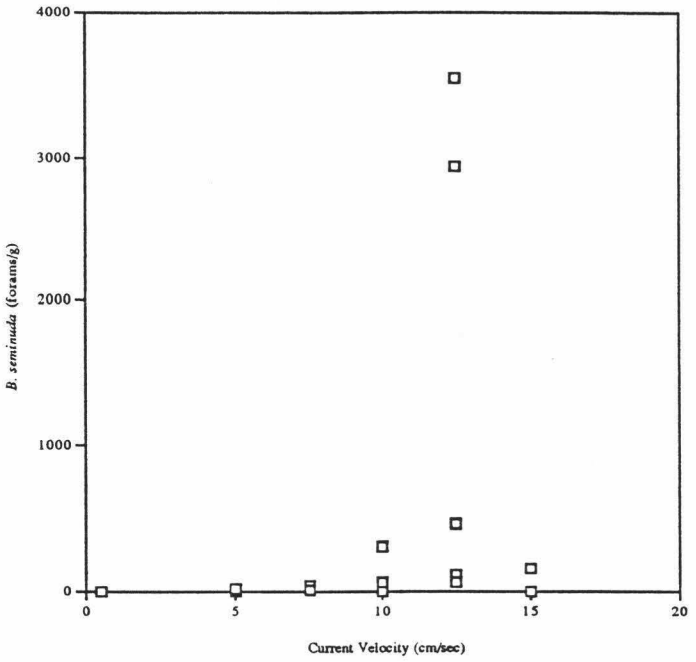

Figure 3.29. Number of specimens of *B. humilis* per gram dry sediment versus bottom water current velocity.

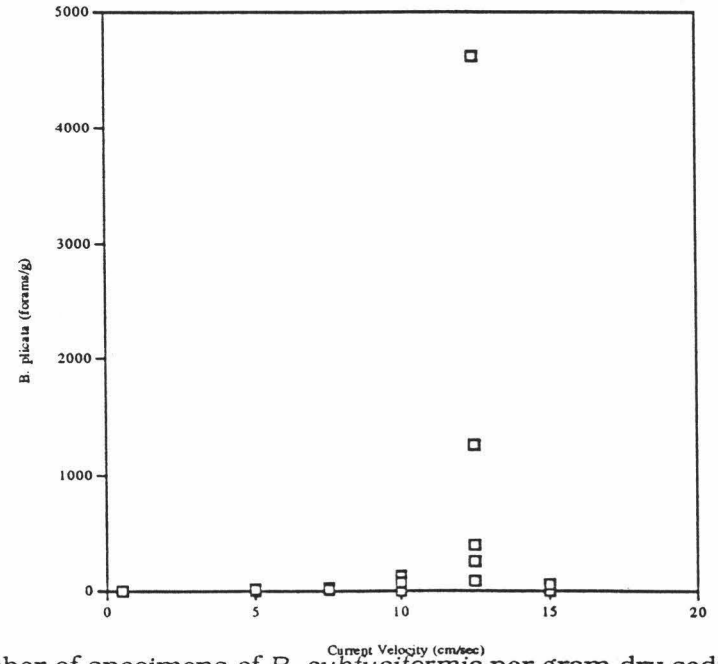

Figure 3.30. Number of specimens of *B. subfusiformis* per gram dry sediment versus bottom water current velocity.

1987). Also, intense anaerobic conditions dominate many areas in this region and such highly anoxic conditions may prohibit benthic foraminiferal habitation. As explained below, foraminifers are absent in many areas — this primary absence of foraminifers may play an important role in barren sediments in cores.

Environmental conditions for sediment samples barren of foraminifers are summarized and compared (Table 3.10). Averages of the various enviromental parameters are statistically compared using a Student t-test and are evaluated at the 90% confidence level. The only factor that is significantly different at the 90% confidence level between the barren and non-barren samples is the percentage of sediment fraction greater than 63 μm. Samples with a very high percentage (>75%) of clay and silt sized sediments are commonly barren of foraminifers. Because foraminifers themselves are part of the sand fraction of the sediments it is important to verify that they do not make up 100% of the sand content. If sediments are found with only foraminifers and clay and silt sized sediment, that would imply that the clay size fraction may not be important in prohibiting infaunal habitation. Samples with foraminifers present were observed and the sand fraction was classified (Table 3.11). In no sample, with foraminifers present, were foraminifers 100% of the sand fraction. The barren sediments are observed to be very dense, sticky, clays. It is very likely that the dense, sticky nature of the sediments prohibits burrowing and habitation by benthic foraminifers.

Among the environmental factors I have available for these surface sediments, no strong correlation exists between them and the percent clay fraction. It has been suggested that barren, very fine grained, laminated intervals in cores may represent deposition in extremely anoxic environments resulting from very high primary surface productivity (Stein, 1991). There may be a correlation between the productivity indicator that I have (weight percent organic-carbon of sediment) and the clay fraction of the sediments. Figure 3.31 shows the variation between the sand fraction and weight percent organic carbon. The plot shows higher weight percent organic carbon contents in sediments with

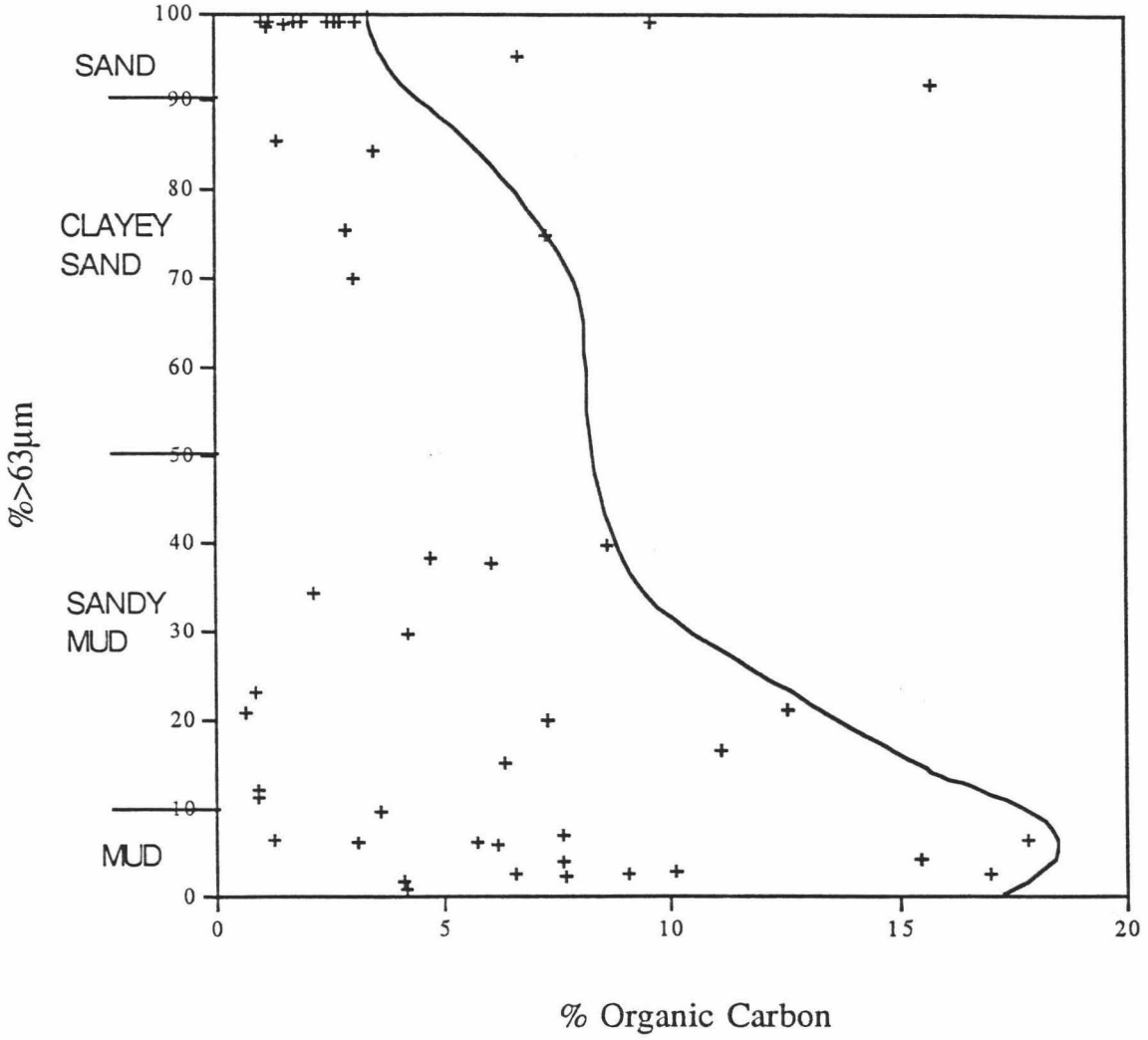

Figure 3.31. Percent of sediment greater than 63µm versus organic carbon weight percent. Sands with low organic carbon content (<5%) are glauconite pellets. Sands with high organic carbon content appear to be winnowed fish debris and foraminifers.

less sand sized particles. Samples with less than 25% of the sediment greater than 63μm generally consist of approximately 5% diatom frustules, <5% fish debris with the rest being terrigenous clays or powdered diatom frustules and other unidentifiable debris. On the Peru Margin, mixed diatom ooze/ terrigenous sediments are believed to originate from suspension fallout (diatoms) and tractional deposition from low density turbidity and/or bottoms currents containing resuspended sediments (Kemp, 1990). With respect to the surface sediment samples of this study, this is a reasonable explanation. However, the final depositional environments must represent areas of significantly decreased energy for the clay fraction to settle. The current strength data do not support this assumption. Low >63μm fractions are found in areas of significant current strength (Fig. 3.32).

Phosphorite absolute ages

Uranium-series radionuclide analyses have been completed for two samples collected during the R/V Seward Johnson cruise (Table 3.7). Phosphatic material taken from Box Core 57 (BC-57) reveals an age that is much older that the surrounding sediments. In the upper 25 mm of phosphatic material found at the sea floor surface, ages ranged from 4.7 to 8.2 ky. Within the error bars of the ages, the dates decrease with depth, implying that the phosphorite is growing downward into the sediment. A phosphatic 'protocrust' taken from Dive 3362 gave a age date very near zero years. Apparently this sample was collected during incipient growth. The analyses of these two samples indicate that phosphatic material at the seafloor can be of different ages. Surface currents probably play the principle role in keeping older phosphatic material at the surface. The results of the phosphorite age analyses imply that the ages of phosphatic materials are not useful in assigning absolute age dates to sediments in this region.

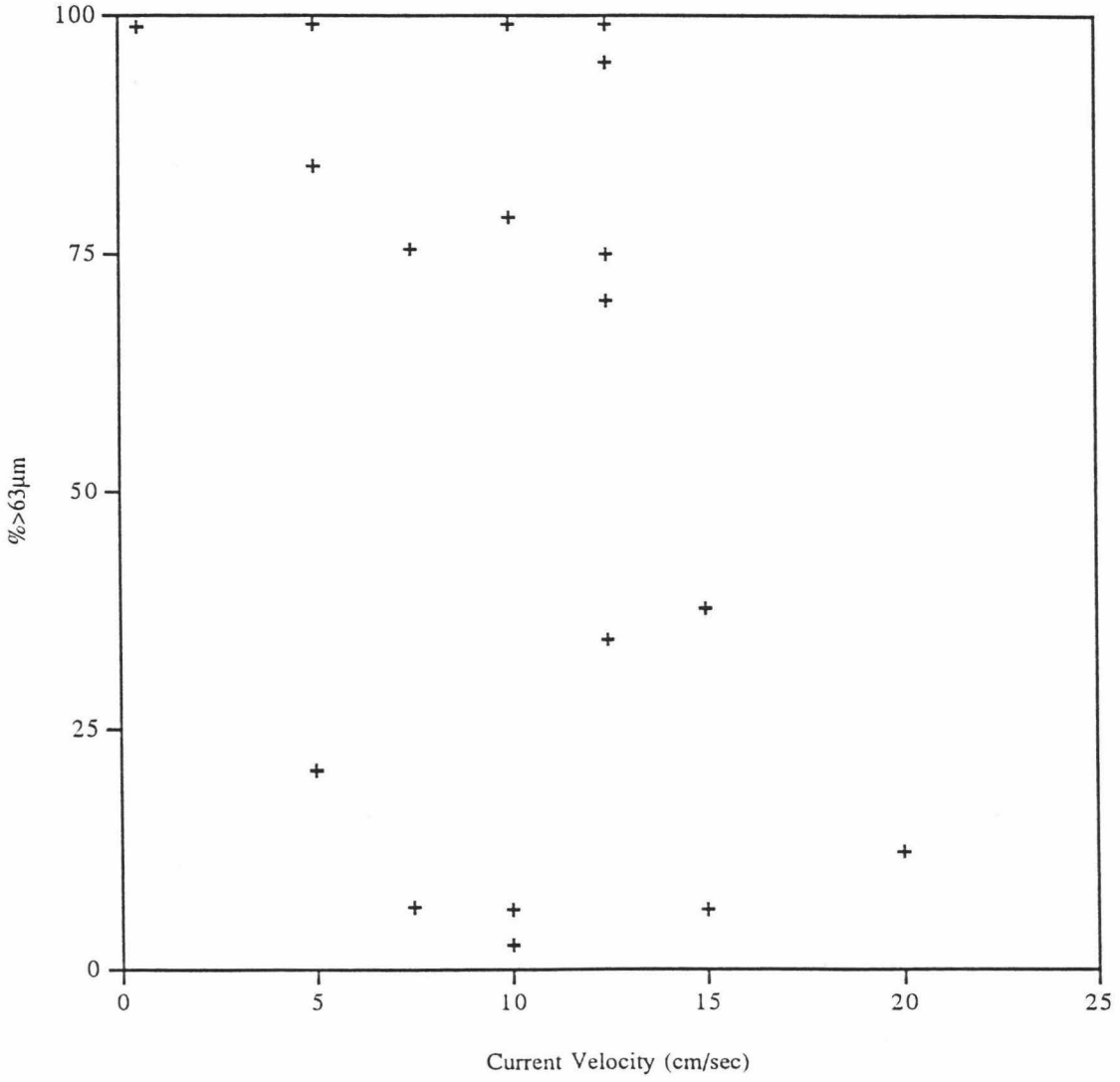

Figure 3.32. Percent of sediment greater than 63µm versus bottom water current velocity.

Conclusions

The organic carbon weight percentages of the surface sediments from the Peru Margin are influenced by overlying surface primary productivity, i.e., sediments underlying areas displaying higher historical records of primary productivity display higher organic carbon contents. Organic carbon weight percent of ODP core sediments may be used as a rough indicator of surface productivity. There was some correlation between the various sediment facies and the amount of organic carbon in the sediment; mud-rich facies retained a higher percent of organic carbon, while the more coarse grained sediments generally retained less organic carbon, especially glauconitic sands which contained nearly no organic carbon. Low bottom-water dissolved oxygen levels were found with relatively high organic carbon weight percents. High organic carbon flux will consume more oxygen and this increased consumption is likely the main reason for the correlation between oxygen levels and organic carbon. Additionally, low oxygen levels may restrict metazoan grazers and this may enhance organic carbon preservation in sediment. Porosity was somewhat correlated with organic carbon content. Very low permeabilities of sediments and high adsorbtion rates onto clay minerals may be the cause of these higher organic carbon contents. 1992 current velocity did not show a correlation with organic carbon content.

$\delta^{13}C$ values of benthic foraminifera showed no correlation with organic carbon weight percents or with bottom water dissolved oxygen levels. $\delta^{13}C$ ratios of benthic formainifera are probably not useful indicators of productivity or anoxia.

Benthic foraminiferal populations were found to comprise four principle assemblages which are useful in determining water depth and bottom water oxygen levels. Current activity does concentrate benthic foraminifera in sediments although current activity does not seem to discriminate much among foraminifera species. Species are affected equally

in sediments. Possibly, the percentages of *C. inflatus*, *C. carmenensis*, and *Uvigerina* spp. in populations is affected by current velocity, but the correlation revealed by the data is very weak. From this analysis, benthic foraminiferal assemblages are not good indicators of current activity.

Many surface samples are barren of benthic foraminifera. The only environmental factor measured for these sediments that correlates with the barren samples is the percent clay-sized fraction, with sediments dominated by mud being commonly barren of foraminifera.

Phosphatic material age data were ambiguous with respect to surrounding sediments. Phosphatic material was found in contemporaneous and non-contemporaneous sediment. Because of this ambiguity, phosphatic material is not useful in assigning absolute ages to sediments from the Peru Margin.

Chapter 4
ODP Core Sediments

Results

Site Description, Sedimentology, and Stratigraphic Columns

To characterize both seaward-landward and latitudinal shifts of upwelling centers along the Peru Margin, ODP drilling sites were selected along two transects (Suess et al., 1988). Site 680 lies at the center of the sampling pattern. Sites 679 (440m), 680 (253m), and 681 (151m) compose the water depth, east-west transect crossing the margin through the high productivity center at 11° S. Sites 684 (426m), 679 (440m), 686 (447m), and 687 (307m) compose the latitudinal north-south transect through Quaternary sediment parallel to the coast. Except for Site 687, the sites of the latitudinal transect are all within the same water depth (450±30m) (see Fig. 1.1 for site locations).

The sedimentology of the upper 18 m of cores from these sites were inspected and described by C. Glenn at the ODP Repository at College Station, TX. Below, I summarize the site location and sedimentology, and present a stratigraphic column based on Glenn's core descriptions for each site.

Hole 679B

Site 679 is located at the seaward flank of the structural ridge separating the Lima Basin from the Salaverry Basin. The site is at the edge of a pronounced upper-slope mud facies, which underlies the center of high productivity at 11° S. The position of this facies at upper-slope water depths is believed to be controlled by the poleward-flowing undercurrent, the on- and off-shore Eckman flow, and the upper-slope and shelf morphologies (Kulm et al., 1984; Suess et al., 1987). The site was selected to provide data for reconstructing the current and upwelling regimes during times of different sea-level

stands. It is the center of the east-west and north-south transects across the lens-shaped sedimentary body of coastal upwelling deposits. The site lies at a depth of 460 m.

The upper 17 m of Hole 679B is composed chiefly of olive green, diatomaceous mud with varying amounts of silt and sand/foraminifera. The fine-grained fraction of sediment from the Peru coastal margin is dominated by clay (smectite, illite, and chlorite) (Clayton and Kemp, 1990) and feldspathic silt (Kemp, 1990). The sediment texture ranges from laminated to bioturbated. The core contains numerous phosphorite nodule beds 1 to 20 cm thick (Fig. 4.1) (Glenn et al., 1994).

Hole 680A

Site 680 is located within the present-day zone of maximum coastal upwelling (Suess, von Huene, et al., 1988) and within the present-day core of a pronounced oxygen-minimum layer. Due to the site's position in the center of the upwelling system, it was believed that high sedimentation rates should preserve a high resolution record of sedimentary and geochemical signals of vertical and lateral shifts of the oxygen-minimum layer in response to the fluctuations of sea level.

The sediment of the upper 18m of Hole 680A is dominated by laminated to massive olive green to gray diatom mud with varying amounts of silt and sand. The silt and sand fractions are composed of diatoms, fish debris, foraminifer tests, terrigenous sediment, and phosphatic pellets. Bioturbation is present in limited sections. Several thin phosphorite nodule beds are present (Fig. 4.2).

Hole 681A

Site 681 is the most landward site of the east-west transect and is located nearest the origin of coastal upwelling around the headlands near 11°S. The water depth is only

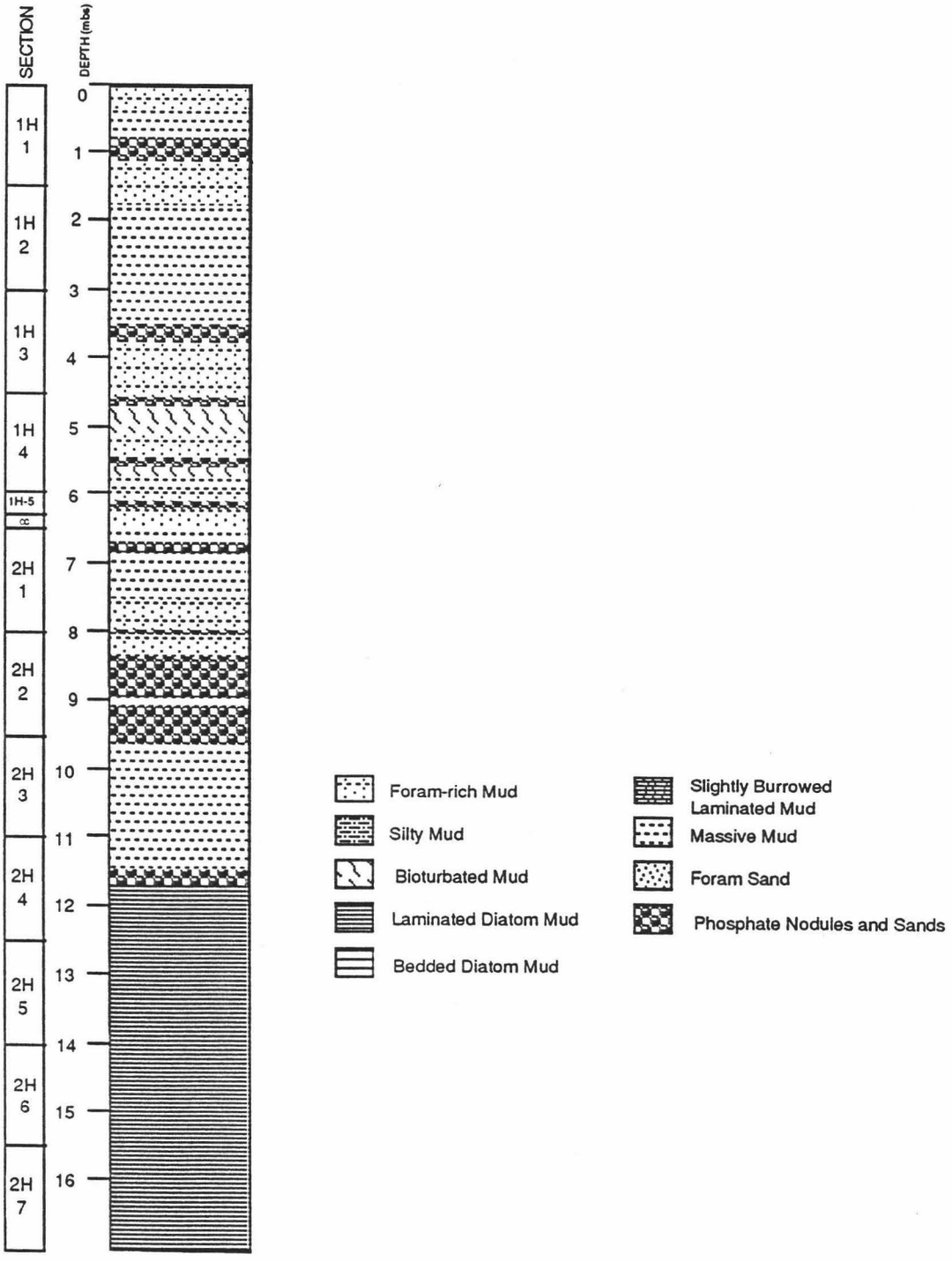

Figure 4.1. Stratigraphic column - Hole 679B.

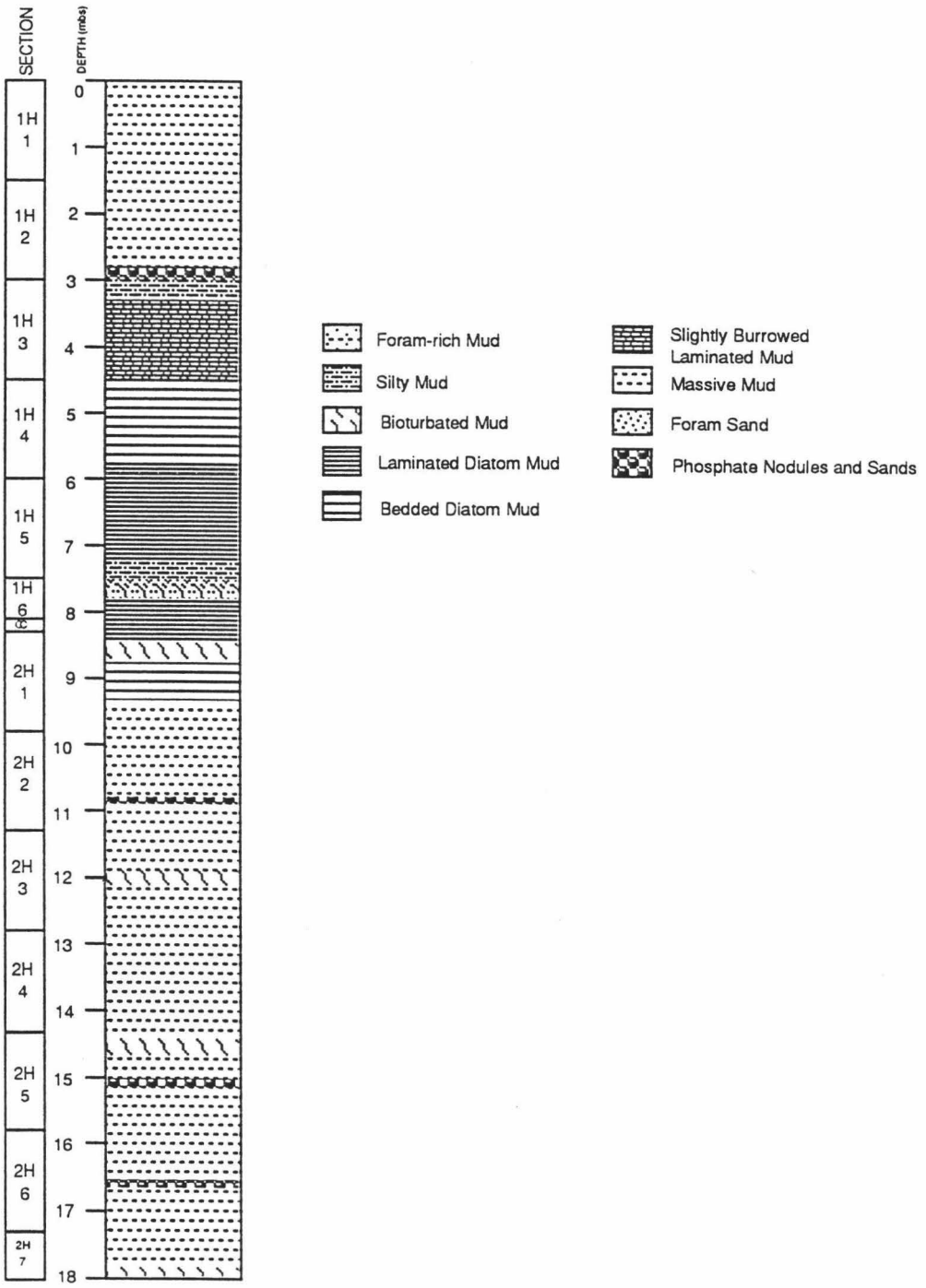

Figure 4.2. Stratigraphic column - Hole 680A.

146m. At Site 681, the seafloor intersects the oxygen minimum zone near its upper boundary. Sedimentation rates in the area are high and it was believed that Site 681 would be the most complete and expanded section of the transect at 11°S. The site may reflect in great detail the seaward-landward shift of upwelling centers during changes in sea level. This shift may have been so dramatic in the past that the most land-ward part of the shelf may have been entirely removed from the influence of coastal upwelling during extremely low stands of sea level.

The upper 16m of sediment of Hole 681A is composed chiefly of massive olive green, diatomaceous mud (Fig. 4.3). Some short intervals show noticeable amounts of silt and sand. In the coarser sediments, the silt and sand fractions are composed of diatoms, fish debris, foraminifer tests, terrigenous sediment, and phosphatic pellets. Some sections in the core show signs of bioturbation. The core contains four thin phosphorite nodule layers.

Holes 686A and 687A

The drilling area for Sites 686 and 687 is located between two structural ridges that separated the shelf and upper-slope region. The West Pisco Basin is heavily sedimented and has undergone continuous subsidence and, hence, has preserved a largely undisturbed record (Thornburg and Kulm, 1981). The basin is adjacent to exposures on land of the famous Miocene Pisco Formation, a classic association of diatomites, cherts, and dolomites believed to have formed under coastal upwelling conditions (Muizon and Bellon, 1980). Site 687 is located on the seaward flank of the Lima Platform which, in this area, forms the eastern and southern boundaries of the Lima Basin.

The upper 15 m of sediment from Hole 686A is composed chiefly of massive to laminated diatom-rich mud (Fig. 4.4). Three phosphorite nodule layers are present in the

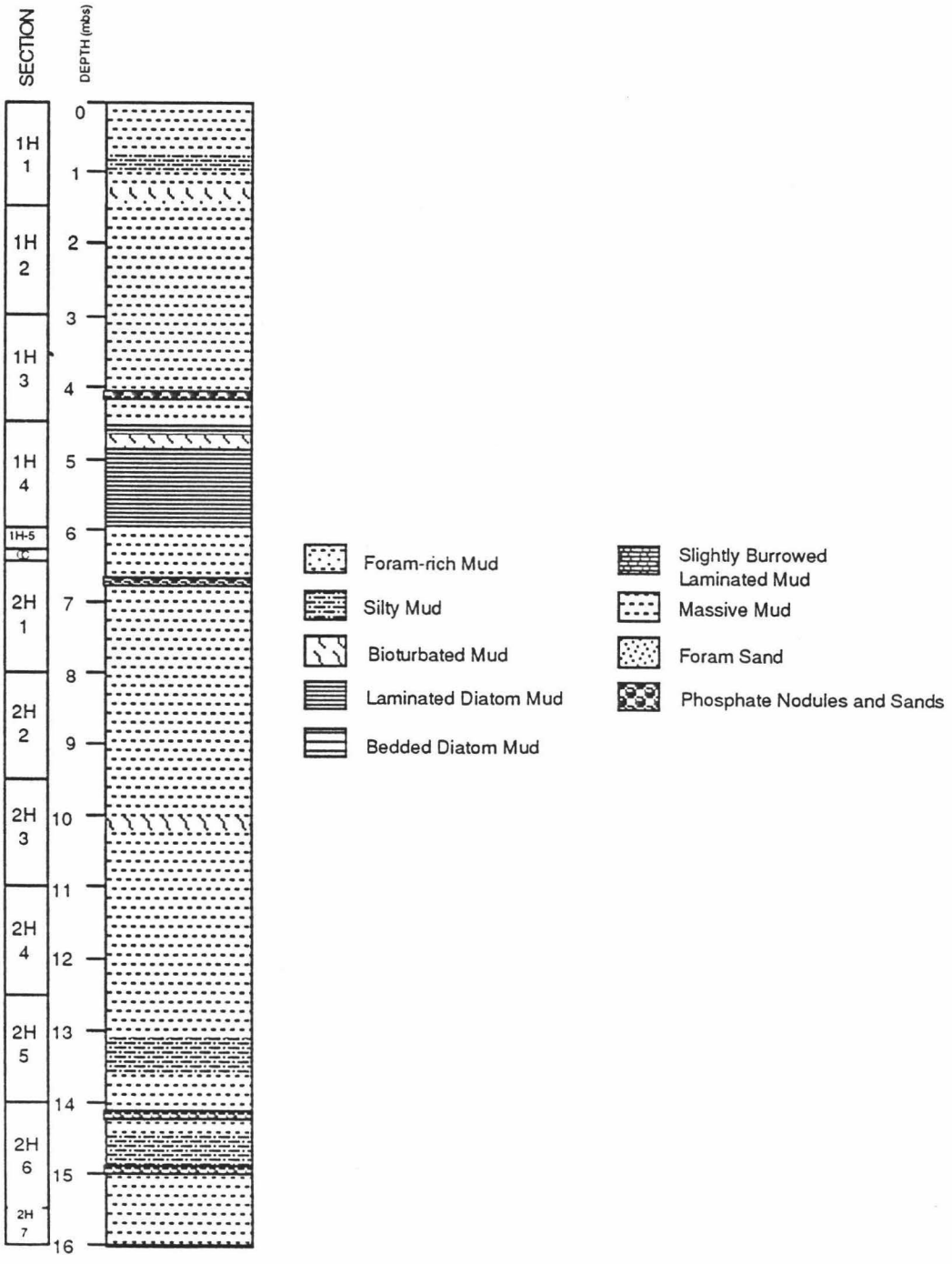

Figure 4.3. Stratigraphic column - Hole 681A.

section. The upper 17 m of Hole 687A is also nearly entirely composed of green massive diatom-rich muds (Fig. 4.5). Two phosphorite nodule layers are present near the bottom of the section.

Foraminifer Census Counts

Hole 679B

The benthic foraminiferal assemblages of the upper 18 m of Hole 679B are very diverse (Fig. 4.6) (assemblage data are summarized in Table 4.1). Species that are found in significant abundance throughout the studied section of the core include *B. humilis, P. subperuviana, A. carinata, B. plicata, and Uvigerina* spp. Preservation of benthic foraminifera in the sediment is fairly good. Barren intervals account for approximately 5 m of the studied section.

Hole 680A

Benthic foraminiferal assemblages in this core are strongly dominated by *B. humilis*, a mid-depth species typical of very low oxygen levels (Fig. 4.7) (assemblage data are summarized in Table 4.1). *P. subperuviana* also has a strong presence throughout the core. Between 9 and 10.5 m the assemblages show a significant percentage of *B. costata* and *N. auris*. Barren intervals are common; no foraminifers were observed in approximately 8 m of the 18 m of core sediment studied.

Hole 681A

The upper 16 m of sediment from Hole 681A is nearly barren of all foraminifera. Only eight sediment samples contained preserved foraminiferal tests and in all but one sample the sediment sample contained less than 100 specimens in the entire sample plug

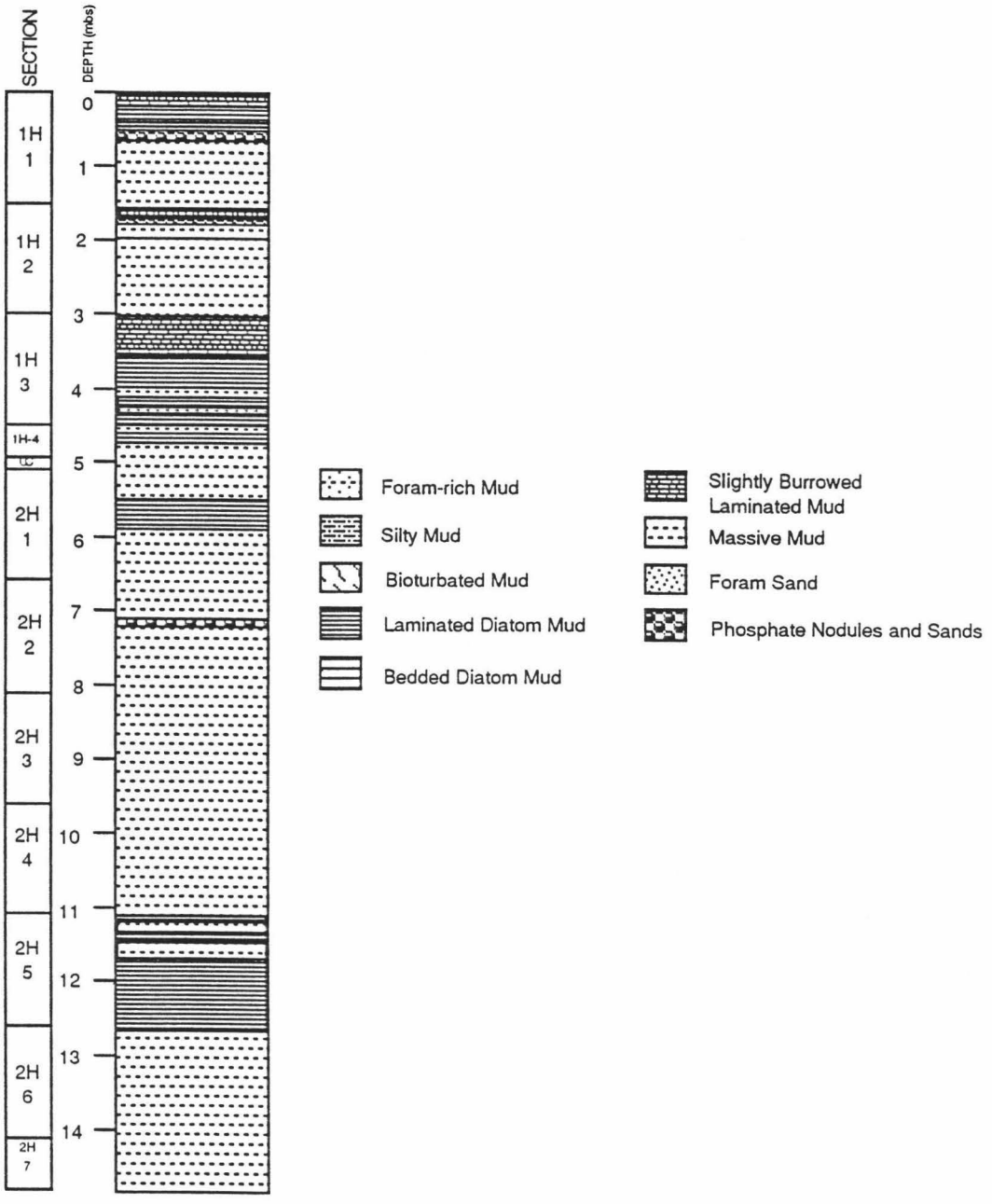

Figure 4.4. Stratigraphic column - Hole 686A

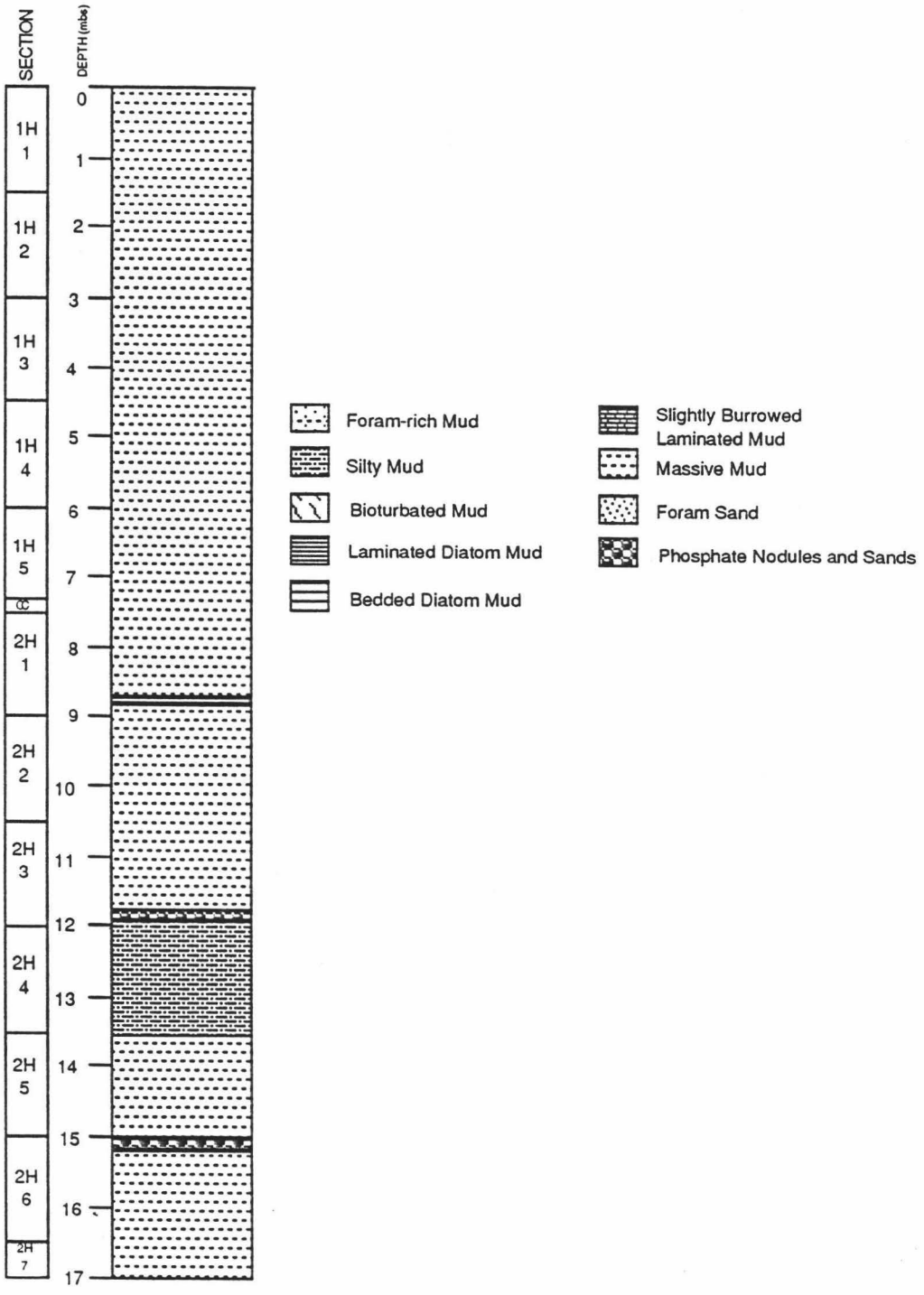

Figure 4.5. Stratigraphic column - Hole 687A

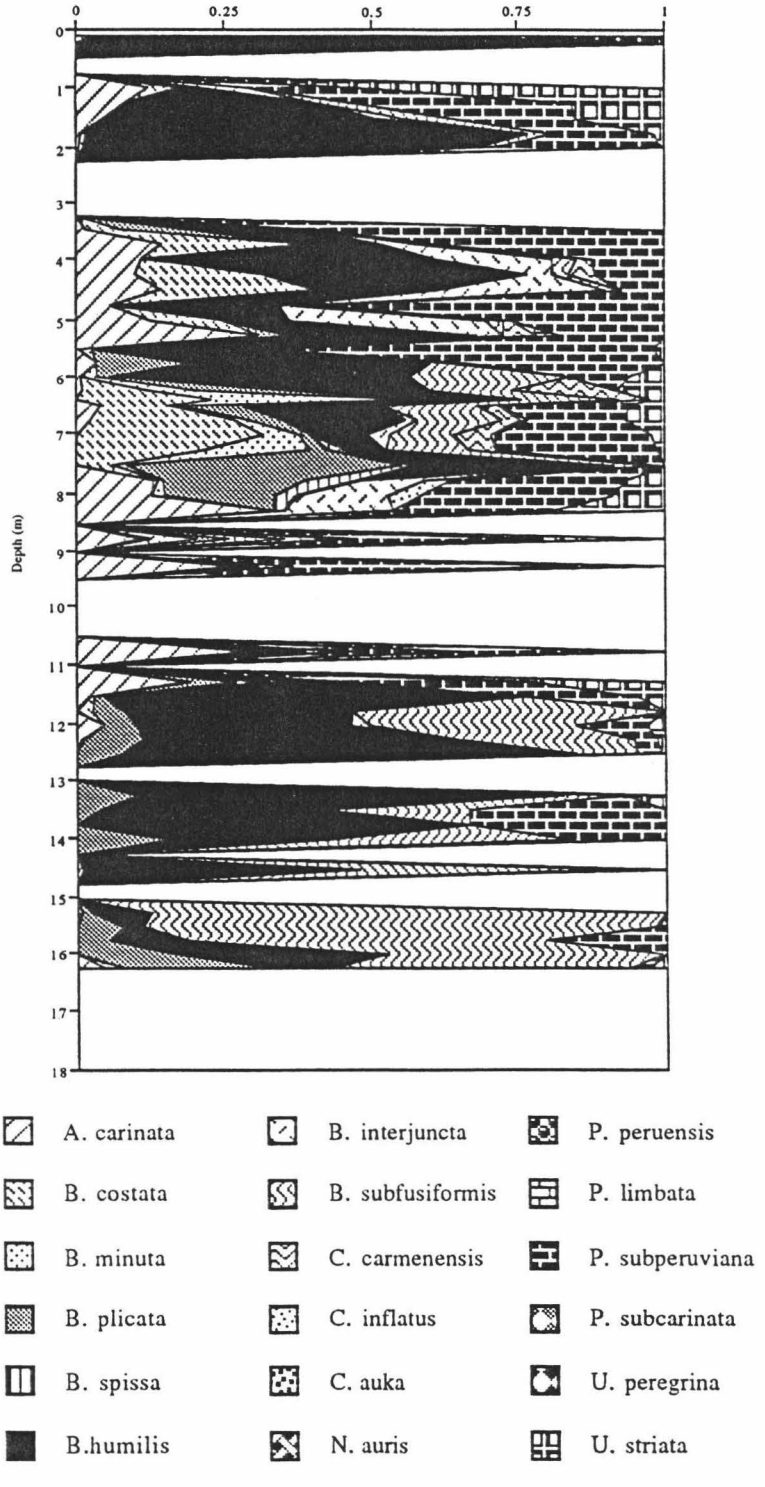

Figure 4.6. Distribution of benthic foraminifera in Hole 679B.

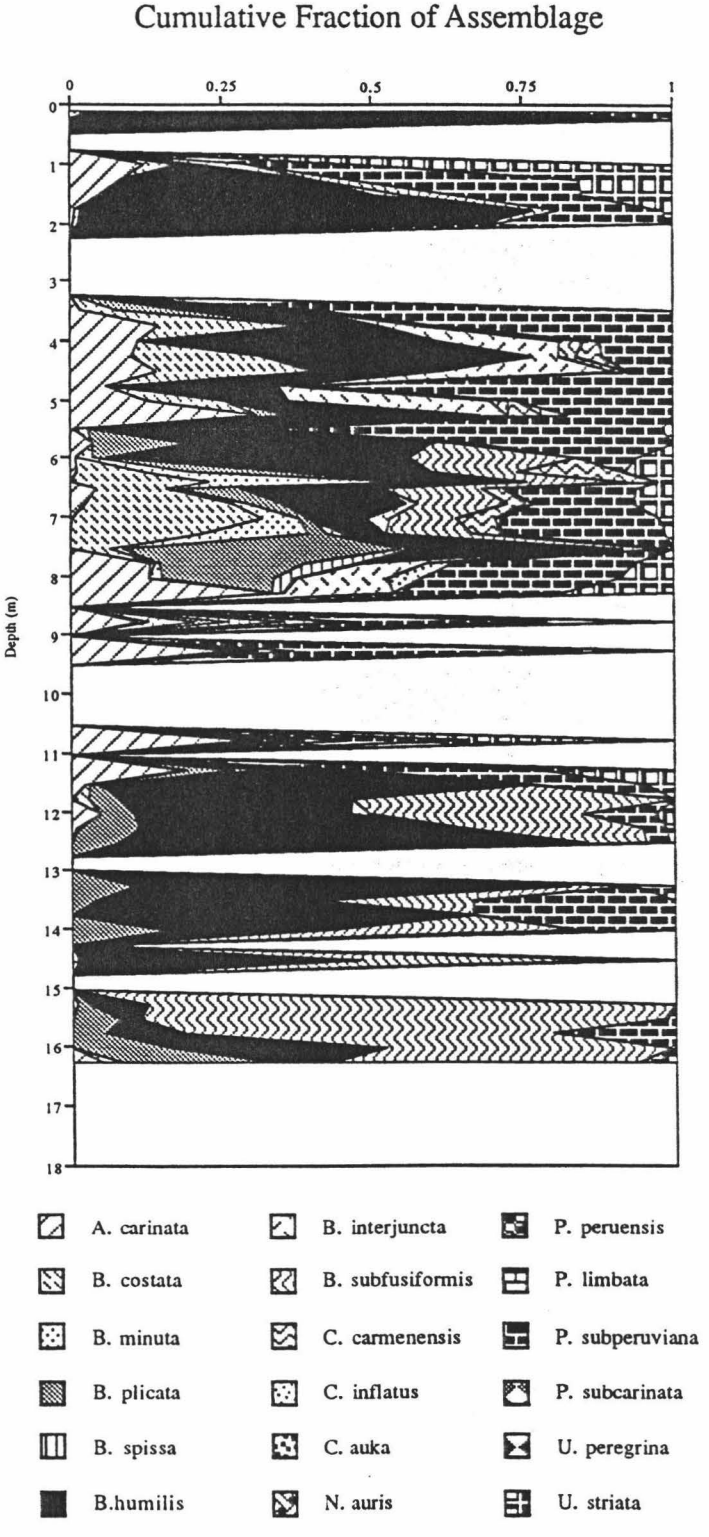

Figure 4.7. Distribution of benthic foraminifera in Hole 680A.

(Fig. 4.8) (assemblage data are summarized in Table 4.2). Due to the highly discontinuous nature of foraminifera preservation in Hole 681A, interpreting environmental changes from assemblages will be of limited value. The assemblages present are largely dominated by *B. costata*, *B. humilis*, and *B. plicata*.

Hole 686A and Hole 687A

The upper 15 m of sediment from Hole 686A was barren of benthic foraminifera. Benthic foraminiferal distribution in the upper 17 m of Hole 687A shows two major assemblages: one dominated by *B. humilis*, and the other dominated by *P. subperuviana* (Fig. 4.9) (assemblage data are summarized in Table 4.3). In the sections dominated by *B. humilis*, appreciable percentages of *B. costata* and *N. auris* are present. The sediments in this core are widely barren of foraminifers. Approximately 11 m of the sediment contained no benthic foraminifera.

Foraminifers Per Gram

Total number of foraminifers per gram dry sediment for Hole 679B and Hole 680A are shown in Figure 4.10. Some sediments show extremely high values e.g., ~8000 at 1.2 m in Hole 679B and ~7500 at 7.75 m in Hole 680A.

Coulometry Results

Organic-carbon

Organic carbon and calcium carbonate weight percent were determined for Holes 679B, 680A, 681A, 686A, and 687A (coulometric data for all ODP cores are summarized in Tables 4.4 through 4.9). Figures 4.11 shows the variation of the weight percent of organic carbon. Table 4.10 summarizes the maximum, the minimum, the mean and the standard deviation of the carbon data for each core. The organic carbon weight percent is

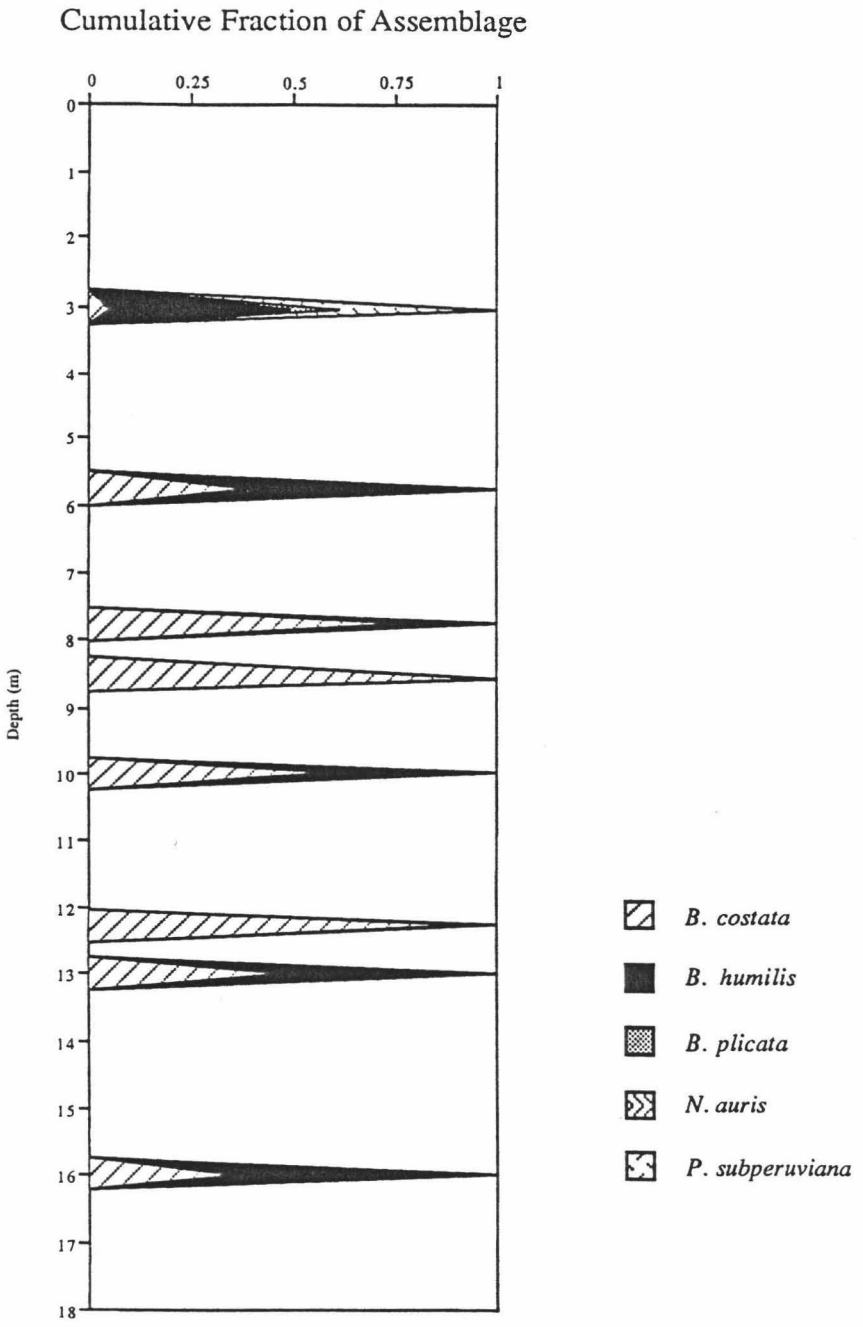

Figure 4.8. Distribution of benthic foraminifera in Hole 681A.

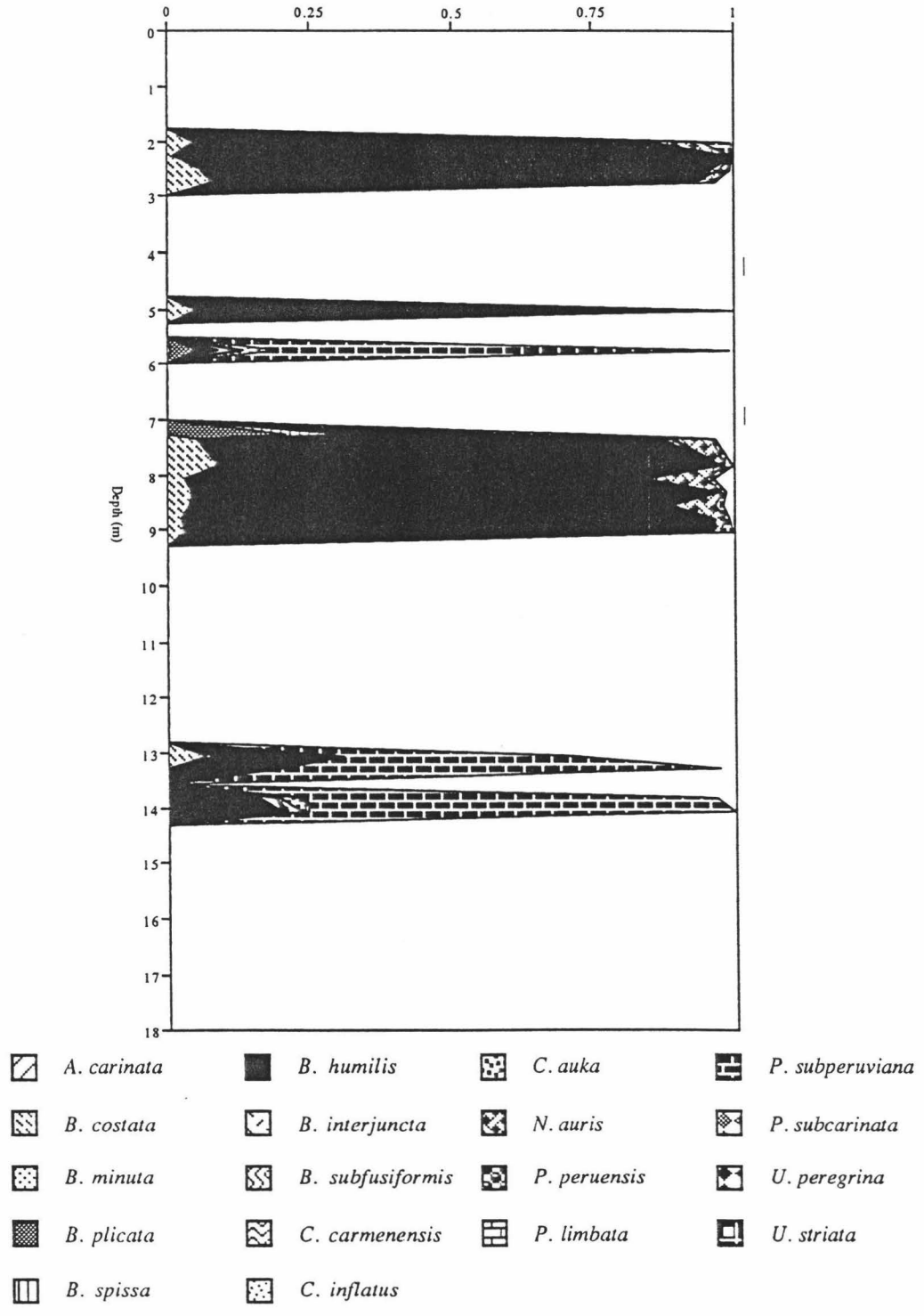

Figure 4.9. Distribution of benthic foraminifera in Hole 687A.

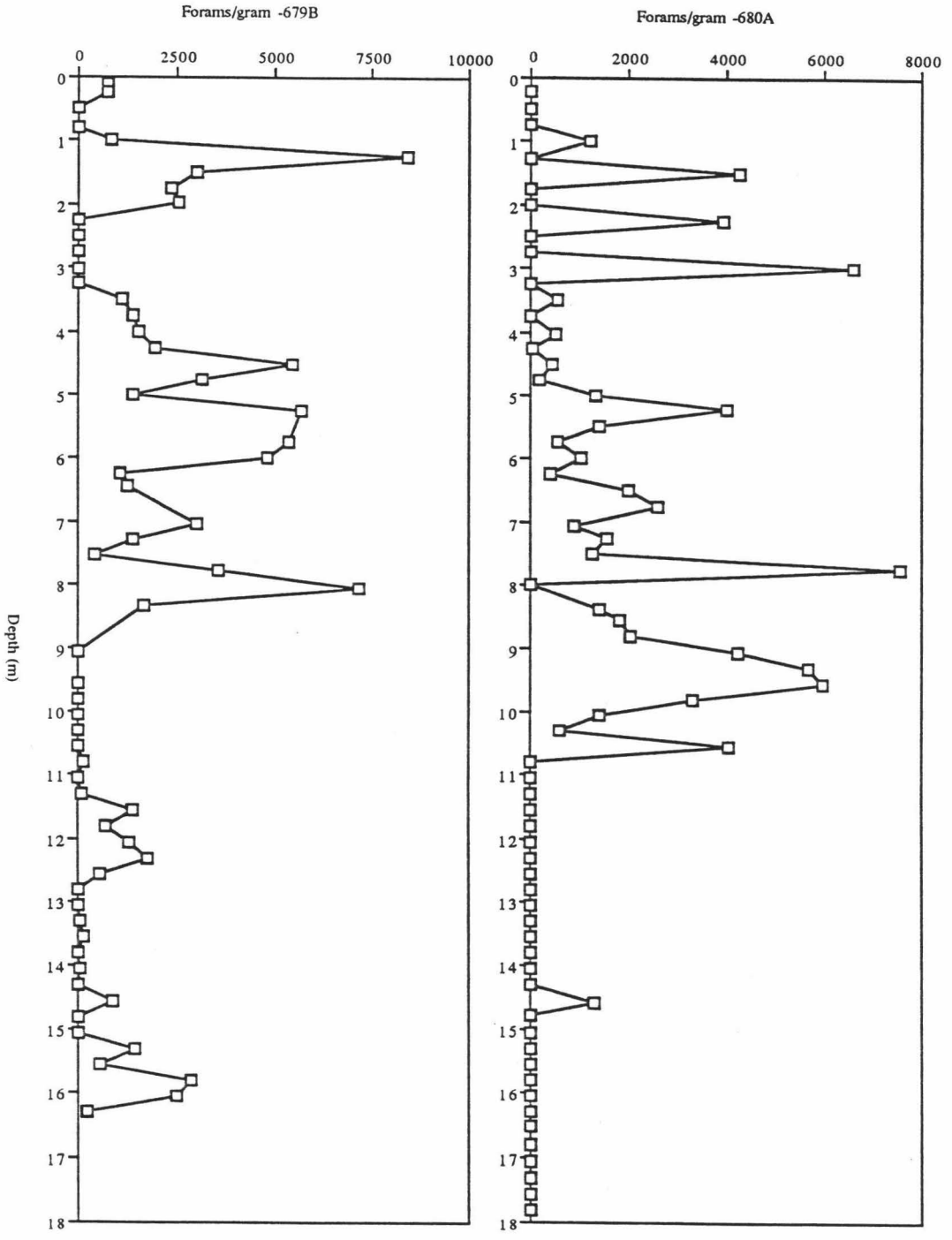

Figure 4.10. Number of foraminifer specimens per gram dry sediment for Holes 679B, and 680A.

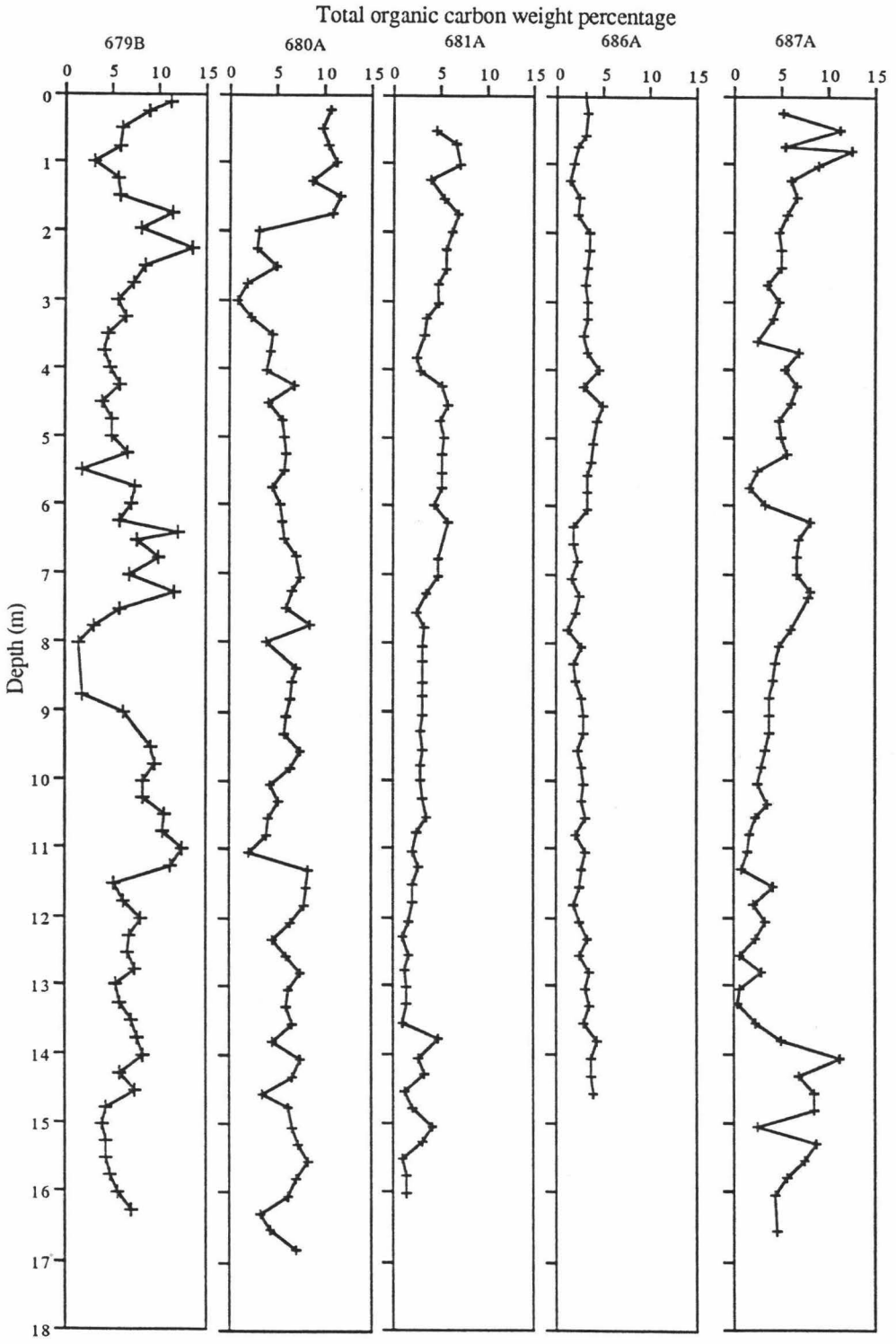

Figure 4.11. Organic carbon weight percents for Holes 679B, 680A, 681A, 686A, and 687A.

very high in all these sediments. Relatively, Holes 679B, 680A, and 687A show higher and more variable values than do Holes 681A, and 686A which have lower and more consistent values.

Sulfur

Sulfur weight percent was determined for Holes 679B and 680A. Figure 4.12 shows the variation of weight percent sulfur with depth. Table 4.11 summarizes the maximum, the minimum, the mean and the standard deviation of the sulfur data. These data are discussed below.

Light Stable Isotope Analysis

The benthic foraminifer *B. humilis* was analyzed for $\delta^{18}O$ and $\delta^{13}C$ throughout Hole 679B (Tables 4.12). Hole 680A did contain sufficient foraminifera to conduct isotope analysis, however, this analysis was not completed because a very detailed oxygen isotope curve has been previously generated for 680B (Wefer et al., 1990; Heinze, 1990) (Fig. 4.13). The isotope curve for 680B will be used for 680A (discussed below). Hole 680B and Hole 680A were drilled 8 m apart (von Huene et al., 1988). The remaining holes, 681A, 686A, and 687A were essentially barren of foraminifera and isotope analysis was, thus, not possible.

Figure 4.14 shows the $\delta^{18}O$ and $\delta^{13}C$ data for the benthic foraminifera *B. humilis* for 679B. Several extended barren intervals interrupt the curve. This lack of data will have a negative effect on glacial stage assignments.

Three samples of *B. humilis* were taken from sediment sample 679B 1H02, 47-52cm and they were analyzed for $\delta^{18}O$ and $\delta^{13}C$. Table 4.13 summarizes the results. The standard deviation of the three analyses was 0.265‰ for $\delta^{13}C$ and 0.144‰ for $\delta^{18}O$. The

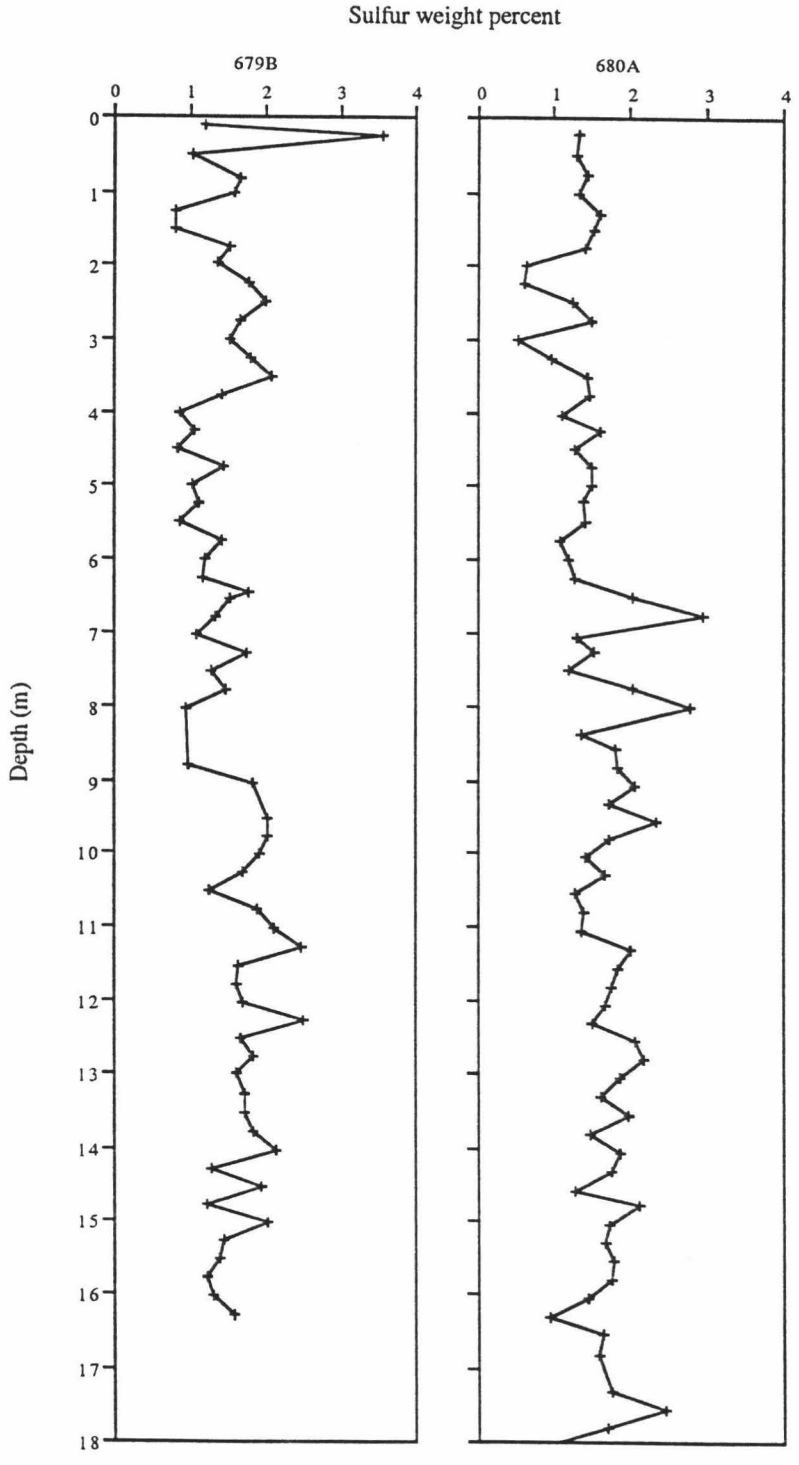

Figure 4.12. Sulfur weight percents for Holes 679B, and 680A.

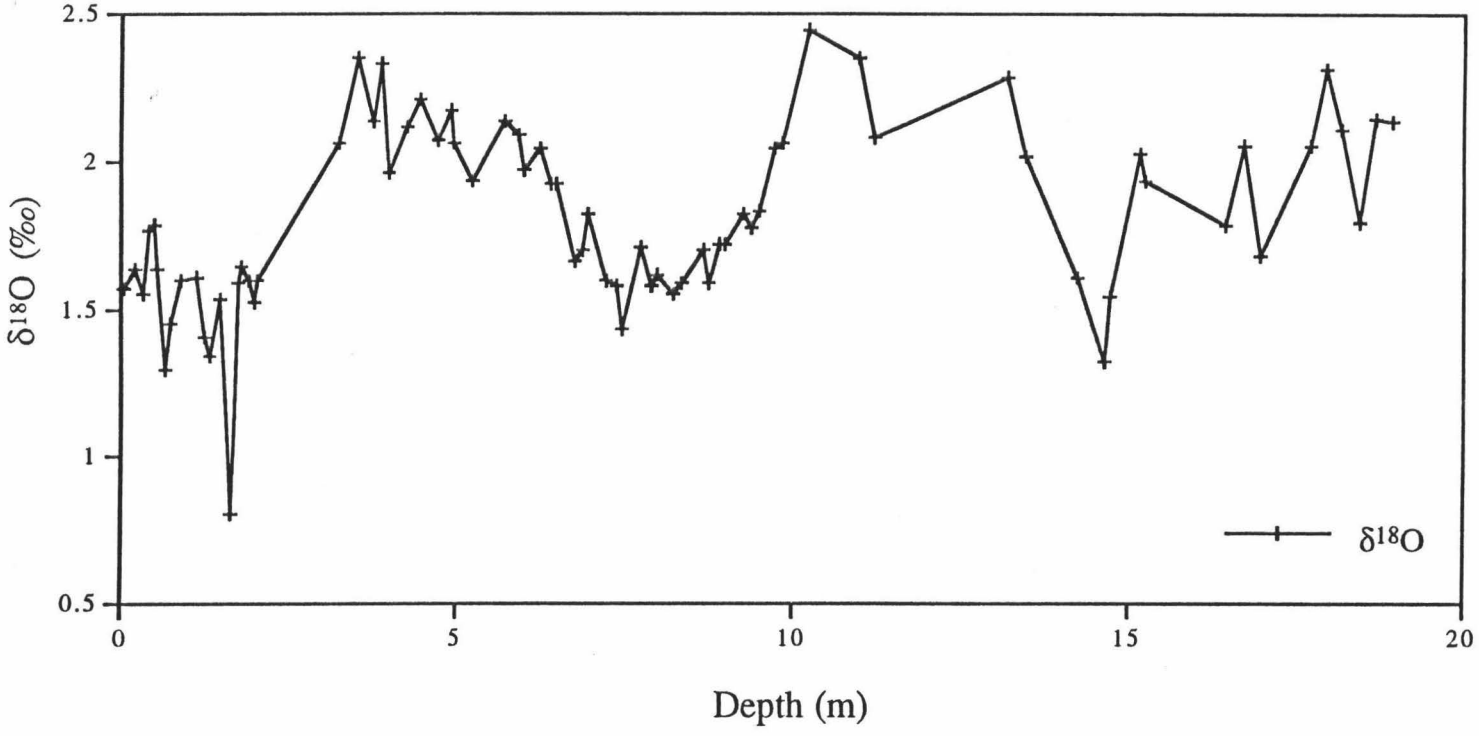

Figure 4.13. $\delta^{18}O$ values for the benthic foraminifer *B. humilis*—Hole 680B (Wefer et al., 1990).

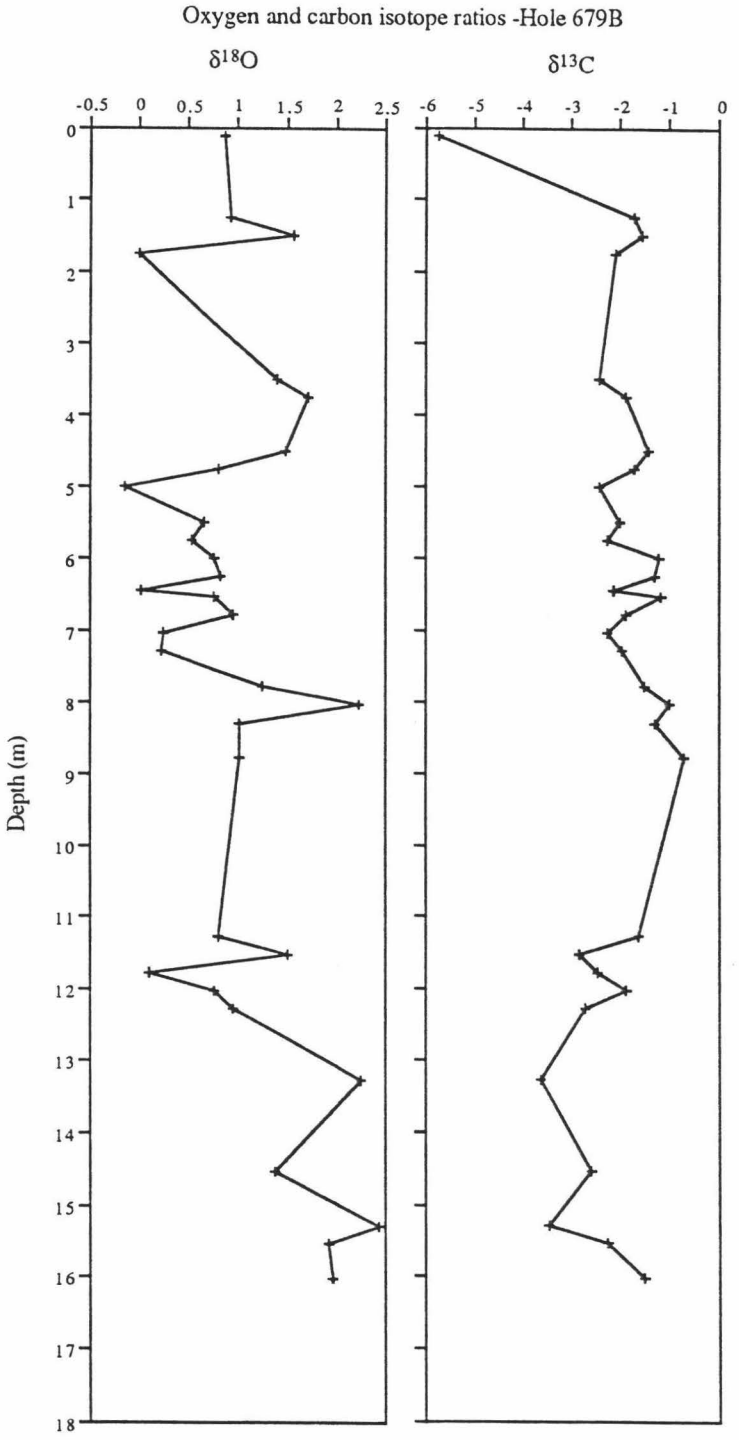

Figure 4.14. $\delta^{18}O$ and $\delta^{13}C$ values for the benthic foraminifer *B. humilis*—679B.

relatively poor reproducibility is likely due to inhomogeneity of the sediment sample. The sediment samples are taken from a 2.5cm vertical section in the ODP cores and this vertical distance can include several hundreds of years of deposition. Benthic foraminifera living at different times and under different isotopic conditions will be present in the sediment samples. A standard sample of NBS-19, analyzed with the foraminifer samples produced values within 0.009‰ of the expected $\delta^{13}C$ value and 0.043‰ of the expected $\delta^{18}O$ value.

Interpretations

Foraminiferal Assemblages - Sea Level Change/Bottom Water Oxygen Levels

In Chapter 3, I concluded that modern foraminiferal assemblages from the Peru coastal margin showed a clear distribution pattern with respect to water depth and bottom water oxygen levels. I determined four basic assemblages that dominate in four different environments with respect to water depth and bottom water oxygen levels (see Fig. 3.24). I apply these four assemblage factors to the benthic foraminiferal assemblages found in the sediment taken from the ODP cores. The foraminiferal population percentages from the cores are projected onto the four factor axes of the four major assemblages. A matrix of the percentage of each foraminifer for each sample in a core is multiplied by the matrix of the significant surface sediment factor loadings. The relative influence of each factor in a given sample is calculated by normalizing the factor scores for each sample by dividing each factor score by the sample vector length in the four dimensional space of the factors so that values range from 0 to 1, with 1 representing perfect coincidence with a factor. Starting at the top of each core and proceeding down, I use the individual strengths of the four factors to qualitatively interpret changes in water depth and changes in oxygen levels for Holes 679B (Fig. 4.15), 680A (Fig. 4.16), 681A (Fig. 4.8), and 687A (Fig. 4.17). These interpretations are made without regard to the $\delta^{18}O$ data for Holes 679B and 680B.

Site 679B

Between 0.5 and 1.5 mbsf there are significant percentages of factor 3 and factor 4 assemblages. This indicates relatively high sea level. Oxygen levels should range between approximately 6 and 20 μMol. Between 3.5 and 5 mbsf factor 2 shows a strong influence in four samples; this is accompanied by a significant decrease in the presence of factor 3 species and an increase in the presence of factor 1 species. I interpret this interval as a time of lowered sea level and very low oxygen levels - between 4 and 6 μMol. Between 2.0m and 3.5m is an interval barren of foraminifers. I infer that at least the lower part of this barren interval represents a stage of sea level decline and the oxygen level was minimum. Between 5 and 6 mbsf there is a strong signal from factors 3 and 4, representing a rise in sea level. Oxygen levels are increasing (>7 μMol). Immediately below this interval, a 1.5 m section shows a very strong presence of both factor 2 and factor 3 species. Although these species are found together in modern sediments, the combination is suspicious. Likely, this interval represents reworked sediment. C. Glenn identified this interval as a possible turbidite. The section from 7.5 to 11 mbsf is consistently dominated by species of factor 3 with a significant presence of factor 4 species. I interpret this to represent a prolonged period of relatively high sea level. Oxygen levels ranged between 7 and 20 μMol. Below this section, the core is dominated by factor 1 species except for two factor 3 spikes at 13.3 and 15.5 m; water depths were relatively high and bottom waters oxygen levels were minimum.

Site 680A

In this core, the presence of species of factor 4 never reaches a significant level in any sample. During maximum periods of maximum sea level the depth at the area should not

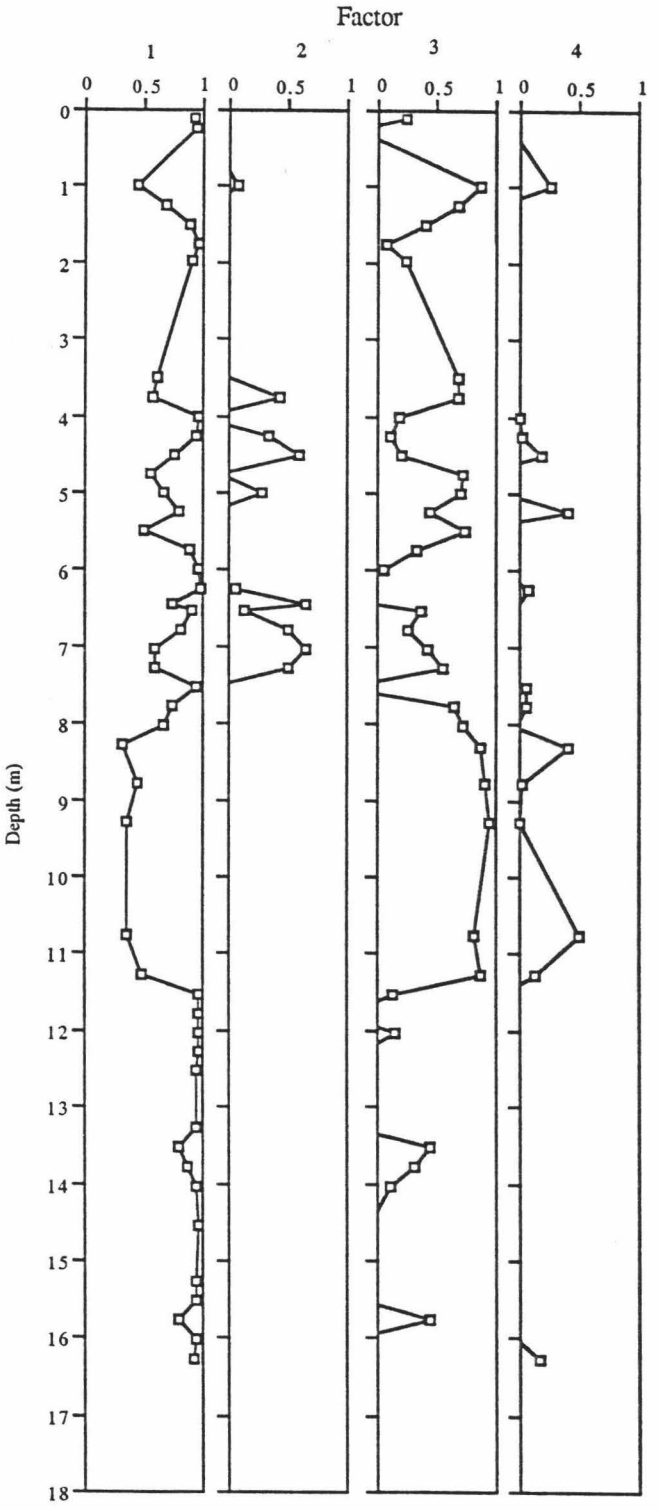

Figure 4.15. Principle assemblage scores for Hole 679B.

be much greater than present depths, which is significantly shallower than factor 4 species environments. I identify two distinct intervals in the core. The interval from 1 to 8.5 mbsf shows alternating spikes of factor 1 and factor 3. This is typical in modern sediments of assemblages found at depths of approximately 300 to 600 m and oxygen levels ranging from 3 to 7 μMol. Between 9 and 10 mbsf there is a significant presence of factor 2 species; I interpret this as a period of lowered sea level -100 to 200m, and low oxygen levels -3 to 7 μMol.

Site 681A

Despite the abundance of barren intervals in Hole 681A, the assemblages present are dominated by factor 2 species with factor 1 species present. The record in the upper section of the site is thus interpreted to have remained at relatively shallow depths (50 to 200m) and to have been consistently bathed in oxygen-deficient waters.

Site 687A

Hole 687A is almost entirely dominated by factor 1 foraminifer species. Water depth have remained in the range of 200 to 300 m and oxygen levels have been very low, 3 to 8 μMol. Two small intervals show deviations from this environment: at 5.75 and 13-14 mbsf there are significant increases in factor 3 species. This may indicate a sea level rise and a small increase in the level of bottom water oxygen.

Foraminifers Per Gram and Current Activity

In Chapter 3, I concluded that current activity may concentrate foraminifera in sediment. A relation exists between the number of foraminifers per gram sediment and some of the phosphorite nodule layers in Hole 679B and Hole 680A. Phosphorite nodules and hard grounds are believed to form under zero or very low net sedimentation rates. To

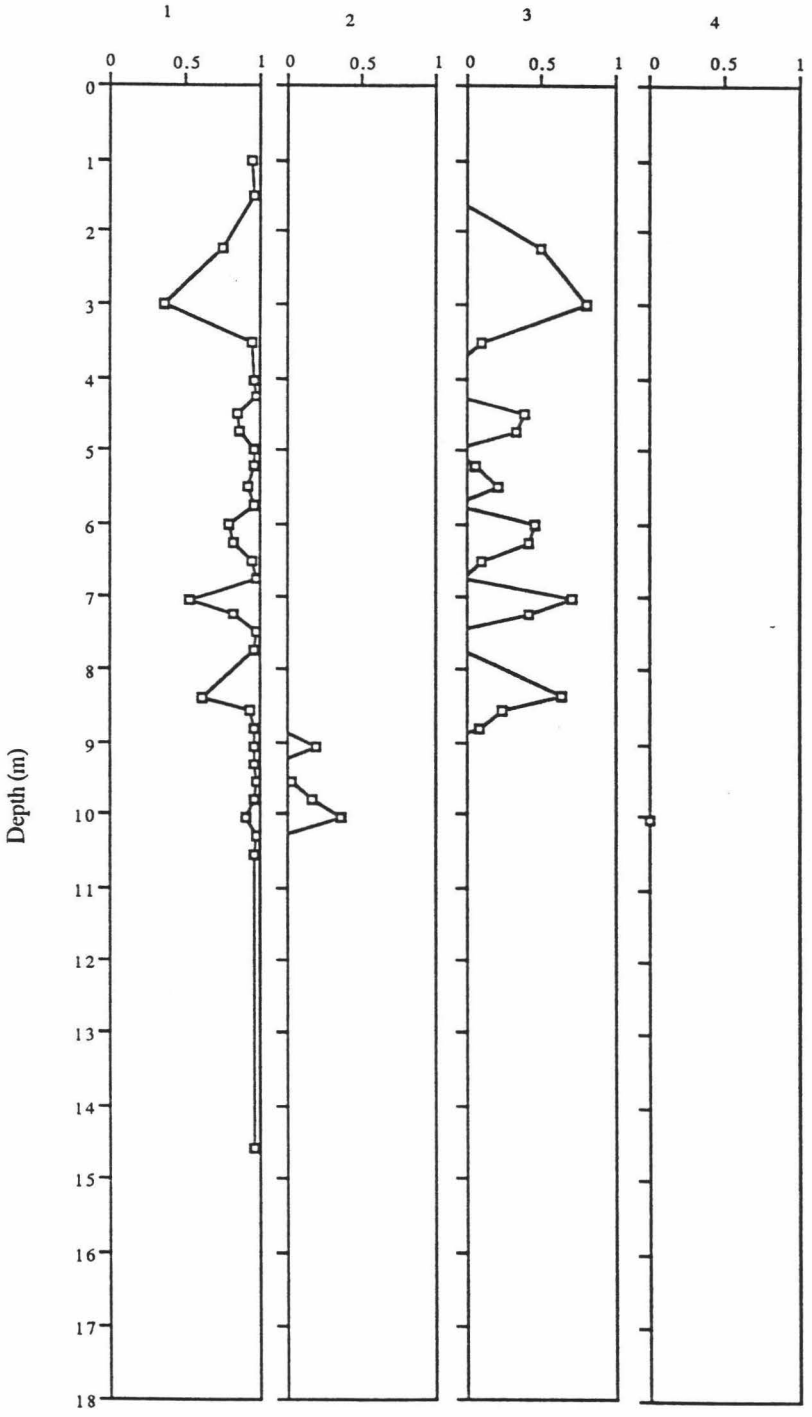

Figure 4.16. Principle assemblage scores for Hole 680A.

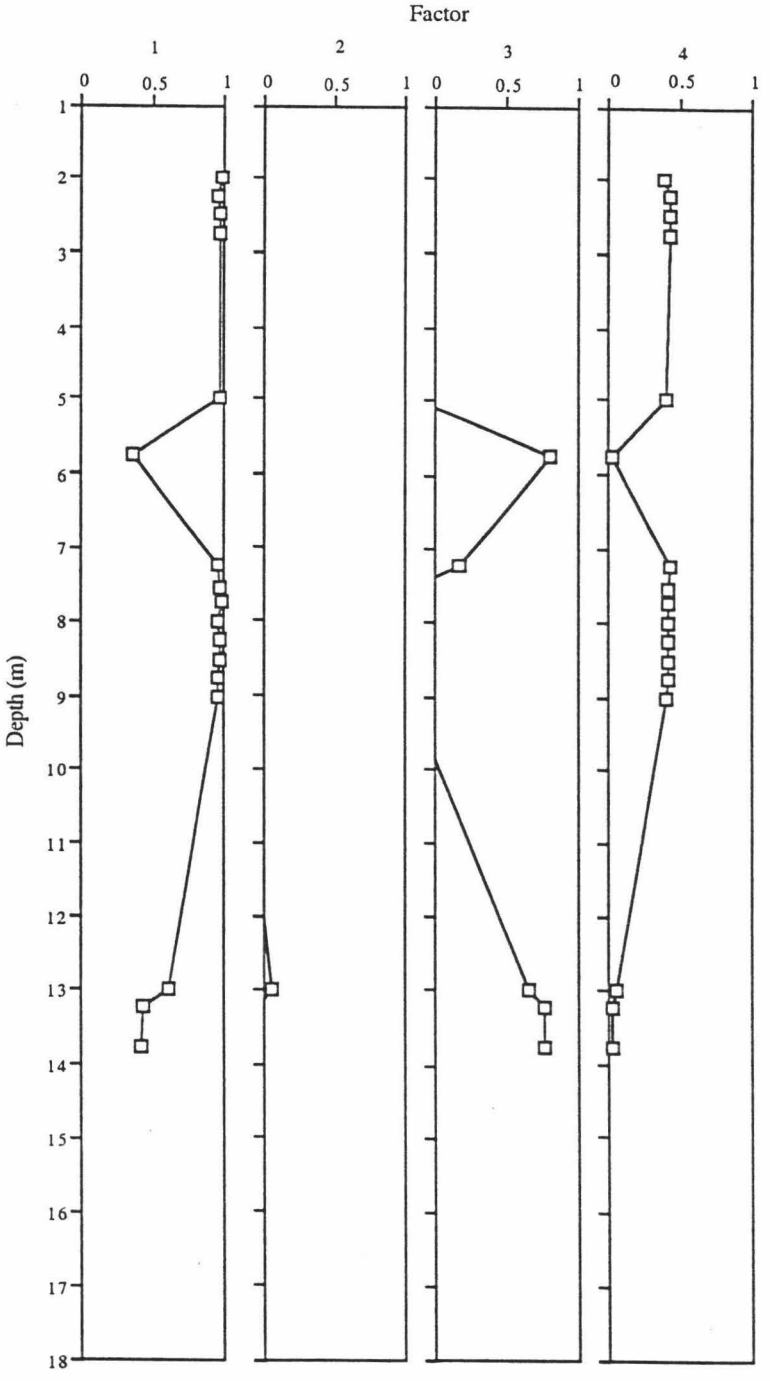

Figure 4.17. Principle assemblage scores for Hole 687A.

grow, phosphatic material must be maintained at a certain depth in the sediment. The most likely mechanism working to reduce sedimentation is bottom current activity. It can be inferred that phosphorite layers represent periods of increased bottom water current strength. At intervals in Hole 679B, the number of foraminifers per gram increases upward in the sediment, reached a maximum near a phosphorite nodule layer, then decreases. This is apparent at 1.2, 4.7, 5.5, 7.0, and 8.0 mbsf (see indicated areas on Fig. 4.18). The increases in foraminifers per gram may be a result of the current winnowing. Several locations with significant phosphorite content do not, however, follow this trend, e.g., at 3.75, 6.3, and 9.0-9.5 mbsf. While current activity may have an effect of the preservation of foraminifers in sediment, from the data I present I cannot conclude that the number of foraminifers per gram is a good representation of current strength.

Age Assignments

Assigning absolute ages to sediments in the ODP cores is important in order to reconstruct the paleoceanography in the area. Ages are necessary to correlate cores, determine sedimentation rates, and detect any temporal shift in upwelling centers. The principal method of assigning age dates to these cores that I will employ is glacial/ interglacial isotope stages determined from $\delta^{18}O$ curves of benthic foraminifera and organic carbon weight percent of sediment. An auxiliary data set of absolute ages of phosphorite samples taken from the cores is also available. I will try to use these ages to better constrain age assignments. In addition, when available, I will use published magnetic stratigraphy and other sedimentation rate data to validate age assignments.

Isotope stage assignment

For the cores recovered form the Peru/Chile Margin, establishing $\delta^{18}O$ stratigraphies is difficult due to the discontinuous preservation of benthic foraminifera in cores. Of the

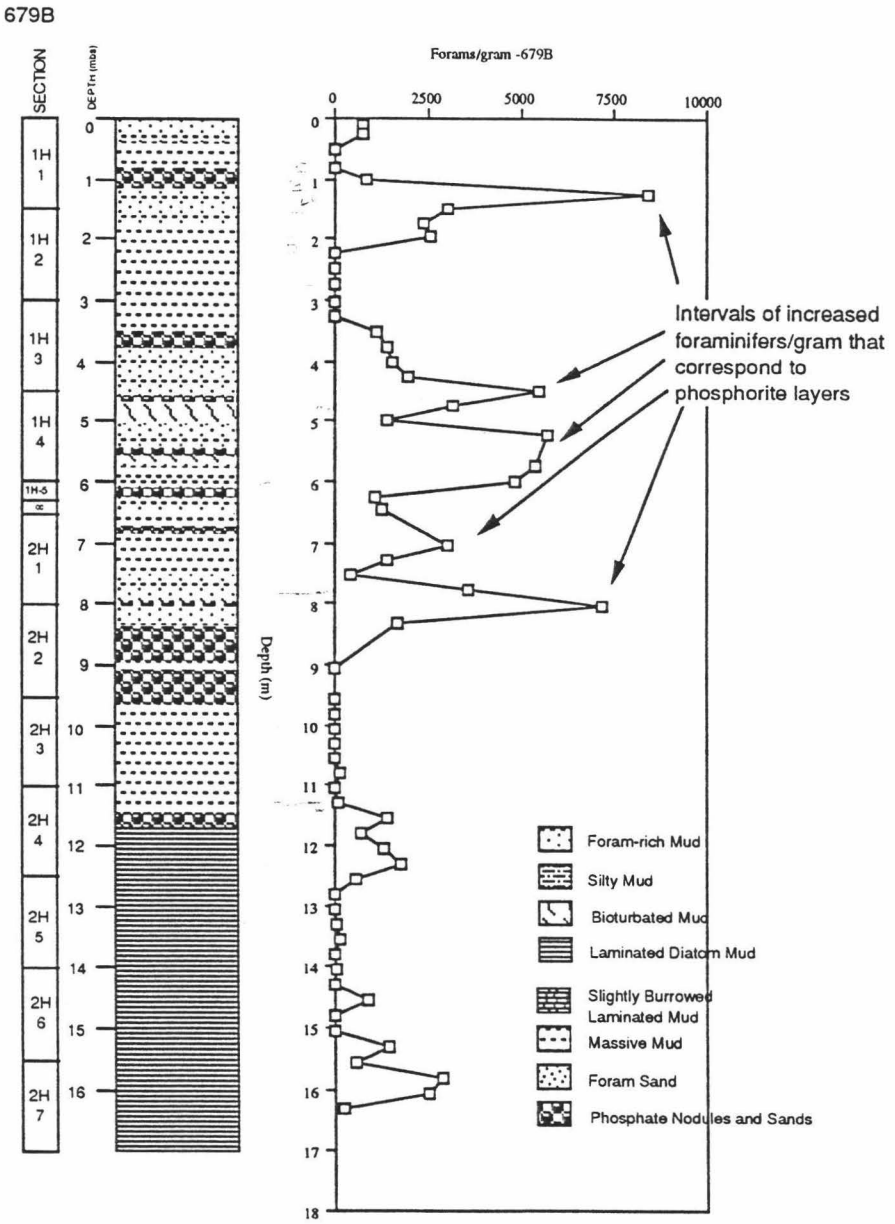

Figure 4.18. Stratigraphic column, Hole 679B, with total benthic foraminifers per gram dry sediment. Several phosphorite beds are characterized by underlying sediment with a significant increase in the number of foraminifers per gram.

cores I have examined, only 680A and 679B contain sufficient foraminifera to justify $\delta^{18}O$ analysis.

Site 680A.

An oxygen isotope curve has been established for Hole 680B by Wefer et al. (1990). These authors had access to a much finer sampling interval in the core than was available to me. For this reason, although Hole 680A did have sufficient benthic foraminifers for $\delta^{18}O$ analysis, I have not generated another $\delta^{18}O$ curve for Hole 680A. Because Wefer et al.'s $\delta^{18}O$ data agree well with the standard curve of Imbrie et al. (1984) I accept their isotope stage assignments for 680B and I transfer these to Site 680A through comparison of the organic carbon weight percent curves. Figure 4.19 shows the organic-carbon weight percent curve for 680B (Wefer et al., 1990) with these researcher's oxygen isotope stage assignments and the organic carbon weight percent curve for Site 680A. The overall shape of the two organic carbon curves is similar. I transferred the Wefer et al. (1990) oxygen isotope stages from Site 680B to Site 680A through visual correlation of the two organic carbon curves. Figure 4.19 shows the cross plotted organic carbon content values for the two holes based on my correlation. The correlation coefficient (r^2) for the plot is 0.484.

Site 679B.

Sufficient benthic foraminifers were present in Hole 679B to develop a $\delta^{18}O$ curve. However, several significant barren intervals exist in the core and these make the assignment of isotope stages somewhat tenuous. $\delta^{18}O$ data from Hole 679B is compared to the $\delta^{18}O$ curve from Hole 680B (which is used as a reference) and to the foraminifera factor analysis results described above; the latter were used to indicate sea level changes and can thus be used here as a further guide in establishing glacial stages (Fig. 4.20). The

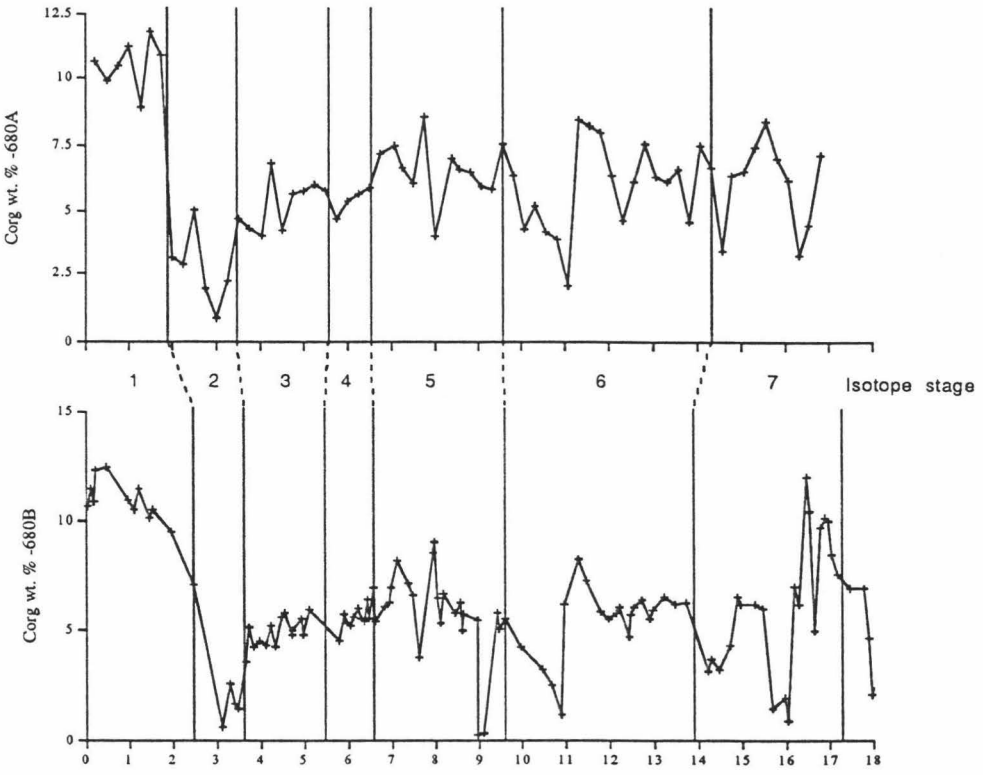

a)

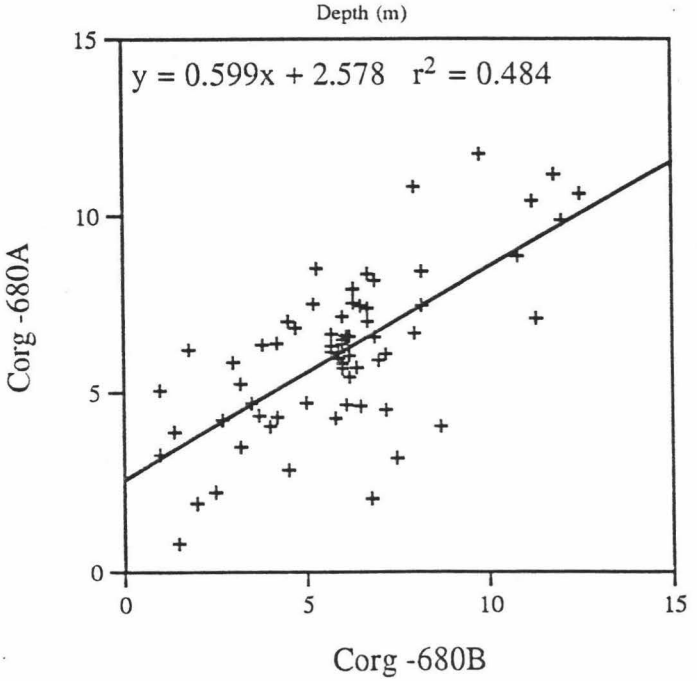

b)

Figure 4.19. a) Organic carbon weight percent curves of Holes 680A and 680B. 680B data and isotope stages from Wefer et al., 1990. Isotope stages are transferred from 680B to 680A through visual correlation. b) Cross plot of Corg data.

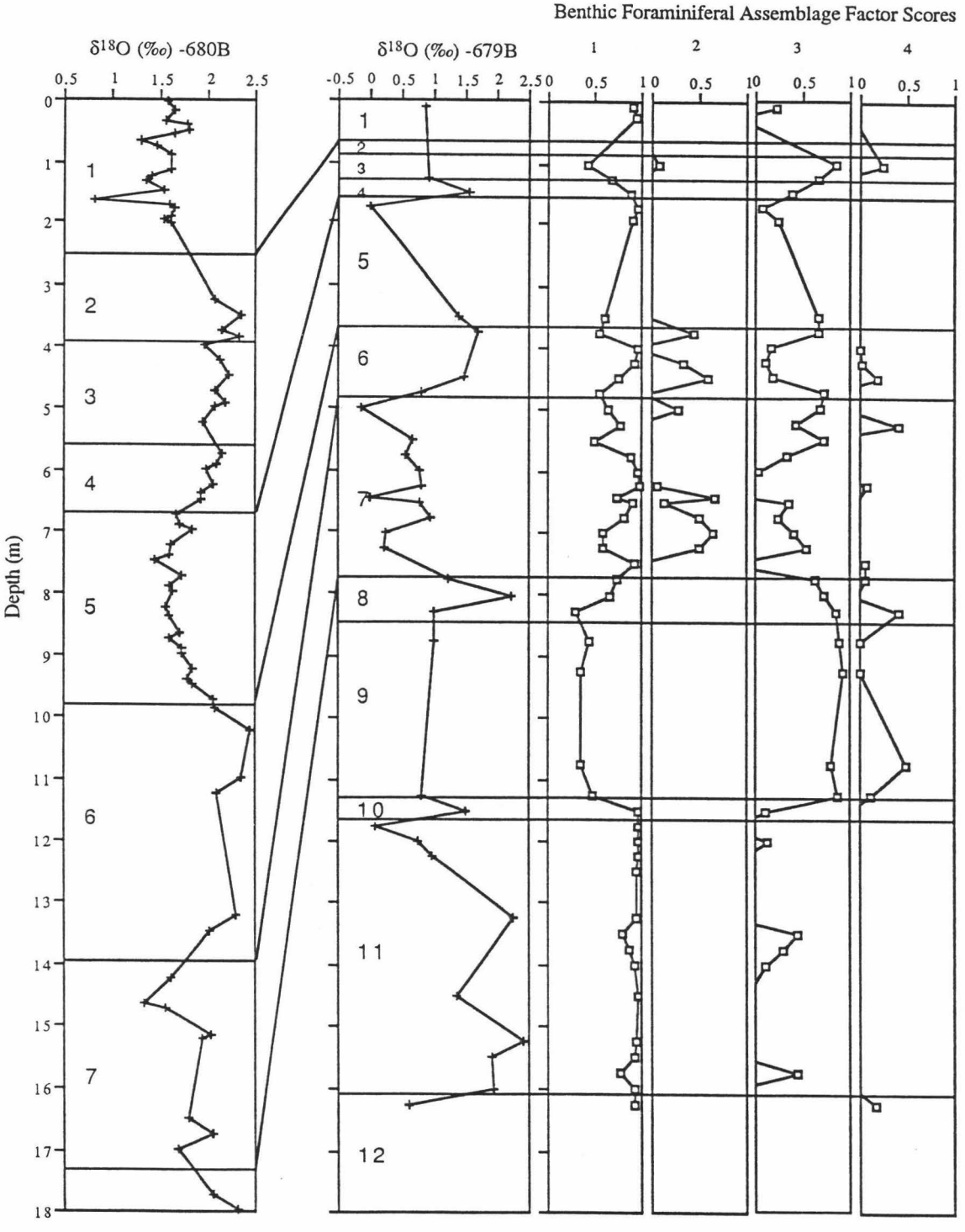

Figure 4.20. Comparison of the $\delta^{18}O$ curve of Hole 679B with the $\delta^{18}O$ curve of 680B and the benthic foraminiferal assemblage scores of Hole 679B.

most developed interval in the $\delta^{18}O$ data in Hole 679B is between 3.5 and 8.5 mbsf. In this interval we see relative high values (between 3.5 and 4.75m) followed by an extended period of low values (between 4.75 and 7.25m) followed by a short interval of high values (between 7.25 and 8.5). With respect to depth, this interval best matches with stages 4, 5 and part of 6 in Hole 680B. This correlation would require sedimentation rates in both cores to be quite similar as the intervals are at similar depths. However, I believe sediment accumulation rates are not similar in these two sites. Site 680 lies at the center of the high productivity zone while Site 679 lies at the distal edge of high productivity zone. Hole 679B also shows many phosphorite nodule layers and beds. These phosphorite bodies may indicate erosional surfaces and winnowing/scouring by ocean currents (Glenn et al., 1994). Fewer erosional surfaces are found in Hole 680A. Silicoflagellate stratigraphy in Hole 679B indicates a sedimentation rate for the upper 37 m of sediment of approximately 2 cm/ky (Martini, 1990). The sedimentation rate over the same interval in Hole 680B is approximately 6.7 cm/ky (Wefer et al., 1990). Due to the lower sedimentation rate, I choose to correlate the $\delta^{18}O$ data from 3.5 to 8.5 mbsf in Hole 679B to a lower section in Hole 680A at 10 to 19 mbsf corresponding to stages 6, 7, and 8. The interval between 8.5 and 11.25 mbsf in Hole 679B is barren of *B. humilis*, the species used for isotope analysis. Due to the lack of $\delta^{18}O$ data, I rely only on the foraminiferal assemblage data to indicate glacial or interglacial conditions. The foraminiferal data indicate increased water depths for this interval. I conclude that this represents an interglacial period and I correlate it to stage 9. There is a short upward spike at 11.5 mbsf; I assign this general area to stage 10, a relatively short stage. Below this region the interpretation becomes difficult. The sediment in this part of the core should belong to stage 11, which is a relatively long stage. The $\delta^{18}O$ values from this section, however, are relatively high indicating a glacial stage. The lithology of this section does not indicate extensive erosion. Considering that stage 11 is, relatively, an extremely long stage and that there is no sign of erosion, I consider it unlikely that the stage would be

entirely missing from the sediment record. In spite of the conflicting data, I tentatively assign this general area to stage 11. At 1 mbsf, foraminiferal data indicate a sea level rise. Lacking $\delta^{18}O$ data, I tentatively place stage 3 here. The relatively high $\delta^{18}O$ value immediately below is assigned to stage 4.

Due to the lack of benthic foraminifera in Holes 681A, 686A, and 687A it will not be possible to assign glacial stages by oxygen isotope stratigraphy. Below, I evaluate a method of using the organic carbon curve as a proxy for the oxygen isotope curve and using the organic carbon curve to assign glacial stages.

Organic carbon weight percent curve as a proxy for the $\delta^{18}O$ curve

Wefer et al. (1990) observed a correlation between the oxygen isotope curve and the organic carbon weight percent curve in Hole 680B, and 686B. They advanced the hypothesis that the organic carbon weight percent curve, used as a proxy for the $\delta^{18}O$ curve, may be suitable for assigning isotope stages. I briefly summarize their results. In general, higher organic carbon values are found in laminated sections. In these sections a higher organic carbon flux promoted oxygen depleted conditions which prohibited habitation by burrowing infauna. Conversely, lower organic carbon values are found in bioturbated sections where oxygen levels would have been higher (see visual core descriptions, Shipboard Scientific Party, 1988). The maxima themselves are sharply subdivided by short intervals of low organic carbon contents. Sections having high organic carbon content exhibit low $\delta^{18}O$ values and vice versa. In Hole 686B, below 120 m, the distribution of organic carbon shows two well-developed maxima bracketed by one minimum, as observed in the oxygen-isotope distribution (Fig. 4.21), Specifically in this interval, but generally throughout the core, the organic carbon maxima coincide with interglacial oxygen-isotope stages, while the minima correspond to glacial stages. The correlation between interglacial stages, as indicated by low $\delta^{18}O$-values, and the weight

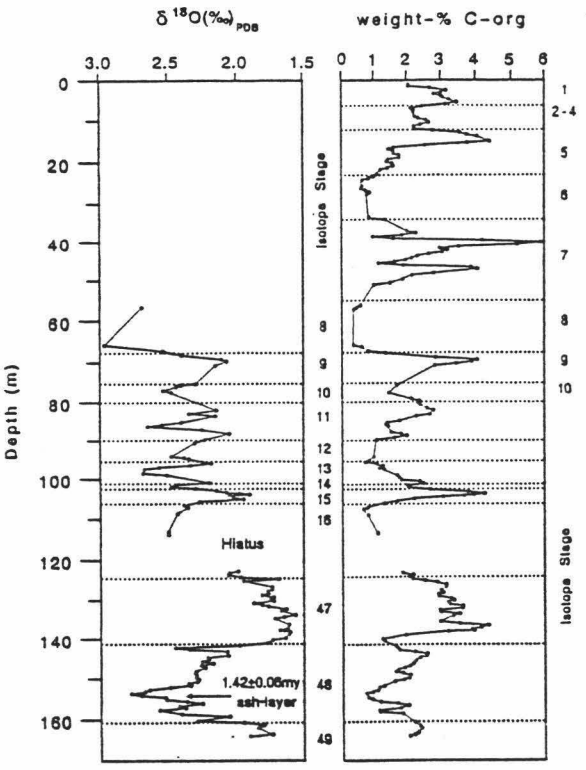

a)

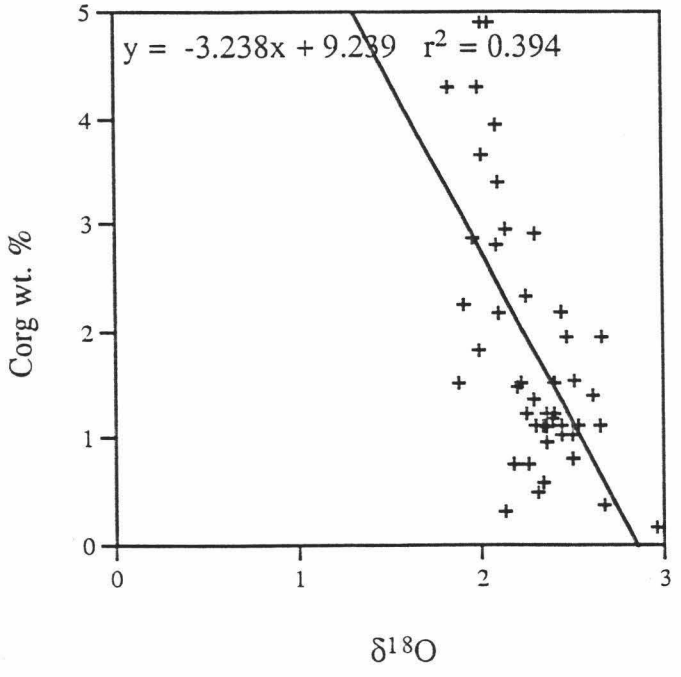

b)

Figure 4.21. a)$\delta^{18}O$ and organic carbon weight percent for Hole 686B (from Wefer et al., 1990). b) Cross plot of data.

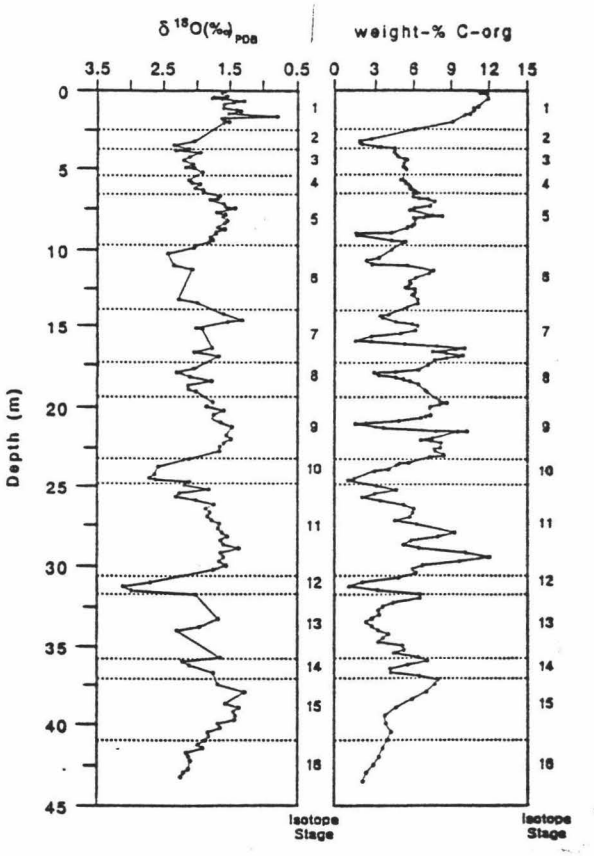

a)

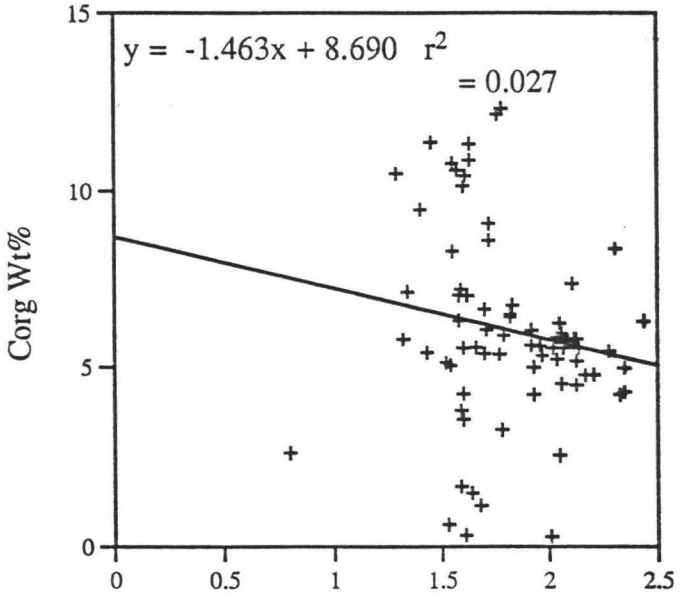

b)

Figure 4.22. a) $\delta^{18}O$ and organic carbon weight percent for Hole 680B (from Wefer et al., 1990). b) Cross plot of data.

percent of organic carbon was clearly observed in the interval between 57 and 85 m. Isotope stages 1 to 15 could be, thus, tentatively identified from the organic carbon contents. While these curves do show similarities there does not seem to be a statistically significant relation between $\delta^{18}O$ and organic carbon percent. Figure 4.21 shows the cross plot for $\delta^{18}O$ and organic carbon percent for Hole 686B. The correlation coefficient for these data is 0.394.

The same similarity between $\delta^{18}O$ and organic carbon percent was found for the upper 40 m of Hole 680B. Figure 4.22 shows the two curves and the cross plot of the data. As with the data for Hole 686B, the curves do show a similarity but there is no statistically valid correlation ($r^2 = 0.027$). Wefer et al. (1990) acknowledged that the stratigraphy resulting from observed correlation between $\delta^{18}O$ and organic carbon is tenuous.

The $\delta^{18}O$ and organic carbon data presented above for Holes 686B and 680B did not show a statistically significant correlation, nonetheless the data curves do show similarities in shape that appear related to one another.

Justification for correlating holes by organic-carbon weight percent

A major assumption in using organic carbon wt.% to assign glacial stages and subsequently absolute ages to sediments is that organic carbon preservation is affected in equal proportion throughout the entire area, i.e., sediments at all sites have simultaneous higher and lower organic carbon preservation rates. This cannot be taken for granted. Shifts in the positions of upwelling centers or variations in the flux of terrigenous or other non-organic material could dilute or enhance the organic carbon wt.% at a particular site. These phenomena do not necessarily have to affect the entire region equally.

Some evidence suggests that changes in productivity are not local events, but rather they affect the entire region. Schrader (1992) has estimated primary productivity for Hole 680B and 681A through evaluation of diatom assemblages. Schrader estimated the

primary production of Hole 680B for the last 400,000 yr representing oxygen isotope stages 1 through 11. He found decreased paleo-production during oxygen isotope stage 3, 4/5 and 5e and concluded that it is a clear indication that periods of relaxation of productivity are not related to periods of major sea-level change, and thus not to a relocation of the upwelling centers away from their present location at Sites 680 and 681. In the event that the decreases in productivity were related only to lowering of sea level during stage 4/5 at the shallow shelf location, then the deeper Site 686 should not have been subjected to the same phenomena. This is not observed. The sedimentary sequences recovered from the shelf and the upper slope at 11° and 13° S off the Peruvian coast, show good correlation between the various diatom indices. These simultaneous changes in productivity indicators during glacial and interglacial stages show that changes in productivity affect the entire area. Simultaneous recording of productivity changes over the entire area is essential for developing a method that uses a productivity indicator (in this case organic-carbon content (Schrader, 1992)) to correlate and assign isotopic stages to cores. Establishing this criterion, however, does raise a complication. A major assumption for using the organic-carbon content as a proxy for $\delta^{18}O$ is that the two track each other i.e., production is reduced during glacial stages and increased during interglacial stages. If changes in productivity are independent of sea-level change, the organic-carbon content should not follow changes in the $\delta^{18}O$ record. This apparent incompatibility can be resolved by noticing that although high and low productivities are observed in both glacial and interglacial stages, diatom assemblages indicate that, in general, higher productivity does occur during interglacial periods and lower productivity does occur during glacial periods (Schrader, 1992). For this reason we may see a correlation (although not perfect) between organic-carbon content and $\delta^{18}O$, as explained further below.

Comparison of $\delta^{18}O$ and organic-carbon weight percent from Hole 679B

I compare the $\delta^{18}O$ curve and the organic carbon weight percent curve for Hole 679B. Figure 4.23 shows the two curves and the cross plot of the data. As with the data from Hole 680B and 686B, the two curves do have similar shapes, however, the relationship is not statistically valid. The correlation coefficient for the data is 0.230.

Age Assignments for 681A, 686A, and 687A

The analysis of the relation between $\delta^{18}O$ and organic carbon percent above did not reveal a statistically substantiated correlation between the two. However, the data do consistently show similarities stratigraphically that do seem to be related to one another. Lacking another method of correlation, I assume that the organic carbon proxy for $\delta^{18}O$ is approximately valid, however, as discussed above, the method is still very subjective.

I visually correlate the organic-carbon weight percent curves of Holes 681A, 686A, and 687A with the organic-carbon weight percent curve of 680B (which I accept as a standard reference) and I assign isotope stages from 680B to the other holes based on the correlation (Fig. 4.24). This visual correlation is not obvious in any of the holes; the organic-carbon curves of the four holes vary significantly from one to another and make a unique correlation impossible. Below I explain in detail my course of reasoning in correlating the holes. First, I identify several intervals in the various curves that do show similarity with one another. In the middle section of each hole (at approximately 5-10m) there is a section (labeled "1" on Fig. 4.24) of relatively high spikes in the curve followed by a steady down-core decrease (arrow on Fig. 4.24) in the organic-carbon weight percent down core. Due to the similar shape I assign this section to the same section as interglacial stage 5 in Hole 680B. At the deepest part of the curve for all the cores the organic-carbon weight percent increases significantly. I assign this general area (labeled "2" on Fig. 4.24) to interglacial stage 7 in each of the curves. Glacial stage 2 shows a very

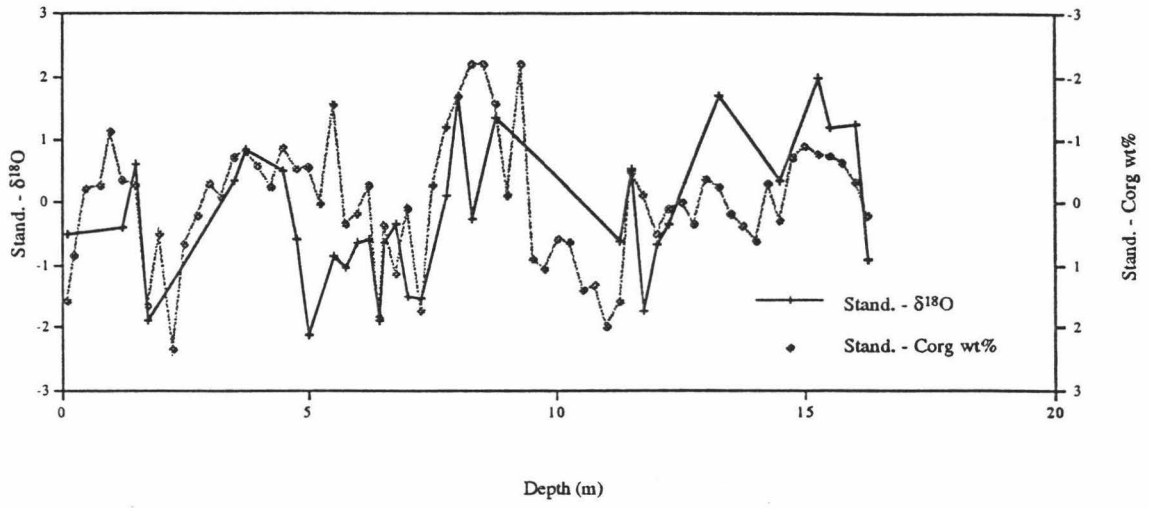

a)

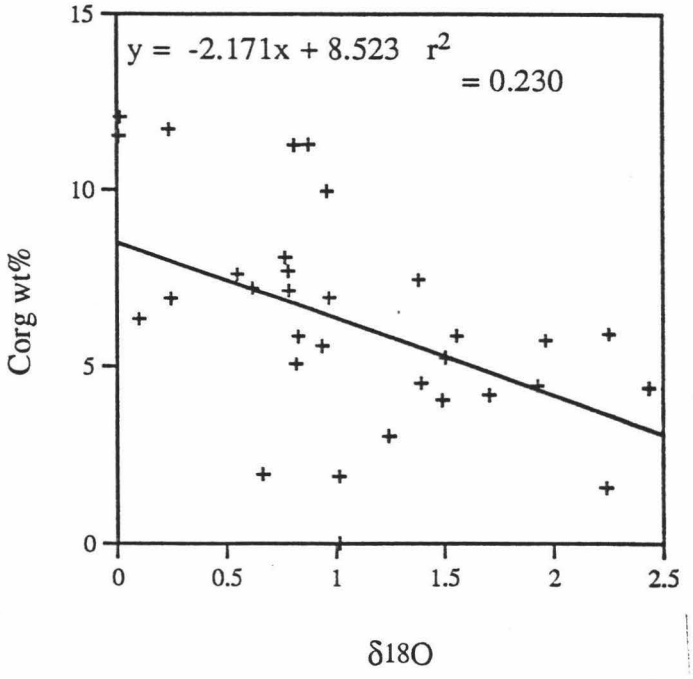

b)

Figure 4.23. a) Comparison of standardized $\delta^{18}O$ and organic carbon weight percent for Hole 679B. Values are standardized by subtracting the average of all the points and dividing by the standard deviation. b) Cross plot of data.

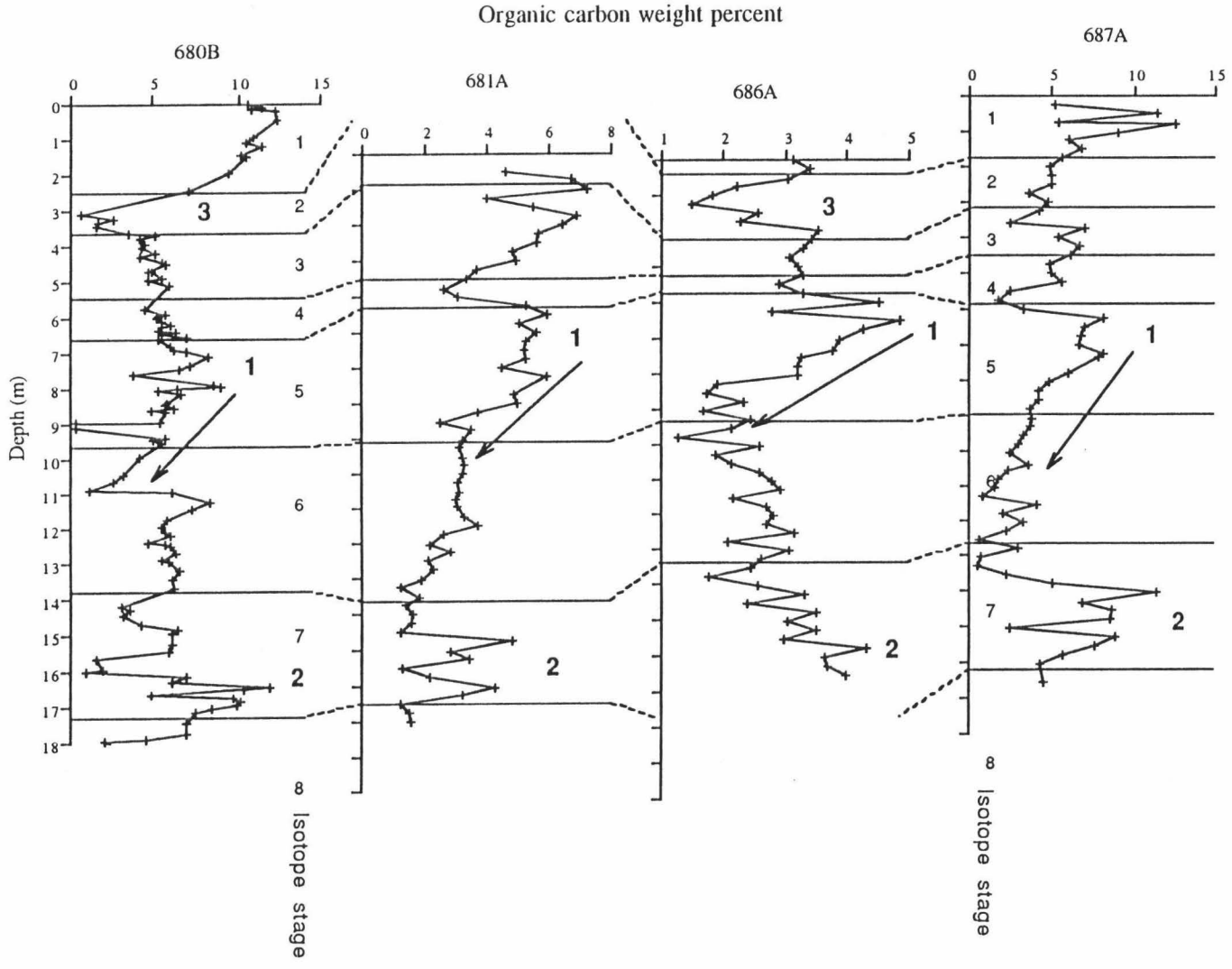

Figure 4.24. Correlation of organic carbon weight percent curves for Holes 680B, 681A, 686A, and 687A.

dramatic decrease in the curve for 680B (labeled "3" on Fig. 4.24). This same decrease is seen in Hole 686A and I assign stage 2 to that interval. No pronounced decrease in Hole 687A and poor recovery of sediment from the top of Hole 681A make stage 2 assignment to those cores more difficult; the top of Hole 681A is believed to be missing sediment from glacial stage 1 (Schrader, 1990b). In Hole 681A, I place the area above the first organic carbon maximum to glacial stage 2. In Hole 687A, I place the section around 2-3m in stage 2 due to the relatively low organic carbon contents. Remaining intervals above stage 2 assignments were subsequently assigned to stage 1. Between stage 2 and 5 the trends in the curves are not well defined. I have tried to assign the generally higher values to stage 3 and lower values deeper in the holes to stage 4. Stage 6 is assigned to the intervals between stage 5 and 7 in each hole. In each hole, the values I have assigned to stage 6 are relatively lower than the surrounding intervals.

I am aware that the correlations I have made and the subsequent assignment of glacial stages are somewhat tenuous. To validate the isotope stages assignments in the holes, I have collected from the literature independently measured sedimentation rates and I compare them to sedimentation rates calculated from my isotope stage assignments, as discussed below. I calculate the overall sedimentation rate of each hole by dividing the length of sediment from the top of the hole to the base of the last complete glacial cycle by the beginning age of the last complete glacial cycle. This overall sedimentation rate is what I compare to other independently determined sedimentation rates. Intervals of erosion will lower the sedimentation rates in some core intervals. These intervals will not seriously affect the comparisons I make because the eroded sections are incorporated in all the sedimentation rate estimates.

In Hole 681A, the Brunhes/Matuyama boundary (0.73my) is identified at 83 mbsf (Shipboard Scientific Party, 1988). This boundary defines a sedimentation rate for the upper 83m of sediment of 114 m/m.y. Schrader (1992) determined a sedimentation rate

of 61.4 m/m.y. based on interpolating ages to Hole 681A from 680B through the comparison of organic carbon and $\delta^{18}O$ curves and adopting the benthic oxygen isotope stratigraphy of Hole 680B (Wefer et al., 1990). The overall sedimentation rate for Hole 681A based on my isotope stage assignments is 58 m/m.y which agrees fairly closely with the value of 61 m/m.y. determined by Schrader, but it is much lower than the rate determined by magnetic stratigraphy (114 m/m.y.).

Sedimentation rates for Hole 686A are at least 160 m/m.y., according to nannoplankton data (Shipboard Scientific Party, 1988). The sedimentation rate calculated from my glacial stage assignments is 58 m/m.y. Schrader and Sorknes (1991) established a correlation between 680B and 686 through analyses of diatom last appearance datums (LAD), mass occurrences of diatom species, peaks and troughs in their diatom-upwelling index, and the shapes of the organic and stable oxygen isotope curves. My isotope stage assignments do not agree with theirs. Their stratigraphy indicates a much higher sedimentation rate (approximately 92 m/m.y.).

For Site 687, sedimentation rates, based on the last appearance datum (LAD) of the diatoms *Rhizonsolenia matuyama* and *Pseudoeunotia doliolus*, are about 65 m./m.y. (Shipboard Scientific Party, 1988). Based on the occurrence of the calcareous nannoplankton, *Cyclococcolithus macintyrei*, the sedimentation rate in the Quaternary at this site has been at least 56 m./m.y. (Shipboard Scientific Party, 1988). My stage assignments indicate a sedimentation rate of 66 m/m.y. and this value agrees very well with the biostratigraphically determined sedimentation rates.

In general, there is some discrepancy among the sedimentation rates. The disagreement is within a factor of two for Site 681 with respect magnetic stratigraphy but is in excellent agreement with Schrader's sedimentation rate (Schrader 1992). The disagreement between my sedimentation rates and the rates of other researchers if slightly greater for Site 686. Site 687 shows very good agreement among the sedimentation rates. I

conclude that my glacial stages are placed within reason, that is, they are not many orders of magnitude different from independently derived ages.

Dating of Phosphorites from Cores

Several phosphatic nodules and sediment samples from Holes 679B, 686A, and 687A have been dated by W. C. Burnett and colleagues at The Florida State University using uranium-series radionuclide analyses (Table 4.15, unpublished). These age dates are compared to the isotope stage age assignments I determined by $\delta^{18}O$ and organic-carbon weight percent above.

Figure 4.25 shows the depths and the ages of the phosphatic samples and isotope stage ages in Hole 679B. The ages of the phosphatic samples do not reveal a simple pattern, nor do they correspond well to the isotope stages. Figure 4.26 shows the depths and the ages of the phosphatic samples and isotope stage ages in Hole 686A. The ages of phosphatic samples are in serious disagreement with isotope stage ages. Figure 4.27 shows the depths and the ages of the phosphatic samples and isotope stage ages in Hole 687A. The ages of phosphorites in this core show better agreement with isotope stage ages than in 686A but there still remain major discrepancies. Most notable is the sample dated 236 ky found at approximately 0.9m depth.

In general, ages of the phosphatic samples do not correlate well with the assigned isotope stage ages and they often show a complicated pattern of distribution, such as older samples found well above younger samples. The non-contemporaneous nature of phosphorite nodules with surrounding sediments is consistent with the modern surface phosphorite data discussed in the Chapter 3. Due to the large discrepancy between the two age assigning methods the results indicate that the absolute ages of these phosphatic sediments are not useful in this work in assigning ages to the cores.

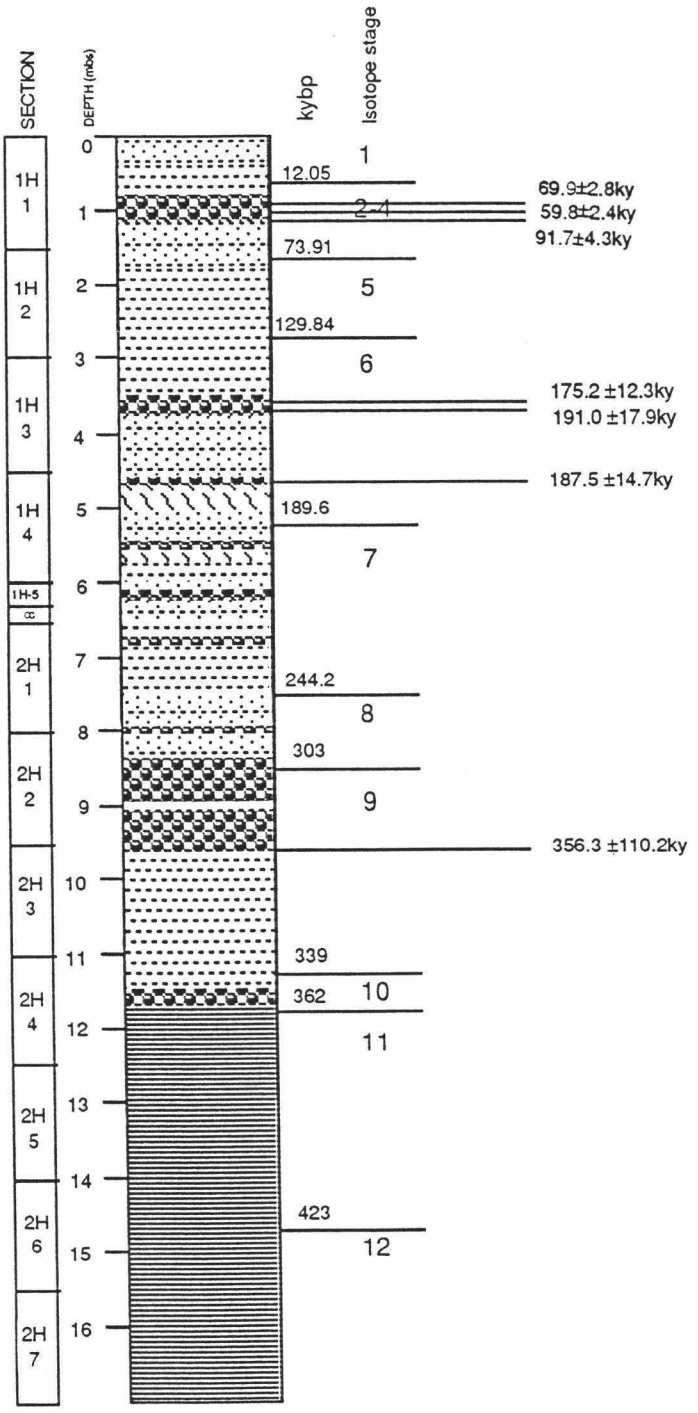

Figure 4.25. Ages of phosphorite samples in Hole 679B.

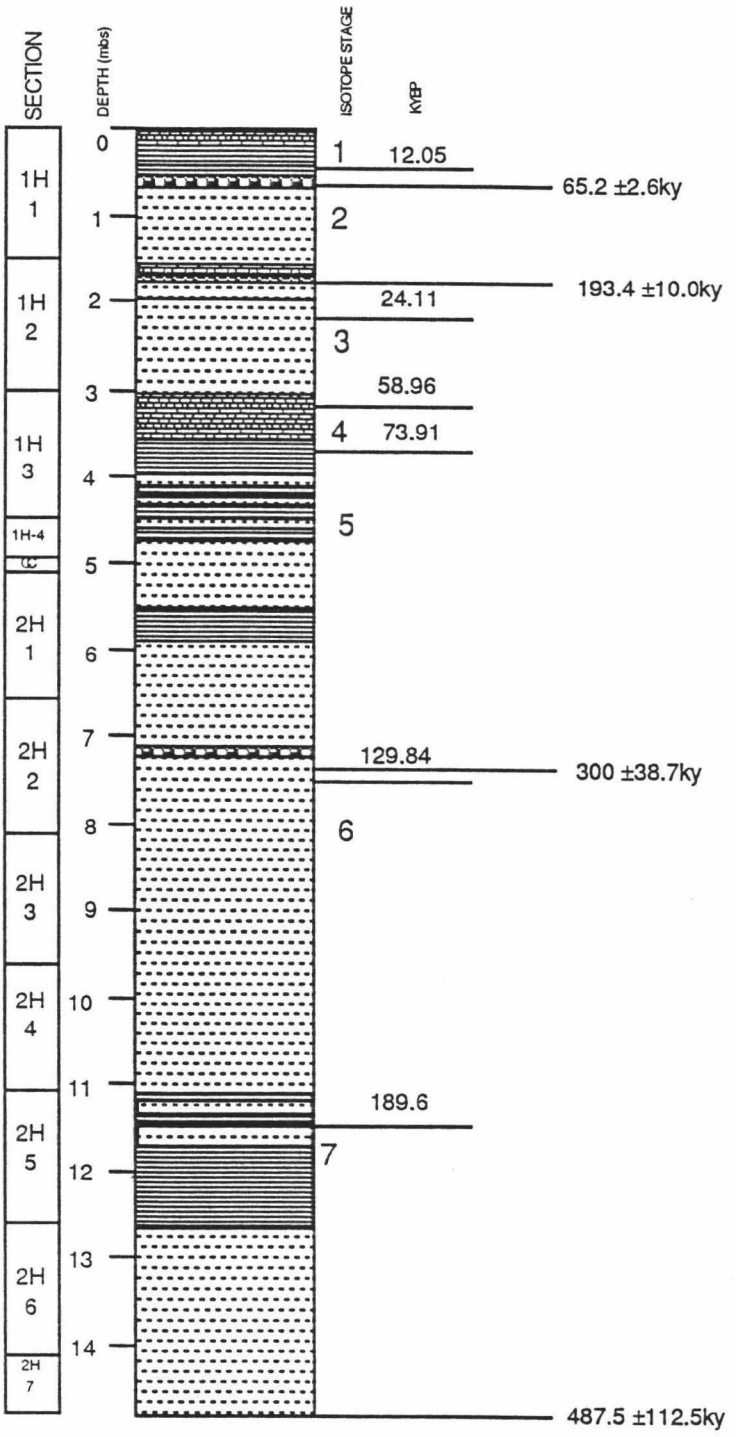

Figure 4.26. Ages of phosphorite samples in Hole 686A.

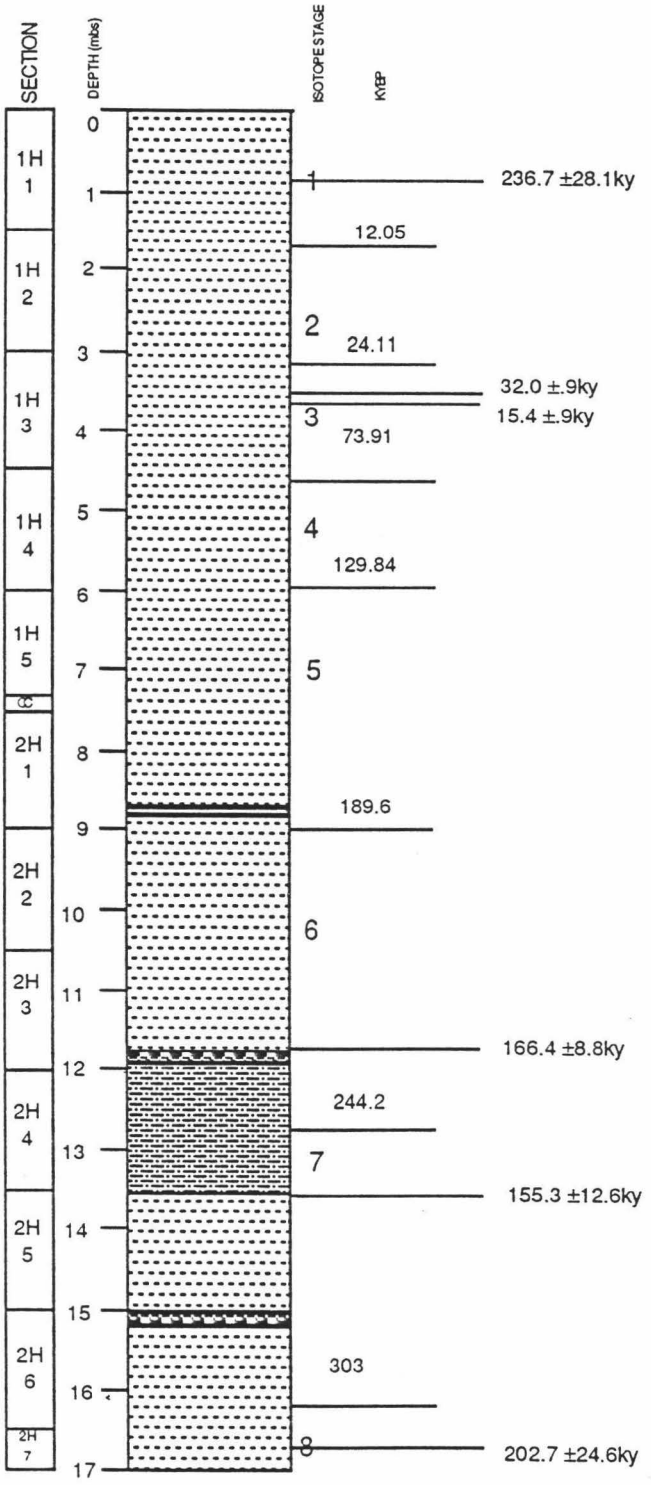

Figure 4.27. Ages of phosphorite samples in Hole 687A.

Discussion - Paleoenvironment

A major goal of this research is to reconstruct the depositional environment of the Peru upwelling region during the Quaternary. Thus, it is of interest to derive information from sediment data about the paleoproductivity of the surface water masses and the oxygen content of the bottom water. While surface productivity and bottom-water oxygen conditions are intrinsically related and therefore not completely separable, I divide the discussion below into two parts with some overlap: the first discusses primarily productivity and the second primarily bottom-water oxygenation.

Productivity

Along the Peru Margin, the atomic H/C ratios of organic materials in sediment are about 1.5 throughout the sediment sequence and indicates a dominantly marine origin of the organic matter (ten Haven et al., 1990). Thus, the accumulation of total organic carbon primarily represents the accumulation of marine organic carbon. In general, high amounts of marine organic carbon can be accumulated in high productivity (e.g., upwelling) areas and/or in oxygen-deficient environments, characterized by a high rate of organic matter flux.

When using the tracers of paleoproductivity it has to be remembered that none of them is completely resistant to changes (e.g., dissolution or decomposition) during transport through the water column, at the sea floor, or in the sediment (Jumars et al., 1989). This means, the sediment data of a specific variable cannot be taken as a direct measure of its production rate in the surface water. Thus, further information about environmental conditions is necessary and different independent tracers should be used for reconstruction of paleoproductivity in order to minimize errors in interpretations. In this section, I interpret several indicators of surface productivity recorded in sediment: organic-carbon weight percent, organic carbon accumulation rates, and $\delta^{13}C$ values of the benthic foraminifer *B. humilis*.

Organic-Carbon Weight Percent

Total organic-carbon (TOC) in weight percent of dry sediment along the Peru Margin ranges from 1% to 20%. TOC weight percent is frequently used both in the deep sea and in shallower continental margin settings to infer changes in the flux of organic matter from the photic zone to the seafloor (Müller and Suess, 1979; Müller et al., 1983; Sarnthein et al., 1988; articles in Berger et al., 1989, and in Suess and Thiede, 1983). Schrader (1992) compared the organic-carbon weight percent of Hole 680B to diatom based calculated primary productivity and found a good correspondence. Schrader noted that the average concentration of organic-carbon in Hole 680B is around 6% and that of Hole 686B is around 2%, i.e., 1/3 of Hole 680B. He concluded that the difference could be attributed to either a reduced organic-carbon flux from the photic zone to the sediment water interface, to a weaker oxygen minimum zone allowing for more oxidation of organic matter or to the 200 m depth difference between the two sites resulting in larger loss of organic-carbon during settling to the deeper Site 686. The average paleo-productivity over the last 160 ky. calculated from diatom assemblages is 180 and 140 $gC/m^2/yr$ at Holes 681A and 686A, respectively (Schrader, 1992). The average paleo-productivity of Hole 686A reaches 78% of the value of Hole 681A; a value that is matched very closely by the difference in average organic-carbon concentration in the two holes. Schrader concluded, therefore, that the offsets in both records of organic-carbon concentrations can best be explained by reduced primary production and by a reduced flux of organic matter from the photic zone to the sediments and, thus, the weight percent organic-carbon content of marine sediments can indicate levels of surface productivity. This is the same conclusion that I came to from the analysis of the modern surface sediments in Chapter 3. Figure 4.28 shows the organic-carbon weight percent versus age for each core. The ages are based on linear interpolations between the oxygen isotope stage

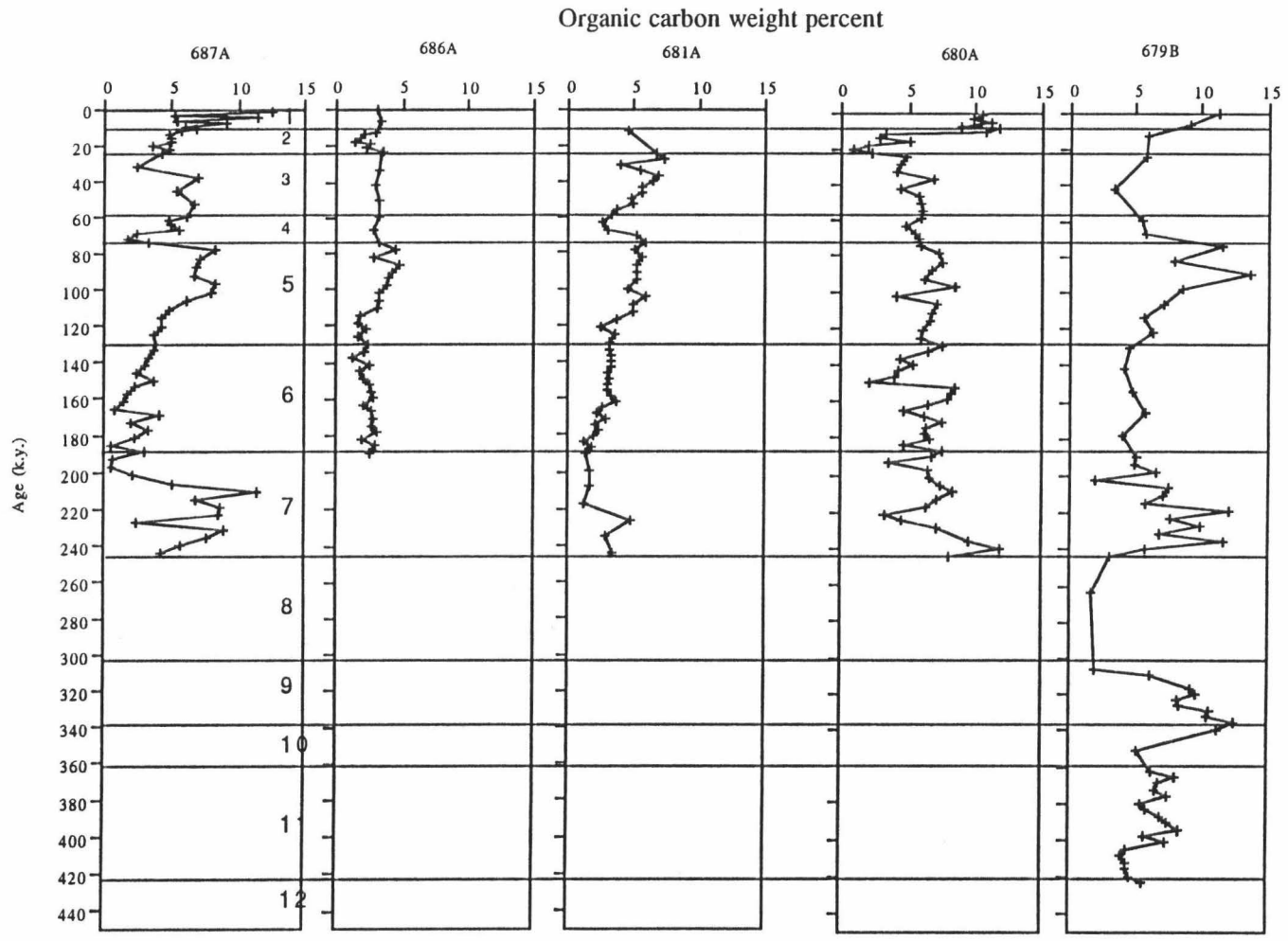

Figure 4.28. Organic carbon weight percent versus age for Holes 679B, 680A, 681A, 686A, and 687A.

boundaries discussed above. Using the organic-carbon weight percent as a measure of productivity, we see from the mean values that all sites underlie high productivity areas with Holes 679B and 680A showing the highest average values of 6.91 % and 6.29 %, respectively, and Hole 686A showing the lowest average value of 3.23 % (Table 4.10). Holes 679B, 680A, and 687A show highly variable organic carbon contents while Holes 681A and 686A show relatively consistent preservation rates. The variable sites appear to experience higher productivity during interglacial stages, but recall that the isotope stages themselves were assigned according to high and low preservation rates of organic-carbon, making the correlation somewhat artificial.

Carbon accumulation rate

Changes in the percentage of organic carbon can result from changes in the supply of both mineral components and organic carbon. Hence, it may be difficult to interpret an organic-carbon weight percent record as presented above for the ODP holes. The values are converted into mass accumulation rates (Tables 4.4, 4.5, 4.6) following the equation developed by Glenn and Arthur (1984). The equation used is:

$$C_{org\ accum} = [(wt.\%\ C_{org})\rho S]/[100 * C_{atomic\ wt.}]$$

where $C_{org\ accum}$= mass accumulation rate of total organic carbon, ρ=dry bulk density of the sediment and S=bulk sedimentation rate. The units of the accumulation rate are $(mol)(cm^{-2})(y^{-1})$.

Fig. 4.29 shows the organic-carbon accumulation rates for Holes 679B, 680A, and 681A vs. age with isotope stages. Hole 679B shows a strong pattern of higher organic-carbon accumulation during interglacial periods than during glacial periods. Also, this hole shows the overall highest values of the three holes. These data suggest that produc-

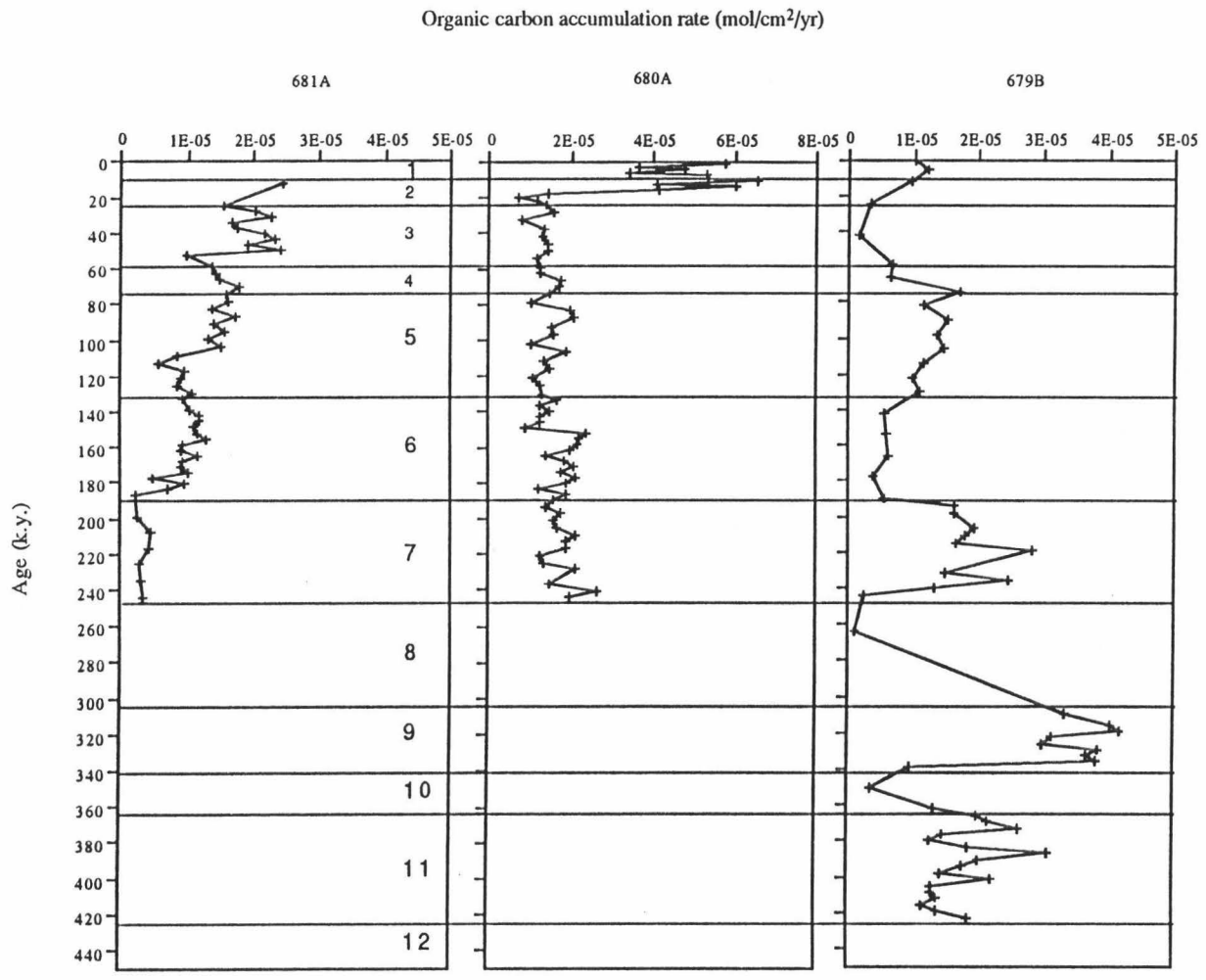

Figure 4.29. Organic carbon accumulation rates (gC/cm²/yr) versus age for Holes 678B, 680A, 681A.

tivity and therefore upwelling in the region is higher during interglacial stages.

At the other two sites, no pattern similar to Hole 679B is observed. Hole 680A shows very high values at the top. These values are the result of an unrealistic sedimentation rate calculated with uncompacted sediment and are not reliable. Below this interval the organic-carbon accumulation rates are rather consistent and do not show the clear trends found in Hole 679B. With less resolution the data do indicate a decrease at the 4/5 boundary, and at the beginning of stage 6. Values are somewhat elevated during stage 5, the lower half of stage 6, and during stage 7. The carbon accumulation rates for Hole 681A show a very curios step-like pattern. Values decrease significantly, then remain fairly stable before decreasing again. These data would seem to imply that production has been steadily increasing in the region.

Organic-carbon weight percent vs. sedimentation rate

Heath et al. (1977) and Müller and Suess (1979) have shown that a positive correlation exists between sedimentation rate and organic carbon content in surface sediments deposited in oxygenated sea-water environments. This relationship may be explained by the fact that high sedimentation rates favor the preservation of marine organic matter by reducing its residence time in the zone of bioturbation and oxic decomposition. Under anoxic conditions, the relation between sedimentation rate and the total organic carbon (TOC) content looks significantly different. In contrast to the positive correlation between sedimentation rate and sedimentary TOC content observed for oxic deep-water conditions, no such correlation appears to exist under anoxic conditions. This may indicate that changes in organic carbon deposited in oxygen-deficient environments are caused by changes in the supply of non-organic matter, i.e., by dilution, rather than by changes in degree of preservation of marine organic matter due to varying sedimentation rates.

From these observations, it seems that the relationship between organic-carbon weight percent and sedimentation rate can indicate the environment of deposition. Stein (1991) derived data from Recent to Miocene sediments that define three fields (Fig. 4.30): Region A— represents sediments deposited in normal open-ocean environments and is based on data from modern surface sediments from the NE and SE Atlantic, the central Pacific, off Peru, off Arabia, and the Baltic Sea and from Quaternary cores from the NE and SE Atlantic; Region A'— represents areas of high productivity and is based on surface sediments collected under areas of high productivity from the same samples as Region A; and Region B— represents an anoxic environment and is based on data from sediments taken from the Black Sea, and Mediterranean sapropels. I use these regions Stein has identified to evaluate the TOC content of the ODP cores. The sedimentation rates that I compare to the TOC contents are derived from the glacial stage assignments that I made to each core. The sedimentation rate for a single glacial stage is determined by taking the length of sediment included in the isotope stage and dividing it by the time duration of that stage. The sedimentation rates for each stage for each core are summarized in Tables 4.17 through 4.21.

Data from Core 679B (Fig. 4.31) indicate that the site has consistently been in an anoxic environment but only occasionally in an area of high productivity. This conclusion stands to reason; Site 679 is presently at the distal edge of the high productivity zone and likely has occupied a similar position during the last 420 ky. Data from Core 680A (Fig. 4.32) indicate that Site 680 has consistently been located in an area of upwelling and high productivity Data from Core 681A (Fig. 4.33) indicate consistent deposition in an anoxic environment with fluctuation in the level of productivity. Approximately one third of the data points fall outside the high productivity region. Data from 686A (Fig. 4.34) indicate consistent deposition in an anoxic, high productivity environment. Data from Core 687A (Fig. 4.35) shows some variability. Most data points fall in the anoxic,

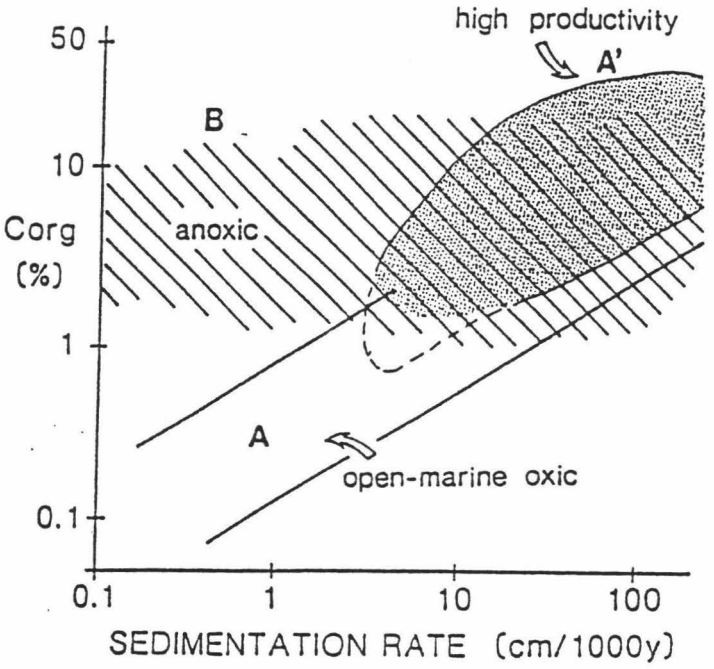

Figure 4.30. Diagram of fields identified by analysis of marine surface sediments (from Stein, 1991).

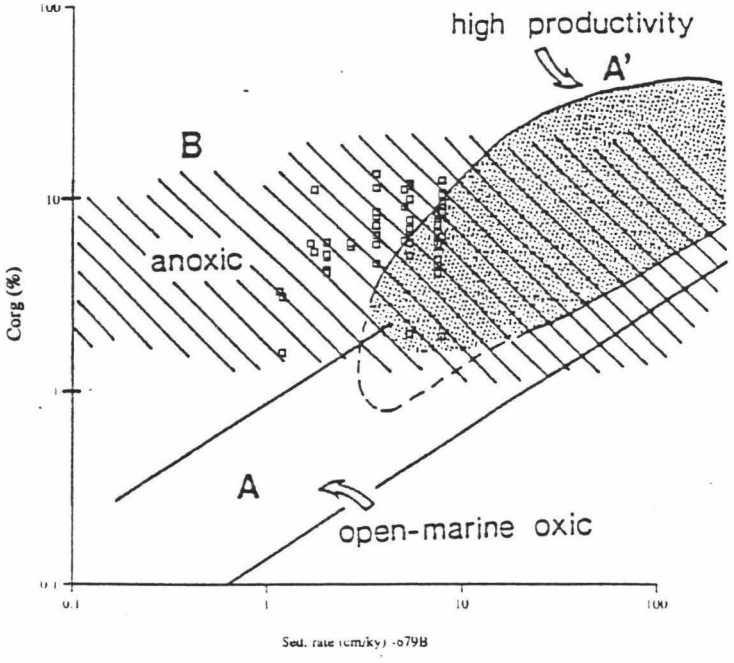

Figure 4.31. Comparison of organic carbon and sedimentation rate data from Hole 679B to fields developed by Stein (1991).

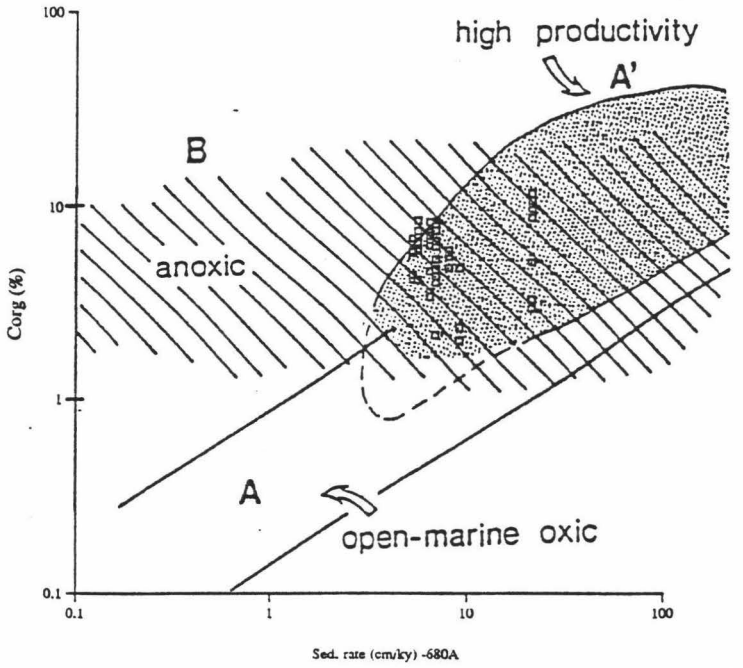

Figure 4.32. Comparison of organic carbon and sedimentation rate data from Hole 680A to fields developed by Stein (1991).

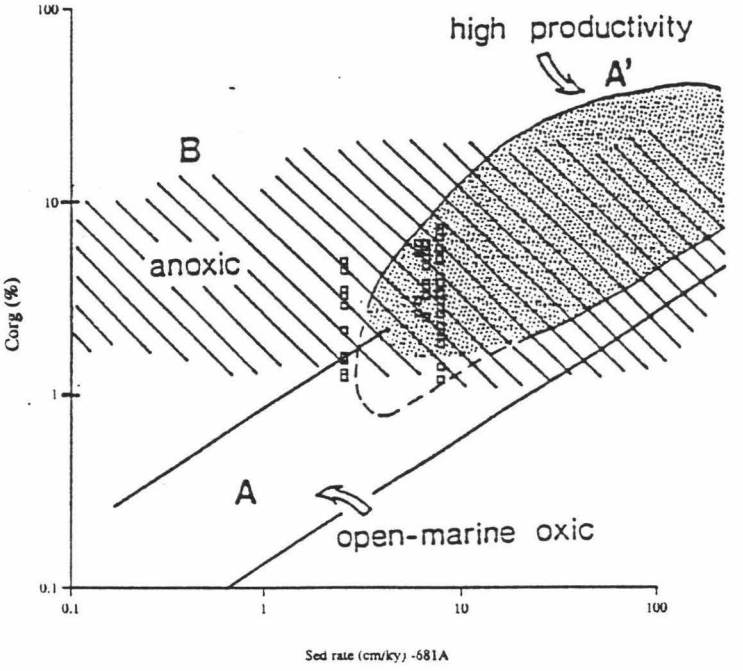

Figure 4.33. Comparison of organic carbon and sedimentation rate data from Hole 681A to fields developed by Stein (1991).

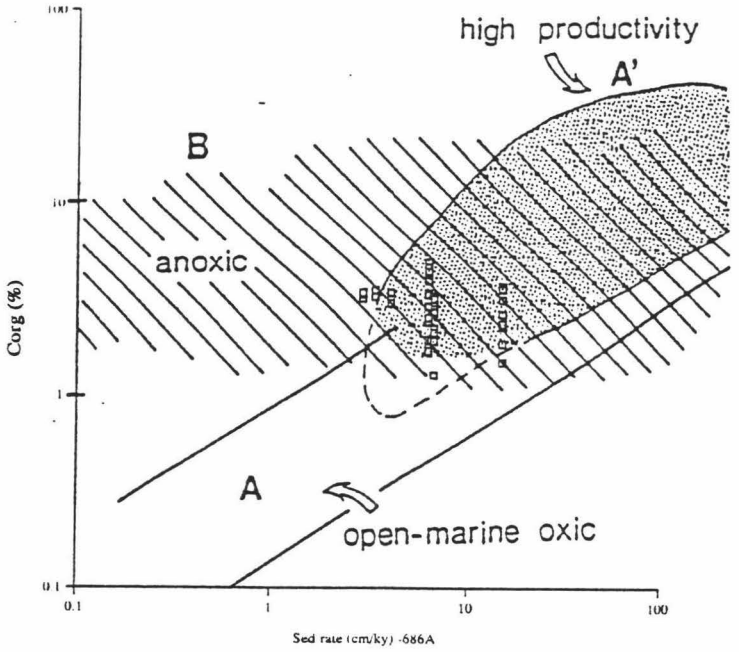

Figure 4.34. Comparison of organic carbon and sedimentation rate data from Hole 686A to fields developed by Stein (1991).

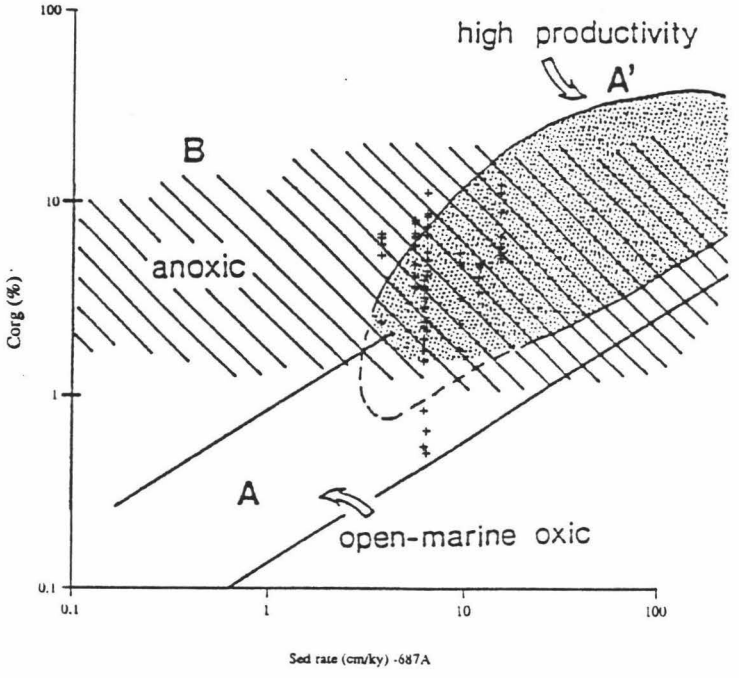

Figure 4.35. Comparison of organic carbon and sedimentation rate data from Hole 687A to fields developed by Stein (1991).

high productivity region. Four points, however, fall in the open-marine oxic environment. These four points may indicate a weakening of productivity in the site's area and an increase in bottom water oxygen levels.

$\delta^{13}C$ as an indicator of productivity

Low $\delta^{13}C$ values may reflect low oxygen levels in sea water and thus, high surface productivity. Changes in the $\delta^{13}C$ of bottom seawater and seawater in sediment can also be the result of increased flux of marine organic material. Marine organic matter is isotopically light with respect to seawater. An increase in particulate organic-carbon (POC) flux will result in a higher percentage of organic carbon in the water column due to oxidation, sediment and, thus, will decrease total dissolved carbon $\delta^{13}C$ values in those waters. If *B. humilis* precipitates its test in relation to the $\delta^{13}C$ of those waters a correlation should, in theory, be present with respect to the sediment's organic-carbon content. Previous studies, however, have found evidence that both environmental (microhabitat) and vital effects determine that final $^{13}C/^{12}C$ ratio in foraminifera tests (McCorkle, 1990). My analysis of benthic foraminifera from surface sediments also showed no correlation between productivity and $\delta^{13}C$ (see Chapter 3). However, while the data show no statistically meaningful relation, $\delta^{13}C$ results from analysis of *B. humilis* in Hole 679B does reveal a curious pattern (Fig. 4.36). For the top 8 m, increases in $\delta^{18}O$ values are mirrored by increases in $\delta^{13}C$ values. Below 8 m, low $\delta^{13}C$ values coincide with high $\delta^{18}O$ values. The isotope values of the upper 8 m of sediment suggests that during glacial periods (high $\delta^{18}O$), bottom water oxygen levels are higher (high $\delta^{13}C$) possibly because upwelling intensity and productivity is lower, and that during interglacial periods (low $\delta^{18}O$), bottom water oxygen level are lower (low $\delta^{13}C$) due to higher upwelling intensity and higher productivity. The two isotopes seem to track each other on a finer scale than glacial/interglacial cycles, perhaps reflecting stadial variations. This suggests that up-

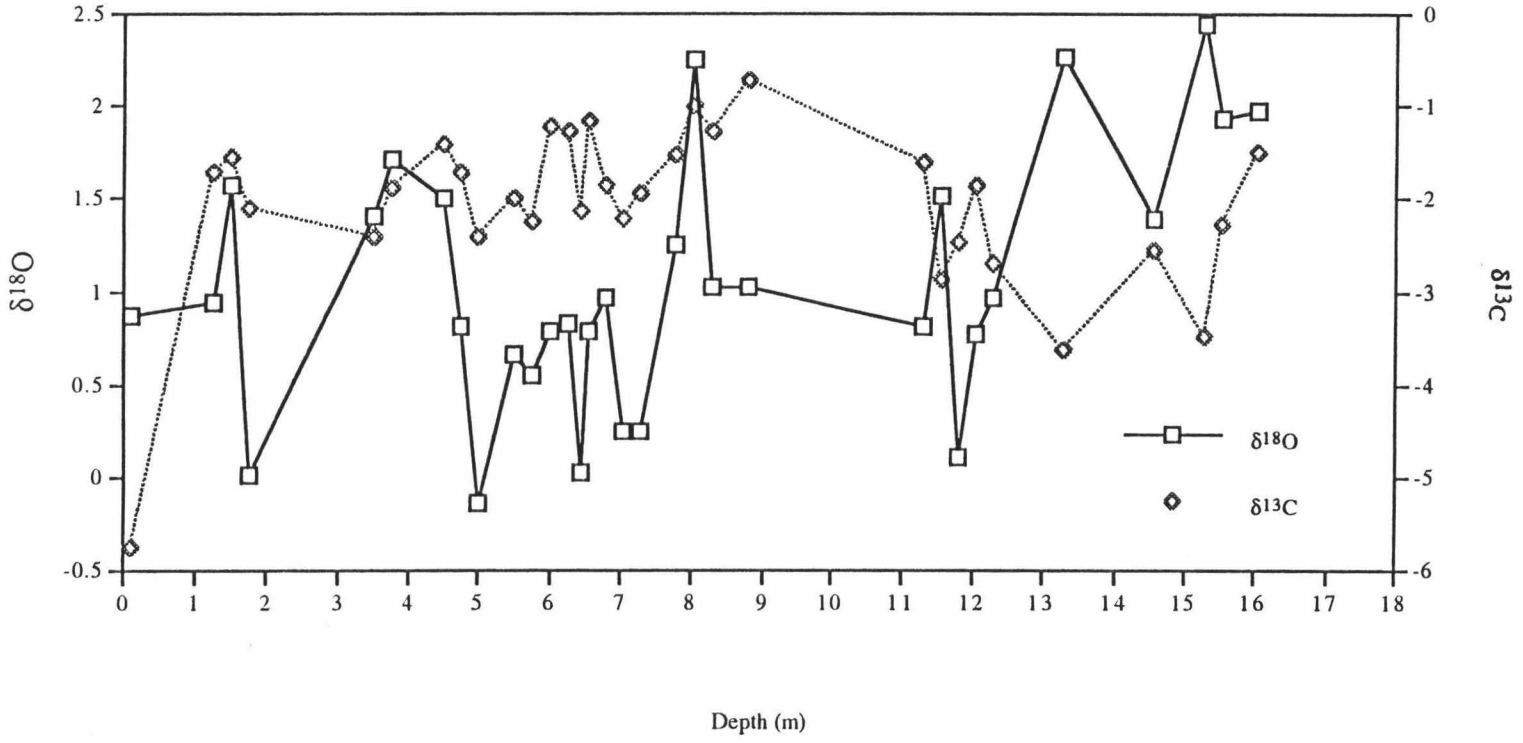

Figure 4.36. Comparison of $\delta^{18}O$ and $\delta^{13}C$ values for Hole 679B.

welling has varied within isotopes stages, perhaps with substage eustatic sea level changes. Below 8 m, however, low $\delta^{13}C$ values coincide with high $\delta^{18}O$ values; this cannot be explained by the glacial period/low upwelling/high oxygen relationship. It is unclear why the pattern reverses below 8 m.

Research on productivity estimates in the Peru Margin region has found evidence for increased productivity during both glacial and interglacial periods. Research by Oberhänsli et al. (1990) evaluating benthic foraminifers and coarse grain-size distribution in Holes 679D, 680B, and 681B found a general increase in upwelling during interglacial stages with increased upwelling activity during stage 1 (lower part), 3, the upper part of 5, the lower part of 6, and 7. They concluded that upwelling was likely at a minimum during stages 5, and 9. Heinze and Wefer (1992) studied the variation in the relative abundances of benthic foraminiferal species in Hole 680B and found productivity to be enhanced during interglacial stages 1, 3, 5, 7, 9, and 11. Schrader and Sorknes (1990a) investigated the composition of the diatom flora in Holes 681A, and 686A. Their results allowed them to identify variations on the upwelling intensity off Peru over the last 400,000 years. The stratigraphy was based on a correlation of the diatom compositions in Holes 681A, and 686A, with the flora in Hole 680B, dated after Wefer et al. (1990) using oxygen isotopes. Time intervals with increased upwelling were found in sections of $\delta^{18}O$-stages 3, 5, 7, and 8, while the upwelling intensity was reduced in $\delta^{18}O$ stages 2, 6, and 10 (Schrader and Sorknes, 1990a). In a more recent paper, Schrader and Sorknes (1990b) revised the stratigraphy and concluded from marine diatom assemblages that paleoproductivity is not in phase with the general glacial-interglacial cycles and that the largest swings in the magnitude of paleoproductivity seem to occur across oxygen isotope stage boundaries. The data that I present above suggest that, in general, productivity and upwelling have been almost persistent during the past 240 ky and that production in-

creased during interglacial periods and decreased during glacial periods although intermittent periods of increased and decreased productivity are found in both glacial and interglacial stages.

Bottom-water Oxic/Anoxic Conditions

Information about the oxygen content of bottom water masses can be derived from different factors. Here, I interpret the organic-carbon/sulfur relationship and the benthic foraminiferal assemblages.

Sulfur/organic carbon relationship

According to Leventhal (1983) and Berner (1984, 1989), the relationship between organic carbon content and (pyritic) sulfur may help to distinguish oxic and anoxic environments. In siliciclastic normal marine sediments, sulfur is mainly bound to pyrite (Berner, 1984). Sulfur is available in excess as sulfate in sea water and iron is available from silicates (clay minerals) and crystalline oxide phases (Goldhaber and Kaplan, 1984; Raiswell and Berner, 1987). The limiting factor for pyrite formation under normal oxic deep-water conditions is the amount of organic matter controlling the formation of reducing conditions in the near-surface sediments. In this environment, there is a positive correlation between (pyritic) sulfur and organic carbon (Berner, 1984; Raiswell and Berner, 1987). Under anoxic sulfidic water conditions, H_2S already exists in the sea water. Thus, framboidal pyrite can already be formed in the water column, resulting in an excess of sulfur in the organic carbon/sulfur diagram shown as a positive intercept and change in slope. In oxic depositional environments, an organic-carbon accumulation rate of zero will result in no sulfide produced. Thus, a plot of organic-carbon weight percent versus sulfur weight percent should indicate oxic water if the regression line passes through the origin and anoxic conditions if the line crosses the y-axis above the origin.

Unfortunately, research concerning sulfur cycling in these sediments has revealed that the reactive iron concentrations are very low (Neil Suites, personal communication). Without reactive iron pyrite can not form. The sulfur to carbon ratio in these sediments will not be useful in determining bottom water anoxia. Plots of sulfur weight percent versus organic carbon weight percent are shown in Figures 4.37, and 4.38. As expected, the plots reveal a low amounts of sulfur compared to organic carbon.

Faunal assemblages

The composition of faunal assemblages may characterize the depositional environment in terms of oxygen content of bottom water (Wetzel, 1983). Previous studies (e.g., Resig, 1990) and the results from my analysis of surface sediments identify certain benthic foraminifer species that are characteristic of minimum oxygen environments. I use the scores of the four assemblage factors in the assemblages of benthic foraminifera in core sediments to interpret dissolved oxygen conditions at the various sites. Figures 4.39, 4.40, and 4.41 show the factor scores, isotope stages, and oxygen isotope stages for Holes 679A, 680B, and 687A, respectively.

While the benthic assemblages in Hole 679B show predominantly anoxic conditions, the percentage of low oxygen species does fall significantly during a few intervals (Fig. 4.39), particularly in the middle of isotope stage 3 and during the end of stage 8 and through stage 9. The benthic assemblages of Hole 680A show a consistent dominance by low oxygen species (Fig. 4.40). Only one sample at the middle of isotope stage 2 shows less than 50% of the low oxygen species. The benthic assemblages of 687A (Fig. 4.41) indicate very low oxygen levels except for two intervals at the end of isotope stage 4 and the beginning of isotope stage 7. The bottom water in the area of these three sites has been persistently very low in oxygen. Bottom water oxygen levels only seems to have changed between oxygen minimum conditions and oxygen depleted conditions.

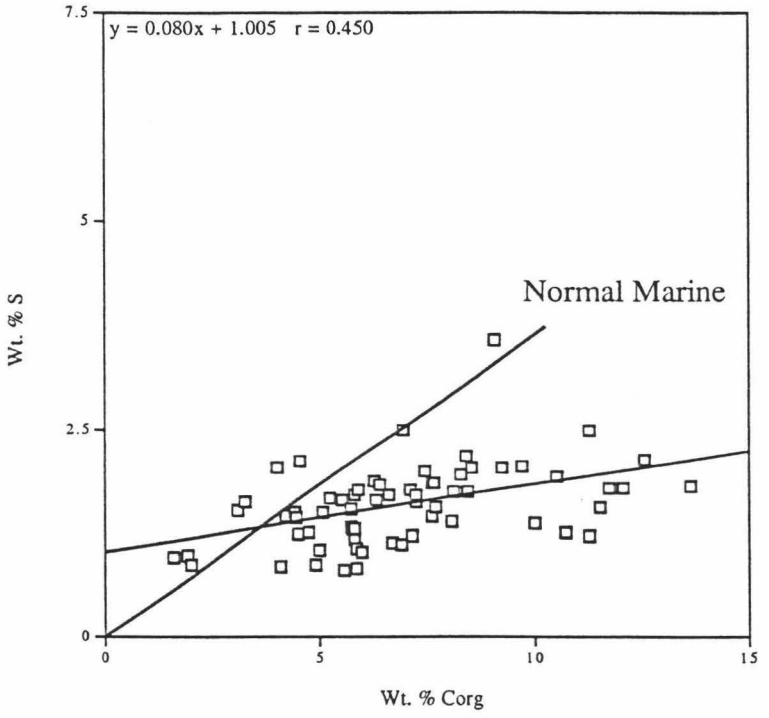

Figure 4.37. Sulfur weight percent versus organic carbon weight percent for Hole 679B.

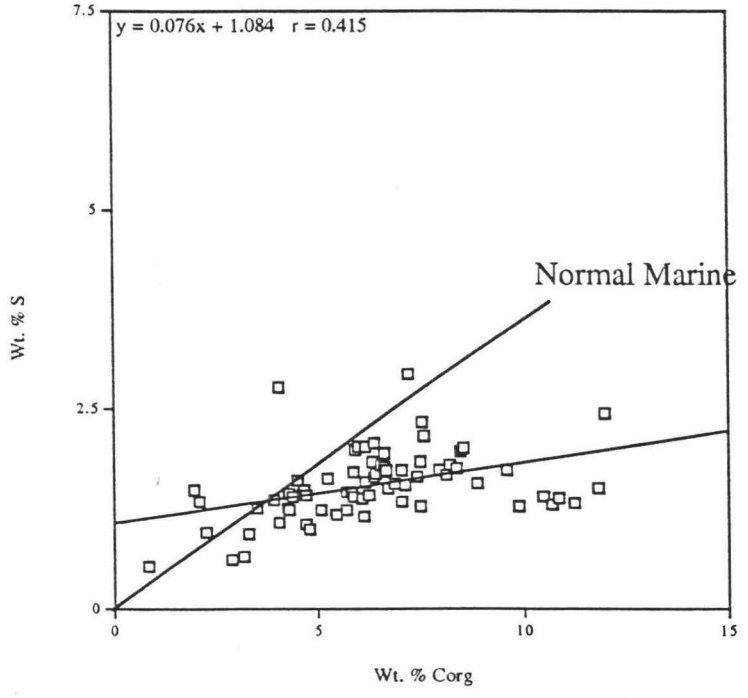

Figure 4.38. Sulfur weight percent versus organic carbon weight percent for Hole 680A.

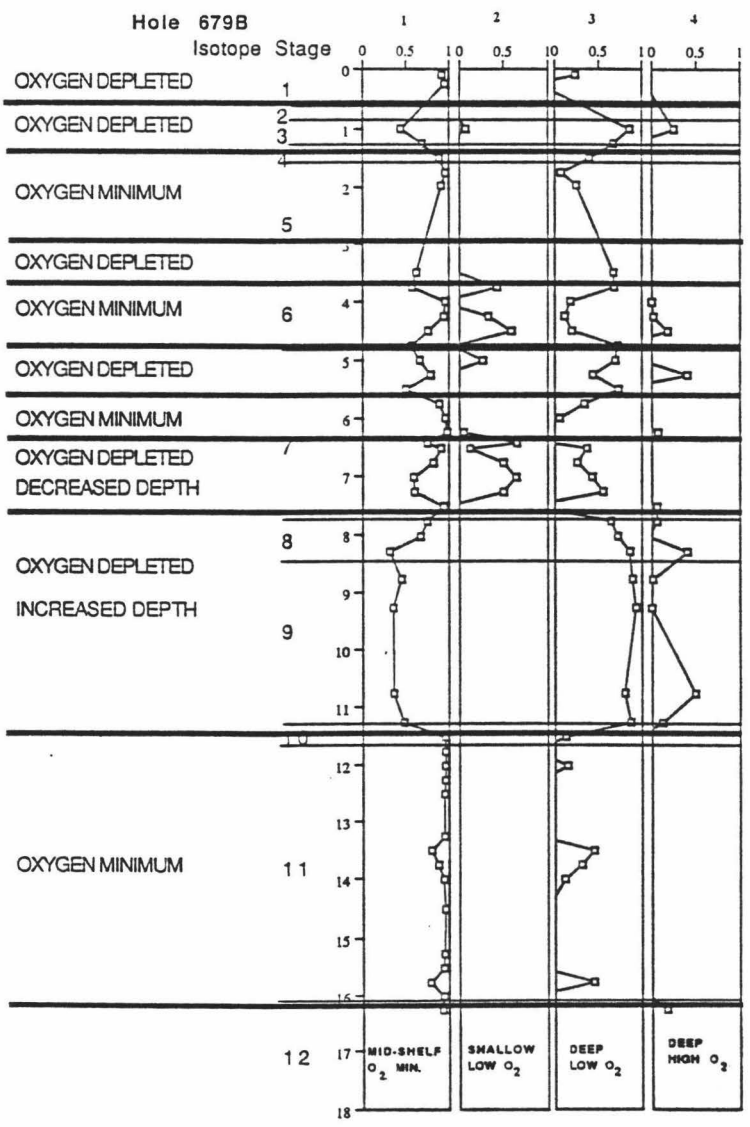

Figure 4.39. Benthic foraminiferal assemblage scores with oxygen level interpretations - Hole 679B.

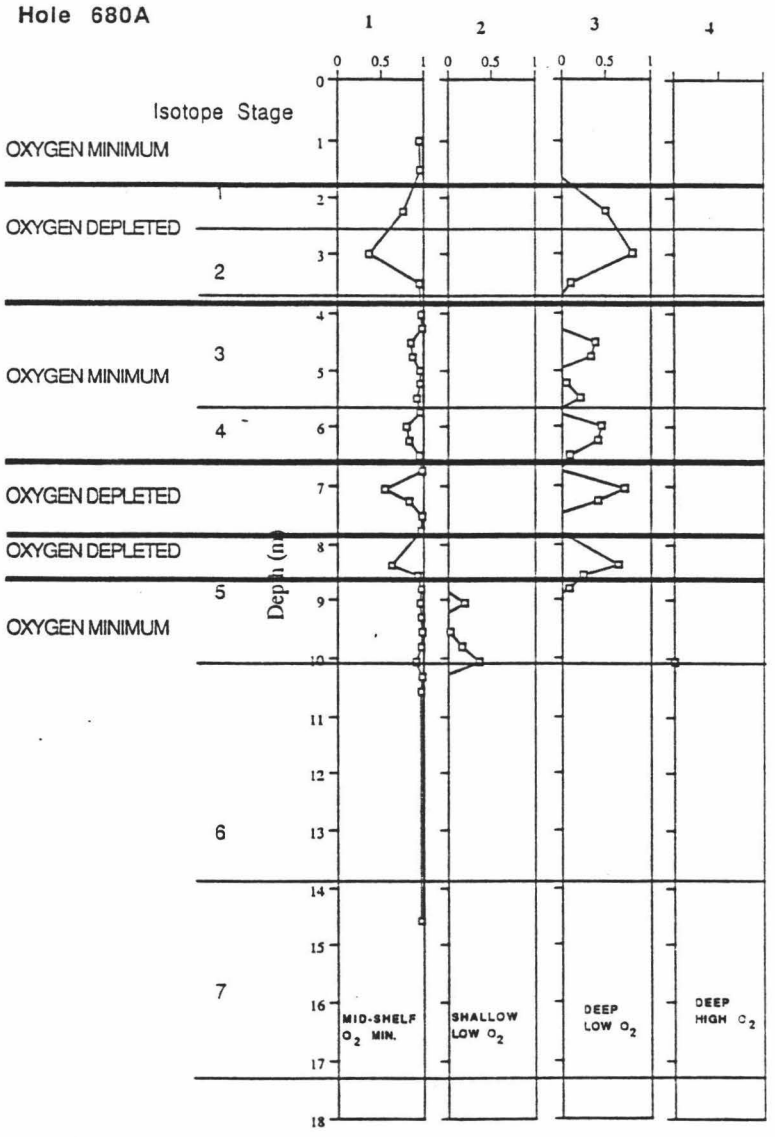

Figure 4.40. Benthic foraminiferal assemblage scores with oxygen level interpretations - Hole 680A.

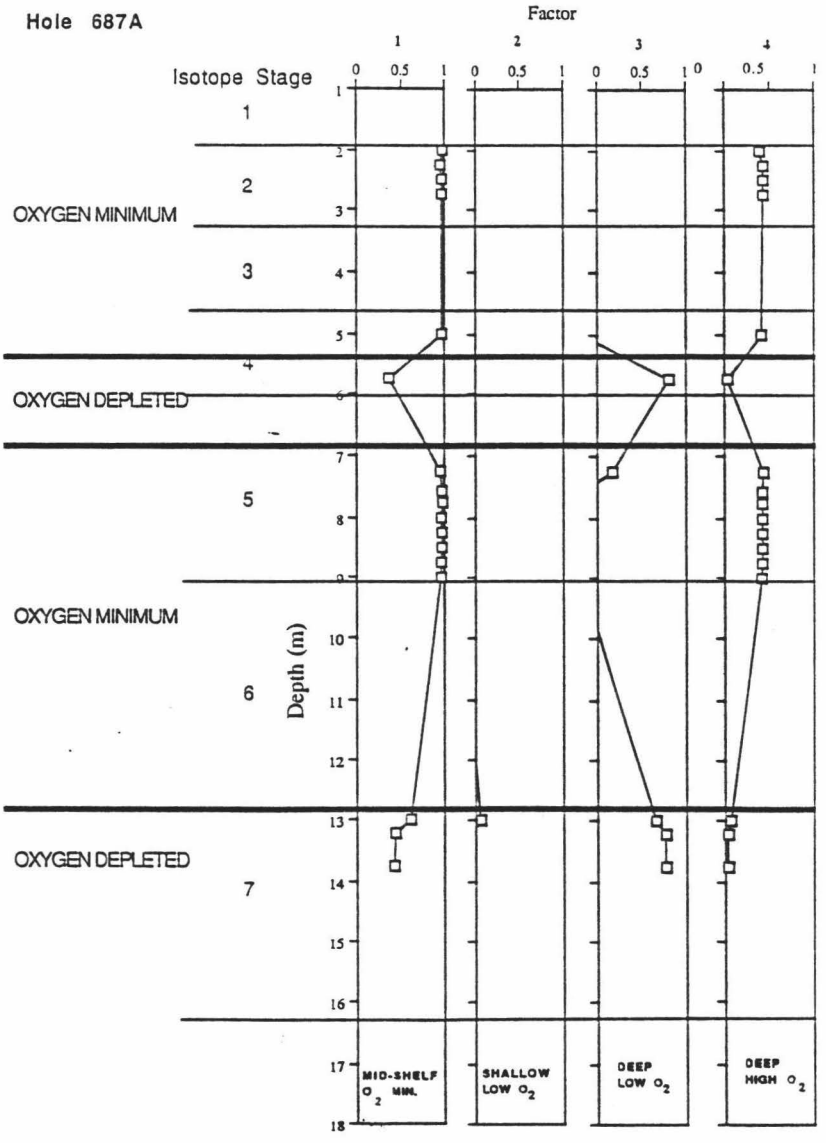

Figure 4.41. Benthic foraminiferal assemblage scores with oxygen level interpretations - Hole 687A.

I illustrate, qualitatively, the position of the oxygen minimum zone over Sites 679 and 680 during oxygen isotope stages 2-11 in Figure 4.42. In general, the oxygen minimum zone moves in response to changes in sea level. This is observed during stages 2 and 6 when there is a significant decrease in sea level and the oxygen minimum zone moves seaward.

Conclusions

Oxygen isotope stages were assigned to Hole 680A by transferring the accepted oxygen isotope stages from Hole 680B. Oxygen isotope stages were assigned to Hole 679B using original $\delta^{18}O$ data and benthic foraminiferal assemblages. The lack of foraminifers in the other ODP core sediments prohibited developing oxygen isotope curves for the cores and subsequently assigning isotope stages and absolute ages. A method of using the organic-carbon weight percent curve as a proxy for the oxygen isotope curve was evaluated and found to be a possible substitute. The method was evaluated using Hole 679B which had both $\delta^{18}O$ and organic-carbon weight percent data. The evaluation was not conclusive and the results are very preliminary. Accepting the method as approximately accurate, isotope stages were assigned to Holes 681A, 686A, and 687A, all of which did not have enough benthic foraminifers for $\delta^{18}O$ analysis.

Organic-carbon weight percent of sediments, organic-carbon accumulation rates, sedimentation rates, and $\delta^{13}C$ of benthic foraminifera were evaluated to interpret paleoproductivity along the Peru Margin. Productivity has been persistently high. In general, high productivities are recorded during interglacial stages, but relatively high and low productivities are observed in both glacial and interglacial stages. The coastal trade winds that blow along the Peru Margin have likely been persistent through the time interval studied in this thesis indicating that upwelling has also been continuous. There-

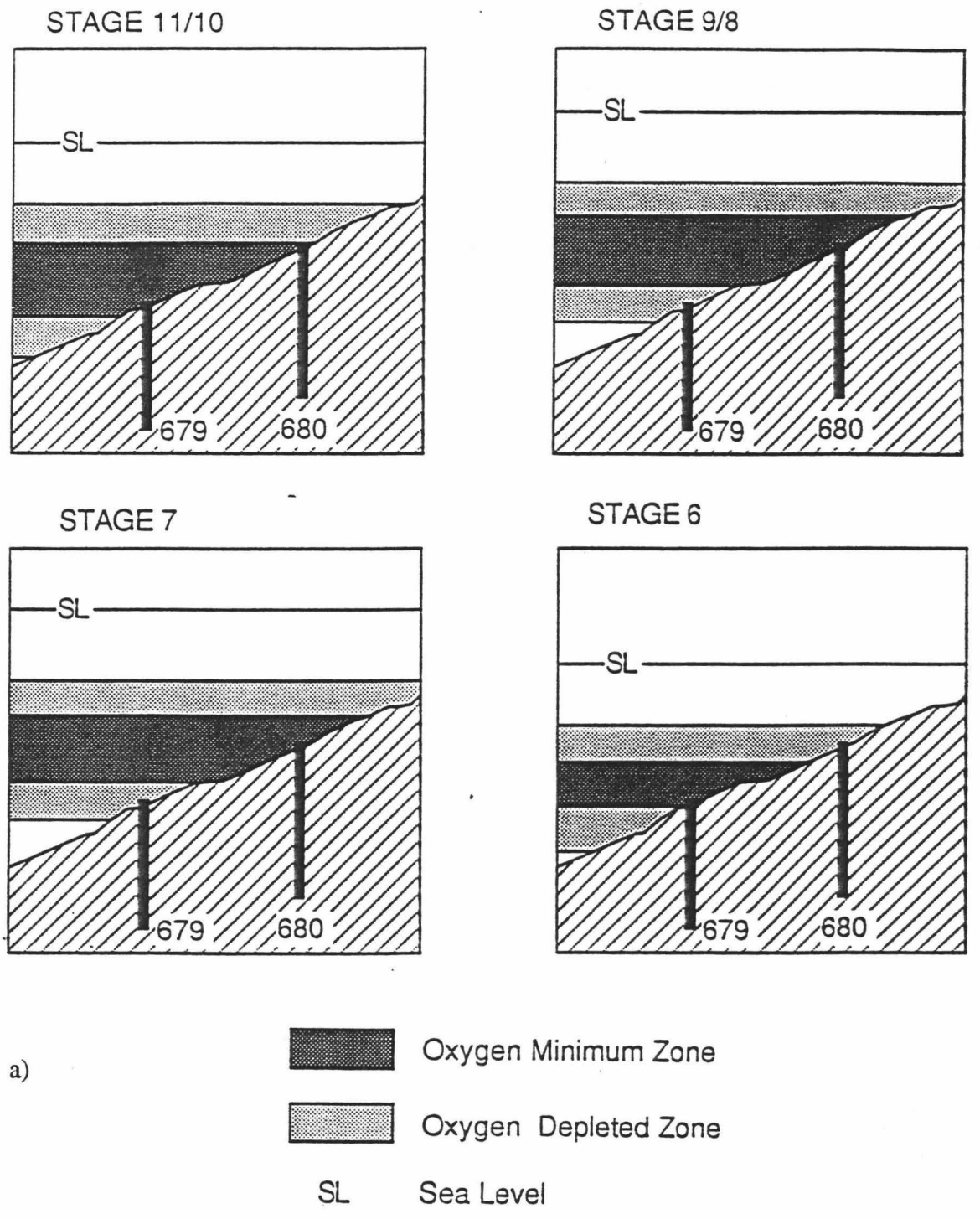

Figure 4.42. a) Position of the oxygen minimum zone over ODP drilling sites 679 and 680 during oxygen isotope stages 11 through 6. b) Position of the OMZ during stages 5 through 2.

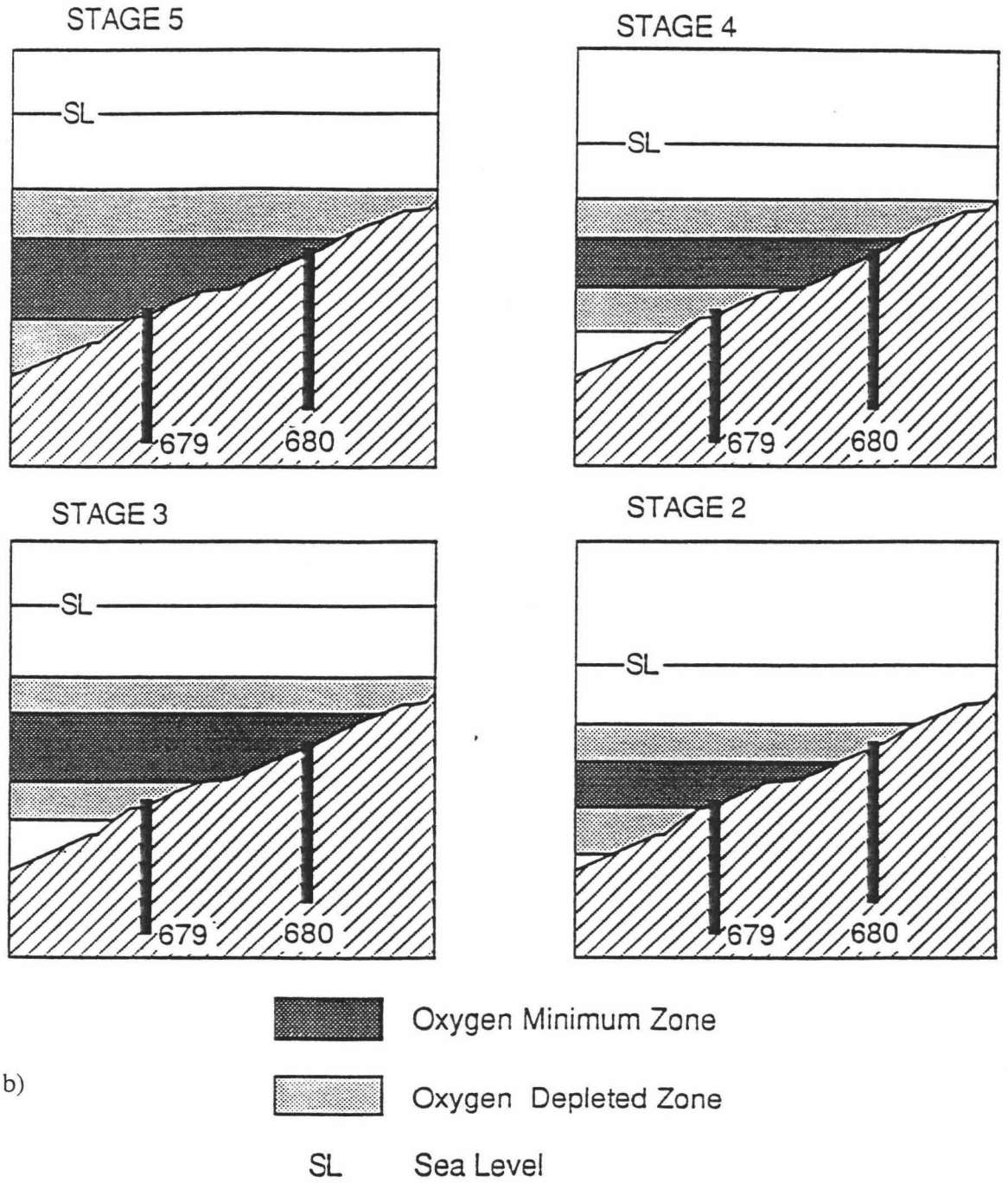

b)

Figure 4.42 (continued).

fore, changes in productivity are probably not related to strengthening or weakening of upwelling intensity. Instead, changes in productivity are more likely related to changes in the location or intensity of the poleward undercurrent and the nutrient content of the upwelled waters. This phenomenon may be analogous to a long term El Niño event. During periods with relatively low surface productivity, there may be a relocation of the poleward undercurrent to a position where its nutrient rich waters cannot be upwelled. Upwelling still occurs, but the upwelled water does not have the high nutrient content to support the high surface productivity

Benthic and planktonic foraminifers are poorly preserved in many sections of ODP core sediments from the Peru Margin. When available, benthic foraminiferal assemblages are good environmental indicators; assemblages can indicate water depth and bottom water oxygen content. In general, benthic foraminiferal assemblages indicate that bottom waters on the Peru Margin have been persistently low in oxygen and that the oxygen minimum zone has moved in response to sea level change. Due to the absence of reactive iron, the sulfur weight percent versus organic-carbon weight percent was not useful in these sediments for interpreting bottom water oxygen conditions.

Table 3.1. Surface sediment data collected during R/V Seward Johnson cruise.

Sample I.D.	Depth (m)	Temp (°C)	O2 (µMol)	Salinity	Current velocity (cm/sec)
BC-02	106				
BC-09	106	13.27	5.16	34.92	
BC-17	106	13.27	5.16	34.92	
BC-21	73	13.67	5.85		
BC-33	373	9.36	2.96	34.69	
BC-33	373	9.36	2.96	34.69	
BC-42	800	5.61	20.3	34.53	
BC-50	898				
BC-51	932	4.43	42.37	34.54	
BC-53					
BC-54	1067	4.34	43.8	34.54	
BC-56	250				
BC-57	172				
BC-62	643	6.89	7.73	34.57	
BC-63	160				
BC-76	725				
BC-79	160				
BC-81	130				
BC-85	106	13.27	5.16	34.92	
BC-87	200				
BC-91	309	11.76	4.3	34.83	
BC-92	309	11.76	4.3	34.83	
BC-116	480				
BC-117	408				
BC-123	376	11.76	4.3	34.83	
BC-125	340				
BC-135	150				
BC-144	100	13.44	5.82	34.93	
BC-153	250				
D-3344	106	13.27	5.16	34.92	
D-3349	264	11.71	4.13	34.84	10
D-3351	823	5.61	20.3	34.53	0.5
D-3353	660	6.89	7.73	34.57	15
D-3354	555	10.5			5
D-3354	546	10.5			5
D-3355	470	8.76	3.05	34.66	10
D-3356	362	9.36	2.96	34.69	12.5
D-3356	383	9.36	2.96	34.69	12.5
D-3357	595	6.89	7.73	34.57	10
D-3358	172	14			20
D-3360	104	13.44	5.82	34.93	10
D-3361	351	11.76	4.3	34.83	12.5
D-3362	459	9.91	3.14	34.72	10
D-3363	517	12			12.5
D-3365	574	5.6			5
D-3366	427	9.91	3.14	34.72	15
D-3367	377	9.91	3.14	34.72	7.5
D-3368	319	11.76	4.3	34.83	7.5
D-3370	190	12.8			12.5
KC-111	297	11.76	4.3	34.83	

Table 3-2. Number of different foraminifer species per gram dry sediment in Peru Margin surface sediments.

Site	*Angulogerina carinata*	*Bolivina costata*	*Bolivina minuta*	*Bolivina plicata*	*Bolivina spissa*	*Bolivinellina seminuda humilis*	*Brizalina interjunsta*	*Buliminella subfusiformis*	*Cancris carmenensis*	*Cancris inflatus*	*Cassidulina auka*	*Nonionella auris*	*Parabolivina peruensis*	*Planulina limbata*	*Pseudoparrela subperuviana*	*Pullenia subcarinata*	*Uvigerina perigrina*	*Uvigerina striata*
BC-02	0.0	0.0	0.0	0.0	0.0	0.0	0.0	0.0	0.0	0.0	0.0	0.0	0.0	0.0	0.0	0.0	0.0	0.0
BC-09	0.0	0.0	0.0	0.0	0.0	0.0	0.0	0.0	0.0	0.0	0.0	0.0	0.0	0.0	0.0	0.0	0.0	0.0
BC-17	0.0	0.0	0.0	0.0	0.0	0.0	0.0	0.0	0.0	0.0	0.0	0.0	0.0	0.0	0.0	0.0	0.0	0.0
BC-21	0.0	17.2	0.0	0.0	0.0	1.1	0.0	0.0	0.0	0.0	0.0	0.0	0.0	0.0	0.0	0.0	0.0	0.0
BC-33	0.0	0.0	0.0	0.0	0.0	0.0	0.0	0.0	0.0	0.0	0.0	0.0	0.0	0.0	0.0	0.0	0.0	0.0
BC-33	0.0	0.0	0.0	0.0	0.0	0.0	0.0	0.0	0.0	0.0	0.0	0.0	0.0	0.0	0.0	0.0	0.0	0.0
BC-42	7.5	0.0	0.0	0.0	2.5	0.0	0.0	0.0	0.0	0.0	0.0	0.0	0.0	1.7	2.5	0.0	18.3	0.8
BC-50	1.7	0.0	0.0	0.0	2.3	0.0	0.0	0.0	0.0	0.0	0.0	0.0	0.0	0.0	0.0	0.0	1.7	0.0
BC-51	2.8	0.0	0.0	0.0	1.4	0.0	0.0	0.0	0.0	0.0	0.0	0.0	0.0	0.0	0.0	0.0	0.0	0.0
BC-53	0.0	0.0	0.0	5.4	0.0	4.8	1.8	0.6	0.0	3.6	1.2	0.0	0.0	0.0	0.0	0.0	0.0	0.0
BC-54	0.0	0.0	0.0	0.0	0.0	0.0	0.0	0.0	0.0	0.0	0.0	0.0	0.0	0.0	0.0	0.0	0.0	0.0
BC-56	0.0	0.0	0.0	0.0	0.0	0.0	0.0	0.0	0.0	0.0	0.0	0.0	0.0	0.0	0.0	0.0	0.0	0.0
BC-57	0.0	0.0	0.0	67.9	1.2	9.9	12.4	0.0	9.9	0.0	0.0	0.0	0.0	0.0	2.5	0.0	1.2	0.0
BC-62	0.0	0.0	0.0	0.0	0.0	2.9	0.0	0.0	0.0	0.0	0.0	0.0	0.0	2.9	70.6	0.0	29.4	47.1
BC-63	0.0	0.0	0.0	0.0	0.0	0.0	0.0	0.0	0.0	0.0	0.0	0.0	0.0	0.0	0.0	0.0	0.0	0.0
BC-76	0.0	0.0	0.0	0.0	6.9	1.7	15.6	0.0	0.0	8.7	0.0	0.0	0.0	1.7	110.7	0.0	91.7	0.0

Table 3-2. (Continued) Number of different foraminifer species per gram dry sediment in Peru Margin surface sediments.

Site	*Angulogerina carinata*	*Bolivina costata*	*Bolivina minuta*	*Bolivina plicata*	*Bolivina spissa*	*Bolivinellina seminuda humilis*	*Brizalina interjunsta*	*Buliminella subfusiformis*	*Cancris carmenensis*	*Cancris inflatus*	*Cassidulina auka*	*Nonionella auris*	*Parabolivina peruensis*	*Planulina limbata*	*Pseudoparrela subperuviana*	*Pullenia subcarinata*	*Uvigerina perigrina*	*Uvigerina striata*
BC-79	0.0	0.0	0.0	0.0	0.0	0.0	0.0	0.0	0.0	0.0	0.0	0.0	0.0	0.0	0.0	0.0	0.0	0.0
BC-81	0.0	0.0	0.0	0.0	0.0	0.0	0.0	0.0	0.0	0.0	0.0	0.0	0.0	0.0	0.0	0.0	0.0	0.0
BC-85	0.0	0.0	0.0	0.0	0.0	0.0	0.0	0.0	0.0	0.0	0.0	0.0	0.0	0.0	0.0	0.0	0.0	0.0
BC-87	0.0	1.6	0.0	133.6	0.0	53.1	8.1	1.6	58.0	16.1	185.1	0.0	0.0	0.0	30.6	0.0	0.0	45.1
BC-91	0.0	0.0	0.0	0.0	0.0	0.0	0.0	0.0	0.0	0.0	0.0	0.0	0.0	0.0	0.0	0.0	0.0	0.0
BC-92	0.0	57.6	0.0	0.8	0.0	2.4	0.0	0.0	0.0	0.0	0.0	0.0	0.0	0.0	0.0	0.0	0.0	0.0
BC-116	13.1	65.3	26.1	626.9	130.6	1398	209.0	418.0	274.3	26.1	78.4	13.1	0.0	26.1	222.0	0.0	0.0	91.4
BC-117	0.0	4.3	0.0	8.6	4.3	66.6	38.7	17.2	4.3	0.0	0.0	34.4	0.0	0.0	236.2	0.0	0.0	10.7
BC-123	0.0	0.0	0.0	42.4	0.0	89.4	9.4	21.2	15.3	12.9	0.0	0.0	0.0	0.0	5.9	0.0	0.0	0.0
BC-125	3.8	22.9	7.6	630.1	0.0	523.2	7.6	34.4	26.7	3.8	0.0	0.0	11.5	0.0	122.2	0.0	0.0	0.0
BC-135	0.0	0.0	0.0	0.0	0.0	0.0	0.0	0.0	0.0	0.0	0.0	0.0	0.0	0.0	0.0	0.0	0.0	0.0
BC-144	0.0	0.0	0.0	0.0	0.0	0.0	0.0	0.0	0.0	0.0	0.0	0.0	0.0	0.0	0.0	0.0	0.0	0.0
BC-153	0.0	0.0	0.0	0.0	0.0	0.0	0.0	0.0	0.0	0.0	0.0	0.0	0.0	0.0	0.0	0.0	0.0	0.0
D-3344	0.0	177.5	0.0	0.0	0.6	25.3	0.0	0.0	2.8	3.3	9.3	0.0	0.0	0.0	54.4	0.0	0.0	1.1
D-3349	0.0	0.8	0.4	8.0	1.3	9.2	1.3	2.1	5.0	0.0	0.4	0.0	0.0	0.0	1.3	0.0	1.3	0.0
D-3351	7.5	0.0	1.2	0.0	0.0	0.0	0.0	0.0	0.0	0.0	0.0	0.0	0.0	0.0	0.0	0.0	0.6	4.0
D-3353	0.0	0.0	0.0	0.0	33.5	0.0	26.4	2.4	0.0	0.0	19.2	0.0	0.0	0.0	50.3	0.0	107.8	115.0
D-3354	0.0	0.0	1.7	0.0	1.7	0.0	3.4	0.0	0.6	0.6	4.0	0.0	0.0	2.3	2.3	0.0	1.1	2.8

Table 3-2. (Continued) Number of different foraminifer species per gram dry sediment in Peru Margin surface sediments.

Site	*Angulogerina carinata*	*Bolivina costata*	*Bolivina minuta*	*Bolivina plicata*	*Bolivina spissa*	*Bolivinellina seminuda humilis*	*Brizalina interjunsta*	*Buliminella subfusiformis*	*Cancris carmenensis*	*Cancris inflatus*	*Cassidulina auka*	*Nonionella auris*	*Paraboliviva peruensis*	*Planulina limbata*	*Pseudoparrela subperuviana*	*Pullenia subcarinata*	*Uvigerina perigrina*	*Uvigerina striata*
D-3354	0.0	0.0	128.6	0.0	5.7	5.7	11.4	0.0	0.0	0.0	14.3	0.0	0.0	0.0	628.6	0.0	0.0	25.7
D-3355	5.5	0.0	0.0	24.9	0.0	19.4	5.5	0.0	5.5	0.0	0.0	0.0	0.0	0.0	2.8	0.0	33.2	27.7
D-3356	36.6	18.3	0.0	1262	146.3	3529	310.9	493.7	1902	1865	0.0	0.0	54.9	0.0	36.6	0.0	0.0	0.0
D-3356	10.9	7.3	0.0	385.7	3.6	473.0	43.7	43.7	145.5	0.0	7.3	0.0	0.0	0.0	76.4	0.0	14.6	32.8
D-3357	0.0	3.3	0.0	112.4	0.0	61.9	1.6	0.0	22.8	4.9	11.4	11.4	0.0	0.0	19.6	0.0	1.6	19.6
D-3358	0.0	0.0	0.0	0.0	0.0	0.0	0.0	0.0	0.0	0.0	0.0	0.0	0.0	0.0	0.0	0.0	0.0	0.0
D-3360	0.0	9.2	0.0	0.0	0.0	0.0	0.0	0.0	0.0	0.0	0.0	0.0	0.0	0.0	0.0	0.0	0.0	0.0
D-3361	0.0	0.0	0.0	4624	0.0	2944	176.0	128	2256	2352	0.0	0.0	0.0	16.0	0.0	0.0	0.0	0.0
D-3362	0.0	15.9	0.0	66.0	18.2	318.6	102.4	93.3	113.8	13.7	9.1	0.0	0.0	0.0	109.3	2.3	0.0	9.1
D-3363	3.9	0.0	1.0	77.9	30.8	113.5	39.5	17.3	18.3	11.6	1.9	0.0	0.0	8.7	15.4	0.0	1.0	37.5
D-3365	5.5	0.0	0.0	4.4	3.3	15.3	4.9	0.5	4.9	0.0	2.2	0.0	0.0	0.5	38.7	0.0	1.1	4.9
D-3366	0.0	1.9	0.0	53.5	1.9	161.4	111.8	20.4	18.5	25.3	0.0	6.8	0.0	0.0	79.7	0.0	0.0	6.8
D-3367	0.0	0.7	0.0	22.0	0.0	35.2	1.5	2.9	4.4	0.7	0.7	0.0	0.0	0.0	0.7	0.0	0.0	0.0
D-3368	0.0	0.0	0.0	12.9	0.0	5.5	0.6	0.0	1.2	0.0	0.0	0.0	0.0	0.0	0.0	0.0	0.0	0.0
D-3370	4.3	4.3	0.0	246.3	0.0	59.5	12.7	0.0	135.9	25.5	127.4	0.0	0.0	8.5	21.2	0.0	76.4	25.5
KC-111	0.0	0.0	0.0	0.0	0.0	0.0	0.0	0.0	0.0	0.0	0.0	0.0	0.0	0.0	0.0	0.0	0.0	0.0

Table 3-3. Peru Margin surface sediment physical and geochemical data.

Site I.D.	Dry Bulk Den. (g/cm^3)	Fraction >63µm (%)	Porosity	Inorganic Carbon (%)	Organic Carbon (%)
BC-02	0.14	3.7	0.77	0.18	7.6
BC-09	0.21	6.8	0.84	0.09	7.61
BC-17	0.22	2.76	0.74	0.13	10.09
BC-21	0.32	1.4	0.78	0.25	4.12
BC-33	0.75	0.62	0.72	0.85	4.17
BC-33	0.17	9.4	0.99	0.09	
BC-42	1.01	99	0.32	0.11	1.02
BC-50	1.22	98.43	0.46	0.09	1.15
BC-51	1.14	99	0.38	0.06	1.21
BC-53	0.89	22.88	0.5	1.78	0.85
BC-54	1.13	99	0.46	0.05	1.77
BC-56	0.97	11.16	0.52	0.12	0.93
BC-57	0.18	20.99	0.84		12.55
BC-62	0.57	29.5	0.67	0.71	4.21
BC-63	1.17	6.2	0.49		1.26
BC-76	0.46	19.78	0.73	0.87	7.26
BC-79	0.86	99	0.54	0.23	2.49
BC-81	0.4	39.5	0.96	0.09	8.59
BC-85	0.17	2.25	0.76	0	9.04
BC-87	1.1	85.16	0.45	2.6	1.35
BC-91	0.21	2.42	0.87	0.13	16.92
BC-92	0.17	5.6	0.95	0.24	6.14
BC-116	0.49	28.98	0.56		
BC-117	0.44	9.53	0.65	0.56	3.61
BC-123	0.68	38.24	0.85	0.56	4.7
BC-125	0.19	16.47	0.78	1.11	11.09
BC-135	1.01	99	0.72	0.74	1.91
BC-144	0.17	15.04	0.83	0.16	6.3
BC-153	0.17	91.86	0.86	0.69	15.71
D-3344	0.18	2.2	0.85	0.5	7.63
D-3349	0.53	5.88	0.54	0.96	5.72
D-3351	1.16	98.85	0.43	0.09	1.52
D-3353	0.61	37.72	0.87	1.02	6.03
D-3354	0.94	99	0.55	0.36	3.11
D-3354	0.56	83.93	0.54	0.29	3.48
D-3355	1.16	99	0.69	1.14	2.74
D-3356	0.25	95.14	0.74	4.79	6.64
D-3356	1.17	69.93	0.61	1.87	3.06
D-3357	0.89	78.72	0.73	0.58	
D-3358	0.97	12.05	0.59	0.24	0.92
D-3360	0.23	2.3	0.83	0.07	6.52
D-3361	0.1	75	0.58	3.13	7.27
D-3362	0.94	99	0.63	1.11	2.68
D-3363	1.39	34.28	0.54	1.27	2.16
D-3365	1.22	20.76	0.54	0.69	0.63
D-3366	0.46	5.95	0.64	0.83	3.07
D-3367	0.73	75.46	0.59	0.9	2.86
D-3368	0.22	6.13	0.68	0.15	17.77
D-3370	1	99	0.3	1.46	9.62
KC-111	0.12	4.07	0.77	0.07	15.45

Table 3.4. Sample of duplicate coulometric analyses.

Sample Identification	Corg (Wt. %)	Standard Dev
687A 1H-04, 0-5 DUP	6.00	
687A 1H-04, 0-5 DUP 2	6.13	0.09
687A 2H-01, 7-12	7.83	
687A 2H-01, 7-12 DUP	9.74	
687A 2H-01, 7-12 DUP2	9.75	1.11
687A 2H-03, 0-5	2.35	
687A 2H-03, 0-5 DUP	2.36	0.01
687A 2H-04, 100-105	0.66	
687A 2H-04, 100-105 DUP	0.85	0.13
687A 2H-06, 0-5	2.52	
687A 2H-06, 0-5 DUP	3.16	0.45

Table 3.5. Oxygen and carbon light stable isotope analysis data--surface sediments.

Site	Foram. Species	$\delta^{13}C$ (≡)	$\delta^{18}O$ (≡)
BC-42	*Uvigerina spp.*	0.20	2.04
BC-53	*B. plicata*	-0.28	1.02
BC-76	*Uvigerina spp.*	-0.14	2.27
BC-87	*B. plicata*	0.03	1.35
BC-92	*Uvigerina spp.*	-0.18	2.49
BC-116	*B. humilis*	-1.27	0.49
BC-116	*B. humilis*	-0.89	1.48
BC-117	*B. humilis*	-1.94	-0.52
BC-125	*B. plicata*	-0.42	0.48
D-3351	*Uvigerina spp.*	-0.51	0.86
D-3353	*B. interjuncta*	0.19	1.90
D-3355	*B. humilis*	-0.54	2.03
D-3356	*B. humilis*	-1.22	0.47
D-3356	*B. humilis*	-0.93	1.46
D-3357	*B. plicata*	-0.13	1.40
D-3357	*Uvigerina spp.*	0.14	2.00
D-3362	*B. humilis*	-1.19	0.72
D-3363	*Uvigerina spp.*	-0.34	1.28
D-3363	*B. interjuncta*	-0.14	1.82
D-3366	*B. interjuncta*	-0.18	1.69

Table 3.6. Reproducibility data--surface sediments.

Site I.D.	$\delta^{13}C$ (≅)
1) D-3362	-1.179
2) D-3362	-1.185
Difference	0.006
1) BC-116	-0.887
2) BC-116	-0.738
3) BC-116	-0.821
St. Dev.	0.075

Table 3.7. Absolute age data from sea floor phosphorite sample (BC-57) taken from the Peru Margin sea floor (Burnett, unpublished).

Slice No.	Interval (mm)	Age (ky)
top		
8	0--3	7.5±0.4
7	3--5	7.6±0.6
6	5--8	8.2±0.7
5	8--11	7.2±0.7
4	11--15	7.4±1.0
3	15--20	5.6±1.3
2	20--23	6.9±1.1
1	23--25	4.7±0.7
bottom		

Table 3.8. The four dominant factors of surface sediment benthic foraminiferal assemblages.

	Factor			
Species	1	2	3	4
Angulogerina carinata	0.067	0.020	-0.328	-0.809
Bolivina costata	0.530	-1.707	0.074	-0.036
Bolivina minuta	0.030	0.004	-0.096	0.010
Bolivina plicata	1.241	0.384	0.385	-0.108
Bolivina spissa	0.082	0.021	-0.197	-0.375
Bolivina humilis	1.222	0.264	0.177	0.051
Brizalina interjuncta	0.251	0.069	-0.083	0.033
Buliminella subfusiformis	0.151	0.041	0.012	0.018
Cancris carmenensis	0.359	0.103	0.068	-0.014
Cancris inflatus	0.178	0.051	0.041	-0.003
Cassidulina auka	0.140	0.029	-0.034	-0.011
Nonionella auris	0.024	0.005	-0.023	0.019
Parabolivina peruensis	0.003	0.001	0.001	0.000
Planulina limbata	0.019	0.005	-0.037	-0.015
Pseudoparrela subperuviana	0.524	0.023	-1.056	0.491
Pullenia subcarinata	0.000	0.000	0.000	0.000
Uvigerina peregrina	0.177	0.043	-0.514	-0.333
Uvigerina striata	0.179	0.045	-0.311	-0.155
% Variance	33	26	15	10
Cum. % Variance	33	59	74	84

Table 3.9. Factor loadings for each surface sediment sample and total variance explained.

	Factor				
Site I.D.	1	2	3	4	Total % var.
BC-21	0.11	0.88	0.00	0.00	1.00
BC-42	0.06	0.00	0.50	0.31	0.87
BC-50	0.03	0.00	0.29	0.64	0.96
BC-51	0.01	0.00	0.13	0.74	0.88
BC-53	0.89	0.06	0.04	0.00	1.00
BC-57	0.83	0.07	0.04	0.00	0.95
BC-62	0.20	0.00	0.75	0.02	0.98
BC-76	0.19	0.00	0.76	0.01	0.96
BC-87	0.86	0.06	0.00	0.00	0.92
BC-92	0.11	0.89	0.00	0.00	1.00
BC-116	0.94	0.04	0.00	0.00	0.98
BC-117	0.42	0.00	0.45	0.11	0.98
BC-123	0.90	0.05	0.02	0.00	0.98
BC-125	0.93	0.05	0.02	0.00	1.00
D-3344	0.22	0.76	0.01	0.00	1.00
D-3349	0.95	0.04	0.01	0.00	1.00
D-3351	0.03	0.00	0.23	0.64	0.89
D-3353	0.16	0.01	0.63	0.04	0.85
D-3354	0.32	0.01	0.50	0.00	0.83
D-3354	0.17	0.00	0.67	0.13	0.97
D-3355	0.76	0.05	0.05	0.06	0.92
D-3356	0.88	0.05	0.03	0.00	0.96
D-3356	0.93	0.05	0.01	0.00	1.00
D-3357	0.92	0.05	0.01	0.00	0.99
D-3360	0.09	0.91	0.00	0.00	1.00
D-3361	0.88	0.07	0.05	0.00	0.99
D-3362	0.91	0.03	0.00	0.01	0.95
D-3363	0.93	0.06	0.00	0.00	0.99
D-3365	0.55	0.01	0.38	0.04	0.98
D-3366	0.90	0.04	0.01	0.01	0.97
D-3367	0.91	0.05	0.03	0.00	0.99
D-3368	0.86	0.07	0.06	0.00	0.98
D-3370	0.87	0.06	0.01	0.01	0.94

Table 3.10. Comparison of environmental factors of surface sediments.

Temp. (°C)		O2 (uMol)		Salinity (‰)		Dry Bulk Density (g/cm^3)		% >63um		% Organic Carbon	
Barren	Non-Barren	Barren	Non-Barren	Barren	Non-Barren	Barren	Non-Barren	Barren	Non-Barren	Barren	Non-Barren
13.27	13.67	5.16	5.85	34.92	32.19	0.14	0.32	3.70	1.40	7.60	4.12
13.27	5.61	5.16	20.30	34.92	34.53	0.21	1.01	6.80	99.00	7.61	1.02
9.36	4.43	2.96	42.37	34.69	34.54	0.22	1.22	2.76	98.43	10.09	1.15
9.36	6.89	2.96	7.73	34.69	34.57	0.75	1.14	0.62	99.00	4.17	1.21
4.34	11.76	43.80	4.30	34.54	34.83	0.17	0.89	9.40	22.88	0.00	0.85
13.27	11.76	5.16	4.30	34.92	34.83	1.13	0.18	99.00	20.99	1.77	12.55
11.76	13.27	4.30	5.16	34.83	34.92	0.97	0.57	11.16	29.50	0.93	4.21
13.44	11.71	5.82	4.13	34.93	34.84	1.17	0.46	6.20	19.78	1.26	7.26
14.00	5.61	4.30	20.30	34.83	34.53	0.86	1.10	99.00	85.16	2.49	1.35
11.76	6.89		7.73		34.57	0.40	0.17	39.50	5.60	8.59	6.14
11.38	10.50		3.05		34.66	0.17	0.49	2.25	28.98	9.04	0.00
12.52	10.50		2.96		34.69	0.21	0.44	2.42	9.53	16.92	3.61
2.98	8.76		2.96		34.69	1.01	0.68	99.00	38.24	1.91	4.70
14.00	9.36		7.73		34.57	0.17	0.19	15.04	16.47	6.30	11.09
4.34	9.36		5.82		34.93	0.17	0.18	91.86	2.20	15.71	7.63
	6.89		4.30		34.83	0.97	0.53	12.05	5.88	0.92	5.72
	13.44		3.14		34.72	0.12	1.16	4.07	98.85	15.45	1.52
	11.76		3.14		34.72		0.61		37.72		6.03
	9.91		3.14		34.72		0.94		99.00		3.11
	12.00		4.30		34.83		0.56		83.93		3.48
	5.60		3.14				1.16		99.00		2.74
	9.91		3.14				0.25		95.14		6.64
	9.91		4.30				1.17		69.93		3.06
	11.76						0.89		78.72		0.00
	12.80						0.23		2.30		6.52
							0.10		75.00		7.27
							0.94		99.00		2.68
							1.39		34.28		2.16
							1.22		20.76		0.63
							0.46		5.95		3.07
							0.73		75.46		2.86
							0.22		6.13		17.77
							1.00		99.00		9.62
10.60	**9.76**	**8.85**	**7.53**	**34.81**	**34.59**	**0.52**	**0.68**	**29.70**	**50.40**	**6.52**	**4.60**
3.77	**2.76**	**13.14**	**8.98**	**0.14**	**0.58**	**0.41**	**0.39**	**39.63**	**38.84**	**5.57**	**3.93**
15	**25**	**9**	**23**	**9**	**20**	**17**	**33**	**17**	**33**	**17**	**33**
0.81		**0.33**		**1.13**		**1.38**		**1.77**		**1.41**	
38		**30**		**27**		**48**		**48**		**48**	

Average
St. Deviation
Count

t-score
Degrees of freedom

Table 3.11. Classification of sand fraction in surface sediments.

Site	Foram. %	Fish Debris %	Phos. Pellets %	Glauc. Pellets %	Diatoms %	Gypsum XL's %	Undifferentiated Silt/Sand %
BC-42	1	0	0	99	0	0	0
BC-43	1	0	0	99	0	0	0
BC-50	1	0	0	99	0	0	0
BC-51	1	0	0	99	0	0	0
BC-53	10	30	0	0	0	35	25
BC-57	10	50	0	0	0	12	28
BC-62	5	0	0	50	0	0	45
BC-63	10	50	1	0	0	0	39
BC-87	20	10	5	0	0	0	65
BC-116	85	10	0	0	0	0	5
BC-117	40	10	5	0	5	0	40
BC-123	25	25	10	0	0	0	40
BC-125	55	2	0	0	0	0	43
D-3344	10	0	0	0	0	0	90
D-3349	5	0	0	25	0	0	70
D-3351	1	0	0	99	0	0	0
D-3351	1	0	0	99	0	0	0
D-3353	5	0	0	50	0	0	45
D-3354	1	0	0	99	0	0	0
D-3355	1	50	5	5	0	0	39
D-3356	15	0	0	0	0	0	85
D-3357	5	10	10	0	0	0	75
D-3363	55	20	1	0	0	10	14
D-3365	10	10	10	0	0	70	0
D-3366	50	25	1	0	0	0	24
D-3367	15	20	20	0	0	0	45
D-3368	5	25	0	0	0	50	20
D-3370	5	0	50	0	0	0	45

Table 4.1. Benthic foraminifera census data, specimens counted and percentage of assemblage for Holes 679B and 680A.

Site, interval	Depth (m)	*Bolivina costata*		*Nonionella miocenica*		*Bulimmella elegantissima limbose*		*Angulogerina carinata*		*Bolivina plicata*		*Brizalina interjuncta bicostata*		*Cancris carmenensis*		*Epistominella exiguaensis*		*Pseudoparrella subperuviana*		*Uvigerina striata*		*Cancris inflatus*		*Bolivina humilis*		*Buliminella subfusiformis*		*Parabolivina peruvensis*		*"Ellipsoglandulina" tregilis*		*Cassidulina pulchella*		*Bolivina punctata*		*minuta*		*limbata*		*Pullenia*		*Globocassidulina crassa*		*Brizalina pseudo*		*Buliminella curta*		*Megastomella pursiima*	
		#	%	#	%	#	%	#	%	#	%	#	%	#	%	#	%	#	%	#	%	#	%	#	%	#	%	#	%	#	%	#	%	#	%	#	%	#	%	#	%	#	%	#	%	#	%
679B 1H-01, 10-15	0.1	6	3	0		0		0		0		9	4			0	53	24		0	2	1		0	131	58	24	11		0		0		0		0		0		0		0		0		0		0	
679B 1H-01, 25-30	0.25		0	0		0		0		0		0		12	4		0		0		0		0	263	95	1	0		0	1	0		0		0		0		0		0		0		0		0	
679B 1H-01, 100-105	1	18	5	0		0		43	11		0	28	7			0	63	16		0	190	50		0	14	4		0		0		0		0		0		0		0	27	7		0		0	
679B 1H-01, 125-130	1.25		0	0		0		20	8		0		0			0	93	38		0	38	16		0	76	32	14	6		0	1	0		0		0		0		0		0		0		0	
679B 1H-02, 0-5	1.5	4	1	0		0		16	5		0	17	5			0	75	21		0	52	15		0	155	44	28	8		0	4	1		0		0		0		0		0		0		0	
679B 1H-02, 25-30	1.75	4	1	0		0		5	1		0		0			0	99	17		0	10	2		0	436	75	24	4		0		0		0		0		0		0		0		0		0	
679B-1H-02, 47-52	1.97	4	1	0		0		3	1		0	2	0			0	136	28		0	4	1		0	328	67	13	3		0		0		0		0		0		0		0		0		0	
679B 1H-03, 50-55	3.5	25	6	0		0		8	2	50	11	1	0			0	257	58		0	1	0		0	88	20	12	3		0		0		0		0		0		0		0		0		0	
679B 1H-03, 75-80	3.75	52	24	0		0		31	14	1	0	12	6			0	86	40		0		0		0	27	13	7	3		0		0		0		0		0		0		0		0		0	
679B 1H-03 100-105	4		0	0		0		22	8		0	40	15	5	2	24	9		0		0		0	98	36	8	3		0		0	62	24		0		0		0		0		0		0	
679B 1H-03, 125-130	4.25	15	16	0		0		7	7		0	3	3	3	3	8	8		0		0		0	31	32	2	2		0		0	27	28		0		0		0		0		0		0	
679B 1H-04, 0-5	4.5	44	26	0		0		24	14		0	48	28			0	12	7		0		0		0	36	21	5	3		0		0		0		0		0		0		0		0		0	
679B 1H-04, 25-30	4.75	1	0	0		0		13	6		0	4	2			0	132	58		0		0		0	63	28	10	4		0		0		0		0		0		0	5	2		0		0	
679B 1H-04, 50-55	5	50	12	0		0		48	11		0	130	30	6	1	100	23		0		0		0	42	10	12	3		0		0		0		0		0	40	9		0		0		0	
679B 1H-04, 75-80	5.25		0	0		0		85	25	14	4	12	4	15	4		0	48	14		0		0	84	25	1	0		0		0	56	17	2	1		0	12	4		0		0		0	
679B 1H-04, 100-105	5.5		0	0		0		2	1	1	0	12	4			0		0	207	65	6	2		0	78	25	4	1		0		0		0		0	7	2		0		0		0		0	
679B 1H-04, 125-130	5.75		0	0		0		11	3.6	48	16		0	11	3.6		0	101	33		0		0	125	41	10	3.3		0		0		0		0		0		0		0		0		0		0	
679B 1H-05, 0-5	6		0	0		0		2	0.7	6	2.2		0			0		0	27	10	16	5.9		0	136	50	74	27		0		0	1	0.4		0	8	3		0		0		0		0	
679B 1H-05, 24-28	6.24	30	11	0		0		3	1.1	44	16		0	48	17		0	1	0.4	22	7.9		0	67	24	40	14		0		0	2	0.7		0	22	7.9		0		0		0		0	
679B 1H-CC, 13-18	6.43	59	23	0		0			0	3	1		0	15	5		0	1	0.3	8	2.6		0	55	18	50	17		0		0		0		0	102	34		0		0		0		0	
679B 2H-01,0-5	6.52	38	11	0		0		14	4.2	35	10	2	0.6	12	3.6		0	72	21	20	5.9		0	76	23	54	16		0		0	5	1.5	2	0.6	7	2.1		0		0		0		0	
679B 2H-01, 25-30	6.77	70	23	0		0		7	2.3	17	5.6	6	2	9	2.9		0	47	15	19	6.2		0	59	19	42	14		0		0	19	6.2		0	7	2.3	4	1.3		0		0		0	
679B 2H-01, 50-55	7.02	83	30	0		0		1	0.4	5	1.8	10	3.6	17	6.1		0	70	25	6	2.2		0	25	9	29	10		0		0		0	10	3.6	16	5.8	2	0.7		0	4	1.4		0		0	

Table 4.1. (Continued) Benthic foraminifera census data, specimens counted and percentage of assemblage for Holes 679B and 680A.

Site, interval	Depth (m)	*Bolivina costata*		*Nonionella miocenica*		*Bulimnella elegantissima imbosa*		*Angulogerina carinata*		*Bolivina plicata*		*Brizalina interjunda bicostata*		*Cancris carmenensis*		*Epistominella aberrasensis*		*Pseudoparrella subperuviana*		*Uvigerina striata*		*Cancris inflatus*		*Bolivina humilis*		*Buliminella subfusiformis*		*Parabolivina peruvensis*		*"Ellipsoglandulina" fragilis*		*Cassidulina pulchella*		*Bolivina punctata*		*minuta*		*limbata*		*Pullenia*		*Globocassidulina crassa*		*Brizalina pseudo*		*Buliminella curta*		*Megastomella pursaima*	
		#	%	#	%	#	%	#	%	#	%	#	%	#	%	#	%	#	%	#	%	#	%	#	%	#	%	#	%	#	%	#	%	#	%	#	%	#	%	#	%	#	%	#	%	#	%
679B 2H-01, 75-80	7.27	57	22		0		0		0	8	3.1	1	0.4	12	4.6		0	71	27	4	1.5		0	18	6.9	37	14		0		0		0	1	0.4	46	18		0		0		0		0		0		0
679B 2H-01, 100-105	7.52	10	6.5		0		0		0	71	46		0	2	1.3		0	1	0.7		0		0	53	35	10	6.5		0		0		0		0	3	2		0		0		0		0		0		0
679B 2H-01, 125-130	7.77	3	1		0	1	0.3	40	13	74	24	34	11		0	93	30		0	20	6.5	13	4.2	2	0.7		0		0		0	11	3.6		0	2	0.7		0		0		0		0		0
679B 2H-02, 1-6	8.03		0		0		0	42	13	62	19	50	15		0	108	33		0	29	8.8	18	5.5	2	0.6		0		0		0	18	5.5		0	7	2.1		0		0		0		0		0
679B 2H-02, 27-32	8.29		0		0		0	104	25	1	0.2	57	14		0	82	20		0	58	14		0		0		0		0		0	97	24		0		0	6	1.5		0		0		0		0
679B 2H-02, 75-80	8.77	5	1.6		0		0	30	9.7	15	4.8	25	8.1		0		0	86	28	58	19		0	1	0.3		0		0		0	35	11	1	0.3	21	6.8	8	2.6		0		0		0		0
679B 2H-02, 125-130	9.27	2	0.5		0		0	65	16		0	14	3.4		0	121	30		0	39	9.6		0	8	2		0		0		0	155	38		0		0	1	0.2		0		0		0		0
679B 2H-03, 125-130	10.77	6	1.2		0		0	116	23	16	3.1	28	5.4		0	80	16		0	138	27		0	2	0.4		0		0		0	108	21		0	6	1.2	4	0.8		0		0		0		0
679B 2H-04, 25-30	11.27	1	1		0		0	16	16	7	6.9	6	5.9		0	28	27		0	20	20	2	2	1	1		0		0		0	15	15		0		0	4	3.9		0		0		0		0
679B 2H-04, 50-55	11.52	3	0.9		0		0	7	2.2	5	1.6	5	1.6		0		0	58	18	15	4.7	2	0.6	222	69		0		0		0	5	1.6		0		0		0		0		0		0		0
679B 2H-04, 75-80	11.77	3	1		0		0		0	6	2		0		0		0		0		0		0	43	14	59	20	190	63		0		0		0		0		0		0		0		0		0
679B 2H-04, 100-105	12.02		0		0		0	6	1.5	7	1.8	4	1		0	15	3.9		0	4	1		0	46	12	45	12	261	67		0		0		0		0		0		0		0		0		0
679B 2H-04, 125-130	12.27	1	0.3		0		0	2	0.6	24	6.9	6	1.7		0	10	2.9		0	3	0.9		0	123	36	71	21	105	30		0		0		0		0		0		0		0		0		0
679B 2H-05, 0-5	12.52		0		0		0		0	12	5.5		0		0	6	2.7		0	1	0.5		0	120	55	16	7.3	65	30		0		0		0		0		0		0		0		0		0
679B 2H-05, 75-80	13.27		0		0		0		0	3	6.8		0		0		0		0	2	4.5		0	21	48	3	6.8	15	34		0		0		0		0		0		0		0		0		0
679B 2H-05, 100-105	13.52		0		0		0		0	2	1.5		0		0	17	13		0		0		0	19	15	13	10	79	61		0		0		0		0		0		0		0		0		0
679B 2H-05, 125-130	13.77		0		0		0		0		0		0		0	1	6.7		0		0		0	2	13		0	12	80		0		0		0		0		0		0		0		0		0
679B 2H-06, 0-5	14.02		0		0		0		0	3	4		0		0	3	4		0		0		0	5	6.7	8	11	56	75		0		0		0		0		0		0		0		0		0
679B 2H-06, 50-55	14.52		0		0		0	2	0.6		0	6	1.7		0	6	1.7		0	6	1.7		0	84	23	88	24	168	47		0		0		0		0		0		0		0		0		0
679B 2H-06, 125-130	15.27	1	0.3		0		0		0	3	1		0		0		0		0		0		0	13	4.4	117	39	164	55		0		0		0		0		0		0		0		0		0
679B 2H-07, 0-5	15.52		0		0		0		0	12	3.8	1	0.3		0	2	0.6		0		0		0	4	1.3	132	41	168	53		0		0		0		0	1	0.3		0		0		0		0
679B 2H-07, 25-30	15.77		0		0		0		0	3	1.2		0		0	11	4.4		0		0		0	7	2.8	33	13	196	78		0		0		0		0		0		0		0		0		0
679B 2H-07, 50-55	16.02		0		0		0		0	21	7.7		0		0	1	0.4		0		0		0	46	17	60	22	135	49		0		0		0		0		0		0	0	11	4		0	

Table 4.1. (Continued) Benthic foraminifera census data, specimens counted and percentage of assemblage for Holes 679B and 680A.

Site, interval	Depth (m)	*Bolivina costata*		*Nonionella miocenica*		*Buliminella elegantissima limbose*		*Angulogerina carinata*		*Bolivina plicata*		*Brizalina interjuncta bicostata*		*Cancris carmenensis*		*Epistominella exiguaensis*		*Pseudoparrella subperuviana*		*Uvigerina striata*		*Cancris inflatus*		*Bolivina humilis*		*Buliminella subfusiformis*		*Parabolivina peruvensis*		*"Elliposoglandulina" trapilis*		*Cassidulina patchella*		*Bolivina punctata*		*minuta*		*limbata*		*Pullenia*		*Globocassidulina crassa*		*Brizalina pseudo*		*Buliminella curta*		*Megastomella punsirina*	
		#	%	#	%	#	%	#	%	#	%	#	%	#	%	#	%	#	%	#	%	#	%	#	%	#	%	#	%	#	%	#	%	#	%	#	%	#	%	#	%	#	%	#	%	#	%	#	%
679B 2H-CC, 0-5	16.27		0		0		0	6	1.8	32	9.8	3	0.9		0	4	1.2		0	4	1.2		0	7	2.1	64	20	185	56		0	5	1.5		0	4	1.2		0		0		0		0	12	3.7		0
680A 1H-01, 100-105	1		0	7	2		0		0		0		0		0		0		0		0		0	339	97	1	0.3		0		0	1	0.3		0		0		0		0		0		0		0
680A 1H-02, 0-5	1.5	4	0.8		0		0		0	18	3.7		0		0	33	6.7		0		0		0	433	88	4	0.8		0		0		0	1	0.2		0		0		0		0		0		0
680A 1H-02, 75-80	2.25		0		0		0		0	34	6.6		0		0		0	180	35		0		0	160	31		0		0	138	27		0		0		0		0		0		0		0		0
680A 1H-03, 0-5	3	1	0.3		0		0		0	16	4.1		0	0	331	86			0		0		0	26	6.7		0		0		0	13	3.4		0		0		0		0		0		0		0
680A 1H-03, 50-55	3.5	2	0.5		0		0		0	14	3.8		0	0	74	20			0		0		0	254	69	12	3.2		0		0	12	3.2		0	2	0.5		0		0		0		0		0
680A 1H-03, 102-107	4.02	18	4.2		0	8	1.9		0	8	1.9		0	0	12	2.8			0		0		0	366	89		0		0		0		0		0		0		0		0		0		0		0
680A 1H-03, 125-130	4.25	8	4		0		0		0		0		0		0		0	20	10		0		0	160	80	8	4		0		0		0	4	2		0		0		0		0		0		0
680A 1H-04, 0-5	4.5	1	0.2		0		0	1	0.2	21	4.2		0		0		0	177	36	5	1		0	259	52	30	6		0		0	1	0.2		0	3	0.6		0		0		0		0		0
680A 1H-04, 25-30	4.75		0		0		0		0	10	3.3		0		0		0	101	33		0		0	175	57	7	2.3		0		0	2	0.7		0	10	3.3		0		0		0		0		0
680A 1H-04, 50-55	5	6	0.8		0		0		0	2	0.3		0		0		0	60	8.4		0		0	619	86	15	2.1		0		0	15	2.1		0		0		0		0		0		0		0
680A 1H-04, 73-78	5.23	8	1.3		0		0		0	5	0.8		0	0	105	17			0		0		0	489	79	5	0.8		0		0	2	0.3		0	4	0.6		0		0		0		0		0
680A 1H-04, 100-105	5.5	2	0.4		0		0		0		0		0		0		0	139	26		0		0	363	68	19	3.6		0		0	10	1.9		0		0		0		0		0		0		0
680A 1H-04, 125-130	5.75	1	0.3		0		0		0	3	0.9		0		0		0	27	8.3		0		0	282	87	8	2.5		0		0	3	0.9		0		0		0		0		0		0		0
680A 1H-05, 0-5	6		0		0		0		0	43	8.5		0		0		0	211	42		0		0	224	44	15	3		0		0	1	0.2		0	13	2.6		0		0		0		0		0
680A 1H-05, 25-30	6.25	3	1		0		0		0	13	4.1		0		0		0	124	39		0		0	165	52	5	1.6		0		0	1	0.3		0	4	1.3		0		0		0		0		0
680A 1H-05, 50-55	6.5	5	0.9		0		0		0	5	0.9		0		0		0	102	17		0		0	399	68	26	4.5		0		0	27	4.6		0	1	0.2		0		0		0	18	3.1		0
680A 1H-05, 75-80	6.75	38	5.9		0		0		0	6	0.9		0		0		0	76	12		0		0	462	72	12	1.9		0		0	24	3.7		0		0		0		0		0	10	1.6	16	2.5
680A 1H-05, 105-110	7.05	1	0.3		0		0		0	18	4.8		0		0		0	236	63		0		0	87	23	7	1.9		0		0	3	0.8		0	20	5.3		0		0		0		0		0
680A 1H-05, 125-130	7.25	7	1.5		0		0		0	63	14		0		0		0	188	41		0		0	192	42	3	0.7		0		0		0	1	0.2		0		0		0		0		0		0
680A 1H-06, 0-5	7.5	22	4.7		0		0		0	2	0.4		0	24	5.1		0	28	5.9		0		0	359	76	38	8		0		0		0		0		0		0		0		0		0		0
680A 1H-06, 25-30	7.75	10	3.2		0		0		0		0		0	8	2.5		0	32	10		0		0	263	84	1	0.3		0		0		0		0		0		0		0		0		0		0		0

Table 4.1. (Continued) Benthic foraminifera census data, specimens counted and percentage of assemblage for Holes 679B and 680A.

Site, interval	Depth (m)	*Bolivina costata*		*Nonionella miocenica*		*Bulimnella elegantissima imbose*		*Angulogerina carinata*		*Bolivina plicata*		*Brizalina interjuncta bicostata*		*Canoris carmenensis*		*Epistominella exiguaensis*		*Pseudoparrella subperuviana*		*Uvigerina striata*		*Canoris inflatus*		*Bolivina humilis*		*Buliminella subfusiformis*		*Parabolivina peruensis*		*"Ellipsoglandulina" fragilis*		*Cassidulina pulchella*		*Bolivina punctata*		*minuta*		*limbata*		*Pullenia*		*Globocassidulina crassa*		*Brizalina pseudo*		*Buliminella curta*		*Megastomella pursima*	
		#	%	#	%	#	%	#	%	#	%	#	%	#	%	#	%	#	%	#	%	#	%	#	%	#	%	#	%	#	%	#	%	#	%	#	%	#	%	#	%	#	%	#	%	#	%
680A 2H-01, 7-12	8.37	8	2.3		0		0		0	11	3.2		0		0	181	53		0		0		0	101	29	7	2		0		0	36	10		0		0		0		0		0		0		0		0
680A 2H-01, 25-30	8.56	26	7.9		0		0		0		0		0		0	75	23		0		0		0	168	51	50	15		0		0	3	0.9	6	1.8		0		0		0		0		0		0		0
680A 2H-01, 50-55	8.81	34	8.4		0		0	2	0.5		0	1	0.2	70	17		0		0		0	276	68	19	4.7		0		0	5	1.2		0		0		0		0		0		0		0		0
680A 2H-01, 75-80	9.06	40	13	127	40		0		0		0		0		0		0		0		0		0	131	41	15	4.7		0		0	1	0.3	3	0.9		0		0		0		0		0		0		0
680A 2H-01, 100-105	9.31	15	5.6	65	24		0		0		0		0		0		0		0		0		0	152	57	34	13		0		0		0		0		0		0		0		0		0		0		0
680A 2H-01, 125-130	9.56	32	7.5	198	46		0		0		0		0		0		0		0		0		0	179	42	17	4		0		0		0		0		0		0		0		0		0		0		0
680A 2H-02, 0-5	9.81	52	13	148	37		0		0		0		0		0		0		0		0		0	185	47	10	2.5		0		0		0		0		0		0		0		0		0		0		0
680A 2H-02, 25-30	10.06	68	25	49	18		0		0		0		0		0		0		0		0		0	146	54	6	2.2		0		0		0		0		0		0		0		0		0		0		0
680A 2H-02, 50-55	10.31	21	8.9	6	2.5		0		0		0	1	0.4	2	0.8		0		0		0		0	203	86	3	1.3		0		0		0		0		0		0		0		0		0		0		0
680A 2H-02, 72-77	10.56	24	5.7	19	4.5		0		0		0		0		0		0		0		0		0	375	89	5	1.2		0		0		0		0		0		0		0		0		0		0		0
680A 2H-05, 26-31	14.57	5	1.9		0		0		0		0		0		0	33	13		0		0		0	205	79	2	0.8		0		0	15	5.8		0		0		0		0		0		0		0		0

Table 4.2. Benthic foraminifera census data, specimens counted and percentage of assemblage for Hole 681A.

Site, interval	*Boliniva costata* #	%	*Bolivina humilis* #	%	*Bolivina plicata* #	%	*Nonionella auris* #	%	*Pseudoparrella subperuviana* #	%
681A 1H-03, 3-8	16	4.9	144	43.9	40	12.2		0.0	128	39.0
681A 1H-04, 125-130	8	38.1	13	61.9		0.0		0.0		0.0
681A 2H-01, 125-130	52	76.5	15	22.1		0.0	T	1.5		0.0
681A 2H-02, 54-59	7	100.0		0.0		0.0		0.0		0.0
681A 2H-03, 47-52	31	57.4	23	42.6		0.0		0.0		0.0
681A 2H-04, 125-130	12	92.3	1	7.7		0.0		0.0		0.0
681A 2H-05, 50-55	14	46.7	16	53.3		0.0		0.0		0.0
681A 2H-07, 50-55	62	35.0	105	59.3		0.0	10	5.6		0.0

Table 4.4. Coulometric, accumulation rate, and dry bulk density data for Hole 679B.

Site, interval	Depth (m)	CaCO3 (%)	Corg (%)	S (%)	Corg Acc. Rate (mol/cm^2/yr)	S Acc. Rate (mol/cm^2/yr)	CaCO3 Acc. Rate (mol/cm^2/yr)	Dry Bulk Dens. (g/cm^3)
679B 1H-01, 10-15	0.1	26.8	11.3	1.2	1.0E-05	4.1E-07	2.9E-06	0.22
679B 1H-01, 25-30	0.25	1.8	9.1	3.6	1.2E-05	1.8E-06	2.9E-07	0.32
679B 1H-01, 50-55	0.5	0.1	6.0	1.0	9.7E-06	6.1E-07	1.6E-08	0.39
679B 1H-01, 79-84	0.79	0.0	5.8	1.7	3.5E-06	3.8E-07	0.0E+00	0.44
679B 1H-01, 100-105	1	49.2	3.3	1.6	1.9E-06	3.5E-07	3.4E-06	0.61
679B 1H-01, 125-130	1.25	49.3	5.6	0.8	6.9E-06	3.8E-07	7.4E-06	0.56
679B 1H-02, 0-5	1.5	45.6	5.9	0.8	6.6E-06	3.5E-07	6.2E-06	0.51
679B 1H-02, 25-30	1.75	21.7	11.5	1.5	1.7E-05	8.6E-07	3.9E-06	0.50
679B1H-02, 47-52	1.97	16.9	8.1	1.4	1.1E-05	7.3E-07	2.9E-06	0.48
679B 1H-2, 75-80	2.25	0.3	13.6	1.8	1.5E-05	7.4E-07	4.5E-08	0.38
679B 1H-02 100-105	2.5	5.1	8.5	2.0	1.3E-05	1.2E-06	9.6E-07	0.53
679B 1H-02, 125-130	2.75	0.2	7.2	1.7	1.5E-05	1.3E-06	6.0E-08	0.67
679B IH-03, 1-6	3.01	0.7	5.7	1.5	1.1E-05	1.1E-06	1.8E-07	0.67
679B 1H-3, 25-30	3.25	0.3	6.4	1.8	9.9E-06	1.0E-06	6.2E-08	0.52
679B 1H-03, 50-55	3.5	29.0	4.5	2.1	1.1E-05	1.9E-06	8.5E-06	0.82
679B 1H-03, 75-80	3.75	48.2	4.2	1.4	5.8E-06	7.3E-07	8.0E-06	0.83
679B 1H-03 100-105	4	52.2	4.9	0.9	6.0E-06	4.0E-07	7.7E-06	0.73
679B 1H-03, 125-130	4.25	36.3	5.9	1.0	6.3E-06	4.2E-07	4.7E-06	0.64
679B 1H-04, 0-5	4.5	51.2	4.1	0.9	4.1E-06	3.2E-07	6.1E-06	0.60
679B 1H-04, 25-30	4.75	33.1	5.1	1.5	5.7E-06	6.2E-07	4.5E-06	0.67
679B 1H-04, 50-55	5	46.8	5.0	1.0	1.6E-05	1.3E-06	1.8E-05	0.74
679B 1H-04, 75-80	5.25	40.1	6.7	1.1	1.6E-05	1.0E-06	1.2E-05	0.55
679B 1H-04, 100-105	5.5	29.6	2.0	0.9				
679B 1H-04, 125-130	5.75	27.0	7.6	1.4	1.9E-05	1.3E-06	8.2E-06	0.57
679B 1H-05, 0-5	6	42.6	7.2	1.2	1.8E-05	1.1E-06	1.3E-05	0.56
679B 1H-05, 24-28	6.24	33.8	5.8	1.2	1.7E-05	1.2E-06	1.1E-05	0.64
679B 1H-CC, 13-18	6.43	32.2	12.0	1.8	2.8E-05	1.6E-06	9.1E-06	0.53
679B 2H-01,0-5	6.52	23.1	7.7	1.5				
679B 2H-01, 25-30	6.77	31.9	10.0	1.3				
679B 2H-01, 50-55	7.02	45.5	6.9	1.1	1.5E-05	8.7E-07	1.2E-05	0.48
679B 2H-01 ,75-80	7.27	20.0	11.7	1.8	2.4E-05	1.4E-06	5.0E-06	0.47
679B 2H-01, 100-105	7.52	14.1	5.8	1.3	1.3E-05	1.1E-06	3.8E-06	0.51
679B 2H-01, 125-130	7.77	24.9	3.1	1.5	2.5E-06	4.6E-07	2.5E-06	0.84
679B 2H-02, 1-6	8.03	56.2	1.6	0.9	1.2E-06	2.8E-07	5.2E-06	0.79
679B 2H-02, 27-32	8.29							1.11
679B 2H-02, 50-55	8.52							
679B 2H-02, 75-80	8.77	40.6	1.9	1.0				
679B 2H-02, 100-105	9.02	0.2	6.3	1.8	3.3E-05	3.7E-06	1.1E-07	0.82
679B 2H-02, 125-130	9.27							
679B 2H-03, 0-5	9.52	0.3	9.2	2.0	4.0E-05	3.3E-06	1.7E-07	0.67
679B 2H-03, 25-30	9.77	0.2	9.7	2.0	4.1E-05	3.3E-06	1.3E-07	0.66
679B 2H-03, 50-55	10.02	0.2	8.3	1.9	3.1E-05	2.7E-06	1.1E-07	0.58
679B 2H-03, 75-80	10.27	0.2	8.5	1.7	3.0E-05	2.3E-06	1.1E-07	0.54
679B 2H-03, 100-105	10.52	0.3	10.7	1.3	3.8E-05	1.7E-06	1.4E-07	0.55
679B 2H-03, 125-130	10.77	0.3	10.5	1.9	3.7E-05	2.5E-06	1.4E-07	0.54
679B 2H-04, 0-5	11.02	0.2	12.5	2.1	3.8E-05	2.4E-06	6.0E-08	0.47
679B 2H-04, 25-30	11.27	0.9	11.2	2.5	9.6E-06	8.0E-07	9.4E-08	0.59
679B 2H-04, 50-55	11.52	5.7	5.2	1.6	3.8E-06	4.5E-07	5.0E-07	0.50
679B 2H-04, 75-80	11.77	8.7	6.3	1.6	1.3E-05	1.2E-06	2.2E-06	0.34
679B 2H-04, 100-105	12.02	16.8	8.1	1.7	2.0E-05	1.6E-06	5.0E-06	0.40
679B 2H-04, 125-130	12.27	12.5	6.9	2.5	2.2E-05	2.9E-06	4.7E-06	0.50
679B 2H-05, 0-5	12.52	19.4	6.6	1.7	2.6E-05	2.5E-06	9.3E-06	0.65
679B 2H-05, 25-30	12.77	0.6	7.6	1.8	1.5E-05	1.3E-06	1.3E-07	0.31
679B 2H-05, 48-53	13	1.9	5.6	1.6	1.3E-05	1.4E-06	5.3E-07	0.37
679B 2H-05, 75-80	13.27	3.8	5.9	1.7	1.9E-05	2.0E-06	1.4E-06	0.51
679B 2H-05, 100-105	13.52	5.1	7.1	1.7	3.1E-05	2.8E-06	2.6E-06	0.70
679B 2H-05, 125-130	13.77	1.7	7.7	1.8	2.0E-05	1.8E-06	5.3E-07	0.43
679B 2H-06, 0-5	14.02	6.7	8.4	2.2	1.8E-05	1.7E-06	1.7E-06	0.34
679B 2H-06, 25-30	14.27	7.8	5.8	1.3	1.4E-05	1.2E-06	2.3E-06	0.40
679B 2H-06, 50-55	14.52	4.5	7.5	2.0	2.2E-05	2.2E-06	1.6E-06	0.48
679B 2H-06, 75-80	14.77	9.7	4.5	1.2	1.3E-05	1.3E-06	3.4E-06	0.47
679B 2H-06, 100-105	15.02	6.6	4.0	2.0	1.3E-05	2.5E-06	2.6E-06	0.53
679B 2H-06, 125-130	15.27	13.8	4.4	1.5	1.4E-05	1.7E-06	5.2E-06	0.51
679B 2H-07, 0-5	15.52	22.6	4.5	1.4	1.2E-05	1.4E-06	7.0E-06	0.42
679B 2H-07, 25-30	15.77	25.8	4.8	1.2	1.4E-05	1.3E-06	8.9E-06	0.47
679B 2H-07, 50-55	16.02	37.3	5.7	1.3	1.8E-05	1.6E-06	1.4E-05	0.53
679B 2H-CC, 0-5	16.27	15.7	7.2	1.6	1.9E-05	1.5E-06	4.9E-06	0.42

Table 4.5. Coulometric, accumulation rate, and dry bulk density data for Hole 680A.

Site, interval	Depth (m)	CaCO3 (%)	Corg (%)	S (%)	Corg Acc. Rate (mol/cm^2/yr)	S Acc. Rate (mol/cm^2/yr)	CaCO3 Acc. Rate (mol/cm^2/yr)	Dry Bulk Dens. (g/cm^3)
680A 1H-01, 21-26	0.21	1.0	10.6	1.3	4.4E-05	2.0E-06	4.9E-07	0.31
680A 1H-01, 50-55	0.5	8.8	9.9	1.3	2.7E-05	1.4E-06	2.9E-06	0.21
680A 1H-01, 75-80	0.75	6.7	10.4	1.4	3.6E-05	1.8E-06	2.8E-06	0.26
680A 1H-01, 100-105	1	8.6	11.2	1.3	2.6E-05	1.1E-06	2.4E-06	0.17
680A 1H-01, 127-132	1.27	8.2	8.9	1.6	4.0E-05	2.7E-06	4.4E-06	0.34
680A 1H-02, 0-5	1.5	4.2	11.8	1.5	4.0E-05	2.0E-06	1.7E-06	0.26
680A 1H-02, 25-30	1.75	3.2	10.8	1.4	4.9E-05	2.4E-06	1.7E-06	0.35
680A 1H-02, 50-55	2	7.0	3.2	0.6	3.1E-05	2.3E-06	8.3E-06	0.75
680A 1H-02, 75-80	2.25	5.7	2.8	0.6	3.8E-05	3.0E-06	9.1E-06	1.21
680A 1H-02, 100-105	2.5	0.2	5.1	1.2	2.6E-05	2.4E-06	1.0E-07	0.47
680A 1H-02, 125-130	2.75	0.3	2.0	1.5	2.0E-05	5.9E-06	4.2E-07	0.94
680A 1H-03, 0-5	3	8.2	0.8	0.5	9.9E-06	2.4E-06	1.2E-05	1.10
680A 1H-03, 25-30	3.25	7.2	2.3	1.0	1.7E-05	2.6E-06	6.3E-06	0.67
680A 1H-03, 50-55	3.5	11.9	4.7	1.4	2.0E-05	2.3E-06	6.1E-06	0.38
680A 1H-03, 75-80	3.75	0.2	4.3	1.5	1.8E-05	2.3E-06	1.2E-07	0.82
680A 1H-03, 102-107	4.02	3.7	4.0	1.1	9.1E-06	9.2E-07	9.9E-07	0.45
680A 1H-03, 125-130	4.25	7.1	6.9	1.6	1.5E-05	1.3E-06	1.9E-06	0.45
680A 1H-04, 0-5	4.5	6.3	4.3	1.3	1.5E-05	1.6E-06	2.6E-06	0.69
680A 1H-04, 25-30	4.75	2.2	5.7	1.5	1.6E-05	1.6E-06	7.5E-07	0.58
680A 1H-04, 50-55	5	9.7	5.8	1.5	1.6E-05	1.5E-06	3.3E-06	0.55
680A 1H-04, 73-78	5.23	12.4	6.1	1.4	1.3E-05	1.2E-06	3.3E-06	0.44
680A 1H-04, 100-105	5.5	7.6	5.8	1.4	1.4E-05	1.3E-06	2.2E-06	0.48
680A 1H-04, 125-130	5.75	14.3	4.7	1.1	8.4E-06	7.1E-07	3.1E-06	0.40
680A 1H-05, 0-5	6	12.5	5.4	1.2	1.2E-05	9.5E-07	3.2E-06	0.48
680A 1H-05, 25-30	6.25	18.2	5.7	1.3	1.1E-05	9.3E-07	4.3E-06	0.44
680A 1H-05, 50-55	6.5	16.7	5.9	2.0	9.7E-06	1.2E-06	3.3E-06	0.37
680A 1H-05, 75-80	6.75	12.9	7.2	2.9	1.0E-05	1.6E-06	2.2E-06	0.30
680A 1H-05, 105-110	7.05	18.3	7.5	1.3	2.0E-05	1.3E-06	5.8E-06	0.56
680A 1H-05, 125-130	7.25	25.4	6.7	1.5	2.1E-05	1.8E-06	9.6E-06	0.66
680A 1H-06, 0-5	7.5	30.6	6.1	1.2	1.5E-05	1.1E-06	9.2E-06	0.53
680A 1H-06, 25-30	7.75	5.7	8.5	2.0	1.6E-05	1.4E-06	1.3E-06	0.39
680A 1H-06, 50-55	8	0.2	4.0	2.8	1.0E-05	2.6E-06	5.1E-08	0.53
680A 2H-01, 7-12	8.37	8.1	7.0	1.4	1.9E-05	1.4E-06	2.6E-06	0.57
680A 2H-01, 25-30	8.56	13.1	6.6	1.8	1.4E-05	1.4E-06	3.3E-06	0.44
680A 2H-01, 50-55	8.81	13.2	6.5	1.8	1.5E-05	1.6E-06	3.6E-06	0.48
680A 2H-01, 75-80	9.06	10.6	6.0	2.0	1.1E-05	1.4E-06	2.3E-06	0.38
680A 2H-01, 100-105	9.31	14.0	5.9	1.7	1.3E-05	1.4E-06	3.6E-06	0.45
680A 2H-01, 125-130	9.56	10.5	7.5	2.3	1.9E-05	2.2E-06	3.1E-06	0.37
680A 2H-02, 0-5	9.81	5.1	6.4	1.7	1.4E-05	1.4E-06	1.3E-06	0.45
680A 2H-02, 25-30	10.06	1.2	4.3	1.4	1.0E-05	1.2E-06	3.5E-07	0.50
680A 2H-02, 50-55	10.31	4.0	5.2	1.7	1.2E-05	1.4E-06	1.1E-06	0.49
680A 2H-02, 72-77	10.56	1.2	4.2	1.3	1.0E-05	1.2E-06	3.4E-07	0.50
680A 2H-02, 100-105	10.81	0.1	3.9	1.4	1.0E-05	1.4E-06	2.6E-08	0.55
680A 2H-02, 125-130	11.06	0.7	2.1	1.3	7.2E-06	1.8E-06	3.1E-07	0.73
680A 2H-03, 0-5	11.31	5.7	8.4	2.0	1.9E-05	1.7E-06	1.6E-06	0.49
680A 2H-03, 25-30	11.56	0.2	8.2	1.8	1.8E-05	1.5E-06	6.6E-08	0.46
680A 2H-03, 50-55	11.81	0.2	8.0	1.8	1.8E-05	1.4E-06	6.6E-08	0.46
680A 2H-03, 75-80	12.06	0.2	6.4	1.7	1.6E-05	1.6E-06	5.1E-08	0.54
680A 2H-03, 100-105	12.31	0.1	4.6	1.5	1.1E-05	1.4E-06	2.4E-08	0.51
680A 2H-03, 125-130	12.56	0.9	6.2	2.0	1.5E-05	1.9E-06	2.7E-07	0.52
680A 2H-04, 0-5	12.81	0.2	7.6	2.2	1.7E-05	1.8E-06	4.5E-08	0.48
680A 2H-04, 25-30	13.06	0.2	6.3	1.9	1.4E-05	1.6E-06	4.5E-08	0.48
680A 2H-04, 50-55	13.31	0.2	6.2	1.6	1.7E-05	1.7E-06	5.6E-08	0.59
680A 2H-04, 78-83	13.56	5.9	6.6	2.0	1.5E-05	1.7E-06	1.6E-06	0.49
680A 2H-04 , 100-105	13.81	0.7	4.6	1.5	1.0E-05	1.2E-06	1.8E-07	0.46
680A 2H-04,125-130	14.06	5.2	7.5	1.9	1.7E-05	1.5E-06	1.4E-06	0.47
680A 2H-05, 0-5	14.31	7.3	6.7	1.7	1.4E-05	1.4E-06	1.8E-06	0.43

Table 4.5. (Continued) Coulometric, accumulation rate, and dry bulk density data for Hole 680A.

Site, interval	Depth (m)	CaCO3 (%)	Corg (%)	S (%)	Corg Acc. Rate (mol/cm^2/yr)	S Acc. Rate (mol/cm^2/yr)	CaCO3 Acc. Rate (mol/cm^2/yr)	Dry Bulk Dens. (g/cm^3)
680A 2H-05, 0-5	14.31	7.3	6.7	1.7	1.4E-05	1.4E-06	1.8E-06	0.43
680A 2H-05, 26-31	14.57	9.3	3.5	1.3	1.3E-05	1.8E-06	4.2E-06	0.73
680A 2H-05, 46-51	14.77	10.4	6.4	2.1	1.7E-05	2.1E-06	3.3E-06	0.51
680A 2H-05, 75-80	15.06	0.4	6.6	1.7	1.5E-05	1.5E-06	1.1E-07	0.43
680A 2H-05, 100-105	15.31	11.2	7.4	1.7	1.6E-05	1.3E-06	2.9E-06	0.41
680A 2H-05, 125-130	15.56	0.1	8.4	1.8	2.0E-05	1.6E-06	2.4E-08	0.47
680A 2H-06, 0-5	15.81	0.1	7.0	1.7	1.8E-05	1.7E-06	2.6E-08	0.49
680A 2H-06, 25-30	16.06	0.1	6.2	1.4	1.8E-05	1.5E-06	2.9E-08	0.56
680A 2H-06, 50-55	16.31	0.3	3.3	0.9	1.2E-05	1.3E-06	1.5E-07	0.71
680A 2H-06, 72-77	16.53	0.1	4.5	1.6	1.3E-05	1.7E-06	2.8E-08	0.54
680A 2H-06, 100-105	16.81	3.9	7.1	1.6	2.0E-05	1.7E-06	1.3E-06	0.55
680A 2H-06, 125-130	17.06							0.42
680A 2H-07, 0-5	17.31	8.7	9.6	1.7	1.4E-05	9.8E-07	1.6E-06	0.29
680A 2H-07, 25-30	17.56	0.8	12.0	2.4	2.5E-05	1.9E-06	2.1E-07	0.41
680A 2H-07, 50-55	17.81	0.2	8.1	1.7	1.9E-05	1.5E-06	7.0E-08	0.45
680A 2H-CC, 6-11	18.02	0.7	4.8	1.0	1.5E-05	1.2E-06	2.5E-07	0.60

Table 4.6. Coulometric, accumulation rate, and dry bulk density data for Hole 681A.

Site, interval	Depth (m)	CaCO3 (%)	Corg (%)	Corg Acc. Rate (mol/cm^2/yr)	CaCO3 Acc. Rate (mol/cm^2/yr)	Dry Bulk Dens. (g/cm^3)
681A 1H-01, 53-58	0.53	0.2	4.6	2.5E-05	1.0E-07	
681A 1H-01, 73-78	0.73	0.3	6.7	1.5E-05	1.2E-07	0.47
681A 1H-01, 101-106	1.01	0.2	7.2	2.0E-05	1.1E-07	0.53
681A 1H-01, 125-130	1.25	0.2	4.0	2.3E-05	9.9E-08	0.60
681A 1H-02, 3-8	1.53	0.2	5.5	1.7E-05	7.9E-08	0.58
681A 1H-02, 25-30	1.75	0.2	6.9	1.8E-05	1.6E-07	0.51
681A 1H-02, 50-55	2	0.2	6.4	2.2E-05	1.9E-07	0.41
681A 1H-02, 74-79	2.24	0.4	5.6	2.3E-05	2.9E-07	0.49
681A 1H-02, 101-106	2.51	0.4	5.6	1.9E-05	2.0E-06	0.60
681A 1H-02, 125-130	2.75	0.5	4.8	2.4E-05	2.0E-07	0.75
681A 1H-03, 3-8	3.03	4.2	4.9	9.9E-06	9.2E-07	0.61
681A 1H-03,25-30	3.25	0.2	3.7			1.03
681A 1H-03, 50-55	3.5	2.6	3.3	1.4E-05	1.2E-06	0.46
681A 1H-03, 82-87	3.82	0.2	2.6	1.4E-05	1.2E-06	
681A 1H-03, 101-106	4.01	2.2	3.0	1.5E-05	2.5E-08	0.91
681A 1H-03, 125-130	4.25	3.8	5.3	1.8E-05	0.0E+00	0.54
681A 1H-04, 3-8	4.53	0.1	6.0	1.6E-05	5.2E-07	0.49
681A 1H-04, 25-30	4.75	0.0	5.0	1.6E-05	3.1E-08	0.64
681A 1H-04, 50-55	5	1.5	5.6	1.4E-05	4.5E-07	0.52
681A 1H-04, 75-80	5.25	0.1	5.3	1.7E-05	3.3E-07	0.56
681A 1H-04, 101-106	5.51	1.4	5.2	1.4E-05	1.0E-06	0.48
681A 1H-04, 125-130	5.75	0.8	5.3	1.6E-05	0.0E+00	0.60
681A 1H-05, 0-5	6	2.7	4.5	1.3E-05	1.6E-06	0.56
681A 1H-05, 25-30	6.25	0.0	6.0	1.5E-05	0.0E+00	0.47
681A 2H-01, 25-30	6.77	5.0	4.9	8.4E-06	7.8E-07	0.48
681A 2H-01, 50-55	7.02	0.0	5.0	5.5E-06	1.0E-06	0.55
681A 2H-01, 75-80	7.27	2.8	3.7	9.5E-06	1.2E-06	0.42
681A 2H-01, 102-107	7.54	3.7	2.5	8.9E-06	9.2E-07	0.40
681A 2H-01, 125-130	7.77	3.7	3.5	8.4E-06	9.3E-07	0.49
681A 2H-02, 3-8	8.05	2.7	3.2	1.1E-05	9.3E-07	0.51
681A 2H-02, 25-30	8.27	2.9	3.1	9.4E-06	1.1E-06	0.41
681A 2H-02, 54-59	8.58	2.3	3.2			0.51
681A 2H-02, 75-80	8.77	3.1	3.3	1.0E-05	2.3E-06	0.44
681A 2H-02, 102-107	9.04	2.8	3.2	1.2E-05	2.0E-06	
681A 2H-02, 125-130	9.27	5.5	3.1	1.2E-05	1.1E-06	0.52
681A 2H-03, 3-8	9.55	4.4	3.1	1.1E-05	9.8E-07	0.58
681A 2H-03, 25-30	9.77	2.3	3.0	1.1E-05	9.1E-07	0.60
681A 2H-03, 47-52	9.99	2.2	3.0	1.3E-05	3.5E-08	0.56
681A 2H-03, 74-79	10.26	2.2	3.3	9.2E-06	4.7E-07	0.53
681A 2H-03, 102-107	10.54	0.1	3.7	8.8E-06	0.0E+00	0.53
681A 2H-03, 125-130	10.77	1.1	2.6	1.1E-05	2.8E-07	0.55
681A 2H-04, 3-8	11.05	0.0	2.2	9.3E-06	0.0E+00	0.63
681A 2H-04, 25-30	11.27	0.6	2.8	9.0E-06	0.0E+00	0.62
681A 2H-04, 50-55	11.52	0.0	2.1	1.0E-05	0.0E+00	0.69
681A 2H-04, 75-80	11.77	0.0	2.3	4.8E-06	0.0E+00	0.61
681A 2H-04, 102-107	12.05	0.0	1.9	9.5E-06	5.7E-07	0.83
681A 2H-04, 125-130	12.27	0.0	1.2	7.1E-06	9.3E-07	0.63
681A 2H-05, 3-8	12.55	0.9	1.8	2.4E-06	8.2E-07	0.80
681A 2H-05, 25-30	12.77	1.5	1.4	2.4E-06	3.0E-08	0.79
681A 2H-05, 50-55	13.02	4.5	1.6	2.6E-06	2.1E-08	0.71
681A 2H-05, 75-80	13.27	0.2	1.6	4.4E-06	9.2E-09	0.71
681A 2H-05, 102-107	13.54	0.1	1.2	4.2E-06	5.9E-08	0.99
681A 2H-05, 125-130	13.77	0.1	4.8	2.9E-06	4.4E-07	0.43
681A 2H-06, 3-8	14.05	0.3	2.9	3.2E-06	4.9E-08	0.69
681A 2H-06, 25-30	14.27	4.4	3.4	3.4E-06	2.5E-06	0.39
681A 2H-06, 50-55	14.52	0.2	1.3	4.1E-06	6.5E-07	1.15
681A 2H-06, 75-80	14.77	13.1	2.1	3.4E-06	1.2E-06	0.74
681A 2H-06, 103-108	15.05	5.7	4.3	2.5E-06	2.0E-08	0.44
681A 2H-06, 125-130	15.27	9.2	3.2	2.4E-06	1.8E-07	0.49
681A 2H-07, 0-5	15.52	0.1	1.2	2.6E-06	5.2E-07	0.94
681A 2H-07, 25-30	15.77	0.9	1.5	3.6E-06	2.0E-08	0.77
681A 2H-07, 50-55	16.02	2.6	1.6	2.0E-05	2.4E-08	0.78
681A 2H-CC, 10-15	16.22	0.1	1.9	1.8E-05	2.6E-08	0.92

Table 4-7. Coulometric data for Hole 686A.

Site, interval	Depth (m)	$CaCO_3$ (%)	Corg (%)
686A 1H-01, 0-5	0	5.2	3.1
686A 1H-01, 25-30	0.25	0.0	3.4
686A 1H-01, 58-63	0.58	0.1	3.0
686A 1H-01, 75-80	0.75	0.1	2.2
686A 1H-01, 100-105	1	0.2	1.8
686A 1H-01, 125-130	1.25	3.7	1.5
686A 1H-02, 0-5	1.5	0.7	2.6
686A 1H-02, 25-30	1.75	10.7	2.3
686A 1H-02, 50-55	2	0.2	3.5
686A 1H-02, 75-80	2.25	0.1	3.4
686A 1H-02, 100-105	2.5	0.0	3.3
686A 1H-02, 125-130	2.75	0.0	3.0
686A 1H-03, 0-5	3	0.7	3.2
686A 1H-03, 25-30	3.25	0.1	3.3
686A 1H-03, 50-55	3.5	1.4	2.9
686A 1H-03, 75-80	3.75	0.2	3.3
686A 1H-03, 100-105	4	0.0	4.5
686A 1H-03, 125-130	4.25	0.1	2.8
686A 1H-04, 1-6	4.51	0.1	4.9
686A 1H-04, 25-30	4.75	0.1	4.3
686A 2H-01, 3-8	5.08	0.1	3.9
686A 2H-01, 30-35	5.35	0.1	3.8
686A 2H-01, 50-55	5.55	0.1	3.3
686A 2H-01, 75-80	5.8	0.0	3.2
686A 2H-01, 100-105	6.05	0.1	3.2
686A 2H-01, 125-130	6.3	4.7	1.9
686A 2H-02, 0-5	6.55	4.8	1.8
686A 2H-02, 25-30	6.8	13.6	2.3
686A 2H-02, 49-54	7.04	9.0	1.7
686A 2H-02, 75-80	7.3	5.0	2.4
686A 2H-02, 100-105	7.55	0.1	2.1
686A 2H-02, 125-130	7.8	0.1	1.3
686A 2H-03, 0-5	8.05	2.8	2.6
686A 2H-03, 25-30	8.3	6.1	1.9
686A 2H-03, 50-55	8.55	2.1	2.1
686A 2H-03, 75-80	8.8	0.4	2.6
686A 2H-03, 100-105	9.05	2.8	2.8
686A 2H-03, 125-130	9.3	0.2	2.9
686A 2H-04, 0-5	9.55	0.1	2.2
686A 2H-04, 25-30	9.8	0.1	2.7
686A 2H-04, 50-55	10.05	0.4	2.8
686A 2H-04, 75-80	10.3	0.2	2.7
686A 2H-04, 100-105	10.55	0.2	3.1
686A 2H-04, 125-130	10.8	0.0	2.1
686A 2H-05, 0-5	11.05	0.0	3.1
686A 2H-05, 25-30	11.3	0.1	2.6
686A 2H-05, 50-55	11.55	1.1	2.5
686A 2H-05, 75-80	11.8	1.2	1.8
686A 2H-05, 100-105	12.05	3.1	2.6
686A 2H-05, 125-130	12.3	0.0	3.3
686A 2H-06, 0-5	12.55	0.9	2.4
686A 2H-06, 25-30	12.8	5.4	3.5
686A2H-06,50-55	13.05	1.1	3.0
686A2H-06, 75-80	13.3	0.1	3.5
686A 2H-06, 100-105	13.55	11.9	3.0
686A 2H-06, 125-130	13.8	0.0	4.3
686A 2H-07, 0-5	14.05	0.7	3.6
686A 2H-07, 25-30	14.3	0.0	3.7
686A 2H-07, 50-55	14.55	0.4	4.0
686A 2H-CC, 10-15	14.85	2.0	23.6

Table 4-8. Coulometric data for Hole 687A.

Site, interval	Depth (m)	$CaCO_3$ %	Corg %
687 A 1H-01, 8-13cm	0.8	0.4	12.5
687 A 1H-01, 25-30cm	0.25	0.1	5.2
687A 1H-01, 50-55	0.5	0.2	11.4
687A 1H-01, 75-80	0.75	1.5	5.4
687A 1H-01,101-106	1.01	0.2	9.0
687A 1H-01,125-130	1.25	0.2	6.0
687A 1H-02, 0-5	1.5	0.2	6.7
687A 1H-02, 25-30	1.75	0.1	5.6
687A 1H-02, 50-55	2	3.3	4.9
687A 1H-02, 75-80	2.25	2.2	5.0
687A 1H-02, 100-105	2.5	5.4	4.9
687A 1H-02, 125-130	2.75	2.2	3.6
687A 1H-03, 0-5	3	0.1	4.8
687A 1H-03, 25-30	3.25	0.1	4.2
687A 1H-03, 57-62	3.57	2.1	2.5
687A 1H-03, 75-80	3.75	0.0	6.9
687A 1H-03, 100-104	4	0.2	5.4
687A 1H-03, 125-130	4.25	0.1	6.6
687A 1H-04, 0-5	4.5	0.1	6.1
687A 1H-04, 25-30	4.75	0.1	4.9
687A 1H-04, 50-55	5	8.7	5.0
687A 1H-04, 75-80	5.25	0.1	5.6
687A 1H-04, 100-105	5.5	0.3	2.4
687A 1H-04, 125-130	5.75	11.3	1.8
687A 1H-05, 0-5	6	0.2	3.3
687A 1H-05, 25-30	6.25	4.7	8.1
687A 1H-05, 50-55	6.5	0.1	7.0
687A 1H-05, 75-80	6.75	0.1	6.8
687A 1H-05, 100-105	7	0.2	6.6
687A 1H-05, 125-130	7.25	0.8	8.1
687A 2H-01, 7-12	7.32	16.9	7.8
687A 2H-01, 25-30	7.8	2.2	6.1
687A 2H-01, 50-55	8.05	6.6	4.9
687A 2H-01, 75-80	8.3	3.6	4.3
687A 2H-01, 100-105	8.55	6.2	4.3
687A 2H-01, 125-130	8.8	5.4	3.7
687A 2H-02, 1-6	9.06	5.3	3.8
687A 2H-02, 25-30	9.3	0.0	3.8
687A 2H-2, 50-55	9.55	0.1	3.4
687A 2H-2, 75-80	9.8	0.0	3.0
687A 2H-02, 100-106	10.05	0.0	2.5
687A 2H-02, 132-137	10.37	0.1	3.7
687A 2H-03, 0-5	10.55	0.0	2.4
687A 2H-03, 25-30	10.8	0.1	1.8
687A 2H-03, 50-55	11.05	0.1	1.5
687A 2H-03, 75-80	11.3	0.5	0.8
687A 2H-03, 100-105	11.55	0.1	4.1
687A 2H-03, 125-130	11.8	0.0	2.0
687A 2H-04, 0-5	12.05	0.0	3.3
687A 2H-04, 25-30	12.3	0.0	2.3
687A 2H-04, 50-55	12.55	0.1	0.6
687A 2H-04, 76-81	12.8	0.0	3.0
687A 2H-04, 100-105	13.05	2.1	0.7
687A 2H-04, 122-127	13.27	1.1	0.5
687A 2H-05, 0-5	13.55	0.1	2.2
687A 2H-05, 25-30	13.8	21.7	5.1
687A 2H-05, 50-55	14.05	0.2	11.4
687A 2H-05, 76-81	14.31	0.1	6.8
687A 2H-05, 100-105	14.55	0.1	8.6
687A 2H-05, 125-130	14.8	0.1	8.5
687A 2H-06, 0-5	15.05	4.9	2.5
687A 2H-06, 25-30	15.3	0.1	8.8
687A 2H-06, 50-55	15.55	0.0	7.6
687A 2H-06, 75-80	15.8	0.0	5.7
687A 2H-06, 100-105	16.05	0.0	4.3
687A 2H-07, 0-5	16.55	0.0	4.5

Table 4-9. Summary of statistics for carbon coulometry data.

	679B		680A		681A		686A		687A	
	% $CaCO_3$	% Corg	% $CaCO_3$	% Corg	% $CaCO_3$	% Corg	% $CaCO_3$	% Corg	% $CaCO_3$	% Corg
Max	56.20	13.61	30.56	11.95	13.07	7.24	13.57	23.60	21.73	12.50
Min	0.00	1.59	0.08	0.82	0.00	1.18	0.00	1.30	0.00	0.50
Mean	18.85	6.91	6.20	6.29	1.82	3.62	1.75	3.20	1.86	4.90
Stdev	17.78	2.65	6.37	2.34	2.39	1.61	3.08	2.80	3.92	2.60

Table 4-10. Summary of statistics for sulfur coulometry data.

	Weight % Sulfur	
	679B	680A
Max	3.55	2.93
Min	0.81	0.53
Mean	1.56	1.56
Stdev	0.47	0.43

Table 4-11. Oxygen and carbon isotope data--Core 679B.

Site, interval	Benthic δ^{13} C	Benthic δ^{18} O
679B 1H-01, 10-15	-5.77	0.87
679B 1H-01, 100-105		
679B 1H-01, 125-130	-1.73	0.94
679B 1H-02, 0-5	-1.57	1.56
679B 1H-02, 25-30	-2.12	0.01
679B 1H-03, 50-55	-2.44	1.39
679B 1H-03, 75-80	-1.90	1.71
679B 1H-03 100-105		
679B 1H-03, 125-130		
679B 1H-04, 0-5	-1.43	1.49
679B 1H-04, 25-30	-1.74	0.82
679B 1H-04, 50-55	-2.44	-0.14
679B 1H-04, 75-80		
679B 1H-04, 100-105	-2.01	0.67
679B 1H-04, 125-130	-2.26	0.55
679B 1H-05, 0-5	-1.24	0.78
679B 1H-05, 24-28	-1.30	0.83
679B 1H-CC, 13-18	-2.15	0.02
679B 2H-01,0-5	-1.17	0.78
679B 2H-01, 25-30	-1.88	0.96
679B 2H-01, 50-55	-2.25	0.25
679B 2H-01 ,75-80	-1.97	0.24
679B 2H-01, 125-130	-1.54	1.25
679B 2H-02, 1-6	-1.02	2.24
679B 2H-02, 27-32	-1.30	1.02
679B 2H-02, 75-80	-0.73	1.02
679B 2H-03, 125-130		
679B 2H-04, 25-30	-1.63	0.81
679B 2H-04, 50-55	-2.87	1.51
679B 2H-04, 75-80	-2.49	0.10
679B 2H-04, 100-105	-1.89	0.77
679B 2H-04, 125-130	-2.71	0.97
679B 2H-05, 75-80	-3.63	2.26
679B 2H-06, 50-55	-2.58	1.38
679B 2H-06, 125-130	-3.47	2.44
679B 2H-07, 0-5	-2.28	1.93
679B 2H-07, 50-55	-1.51	1.96
679B 2H-CC, 0-5	-1.76	0.62

Table 4.12. $\delta^{18}O$ data for Hole 680B (Wefer et al., 1990).

Depth (m)	$\delta^{18}O$
0.03	1.57
0.18	1.63
0.32	1.55
0.4	1.76
0.48	1.78
0.52	1.63
0.65	1.29
0.73	1.45
0.87	1.6
1.12	1.61
1.23	1.4
1.31	1.34
1.46	1.53
1.64	0.8
1.73	1.59
1.79	1.64
1.91	1.6
1.98	1.52
2.04	1.6
3.23	2.06
3.48	2.35
3.73	2.13
3.83	2.33
3.98	1.96
4.23	2.12
4.46	2.21
4.73	2.07
4.93	2.17
4.98	2.06
5.23	1.93
5.73	2.13
5.9	2.09
5.98	1.97
6.23	2.04
6.37	1.92
6.48	1.92
6.73	1.66
6.88	1.7
6.96	1.82
7.23	1.6
7.4	1.58
7.48	1.43
7.73	1.71
7.88	1.58
7.98	1.62
8.23	1.55
8.35	1.59
8.64	1.7
8.73	1.59
8.9	1.72
8.98	1.72
9.23	1.82
9.38	1.77
9.48	1.83
9.73	2.04
9.85	2.06
10.23	2.44
10.98	2.35
11.23	2.08
13.23	2.28
13.48	2.01
14.23	1.61
14.64	1.32
14.73	1.54
15.16	2.02
15.23	1.93
16.46	1.78
16.73	2.05
16.98	1.68
17.73	2.05
17.96	2.31
18.23	2.11
18.48	1.79
18.73	2.14
18.98	2.13
19.1	2.03

Table 4.13. Duplicated isotope analyses for the benthic foraminifer *B. humilis* from ODP core sediments.

Sample I.D. 679B 1H-02, 47-52cm		
	$\delta^{13}C$ (≡)	$\delta^{18}O$ (≡)
1)	-1.128	2.111
2)	-1.394	1.964
3)	-1.658	1.823
Standard Deviation	0.265	0.144

Table 4.14. Age dates of phosphorite samples from ODP Holes 679B, 686A, and 687A.

Site, interval	Depth (m)	Sample type	Th-230 Age (1000 yrs)
679B 1H-1 88-89cm	0.88	hard nodule	69.9±2.8
679B 1H-1 95-97cm	0.95	hard nodule	59.8±2.4
679B 1H-1 112-114cm	1.12	hard nodule	91.7±4.3
679B 1H-3 57-58cm	3.57	hard nodule	175.2±12.3
679B 1H-3 59-61cm	3.59	hard nodule	191.0±17.9
679B 1H-4 11-13cm	4.61	hard nodule	187.5±14.7
679B 2H-2 118-121cm	9.18	hard nodule	356.3±110.2
686A 1H-1 44-45cm	0.44	hard nodule	65.2±2.6
686A 1H-2 22-23cm	1.72	hard nodule	193.4±10.0
686A 2H-2 55-56cm	7.51	hard nodule	300.0±38.7
686A 3H-1 38-46cm	14.98	hard nodule	487.5±112.5
687A 1H-1 91-92cm	0.91	sediment	236.7±28.1
687A 1H-3 52-54cm	3.52	hard nodule	32.0±0.9
687A 1H-3 66-68cm	3.66	mudstone	15.4±0.9
687A 2H-3 137-138cm	11.87	hard nodule	166.4±8.8
687A 2H-5 9-11cm	13.59	sediment	155.3±12.6
687A 2H-7 22cm	16.72	small nodule	202.7±10.5
687A 3H-1 72-74cm	17.72	hard nodule	248.4±24.6

References Cited

Arthur, M,A., Laarkamp, K., Dean, W.E., Glenn, C.R., and Jahnke, R.A., 1993. The modern Peru margin: Organic sedimentation and preservation patterns. Geol. Soc. Amer. Ann. Meeting, Programs with Abstracts, A239.

Barber, R. T. and Smith, R. L., 1981. Coastal upwelling systems. In: A. R. Longhurst (Editor), Analysis of Marine Ecosystems, Acedemic Press, New York, pp. 31-68.

Belanger, P. E., Curry, W. B., Matthews, R. K., 1981. Core top evaluation of benthic foraminiferal isotope ratios for paleoceanographic interpretations. *Palaeogeogr., Palaeoclimatol., Palaoecol.*, 32:205:221.

Berger, W. H., Smetacek, V. S. and Wefer, G. (Editors), 1989. Productivity of the ocean: Present and Past. (Life Science Research Reports.) Wiley, Chichester, UK, pp. 471.

Berner, R. A., 1984. Sedimentary pyrite formation: An update. *Geochim. Cosmochim. Acta*, 48:605-615.

Berner, R. A., 1989. Biogeochemical cycles of carbon and sulfur and their effect on atmospheric oxygen over Phanerozoic time. *Palaeogeogr., Palaeoclim. Palaeoecol.*, 75:97-122.

Blasco, D., 1971. Composition and distribution of phytoplankton in the region of up-welling off the coast of Peru. *Invest. Pesq.*, 35(1):61-112.

Bralower, T. J., and Thierstein, H. R., 1984. Low productivity and slow deep-water circulation in Mid-Cretaceous oceans. *Geology*, 12:614-618.

Brockmann, C., Fahrbach, E., Huyer, A. and Smith, R., 1980. The poleward undercurrent along the Peru coast: 5°S to 15°S. *Deep-Sea Res.*, 27: 847-856.

Burnett, W.H., Veeh, H. H. and Soutar, A., 1980. U-series oceanographic and sedimentary evidence in support of recent formation of phosphatic nodules off Peru. SEPM, Spec. Publ., 29:61-71.

Burnett, W.H., Veeh, H. H. (1977), Uranium-series disequilibrium studies in phosphorite nodules from the west coast of South America. *Geochimica et Cosmochimica Acta*, 41:755-764.

Calvert, S. E., Bustin, R. M., Pedersen, T. F., 1992. Lack of evidence for enhanced preservation of sedimentary organic matter in the oxygen minimum of the Gulf of California.*Geology*, 20:757-760.

Canby, T.Y., 1984. El Niño's ill wind. Natl. Geogr., 165:144-183.

Chappell, J., and Shackleton, N. J., 1986. Oxygen isotopes and sea level, *Nature*, 324:137-140.

Clayton, T., Kemp, A. E. S., 1990. Clay mineralogy of cenozoic sediments from the peruvian continental margin: Leg 112. *Proceedings of the Ocean Drilling Program, Scientific Results,* Ocean Drilling Program, College Station, TX, 112:59-86.

Corliss, B. H., 1985. Microhabitats of benthic foraminifera within deep-sea sediments, *Nature*, 314:435-438.

Csandy, G. T., 1990. Physical basis of coastal productivity. The SEEP and MASAR experiments . EOS Trans., Am. Geophys. Union, 71:1060-1065.

Davie, J. 1986. Statistics and Data Analysis in Geology, John Wiley & Sons, New York, pp. 546-554.

Demaison, G. J., Moore, G. T. 1980. Anoxic environments and oil source bed genesis. *Organic Geochemistry*, 2:9-31.

De Mendiola, B.R., 1981. Seasonal phytoplankton distribution along the Peruvian coast. In: F. A. Richards (Editor), Coastal Upwelling. (Coastal and Estuarine Sciances, 1.) Am. Geophys. Union, pp. 348-356.

De Vries, T. J., and Pearcy, W. G., 1982. Fish debris in sediments of the upwelling zone off central Peru: a late Quaternary record. *Deep Sea Res.*, 28:87-109.

Dunbar, R. B. and Wefer, G., 1984. Stable isotope fractionation in benthic foraminifera

from the Peruvian continental margin. Mar. Geol., 59:215-225.

Farrington, J. W., Davis, A. C., Sulanowski, J., McCaffrey, M. A., McCarthy, M., Clifford, C. H., Dickenson, P., and Volkman, J. K., 1989. Biogeochemistry of lipids in surface sediments of the Peru upwelling area ar 15°S. *In*: L. Matavelli and L. Novelli (Editors), Advances in Organic Geochemistry 1987. Org. Geochem., 13:607-617.

Faure, G., 1986. Principles of Isotope Geology, John Wiley & Sons, New York, pp. 56-58.

Foree, E. G., and McCarty, P. L., 1970. Anaerobic decomposition of algea. *Environ. Sci. Technology*, 4:842-849.

Glenn, C. R., Arthur, M. A., Resig, J. M., Burnett, W. C., Dean, W. E., Jahnke, R. A. 1994. Are modern and ancient phosphorites really so different? *In*: Proc, 29th Geol. Cong., Part C, A. Iijima et al. (Eds), pp. 159-188.

Glenn, C. R., Arthur, M.A., 1984. Sedimentary and geochemical indicatores of productivity and oxygen contents in modern and ancient basins: The Holocene Black Sea as the "type" anoxic basin. *Chemical Geology*, 48:325-354.

Goldhaber, M. B. and Kaplan, I. R., 1974. The sulfur cycle. *In*: Goldberg, E. D. et al. (Eds.), The Sea Vol. 5, J. Wiley & Sons, New York, p.569-655.

Grossman, E. L., 1984. Carbon isotope fractionation in the life benthic foraminifera: Comparison with inorganic precipitate studies. *Geochim, Cosmochim. Acta,* 48:1505-1512.

Heath, G. R., Moore, T. C. and Dauphin, J. P. 1977. Organic carbon in deep-sea sediments. *In*: Andersen, N. R. and Malahoff, A. (eds) *The Fate of Fossil Fuel CO_2 in the Oceans*. Plenum Press, New York. 605-625.

Heinze, P., 1990. Das Auftriebsgeschehen vor Peru im Spätquartär: Ocean Drilling Program (ODP) Forschungsfahrt Nr. 112: Bohrungen 679D, 680B, 681B, 686B. Ph.D. Thesis, Univ. Bremen, Germany.

Heinze, P., Wefer, G., 1992. The history of coastal upwelling off Peru (11°S, ODP Leg 112, Site 680B) over the past 650,000 years. In *Upwelling Systems: Evolution Since the Early Miocene*, Summerhayes, C. P., Prell, W. L., Emeis, K. C. (eds), Geological Society Special Publication No. 64, pp. 451-462.

Huffman, E.W.D., 1977. Performance of a new automatic carbon dioxide coulometer. *Microchem. J.*, 22:567-573.

Huyer,

Imbrie, J., Hays, J., Martinson, D., McIntyre, A., Mix, A., Morley, J., Pisias, N., Prell, W., and Shackleton, N., 1984. The orbital theory of Pleistocene climate:Support from a revised chronology of the marine d18O record, *In* Berger, A., Imbrie, J., Hays, J., Kukla, G., and Saltzman, B. (Eds.), *Milankovitch and Climate. Part I*: Dordrecht (Reidel), 269-305.

Ingle, J. C., Keller, G., Kolpack, R. L., 1980. Benthic foraminiferal biofacies, sediments and water masses of the southern Peru-Chile trench area, southeastern Pacific Ocean. *Micropaleontology,* 26:113-150.

Jumars, P. A., Altenbach, A. V., de Lange, G. J., Emerson, S. R., Hargrave, B. T., Müller, P. J., Prahl, F. G., Reimers, C. E., Steiger, T., and Suess, E., 1989. Transformation of Seafloor-arriving Fluxes into the Sedimentary Record, *In* Berger, W. H., et al. (Eds.), Productivity of the Ocean: Past and Present, Life Sci. Res. Rep., Vol. 44, Wiley & Sons, p. 291-312.

Kemp, A. E. S., 1990. Sedimentary fabrics and variation in lamination style in Peru continental margin upwelling sediments. *Proceedings of the Ocean Drilling Program, Scientific Results,* Ocean Drilling Program, College Station, TX, 112:43-58.

Kulm, L. D., Schrader, H., Resig, J. M., Thornburg, T. M., Masias, A. and Johnson, L., 1981. Late Cenozoic carbonates on the Peru continental margin: Lithostratigraphy, biostratigraphy, and tectonic history. In:L.D. Kulm, J. Dymond, J. Dasch and D. M.

Hussong (Editors), Nasca Plate: Crustal Formation and Andean Convergence. Geol. Soc. Am. Mem., 154:469-508.

Kulm, L. D., Suess, D., and Thornburg, T.M., 1984. Dolomites in organic-rich muds of the Peru forearc basins: analogue to the Monterey Formation. *In* Garrison, R. E., Kastner, M., and Zenger, D. H. (Eds.), *Dolomites of the Monterey Formation and Other Organic-Rich Units*. SEPM, Panifin Section, 41:29-47.

Lee, C. 1992. Controls on organic carbon preservation: The use of stratified water bodies to compare intrinsic rates of decomposition in oxic and anoxic systems. *Geochimica et Cosmochimica Acta* 56:3323-3335.

Leventhal, J. S., 1983. An interpretation of carbon and sulfur relationships in Black Sea sediments as indicators of environments of deposition. *Geochim. Cosmochim. Acta,* 47:133-137.

Martinez-Pardo, R., 1990. Major Neogene events of the Southeastern Pacific: the Chilean and Peruvian record. Paleoceanogr., Paleoclimatol., Paleoecol., 77:263-278.

Martini, E., 1990. Tertiary and Quaternary silicoflagellates, actiniscidians, and ebridians from the Eastern Pacific off Peru (Leg 112). *Proceedings of the Ocean Drilling Program, Scientific Results,* Ocean Drilling Program, College Station, TX, 112:157-173.

Martinson, D., Pisias, N., Hays, J., Imbrie, J., Moore, T., and Shackleton, N., 1987. Age dating and the orbital theory of the Ice Ages: development of a high resolution 0 to 300,000-year chronology. *Quat. Res.*, 27:1-29.

Mayer, L. M., 1994. Relationships between mineral surfaces and organic carbon concentrations in soils and sediments. *In*: C. Lee (Guest-Editor), Controls on Carbon Preservation. Chem. Geol., 114: 347-363.

McCorkle, D.C., Keigwin, L.D., 1990. The influence of microhabitats on the carbon isotopic composition of deep-sea benthic foraminifera. *Paleoceanography*, 5:161-185.

Muizon, C. de, and Bellon, H., 1980. L'age Mio-Pliocène de la formation Pisco, Peru. *C. R. Acad. Sci.*, 290(D):1063-1066.

Müller, P. J. and Suess, E., 1979. Productivity, sedimentation rate and sedimentary organic matter in the oceans: I. Organic Carbon preservation. *Deep Sea Res.*, 26A:1347-1362.

Müller, P. J., Erlenkeuser, H. and Von Grafenstein, R., 1983. Glacial-interglacial cycles in ocean productivity inferred from organic carbon contents in eastern North Atlantic sediment cores. *In* J. Thiede and E. Suess (Editors), Coastal Upwelling, Its Sediment Record, Part B, Sedimentary Records of Ancient Coastal Upwelling. Plenum, New York, pp. 365-398.

Oberhänsli, H., Heinze, P., Diester-Haass, L., Wefer, G., 1990. Upwelling off Peru during the last 430,000 yr and its relationship to the bottom-water environment, as deduced from coarse grain-size distributions and analyses of benthic foraminifers at Holes 679D, 680B, and 681B, Leg 112. *Proceedings of the Ocean Drilling Program, Scientific Results,* Ocean Drilling Program, College Station, TX, 112:369-390.

Orr, W. L., Gaines, A. G., 1974. Observations on rate of sulfate reduction and organic matter oxidation in the bottom waters of an estuarine basin: the upper basin of the Pettaquamscutt River (Rhode Island), *In* Advances in organic geochemistry, 1974: Paris, Technip, pp. 790-812.

Philander, S. G. H., 1983. El Niño Southern Oscillation phenomena. Nature, 302:295-301.

Raiswell, R. and Berner, R. A., 1987. Organic carbon losses during burial and thermal maturation of normal marine shales, *Geology*, 15:853-856.

Reimers, C. E., Suess, E. 1983a. Spatial and temporal patterns of organic matter accumulation on the Peru Continental Margin. *In* Thiede, J., and Suess, E. (Eds.), *Coastal Upwelling: Its Sediment Record, Part B*: New York (Plenum Press), 311-345.

Reimers, C. E., Suess, E. 1983b. The partitioning of organic carbon fluxes and sedimentary organic matter decomposition rates in the ocean. *Mar. Chem.*. 13:141-168.

Resig, J., 1981. Biogeography of benthic foraminifera of the northern Nazca plate and adjacent continental margin. *Geol. Soc. Am. Mem.*, 154:619-666.

Resig, J., 1990. Benthic foraminiferal stratigraphy and paleoenvironments off Peru, Leg 112. *Proceedings of the Ocean Drilling Program, Scientific Results,* Ocean Drilling Program, College Station, TX, 112:263-296.

Sarthein, M., Winn, K., Duplessy, J.-C. and Fontugne, M. R., 1988. Global variation of surface ocean productivity in low and mid latitudes: Influence on CO_2 reservoirs of the deep ocean and atmosphere during the last 21,000 years. *Paleoceanography*, 3(3):361-399.

Savdra, C. E., Bottjer, D. J., 1988. Trace-fossil model for reconstruction of paleo-oxygenation in bottom waters. *Geology*, 14:3-8.

Schrader, H. and Sorknes, R., 1990a. Spatial and temporal variation of Peruvian coastal upwelling during the latest Quaternary. *Proceedings of the Ocean Drilling Program, Scientific Results,* Ocean Drilling Program, College Station, TX, 112:391-406.

Schrader, H. and Sorknes, R., 1990b. Peruvian coastal upwelling: Late Quaternary productivity changes revealed by diatoms. Mar. Geol., 97:233-249.

Schrader, H., 1992a. Comparison of Quaternary coastal upwelling proxies off central Peru. *Marine Micropaleontology*, 19:28-47.

Schrader, H., 1992b. Peruvian coastal primary palaeo-productivity during the last 200,000 years. In *Upwelling Systems: Evolution Since the Early Miocene*, Summerhayes, C. P., Prell, W. L., Emeis, K. C. (eds), Geological Society Special Publication No. 64, pp. 451-462.

Shackleton, N. J., 1987. Oxygen isotopes, ice volume and sea level. *Quaternary Science Reviews*. 6:183-190..

Shepherd. G., 1979., Shallow crustal structure and marine geology of a convergence zone, northwest Peru and southwest Ecuador [Ph. D. dissert.]: Honolulu, University of Hawaii, 201 p.

Shipboard Scientific Party, 1988. Site. *In* Suess, E., von Huene, R. et al., *Proc. ODP, Init. Repts.*, 112: College Station, Tx (Ocean Drilling Program).

Smith, R. L., Mooers, C. N. K. and Enfield, D. B., 1971. Mesoscale studies of the physical oceanography of two coastal upwelling regions: Oregon and Peru. In: J. D. Costlow (Editor), Fertility of the Sea. Gordon and Breach, New York, pp. 512-535.

Soutar, A., Johnson, S. R. and Baumgartner, T. R., 1982. In search of modern depositional to the Monterey Formation. in: R. E. Garrison and R. G. Douglas (Editors), The Monterey Formation and Related Siliceous Rocks of California. SEPM, Tulsa, Okla., pp. 123-147.

Suess, E. 1980. Particulate organic carbon flux in the ocean: surface productivity and oxygen utilization. *Nature*, 288:260-263.

Suess, E., and Thiede, J. (Editors), 1983. Coastal Upwelling, Its Sedimentary Record. Part A: Responses of the Sedimentary Regime to Coastal Upwelling. Plenum, New York, 604 pp.

Suess, E., Kulm, L. D., and Killingley, J. S., 1987. Coastal upwelling and a history of organic-rich mudstone deposition off Peru, *In* Brooks, J., and Fleet, A. J. (Eds.), *Marine Petroleum Source Rocks*, Geol. Soc. Am. Sp. Publ., 24:181-197.

Suess, E., von Huene, R., et al., 1988. Ocean Drilling Program Leg 112; Peru Continental Margin: Part 2—Sedimentary history and diagenesis in a coastal upwelling environment, *Geology*, 16:939-943.

Suess, E., von Huene, R., et al., 1988. *Proceedings of the Ocean Drilling Program, Initial Reports* Ocean Drilling Program, College Station, TX, v.112.

ten Haven, H. L., Littke, R., Rullkötter, J., Stein, R., Welte, D. H., 1990. Accumulation rates and Composition of Organic Matter in Late Cenozoic Sediments Underlying the Active Upwelling Area Off Peru. *In* E. Suess, R. von Huene et al., Proc. ODP, Sci. Results. 112:591-605.

Thornburg, T. M., and Kulm, L. D., 1981. Sedimentary basins of the Peru continental margin: structure, stratigraphy and Cenozoic tectonics from 6°S to 16°S latitude, *In* Kulm, L. D., Dymond, J., Dasch, J. E., and Hussong, D. M. (Eds.), *Nazca Plate: Crustal Formation and Andean Convergence*. Geol. Soc. Am. Mem., 154:393-422.

Tucker, M., 1991. *Sedimentary Petrology: an introduction to the origin of sedimentary rocks*. Blackwell Scientific Publications, Oxford, p. 36.

Vincent, E., Killingley, J. S., Berger, W. H., 1981. Stable isotope composition of benthic foraminifera from the equatorial Pacific. *Nature*, 289:639-643.

Walsh, J. J. 1981. A carbon budget for overfishing off Peru, *Nature*, 290:300-304.

Wefer, G., Heinze, P., Suess, E., 1990. Stratigraphy and sedimentation rates from oxygen isotope composition, organic carbon content, and grain-size distribution at the Peru upwelling region: Holes 680B and 686B. *Proceedings of the Ocean Drilling Program, Scientific Results*, Ocean Drilling Program, College Station, TX, 112:355-368.

Wefer, G., Dunbar, R. B., and Suess, E., 1983. Stable isotopes of foraminifers off Peru recording high fertility and changes in upwelling history, *In* Thiede, J., and Suess, E. (Eds.), *Coastal Upwelling: Its Sediment Record, Part B*: New York (Plenum Press), 295-308.

Wetzel, A., 1983. Biogenic sedimentary structures in a modern upwelling region: Northwest African Continental Margin. *In* Thiede, J., and Suess, E. (Eds.), *Coastal Upwelling: Its Sediment Record, Part B*: New York (Plenum Press), 123-144.

Wyrtki, K., 1967. Circulation and water masses in the eastern equatorial Pacific Ocean. *Int. J. Oceanol. Limnol.*, 1:117-147.

Zahn, R., Winn, K. and Sarnthein, M., 1986. Benthic foraminiferal $\delta^{13}C$ and accumumlation rates of organic carbon: *Uvigerina peregrina* group and *Cibicidoides wuellerstorfi*. *Paleoceanography*, 1:27-42.

Zuta, S. and Guillén, O., 1970. Oceanographía de las aguas costeras del Peru. Bol. Inst. Mar Peru, 2:161-323.